Pile Foundations for Offshore Wind Turbines: Numerical and Experimental Investigations on the Behaviour under Short-Term and Long-Term Cyclic Loading

von Pablo Cuéllar
Ingeniero de Caminos, Canales y Puertos *)
geboren am 16. Januar 1978 in Madrid

von der Fakultät VI - Planen Bauen Umwelt
der Technischen Universität Berlin
zur Erlangung des Akademischen Grades
Doktor der Ingenieurwissenschaften (Dr.-Ing.)
genehmigte Dissertation

Promotionsausschuß:

Vorsitzender:	Prof. Dr.-Ing. Karsten Geißler
Gutachter:	Prof. Dr.-Ing. Stavros Savidis
Gutachter:	Prof. Dr.-Ing. Werner Rücker
Gutachter:	Prof. Dr.-Ing. Manuel Pastor

Tag der Einreichung:	15. Dezember 2010
Tag der Prüfung:	11. Februar 2011

Berlin 2011
D 83

*) Bauingenieur / Civil engineer

ABSTRACT

The behaviour of pile foundations for offshore wind turbines deviates from classical assumptions and accumulated experience mainly due to their large diameter, reduced slenderness and elevated ratio of lateral to vertical loads. The offshore environment poses the additional challenge of large numbers of load cycles from wind and waves and the possible influence of transient changes of pore water pressure around the pile, both of them issues that are still not well understood and also not being contemplated in current design guidelines.

In saturated soils, short-term cyclic loading within the extreme regime often involves a pore-pressure build up that eventually can lead to liquefaction phenomena and foundation failure. On the other hand, the effects of the long-term cyclic loading on the foundation's stability and especially on its serviceability must also be studied.

The purpose of this work was to gain an insight into both aspects, while developing a practicable numerical tool for a short-term prognosis and deriving useful criteria for design. To achieve such goals, the investigations have been broadly divided into a first part with a theoretical orientation for the analysis of short-term transient effects in the frame of the Finite Element Method, and a second empirical block for the study of long-term phenomena by means of model tests in a reduced scale.

The general picture that arises from these investigations is that of a foundation subject to hardening and soil densification in the long term, but also affected by transient episodes of significant softening during the storms as a consequence of pore pressure accumulation.

Hence the importance of considering the coupling effects between soil stress and pore water pressure in design, even for those cases where a soil liquefaction could in principle be disregarded on the grounds of a high relative density of the soil.

For practical design purposes, it seems sensible to distinguish between piles in fully drained conditions, in partially drained conditions and in undrained conditions, and analyse them correspondingly employing different strategies. Some considerations in this respect have been given in the final sections of this thesis.

KURZFASSUNG

Das Verhalten von Pfahlgründungen für Offshore-Windenergieanlagen weicht von den klassischen Annahmen und gesammelten Erfahrungen vor allem wegen der großen Pfahldurchmesser, geringeren Schlankheit und hohen Verhältnisse von lateralen zu vertikalen Lasten ab. Zudem entsteht im Offshore-Bereich die zusätzliche Herausforderung einer großen Anzahl von Lastwechseln aus Wind und Wellen und des möglichen Einflusses von vorübergehenden Veränderungen des Porenwasserdrucks um den Pfahl. Da in diesem Hinsicht noch viel Unkenntniss herrscht, wurden beide Aspekte in den Bemessungsrichtlinien bisher nicht ausreichend in Betracht gezogen.

Es ist aber bekannt, dass wassergesättigte Böden unter zyklischer Belastung oft einen Porenwasserdruckaufbau zeigen, der schließlich bis zur Bodenverflüssigung und einem Gründungsversagen führen kann. Andererseits können grosse Lastspielzahlen erhebliche bleibende Verformungen zur Folge haben, die die Gebrauchstauglichkeit der Gründung progressiv gefährden.

Wesentliche Ziele dieser Arbeit waren, einen Einblick in beide Aspekte zu gewinnen, ihre Folgen aufzuzeigen und sinnvolle Kriterien für die Pfahlbemessung herzuleiten. Dabei wurde aber auch ein praktikables numerisches Werkzeug entwickelt, um den Einfluss von Kurzzeit-Sturmereignissen auf die Offshore-Pfähle prognostizieren zu können. Die Untersuchungen wurden deswegen in zwei Hauptrichtungen gegliedert: ein erster Teil, mit einer theoretischen Orientierung, der der Analyse von kurzzeitigen Ereignisse anhand der Finite-Elemente-Methode gewidmet wurde, und ein zweiter empirischer Teil für die Betrachtung von Langzeitphänomene anhand Modellversuchen in kleinem Maßstab.

In diesen Untersuchungen konnte gezeigt werden, wie sich der Boden an der Pfahlgründung langfristig progressiv verfestigt (long-time hardening). Vorübergehend kann es aber auch zu einer Entfestigung während der Sturmereignisse kommen (short-time transient softening). Sowohl die abgeminderte Bettungssteifigkeit während der Entfestigung, als auch ihre kummulativen Effekte im Sinne von bleibenden Verformungen, zeigen die Relevanz und Notwendigkeit der Berücksichtigung der Wechselwirkung zwischen Porenwasserdruck und Bodenverformung in der Pfahlbemessung. In der Summe werden die Phänomene und praktischen Folgen für die Bemessung der Pfähle in dieser Dissertation hergeleitet.

PROJECT FUNDING

BAM's doctoral program and the German Federal Ministry for the Environment, Nature Conservation and Nuclear Safety (BMU) have kindly provided the funding for these investigations, which were carried out in the frame of the RAVE (research at Alpha Ventus) research program.

PERSONAL ACKNOWLEDGEMENTS

For the completion of this work I have enjoyed the assistance and support of many people, to all of whom I am greatly indebted. First of all, my deepest gratitude is due to my academic advisor, Prof. Manuel Pastor, for his enthusiasm, help and constant encouragement and for always making everything so easy. With him there was never a problem that could not be solved.

For the past years I have also had the great privilege of working at BAM's department for Buildings and Structures under the direction of Prof. Werner Rücker who watched over my work and granted me permanent support, assistance and understanding, especially during the final stages of the doctoral endeavour. I am also very grateful to Prof. Stavros Savidis from the Technical University of Berlin for his interest on my work, his advice on academic matters and for supervising this thesis. Finally, I am grateful to Prof. Karsten Geißler for assuming the chairmanship of the doctoral committee and to Prof. Yuri Petryna for his disposition and gentle substitution at the scientific defense.

Among my direct colleagues, I am particularly indebted to Pablo Mira and José Antonio Fernández Merodo for their selfless support, advice and help. Together with Manolo Pastor, they provided the sources of the GeHoMadrid Finite Element code and were a decisive help for dealing with the intricacies of computational geomechanics. Fernando Pardo and the research group within the Geotechnical Laboratory of CEDEX in Madrid have kindly hosted my "research-and-training" stays at CEDEX.

For the experimental investigations I was able to rely on the experience and wisdom of Fred Ziegler, Wilfried Wuttke and Hans-Joachim Peschke, who, along with many other individuals at BAM (a.o. Margrit Kayser, Steven Georgi, Krassimire Karabeliov, Christian Knaust and all the staff at BAM's division VII.2) made my work in Berlin much easier and particularly rewarding.

Finally, my special appreciation is due to Matthias Baeßler, the leader of my work-group, who has coordinated all of my German projects and has gradually guided me towards becoming an independent researcher. His inquisitive style, sharp insight and critical judgement have been a permanent stimulus and never precluded his unconditional assistance and friendship.

Last but not least, I want to acknowledge the marvellous support provided by my family. I cannot thank them enough for their love and care. This dissertation, which is the product of their constant encouragement and support, is dedicated to them.

Pablo Cuéllar. February 2011, Berlin.

STUDENT:

I have arrived quite recently
And come, full of humility,
To meet the giant intelect
Whom all refer to with respect

MEPHISTO:

This is a charming pleasantry.
A man as others are, you see. –
Have you already called elsewhere?

STUDENT:

I pray you, take me in your care.
I am, believe me, quite sincere,
Have some odd cash and lots of cheer;
My mother scarcely let me go,
But there is much I hope to know.

MEPHISTO:

This is just the place for you to stay.

STUDENT:

To be frank, I should like to run away.
I cannot say I like these walls,
These gloomy rooms and somber halls.
It seems so narrow, and I see
No patch of green, no single tree;
And in the auditorium
My hearing, sight, and thought grow numb.

MEPHISTO:

That is a question of mere habit.
The child, offered the mother's breast,
Will not in the beginning grab it;
But soon it clings to it with zest.
And thus at wisdom's copious breasts
You'll drink each day with greater zest.

STUDENT:

I'll hang around her neck, enraptured;
But tell me first: how is she captured?

MEPHISTO:

Before we get into my views –
What Department do you choose?

STUDENT:

I should like to be erudite,
And from the earth to heaven's height
Know every law and every action:
Nature and science is what I need.

MEPHISTO:

That is the way; you just proceed
And scrupulously shun distraction.

STUDENT:

Body and soul, I am a devotee;
Though, naturally, everybody prays
For some free time and liberty
On pleasant summer holidays.

MEPHISTO:

Use well your time, so swiftly it runs on!
Be orderly, and time is won!
My friend, I shall be pedagogic,
And say you ought to start with Logic
For thus your mind is trained and braced,
In Spanish boots it will be laced,
That on the road of thought maybe
It henceforth creep more thoughtfully,
And does not crisscross here and there,
Will-o'-the-wisping through the air.
Days will be spent to let you know
That what you once did at one blow,
Like eating and drinking so easy and free,
Can only be done with One, Two, Three.
Yet the web of thought has no such creases
And is more like a weaver's masterpieces:
One step, a thousand threads arise,
Hither and thither shoots each shuttle,
The threads flow on, unseen and subtle,
Each blow effects a thousands ties.
The philosopher comes with analysis
And proves it had to be like this:
The first was so, the second so,
And hence the third and fourth was so,
And were not the first and second here,
Then the third and fourth could never appear.
That is what all the students believe,
But they have never learned to weave.
Who would study and describe the living, starts
By driving the spirit out of the parts:
In the palm of his hand he holds all the sections,
Lacks nothing, except the spirit's connections.
Encheirisis naturae the chemists baptize it,
Mock themselves and don't realize it.

STUDENT:

I did not quite get everything.

MEPHISTO:

That will improve with studying:
You will reduce things by and by
And also learn to classify.

STUDENT:

I feel so dazed by all you said
As if a mill went around my head.

Johann Wolfgang von Goethe, 1808, *Faust. Eine Tragödie*

Write to be understood, speak to be heard, read to grow

Lawrence Clark Powell

TABLE OF CONTENTS

Page

1 **INTRODUCTION** 1

1.1 Project Framework. Pile Foundations for Offshore Wind Turbines 3
1.2 Scope of this Work. Offshore Piles under Cyclic Lateral Loading 5
1.3 Research Structure and Methodology 6
1.4 Terminology and Conventions employed here 8

2 **CYCLIC LATERALLY LOADED PILES. AN OVERVIEW** 11

2.1 Static Behaviour and Design Approaches 12
2.1.1 Ultimate lateral resistance 12
2.1.2 Deformational behaviour 15
2.2 Effects of Cyclic Loading. Considerations in Design 22
2.2.1 General cyclic behaviour. Lower bound design methods 23
2.2.2 Particular aspects of cycling 25
2.2.3 Explicit considerations in design 33
2.3 Open Issues for the Large-Diameter Offshore Piles 37
2.3.1 Short-term. Pore pressure accumulation during a storm 38
2.3.2 Long-term. Incremental collapse and embedment stiffening 42

3 **SHORT TERM BEHAVIOUR: NUMERICAL INVESTIGATIONS** 45

3.1 Model Description 46
3.1.1 Mathematical model: The u-p_W formulation 46
3.1.2 Numerical model: The Finite Element approach 54
3.1.2.1 Discretization in space 55
3.1.2.2 Discretization in time 58
3.1.2.3 Solution of the non-linear system 60
3.1.3 Constitutive model 62
3.1.3.1 Sand behaviour and the Generalized Plasticity Theory 62
3.1.3.2 The Pastor-Zienkiewicz model for sands 65
3.1.3.3 Parameter calibration 72
3.2 Element Technology 77
3.2.1 Special issues for the transient simulation of an offshore pile 78
3.2.2 The stabilized enhanced strain Simo-Rifai formulation 80
3.2.3 Pile soil interface and contact problem 83
3.3 Optimization of the Computational Cost 89
3.3.1 Solution strategies 89
3.3.2 Handling of the sparse matrices 91
3.3.3 Parallelism and super-computing 93

3.3.4 Functional software: external solver libraries 95
3.4 Validation 96
3.4.1 Stabilized coupled element 97
3.4.2 No-tension joint element 99
3.5 A Case Study 100
3.5.1 Evolution of Pore Water Pressure 102
3.5.2 Soil stresses and strains. Cyclic mobility 105
3.5.3 Pile deflection and soil settlement 106
3.6 Parameter Relevance for the Accumulation of PWP 108
3.6.1 Influence of load level 110
3.6.2 Influence of soil permeability 114
3.6.3 Influence of loading frequency 118
3.6.4 Influence of pile diameter 120
3.6.5 Comprehensive PWP accumulation trend 124
3.6.6 A note on irregular loading and order effects 126
3.6.7 A note on the computational cost 131
3.6.8 A note on the choice of constitutive model 132
3.7 Computation of a real storm 133
3.8 Recapitulation 136

4 **LONG TERM BEHAVIOUR: EXPERIMENTAL INVESTIGATIONS** 139

4.1 Motivation and Scope 140
4.1.1 Long-term stability: cyclic Axial vs. cyclic Lateral loading 141
4.1.2 Soil subsidence and grain migration 142
4.1.3 Study object: Large diameter offshore monopile 144
4.2 Model Tests 146
4.2.1 Model testing and 1-g scaling laws 146
4.2.2 Experimental setup and testing program 150
4.2.3 Results of test series. Attenuation of displacement rate 155
4.2.4 Displacement accumulation pattern 158
4.2.4.1 Accumulation laws from the literature 162
4.2.4.2 Generalisation of the Log-Linear accumulation law 163
4.3 Soil Densification 166
4.3.1 Photogrammetry: Structured-light 3D scanning 167
4.3.2 Topographic evolution of soil surface 168
4.3.3 Densification and embedment stiffening 170
4.3.3.1 Volume loss and subsidence depth 173
4.3.3.2 Final soil density 174
4.3.3.3 Concluding remarks 174
4.4 Sand Ratcheting Convection 176
4.4.1 Granular convective cells 178
4.4.2 Quasi-static convection and granular ratcheting 183
4.4.3 Incremental collapse vs. localised failure 185
4.5 Practical Implications. Bi-Phasic Model of Long Term Behaviour 186
4.5.1 Densification-dominated phase 186

4.5.2 Convection-dominated phase 188
4.5.3 On the character of the cyclic loading (One-way vs. Two-way) 189
4.5.4 Possible implications for offshore operations 191
4.6 Recapitulation 192

5 **CONSIDERATIONS FOR DESIGN** 195

5.1 Short Term Cyclic Lateral Loading 195
5.1.1 Thresholds for drained and undrained behaviour 197
5.1.2 Piles in Fully Drained Conditions 198
5.1.3 Piles in Partially Drained Conditions 198
5.1.4 Piles in Undrained Conditions 200
5.2 Long Term Cyclic Lateral Loading 201
5.2.1 Long term pile-head displacement 201
5.2.2 Soil subsidence and scouring 202
5.2.3 Embedment stiffening and long term dynamic behaviour 203

6 **CRITICISM, SUMMARY AND OUTLOOK** 205

6.1 Limitations and their relevance 205
6.2 Summary and conclusions 207
6.2.1 Short-Term Behaviour 207
6.2.2 Long-Term Behaviour 210
6.2.3 Concluding Remarks 211
6.3 Outlook 212

7 **REFERENCES** 215

A **APPENDIX** 241

A.1 Weak form of the u-p_w formulation. Gauss's Divergence Theorem 241
A.2 Convergence of the non-linear algorithm. Tolerance criteria 243
A.3 Formulation of the saturated consolidation case 245
A.4 Definitions of stress and strain invariants 248
A.5 Estimation of design loads for an offshore turbine 250
A.6 Adjustment of accumulation law to the experimental data 255

Nomenclature

Roman alphabet

Symbol	*Units* [*)]	*Description*
b_i	[L/T²]	Acceleration of body forces (generally gravity)
B	[-]	FEM matrix, product of the strain operator and the vector of shape functions
C	[L⁵/F]	Compressibility matrix
d_G	[-]	Soil dilatance, ratio of volumetric to shear plastic deformation
D; d	[L]	External pile diameter; of equivalent pile with solid cross section
D_{EP}	[F/L²]	Elastoplastic constitutive tensor
D_R	[-]	Relative density
$D_{(*)}$	[-]	Degradation factor relative to the parameter (*)
e	[-]	Void ratio
E; E_P	[F/L²]	Young's modulus of pile's material; of equivalent solid pile
E_N, G_S	[F/L²]	Normal and tangential interface stiffnesses
EI	[F·L²]	Bending (or flexural) stiffness of the pile
f	[1/T]	Cyclic load frequency
$f_{(*)}$	[-]	Multiplicative function of an accumulation model to take into account the influence of (*)
f_u, f_p	[F], [L³/T]	Load vectors of the FE nodal variables
G_C	[F/L²]	Characteristic shear modulus of subgrade
G_{DYN}	[F/L²]	Dynamic (small strain) shear modulus of the soil
G, G^U, G^P	[F], [L³/T]	Vectors of residua in the FEM
h	[L]	Lever (moment) arm
h_R	[L]	Depth of pile's rotation centre (point of zero deflection)
h_S	[L]	Depth of subsidence cone
H	[F]	Horizontal external load acting on the pile-head
H	[L⁴T/M]	Permeability matrix
H	[F/L²]	Plastic hardening modulus. Scalar magnitude
I	[L⁴]	Second moment of area of the pile's cross section
J	[-]	Jacobian matrix
k	[F/L²]	Coefficient of subgrade reaction

*) [L]: Length; [T]: Time; [F]: Force; [M]: Mass; [°]: Angular units

k	[L/T]	Hydraulic conductivity (also, "engineering permeability")
k_{ij}	[L^3T/M]	Permeability tensor
K	[F/L^3]	Modulus of subgrade reaction
K_0	[-]	Earth pressure coefficient at rest
K_A; K_P	[-]	Rankine's active and passive lateral earth pressure coefficients
K_S; K_T; K_W	[F/L^2]	Volumetric stiffness of the solid particles; of the solid skeleton; of the pore water, respectively. Scalar magnitudes
K_T	[F/L]	Tangent stiffness matrix
L; L_E; L_C	[L]	Pile's embedded length; elastic length; critical length, respectively
L, U	[-]	Lower and upper triangular factors of a decomposed matrix
M	[F·L]	Bending moment
M	[M]	Mass matrix
M_G	[-]	Slope of the CSL line
N	[-]	Number of applied load cycles
N_u, N_p	[-]	Elementary interpolation (shape) functions
n	[-]	Porosity
n; n_G	[-]	Loading direction; plastic flow direction. Tensors
n_H	[F/L^3]	Derivative of subgrade reaction coefficient with respect to depth
p'; q	[F/L^2]	Cambridge stress invariants, mean effective and deviatoric.
p_W	[F/L^2]	Pore water pressure
p, p_U	[F/L]	Soil reaction (force per unit length of pile); ultimate soil reaction
P, P_U	[F/L^2]	Lateral earth pressure; lateral earth pressure at failure
q	[L^3/L^2T]	Water flux, rate of water volume flow across a unit area
Q	[L^3]	Coupling matrix
Q^*	[F/L^2]	Volumetric stiffness of the solid-fluid mixture
R_i	[F]	Viscous drag forces between solid and fluid
S	[-]	Strain operator
t	[L]	Pile's wall thickness
t	[F/L^2]	Traction (stress at the boundary of a material domain)
t	[-]	Cyclic degradation parameter
t, Δt	[T]	Time variable, time step
T	[T]	Time period of a cycle, inverse of the frequency
u_i	[L]	Displacements of solid matrix
V	[L^3]	Volume
w_i	[L]	Displacements of pore fluid relative to the solid
x,y,z; x_i	[L]	Cartesian coordinates

y	[L]	Pile-head lateral displacement

Greek alphabet

Symbol	*Units*	*Description*
β_1, β_2, θ	[-]	Newmark's time integration parameters
δ_N	[-]	Long-term rate-degradation function
ε	[-]	Strain tensor
γ	[F/L^3]	Soil's specific weight
γ	[F/L^2]	Engineering shear strain
η	[-]	Stress ratio, quotient of deviatoric and mean stresses
φ'	[º]	Angle of internal friction
Φ	[-]	Dimensionless horizontal load applied to the pile
ν	[-]	Poisson's ratio
$\varkappa$	[-]	Scaling ratio for gravitational acceleration
λ	[-]	Geometrical scaling ratio
Π	[F/L^2]	Averaged subgrade pressure
Π_i	[-]	Buckingham's dimensionless combinations of physical quantities
ϱ	[M/L^3]	Total density of soil's solid-fluid mixture
σ	[F/L^2]	Total stress tensor
σ'	[F/L^2]	Effective stress tensor
τ	[F/L^2]	Shear stress
θ	[º]	Pile-head rotation, deflected angle from the vertical
θ	[º]	Lode's angle, stress invariant
ξ	[-]	Accumulated deviatoric plastic strain
ζ	[F/L^2]	Variable of mobilized stress level
ξ, η, ζ	[L]	Isoparametric (natural) coordinates of the finite elements

Subscripts

Symbol	*Description*
1, 2, ... , i	Relative to the 1st, 2nd, ..., ith load cycle
,S	Relative to deviatoric components
,V	Relative to volumetric components
,θ	Relative to components outside the triaxial (p'-q) plane
ACC	Relative to an accumulated magnitude during cycling

AMP	Relative to a double-amplitude (difference between local maxima and minima)
CYC	Relative to a cyclic type of loading or a cyclic magnitude
DC; SC	Relative to the double and single cone densification geometries
E; P	Relative to an elastic condition; relative to a plastic condition
EP	Relative to an elasto-plastic condition
L; U	Relative to loading and unloading stress increments, respectively
M; P	Relative to model and prototype scales, respectively
MAX	Relative to a cyclic peak (local maxima)
MIN	Relative to a cyclic trough (local minima)
p	Relative to the pressure variable
u	Relative to the displacement variables
S	Relative to the solid phase of the soil-fluid mixture
STAT	Relative to a static type of loading
W	Relative to the fluid phase of the soil-fluid mixture

Superscripts

Symbol	*Description*
e	Relative to a single element (generally, nodal variables)
p	Relative to the pressure variable
S	Relative to the solid phase
u	Relative to the displacement variables
W	Relative to the fluid (water) phase

Abbreviations

Symbol	*Description*
API	American Petroleum Institute (also, its offshore design standard)
BAM	Federal Institute for Materials Research and Testing (Bundesanstalt für Materialforschung und -prüfung)
BEF	Beam on Elastic Foundation (Winkler's approach)
BEM	Boundary Element Method
BLAS	Basic Linear Algebra Subprograms
CSL	Characteristic State Line (also, Critical State Line)

DNV	Det Norske Veritas (offshore design standard)
DOF	Degree of freedom
EAS	Enhanced Assumed Strain formulation (Simo-Rifai element)
FD, FDM	Finite Differences Method
FE, FEM	Finite Element Method
GL	Germanischer Lloyd (offshore design standard)
GNpj	Generalized Newmark method of order p for a differential equation of order j
h(i)p(j)	Hexahedric finite element with displacement DOFs defined in (i) nodes, and pressure DOF defined in (j) nodes
MPI	Message Passing Interface (standard for parallel computing)
OpenMP	Open Multi-Processing (standard for parallel computing)
OWT	Offshore Wind Turbine
PIV	Particle Image Velocimetry
P-M	Palmgren-Miner damage superposition rule
PWP	Pore water pressure (or the excess of it over the hydrostatic one)
PZ	Pastor-Zienkiewicz Mark III constitutive model for sands
SLS	Serviceability Limit State
SWM	Strain Wedge Method
ULS	Ultimate Limit State

Any deviations from these conventions are described in the text wherever applicable.

1 INTRODUCTION

The world-wide landscape of energy production is nowadays being conditioned by two issues of growing importance, namely the progressive depletion of the finite hydrocarbon reserves and the pressing need for clean and sustainable sources of energy. In this context, several countries of the European Union are adopting ambitious policies for the branch of renewable energies, where for instance Germany and the UK have set global targets of 20% of electricity production from renewable sources by 2020 [Baeßler *et al.*, 2009; Byrne & Houlsby, 2003].

In order to achieve such goals, the harvest of wind energy through the use of large wind turbines is likely to play a key role, particularly as the political and industrial interests are starting to focus on the offshore wind energy production (see e.g. [Matthies *et al.*, 1995]). The offshore environment is generally characterised by stronger and less variable wind conditions than its onshore counterpart, which permits the installation of larger turbines and a much greater power output. Typical onshore turbines have a power capacity of 0.66 MW, while the offshore turbines being installed currently in the North Sea already feature 5 MW of capacity, which approximately represents the electrical power consumed by up to 10,000 homes*).

As of November 2010, there are already 25 wind farms with over 2,000 turbines approved for construction in German waters, and around 50 additional projects in the process of approval by the German authorities (see Figure 1.1).

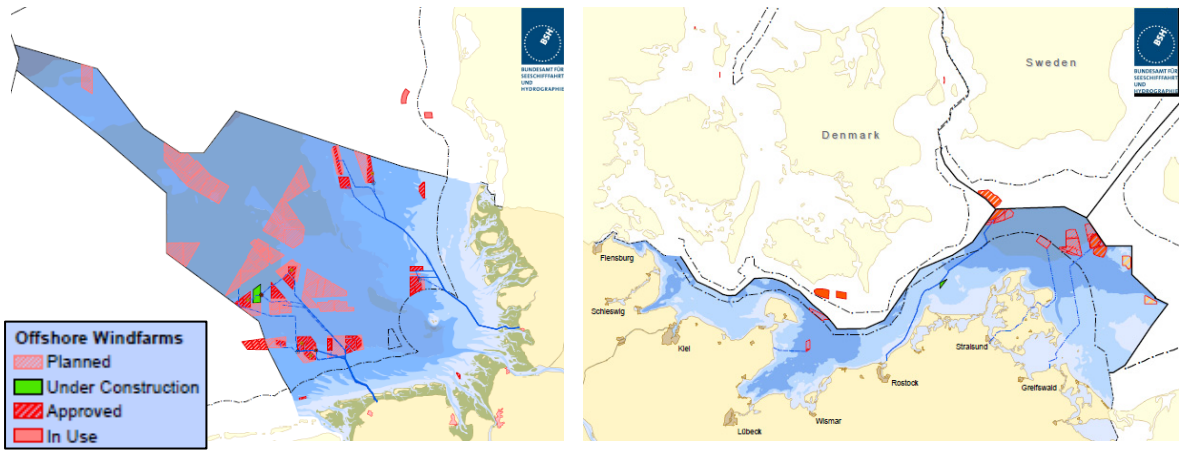

a) b)

Figure 1.1 Offshore wind farms in the German waters of the North Sea (a) and Baltic Sea (b). Source: BSH, Federal Maritime and Hydrographic Agency (http://www.bsh.de/en/)

*) Based on the assumption of a typical annual household energy consumption of 4200 kWh for a three bedroom house (Source: Strathclyde University, http://www.esru.strath.ac.uk/EandE/Web_sites/01-02/RE_info/hec.htm)

However, the challenges and questions faced by the geotechnical specialists for the foundation of such turbines in the seabed are far from closed, which is partly due to the growing interest in exploiting deeper waters and the fact that each site may require different engineering strategies depending on the soil conditions and water depth. Moreover, there are several phenomena inherent to the offshore environment, such as the effects on the foundation of a permanent exposure to cyclic loading from wind and waves, which are still not well understood and do require considerable efforts in research [Randolph *et al.*, 2005; Rücker, 2007; Richter, 2009].

Currently, the most common solutions being considered for the foundation of offshore wind turbines (OWT) are either the gravity-based shallow foundations or some kind of support structure incorporating one or more driven piles (see Figure 1.2). Other concepts such as the suction caissons or the tension-leg floating substructures have also been proposed and are under development, but their suitability is in general more restricted.

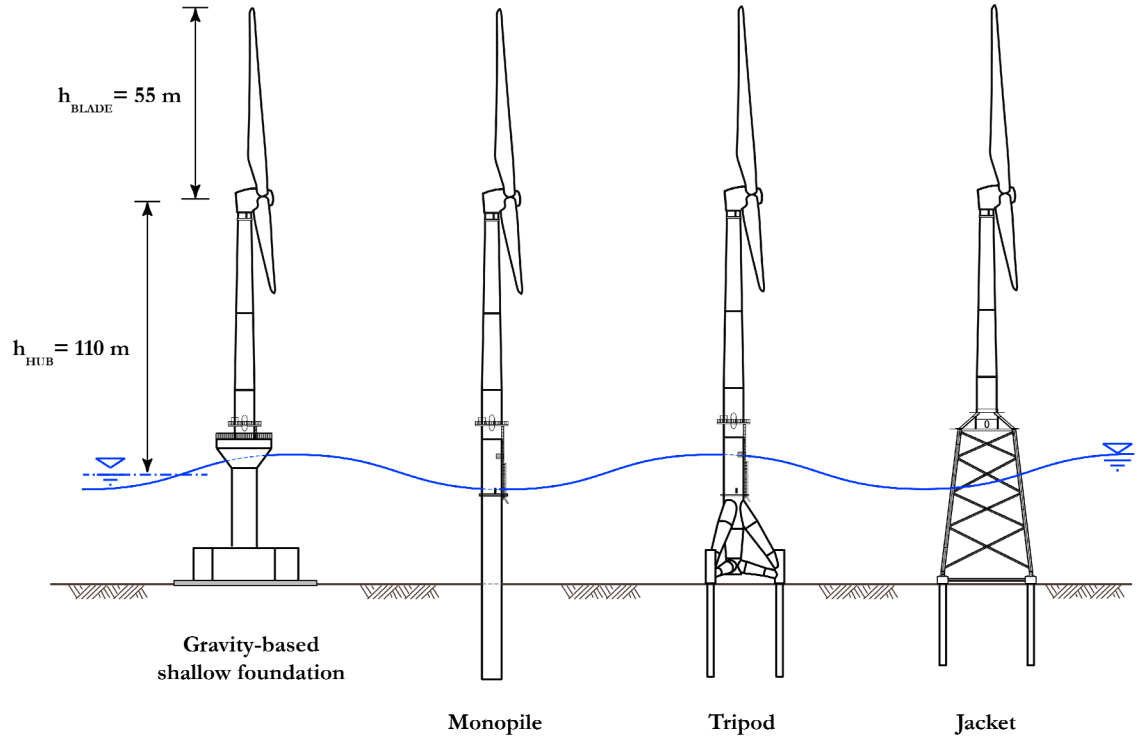

Figure 1.2 Conventional foundation configurations for offshore wind turbines, sketched with the typical dimensions of a 5-MW class turbine

The choice of a particular foundation type normally depends on the specific soil profile of the wind farm site, although for the predominantly homogeneous sandy soils of the North Sea in principle all of the conventional foundations could be suitable [Lesny, 2008]. Therefore, in practice other strategic criteria such as the availability of appropriate installation and transport equipment or the possibilities for mass production and storage can become decisive.

The foundation type prevalent so far has been the monopile, mainly due to its relative low costs of production, storage and installation. As an order of magnitude, it is estimated that from all of the constructed and projected OWTs in the Irish Sea, North Sea and Baltic Sea in the time frame from 2007 to 2020, only 1.5% will be founded in shallow foundations, while the monopile option will cover up to 57% of the total amount (up to 4,000 units). On the other hand, the multi-pile variants, mainly the tripod and jacket types, constitute the next main option, with up to 41% of the total number of installed units. In any case, it seems likely that the monopile foundations will keep on being the choice of preference in the future and also be installed up to water depths of 40 m, although at depths greater than 25 m the multi-pile options gain relevance [Kahle, 2009].

1.1 **Project Framework.** Pile Foundations for Offshore Wind Turbines

The first major offshore wind farm incorporating the tripod and jacket foundations for large turbines of the 5-MW class is the Alpha Ventus site, Germany's first offshore wind park, which started operating in April 2010 (see Figure 1.3). In this context, the German Federal Ministry for Environment and Nuclear Safety (BMU) has launched a large research initiative called RAVE (Research at Alpha Ventus) to support the construction and learn from the experience at the alpha ventus site.

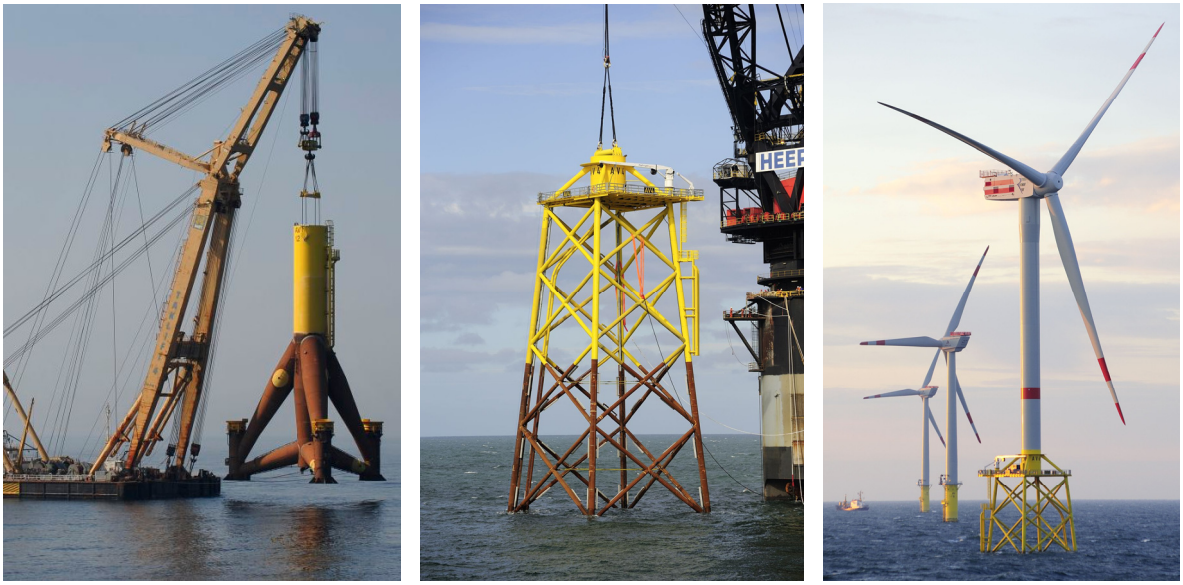

Figure 1.3 Installation of the tripod and jacket foundations for the turbines of the Alpha Ventus offshore wind farm (images courtesy of the Alpha Ventus Consortium, http://www.alpha-ventus.de)

In the frame of the RAVE initiative, two large parallel research projects on the cyclic behaviour of offshore pile foundations are being carried out at BAM, the Federal Institute for Materials Research and Testing in Berlin, where the author has performed the doctoral investigations presented here. The main focus of the first project has been placed on certain open issues of the cyclic soil-structure interaction of both monopile and multi-pile foundation types, while the objective of the second project has been the continuous monitoring of the short-term and long-term behaviour of the pile foundations at the Alpha Ventus site and the assessment of the progressive changes in the pile embedment due to the cyclic loading (see e.g. [Quell *et al.*, 2007]).

Apart from their distinct dynamic behaviour, the main difference between the monopile and the multi-pile foundations is the way they transfer the applied loads to the surrounding soil, in particular the large cyclic bending moments caused by the action of wind and waves. While the monopiles carry the cyclic moments through lateral resistance of the embedment, the multi-pile variants do so by generating pairs of "tension-compression" axial forces in opposed piles. Therefore, the cyclic loads that affect the monopiles can be described as being predominantly lateral, while for the case of the multi-pile foundations, the cyclic loading has mainly an axial character. Such distinction might be important for design, in particular for the multi-pile variants, since the cyclic axial loads have the potential to cause an abrupt failure of the pile foundation, as has been shown in the past (for instance in [Jardine & Standing, 2000; Schwarz, 2002]).

On the other hand, monopiles of around 4 to 5 metres in diameter are nowadays state of the art (for instance in the offshore wind parks of North Hoyle and Horns Rev II) and plans for future wind farms in the North Sea already contemplate the possibility of monopiles with up to 8 meters in diameter. Current design estimates show that the strict limits for the pile-head rotation, which are necessary for a trouble-free operation of the turbines, require monopile diameters of at least 5.5 m to 6.5 m depending on the water depth [Lesny, 2008; Achmus *et al.*, 2009].

However, the use of piles with such large diameters entails several engineering challenges that have not been faced before, not the least being the impossibility of driving such piles with the conventional hammers employed so far by the offshore industry. Another potentially critical issue for the monopile foundations is their relatively soft dynamic behaviour, particularly in comparison to their tripod and jacket counterparts which feature a much stiffer dynamic response. The first eigenfrequency of the turbines founded in monopiles tends to be close to the lower limit to avoid dynamic resonance of the structure during operation, which might be relevant or even decisive for design.

1.2 **Scope of this Work.** Offshore Piles under Cyclic Lateral Loading

This work aims to investigate the complex behaviour of the large-diameter offshore piles under the effects of cyclic lateral loading, not only in the short-term but also as a long-term transient phenomenon.

Its focus lies exclusively on pile foundations embedded in cohesionless siliceous sands, which is the soil type predominant in the German Bight of the North Sea, and hence the most relevant for the majority of the future German offshore wind farms.

Concerning the short-term behaviour, the main questions that will be addressed in this thesis are the following:

- Can the cyclic lateral displacements of the pile due to cyclic loading from wind and waves produce a net accumulation of pore water pressure (PWP) in the surrounding soil? If so, to what extent and what are its consequences?
- Is the stability of the foundation endangered by the possibility of soil liquefaction due to PWP accumulation? If not, can it lead to the appearance of residual displacements that would compromise the serviceability of the turbine?
- What are the main factors that influence the generation of pore pressure around the pile and what is their relevance for the overall behaviour of the pile? Does an increase of pile diameter have a negative effect on the absolute levels and accumulation rate of excess of PWP due to the elongation of the drainage paths around the pile?
- What are the effects of an irregular cyclic loading, and what is the foundation's response to a realistic storm load signal? Does the order of application of the loads play any significant role?

Regarding the long-term behaviour of the offshore piles, the main open issues driving this work have been the following:

- What is the general trend of pile displacement due to cyclic lateral loading in the very long term range, after the application of millions load cycles?
- Can a sudden failure due to cyclic loading also be expected for the laterally loaded pile in the long-term, analogous to the abrupt failure that can potentially take place in piles under cyclic axial loading?

- Does the embedment stiffness degrade with cyclic loading, as commonly assumed in design?
- What are the main physical phenomena occurring in the surrounding soil in the long-term, and what is their extent and influence on the pile behaviour? Can they modify the dynamic properties of the soil and hence alter the dynamic response of the whole turbine?

In order to examine all of these questions and derive some practical implications for design, the investigations on the short-term behaviour have been based on a comprehensive theoretical model of the pile foundation including the interaction of the soil skeleton with the pore water, while the study of the long-term behaviour has relied on the performance of physical tests in a reduced scale.

1.3 Research Structure and Methodology

This dissertation has been structured around the two main lines of investigation behind this work, namely, a first part with a theoretical orientation for the analysis of short-term transient effects of cyclic loading (Chapter 3), and a second empirical block for the study of long-term phenomena (Chapter 4). Subsequently, an effort has been made to derive practical conclusions for design (Chapter 5).

The first chapter after these introductory remarks aims to provide a conceptual background on the behaviour of laterally-loaded piles as well as a general overview on the different aspects and effects of cyclic loading. Therein, a review of the most common approaches for the consideration of cyclic lateral loads in design is presented and the main open issues for the large-diameter offshore piles are outlined.

In the first part of Chapter 3, the basic requisites for the coupled transient analysis of an offshore pile foundation are introduced and some suitable options are described. Concerning the saturated seabed soil, a general dynamic formulation for a bi-phasic solid-fluid mixture and the particular case of saturated consolidation are presented. The numerical technique for the discretisation of the equations in the frame of the Finite Element Method is then given. Afterwards, a constitutive model for the soil that reproduces the main aspects of sand behaviour and is able to generate a

residual excess of pore pressure upon cyclic loading is introduced in the frame of the Theory of Generalized Plasticity.

Then, some aspects indispensable for the simulations are addressed, namely the particular conditions to ensure the stability of the pressure field, the provision of a suitable pile-soil interface, and specially, the optimization of the computational cost, for which some practicable techniques are discussed.

Afterwards the capabilities of the numerical model are examined through the detailed analysis of a case study, and a parametric study explores the main factors that affect the generation of pore pressure around the pile.

Finally, as a closure to the chapter, the so-called order effects and the influence of load irregularities are briefly discussed on the basis of two simple examples and the loading case of a realistic storm time signal is presented and analysed.

In Chapter 4, the first sections have been devoted to introduce the experimental results from several model tests with up to five million load cycles and a give qualitative description of the different stages of pile-head displacement. Additionally, a tentative accumulation law to describe the experimental results in the very high cycle range, beyond the first million of load cycles, is proposed therein.

Then, the soil subsidence around the pile caused by the cyclic loading and the long-term densification of the soil are examined in the light of several topographic investigations of the soil surface with a photogrammetric device.

Finally, some empirical evidence of a granular convective flow within the shallow layers of soil around the pile is brought forward, and the existence of a distinct limiting surface within the soil where a direct shear of the convecting material takes place is discussed. Then, a mechanical explanation of such convective migration of the sand is proposed and to conclude the chapter a broad phenomenological model of the long-term lateral pile-soil interaction encompassing all of the observed facts is outlined.

The purpose and object of Chapter 5 is to explore the main implications for design that can be drawn out of the presented investigations, and Chapter 6 summarises the main conclusions from the preceding chapters and provides an outlook on further research.

1.4 Terminology and Conventions employed here

The conventions and terms employed in the past for the description of cyclically loaded piles have been variable, and not only chronologically but also geographically, with specific designations being used in the German literature. This section summarises the main terms and definitions that have been adopted for this work, where a certain consistency with the recent German literature on the field has been intended.

Temporal scopes. For the remainder of the thesis, "short-term" will refer to cyclic events with a number of repetitions N between 2 and 10^4, "mid-term" shall designate events that encompass up to 10^6 cycles, and "long-term" will allude any events beyond that (i.e. $N>10^6$). In the context of extreme offshore loading, "short-term" will imply a single storm (typical duration of 36 hours), while "long-term" will in general address the cumulative effects of several storms over years.

Pile slenderness and relative stiffness. It is usually convenient to distinguish between the behaviour of short rigid piles and long flexible ones, but their limits are usually rather vague. In order to classify the pile's slenderness and relative bending stiffness the following criteria have often been used in the literature (for instance in [Davisson & Prakash, 1963], [Broms, 1964] or [Han & Frost, 2000]):

$$T = \sqrt[5]{\frac{EI}{n_H}} \tag{1.1}$$

$$\frac{L}{T} \leq 2 \quad \Rightarrow \quad \textit{Short rigid pile} \tag{1.2}$$

$$\frac{L}{T} \geq 4 \quad \Rightarrow \quad \textit{Long flexible pile} \tag{1.3}$$

where L is the pile´s embedded length, T is a relative stiffness factor, n_H is the constant depth rate of the horizontal subgrade reaction for granular soils (see Section 2.1.2) and EI is the flexural stiffness of the pile.

Cyclic loads and displacements. In general, the resultant of the external lateral loads acting on the pile, H, will not be applied at the soil surface level (the so-called pile-head), but with a certain

lever arm ***h***, thereby introducing bending moments at the pile-head. The cyclic variations of ***H*** will be described here with the following parameters:

- The maximum load applied during a cycle of loading, H_{MAX}
- The minimum load applied during a cycle of loading H_{MIN}
- The average cyclic load level, H_{AVG}, half the sum of H_{MAX} and H_{MIN}
- The cyclic load amplitude, H_{AMP}, difference of H_{MAX} and H_{MIN} (some authors refer to this concept as "double amplitude")
- The cyclic period, T, and its inverse, f

The consequent pile deformations will in general be described by means of the pile-head lateral displacement y, and its cyclic variations y_{MAX}, y_{MIN} and y_{AMP}, analogous to those of H. An additional sub-index may refer to the specific load cycle to which they pertain (see Figure 1.4).

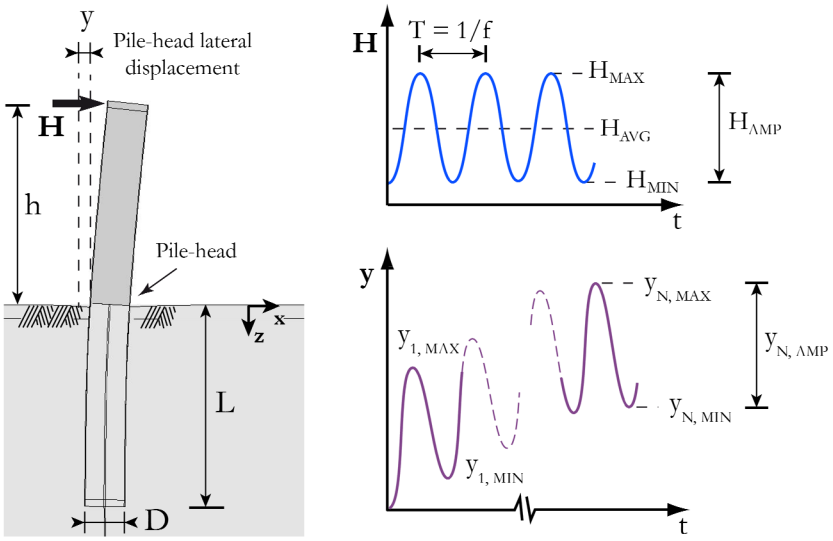

Figure 1.4 Convention for pile dimensions and load and displacement magnitudes

Normalization of variables. A parameter useful for normalization and widely employed in the German literature is the so-called pile´s elastic length L_e, for which several definitions have been proposed. For consistency with recent related works in the field (e.g. [Grabe & Dührkop, 2008; Hinz, 2009; Dührkop, 2010]), the expression used by Hettler will be adopted here, which reads [Hettler, 1981]:

$$L_e = \sqrt[4]{\frac{EI}{\gamma L}} \tag{1.4}$$

where γ is the specific weight of the soil. Based on this magnitude, Hettler also derived a dimensionless load Φ for the dimensional analysis of model tests in the following form:

$$\Phi = \frac{H}{\gamma L^2 L_e} \tag{1.5}$$

Finally, an additional parameter for the normalization of the excess of pore pressure generated by the pile displacements shall be used in Chapter 3. For that purpose it was found convenient to employ an averaged subgrade pressure Π, defined as follows:

$$\Pi = \frac{H}{D L_e} \tag{1.6}$$

Stress and strain invariants. The conventions that shall be used here regarding the invariants of the stress and strain tensors are summarised in the Appendix A.4.

2 CYCLIC LATERALLY LOADED PILES. AN OVERVIEW

The cyclic behaviour of laterally loaded piles has received considerable attention in the literature in the past decades, especially since the 60s and 70s motivated by the sharp increase in offshore operations by the oil and gas industry. The construction and maintenance of expensive extraction platforms in the harsh offshore environment, constantly exposed to the cyclic action of wind and waves, demanded reliable design procedures for the pile foundations that would take into account possible cyclic degrading effects and/or accumulation of plastic deformations.

However, the apparent excessive conservatism of the early design approaches, highlighted by the very low failure rate of actual offshore structures on pile foundations [McClelland & Cox, 1976], and the appearance of new offshore foundation concepts, such as the large-diameter monopiles, the winged piles or the so-called suction piles (see Figure 2.1), have led to a revision of the established design methods and emphasized the need for a better understanding of the cyclic behaviour of laterally loaded piles (see for instance [Swane, 1983], [Randolph *et al.*, 2005] or [Grabe, 2008]).

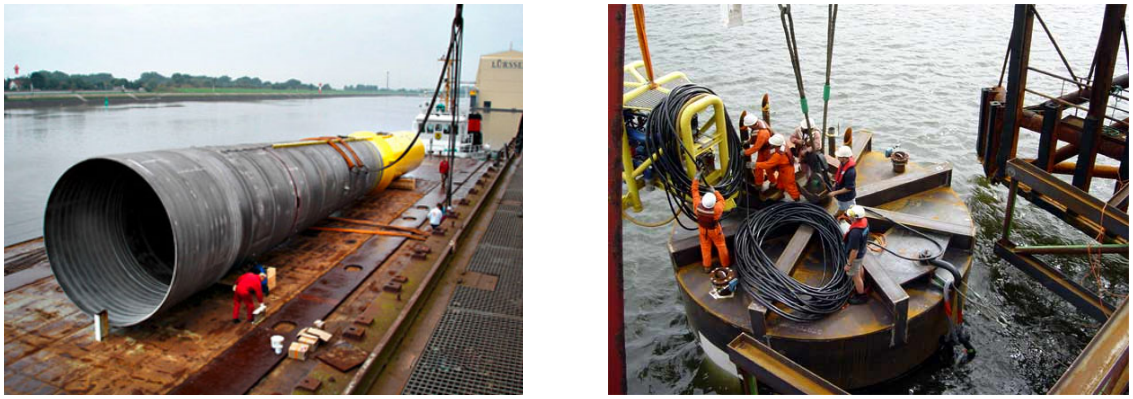

a) b)

Figure 2.1 Developing trends for offshore deep foundations. a) Large-diameter monopile (source: Ambau GmbH, www.ambau-gmbh.de). b) Large-diameter suction pile (source: SPT Offshore www.sptoffshore.com).

With no claim of completeness being raised here, this chapter aims to provide a general overview on the different effects of cyclic loading on the behaviour of laterally loaded pile foundations, as well as on their consideration within the most popular methods for design. The overview will however be restricted to free-headed single piles embedded in sand and subject to cyclic quasi-static loads (i.e. inertia effects and dynamic considerations will not be reviewed here).

Given that most design considerations for cyclic effects are based on pseudo-static approaches where the pile response is calculated from a static analysis using modified (degraded) soil properties, the first part of the chapter is devoted to a brief review of the most common methods for the static design.

2.1 Static Behaviour and Design Approaches

In general, the analysis of the pile-soil interaction can be divided into two different aspects that are normally treated separately, namely the deformational behaviour of the system for a prediction of the pile-head displacements and rotations, and the calculation of the ultimate resistance for the overall stability of the foundation.

2.1.1 Ultimate lateral resistance

Concerning the ultimate lateral resistance of piles, two possible failure mechanisms can be distinguished, mainly depending on the pile's slenderness (i.e. its length-to-diameter ratio), on the yield resistance of its section as well as on the strength of the soil. For short piles, failure typically takes place when the external capacity of the foundation is exhausted, i.e. when the lateral earth pressure reaches the ultimate lateral resistance of the soil along the total embedded length of the pile, leading to a rigid body rotation of the pile around a point located close to its toe [Broms, 1964]. In contrast, the failure mode of a long (slender) pile is characterised by the formation of a plastic hinge at a certain point of the pile when the maximum bending moment reaches the yield resistance of the pile section, i.e. when the internal capacity of the pile is exceeded. Both mechanisms are illustrated in Figure 2.2.

The location and magnitude of the maximum bending moment can be calculated by assuming a certain profile of soil reaction and imposing the mechanical balance, so that the former can be determined as the depth where the total shear force is equal to zero and the latter by simple moment equilibrium requirements [Broms, 1964; Wilson & Hilts, 1967].

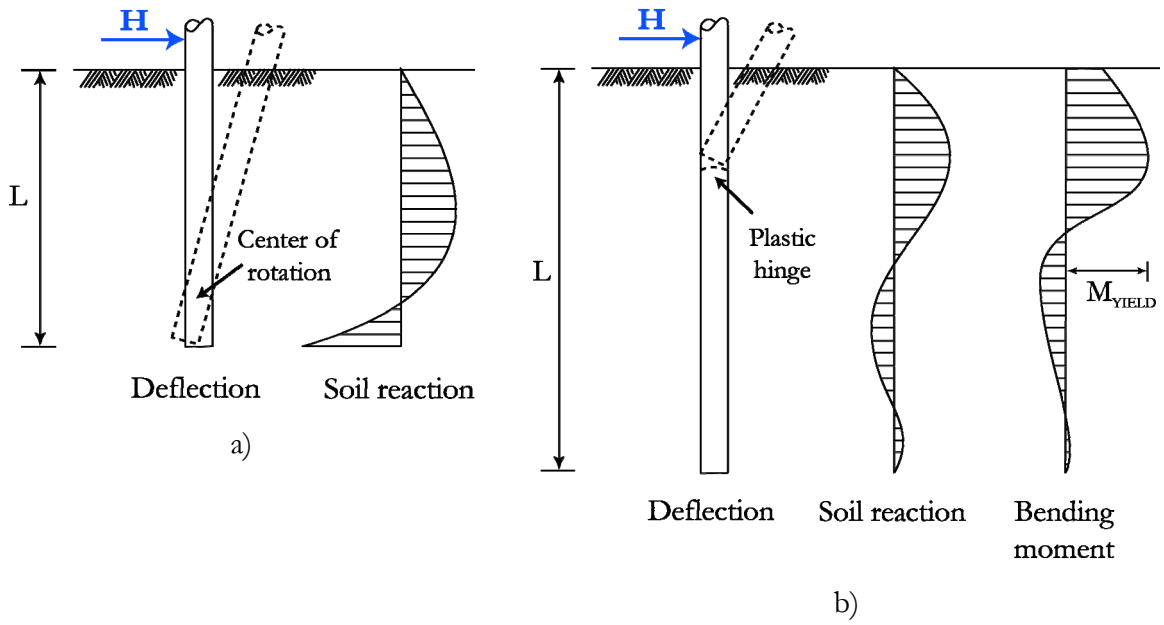

Figure 2.2 Failure modes of a free-headed laterally loaded pile, after [Broms, 1964]. a) Short pile (rigid-body rotation) b) Long-pile (formation of plastic hinge).

Therefore, the ultimate lateral pile resistance will strongly depend on the limiting pressure that the soil is assumed to apply, for which a number of expressions have been proposed in the literature (e.g. in [McClelland & Focht, 1958], [Brinch Hansen, 1961], [Broms, 1964] or [Reese *et al.*, 1974]). Most of these expressions make use of the concept of active and passive lateral earth pressure coefficients, $\boldsymbol{K_A}$ and $\boldsymbol{K_P}$ respectively, which define the ratios of horizontal to vertical stress within the soil in the active and passive sides of the foundation and were introduced by Rankine [1857] as

$$K_A = \tan^2\left(45 - \frac{\varphi'}{2}\right) \tag{2.1}$$

$$K_P = \tan^2\left(45 + \frac{\varphi'}{2}\right) \tag{2.2}$$

where $\boldsymbol{\varphi'}$ is the angle of internal friction of the soil.

This way, Broms proposed that the lateral earth pressure $\boldsymbol{P_U}$ at failure would amount to three times the passive Rankine earth pressure [Broms, 1964], and thus

$$P_U = 3 D \gamma z K_P \tag{2.3}$$

while Reese *et al.* [1974] distinguished between the soil failure mechanisms taking place near the soil surface (passive wedge type of failure, see Figure 2.3) and below a certain depth (flow failure

around the pile), which led to two alternative expressions for the ultimate soil reaction $\boldsymbol{P_U}$, being the governing expression at each depth the one leading to the lowest value of $\boldsymbol{P_U}$. Both expressions, which were originally introduced as functions of Rankine's active and passive earth coefficients, as well as on the coefficient of earth pressure at rest $\boldsymbol{K_0}$ (assumed there to be equal to 0.4), where later simplified by several authors (e.g. by [Borgard & Matlock, 1980] or [Murchison & O'Neill, 1984]), leading to the following formulation, which is the one currently included in the main standards for offshore operations (for instance in [API, 2007], [DNV, 2004], [GL WIND, 2005] or [ISO, 2007]):

$$P_{U,SHALLOW} = \left(C_1 z + C_2 D\right)\gamma z D \tag{2.4}$$

$$P_{U,DEEP} = C_3 \gamma z D^2 \tag{2.5}$$

$$P_U(z) = \min\left\{P_{U,SHALLOW}, P_{U,DEEP}\right\} \tag{2.6}$$

being C_1, C_2 and C_3 functions of the soil's internal friction angle $\boldsymbol{\varphi'}$ alone.

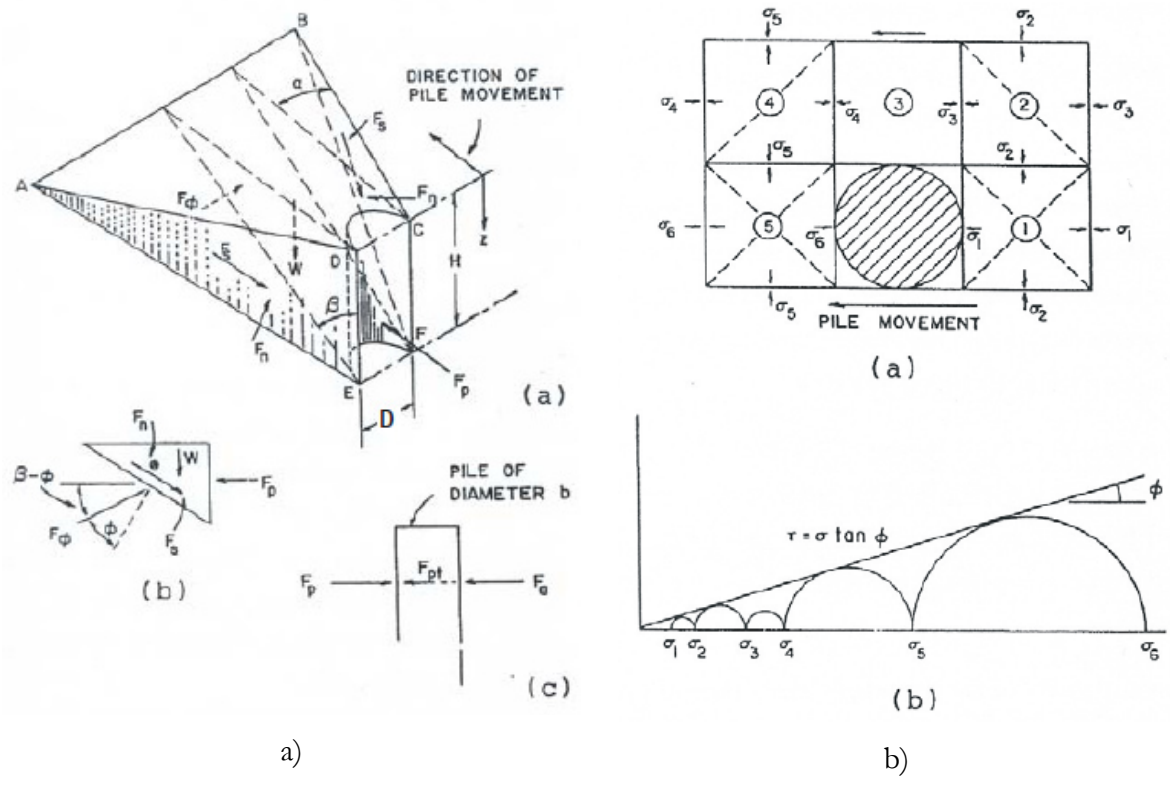

Figure 2.3 Sand failure modes for a laterally loaded pile, after [Reese *et al.*, 1974]. a) Passive wedge failure at shallow depths b) Lateral flow failure around the pile [Juirnarongrit & Ashford, 2005].

In any case, and despite the great diversity of formulations for $\boldsymbol{P_U}$, the existing methods have in general led to conservative estimates of the stability of the laterally loaded piles, although in this

respect it must be noted that the formulation included in the offshore guidelines appears to be less conservative than other approaches (e.g. those due to Broms, Barton or Brinch Hansen) [Fleming *et al.*, 2009; Randolph *et al.*, 2005].

In practice, however, failure usually does not take place at a clearly distinct load level, so that different *definitions* of failure have been proposed (such as the load causing a pile-head displacement of 0.1D, or the tangent-asymptote method in [Verdure *et al.*, 2003], or the hyperbolic method of Manoliu *et al.* [1985]). An illustrating comparison of eight different definitions of pile failure, describing the same experimental data but nonetheless showing differences in the failure value of up to 40%, can be found in [Fellenius, 1975].

Nevertheless, the lateral design of the large-diameter piles required for offshore wind turbines is normally governed by the deformational behaviour rather than by the ultimate resistance, since the strict serviceability conditions for pile-head rotation and for the structure's inclination normally imply soil reactions well below the ultimate lateral resistance [Lesny, 2008].

2.1.2 Deformational behaviour

The analysis of the static lateral response of pile foundations has evolved from the early idealizations of a beam interacting with a linear elastic embedment (e.g. in [Winkler, 1867], [Hetenyi, 1946] or [Titze, 1970]) to a great variety of techniques allowing to some extent for non-linear behaviour and mainly based on the theory of subgrade reaction, the boundary element method and the finite element method.

The early approaches, based on the pioneering work of Winkler in the late 19th century for railway foundations [Winkler, 1867], treated the embedding soil as a series of independent discrete springs down the length of the pile (see Figure 2.4) and have been collectively termed as Beam on Elastic Foundation approaches (BEF), or simply Winkler's foundation. The behaviour of such pile can be described with the following fourth-order differential equation

$$EI\frac{d^4y}{dz^4} = -P \tag{2.7}$$

where $\boldsymbol{EI}$ is the bending stiffness of the pile and $\boldsymbol{P}$ is the pressure exerted by the soil at any given point of the pile, which is usually defined in terms of the coefficient of subgrade reaction $\boldsymbol{k}$ and

pile displacement ***y***. The terminology employed in the literature is here rather inconsistent*), where the soil reaction ***p*** is also often used (in terms of force per unit length of pile), while the German literature usually makes reference to the modulus of subgrade reaction ***K*** (Bettungsmodul) in dimensions of (F/L^3). The relationship of all these terms, involving the diameter ***D*** of the pile, can be summarised as follows

$$p = k\,y = K\,D\,y = P\,D \tag{2.8}$$

Simple analytical solutions of (2.7) are possible if for instance ***k*** is assumed to be constant all over the pile or vary linearly with depth ***z***, so then the deflected shape of the pile as well as the profiles for shear force and bending moment can be analytically derived (see for instance [Hetenyi, 1946; Reese & Matlock, 1956; Matlock & Reese, 1960]).

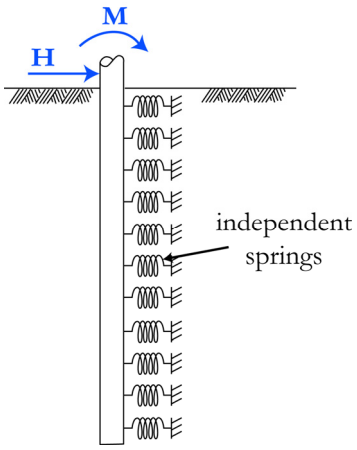

Figure 2.4 Subgrade reaction model of soil around the pile. Beam on elastic foundation idealization

Depending on the pile's bending stiffness ***EI*** and on the assumed profile of ***k***, a critical length of the pile can be defined beyond which the pile behaves as if it were infinitely long. For the particular case of a constant profile of ***k*** with depth, the critical length L_C takes the following form [Fleming *et al.*, 2009]:

$$L_C = 4\left(EI / k\right)^{1/4} \tag{2.9}$$

so that the deflection ***y*** and rotation ***θ*** of the pile-head under the action of an applied lateral load ***H*** and moment ***M*** can be derived in terms of $\boldsymbol{L_C}$, leading in the case of a long pile to

*) Some authors (e.g. [Alizadeh & Davisson, 1970]) employ the term coefficient of subgrade reaction for its rate of increase with depth, n_H , which for sands is often assumed linear (i.e. $k = n_H z$).

$$y = \sqrt{2}\,\frac{H}{k}\left(\frac{L_C}{4}\right)^{-1} + \frac{M}{k}\left(\frac{L_C}{4}\right)^{-2} \tag{2.10}$$

$$\theta = \frac{H}{k}\left(\frac{L_C}{4}\right)^{-2} + \sqrt{2}\,\frac{M}{k}\left(\frac{L_C}{4}\right)^{-3} \tag{2.11}$$

The variation of the subgrade reaction coefficient with depth and its dependence on the pile and soil properties have been discussed by many authors (e.g. in [Terzaghi, 1955], [Verdeyen & Gillet, 1968], [Titze, 1970] or [Hettler, 1986]) and has been well documented in [Wiemann, 2007]. In this respect, and for the case of cohesionless soils, Terzaghi [1955] advocated the use of a coefficient of subgrade reaction growing linearly with depth (i.e. $\boldsymbol{k} = \mathbf{n}\cdot\boldsymbol{z}$) which was found to give reasonable results by a number of authors (e.g. in [Broms, 1964], [Matlock & Reese, 1960] or [Alizadeh & Davisson, 1970]), although as noted by Wiemann [2007] at great depths it might lead to unrealistic values.

A further development of the subgrade reaction theory was the introduction of non-linear springs by defining a complete load transfer curve at each depth, the so-called p-y curves (see Figure 2.5). This approach, firstly explored by McClelland & Focht [1958] and currently included in the main offshore standards (e.g. in [API, 2007; GL WIND, 2005; DNV, 2004; ISO, 2007]), allows for a more realistic description of the evolution of soil reaction with the pile displacement and can be suitably implemented in a computer program through simple finite difference modelling of the pile's differential equation (2.7) (see for instance [Reese, 1977] or [Reese & Van Impe, 2001]).

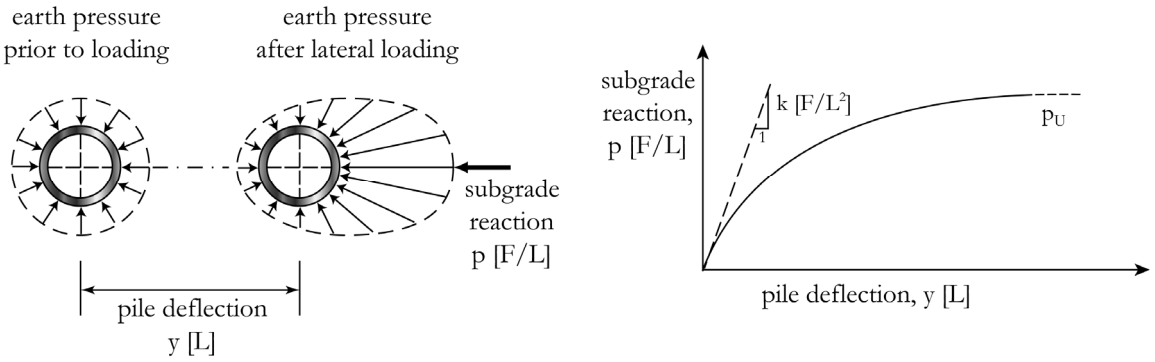

Figure 2.5 Graphical definition of $\boldsymbol{p}$ and $\boldsymbol{y}$, after [Reese *et al.*, 1974]

The shape and magnitude of the p-y curves has often been defined on the basis of full-scale field tests, simply by measuring the curvature (i.e. bending moment) of the pile with strain gauges, so that the double integration (eq. 2.12) and double derivation (eq. 2.13) of the pile's moment profile

provide the lateral displacement and soil's reaction respectively (a detailed description of the process and common pitfalls is given for instance in [Yang & Liang, 2007]).

$$y(z) = \iint \frac{M(z)}{EI} dz^2 \tag{2.12}$$

$$p(z) = \frac{d^2 M(z)}{dz^2} \tag{2.13}$$

For the case of piles embedded in sand, the piece-wise definition of the curves proposed by Reese *et al.* [1974] was later examined and simplified by Murchinson & O'Neill [1984] in what is the version ultimately adopted by the API committee. Given its relevance in the practice it may be worth to briefly summarise the procedure here:

1) Define at each depth the ultimate soil resistance p_U, as the smallest of the values given by the two types of failure (the passive wedge and the lateral flow types of failure described before) by means of equations (2.4) and (2.5) and taking into account that $p = PD$. The coefficients C_1 through C_3 can be obtained from Figure 2.6-a.

2) Compute the adjustment coefficient $A(z)$ as

$$A(z) = \left(3.0 - 0.8\frac{z}{D}\right) \geq 0.9 \tag{2.14}$$

$$A(z) = 0.9 \quad \text{whenever the load is cyclic} \tag{2.15}$$

3) Estimate the initial modulus of subgrade reaction K on the basis of the angle of internal friction φ', using the chart in Figure 2.6-b.

4) Approximate the p-y curve at each depth by the following expression

$$p(y) = A\, p_U \tanh\left(\frac{K\, z}{A\, p_U} y\right) \tag{2.16}$$

At this point it can be noted that the *modulus* of subgrade reaction K is here assumed to be independent of the pile's diameter D, which stems from Terzaghi's idea that the *coefficient* of subgrade reaction k is inversely proportional to D [Terzaghi, 1955]. This was confirmed in [Juirnarongrit & Ashford, 2005] on the basis of FE calculations and full-scale tests, but its adequacy for the large pile diameters that could be required for the monopile foundations of offshore wind turbines was questioned in [Wiemann, 2007], where the following correction for the initial modulus of subgrade reaction was proposed

$$K^*(D) = K_{REF}\left(\frac{D_{REF}}{D}\right)^{\frac{4(1-a)}{4+a}} \tag{2.17}$$

where $\boldsymbol{K_{REF}}$ would take the values provided in the literature for small diameters (for instance those given in Figure 2.6-b), $\boldsymbol{D_{REF}}$ is the diameter of the test pile used to derive $\boldsymbol{K_{REF}}$ ($\boldsymbol{D_{REF}}$ = 0.6 m for the values given in [Reese *et al.*, 1974]), and the constant $\boldsymbol{a}$ in the exponent would solely depend on the soil's relative density. However, this modification has been found to have little influence in the overall behaviour of the large-diameter piles and to still underestimate the pile-head displacement when compared to FE solutions [Lesny *et al.*, 2007]. An alternative correction to the initial stiffness of the p-y curves analogous to (2.17) has also been proposed recently in [Sørensen *et al.*, 2010] and [Augustesen *et al.*, 2010] on the basis of numerical FD calculations with a simple elastic-perfectly-plastic constitutive model for the soil.

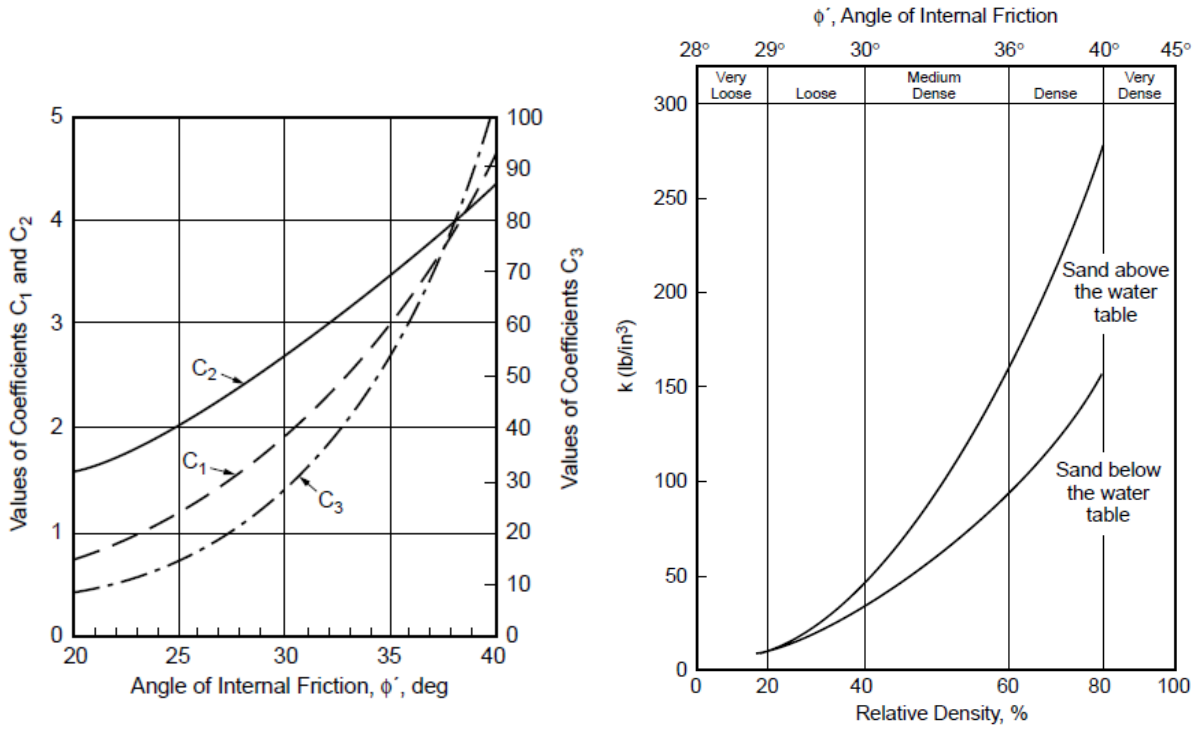

Figure 2.6 Determination of constants for the p-y curves of a pile embedded in sand [API, 2007]. a) Coefficients for the ultimate soil resistance. b) Initial modulus of subgrade reaction.

The main criticism in the literature to the p-y approach usually focuses on the following issues

- The soil is not treated as a continuum, and the shear interaction between the different discrete layers is disregarded. However, this limitation may be compensated, at least partially, by the fact that the curves are mostly derived based on the results of

full-scale tests, where the continuity of the soil is obviously satisfied [Reese & Van Impe, 2001].

- A correct assessment of the subgrade reaction coefficient ***k*** should take into account not only the soil properties, but also the influence of other factors such as the pile's flexural stiffness or the form of loading.
- It is basically unable to reproduce the interaction effects between neighbouring piles.
- The usefulness of this approach depends to a great extent on the similarity between the actual pile and soil conditions to those in which the method was developed.

Such restrictions have often been avoided by the use of finite element and boundary element solutions (e.g. in [Poulos, 1971], [Kuhlemeyer, 1979], [Poulos & Davis, 1980], [Randolph, 1981] or [Wiemann, 2007]).

The boundary element approach is based on the solution of Mindlin's equation for the deformation of an elastic half-space under the action of a concentrated force [Mindlin, 1936]. Applying the principle of superposition for the consideration of loads at every depth, and coupling it with the beam equation (2.7) at discrete points, a finite difference solution can be derived (see for instance [Douglas & Davis, 1964], [Banerjee & Davies, 1978] or [Poulos & Davis, 1980]), while it also allows a certain consideration of non-linear behaviour, for instance by the introduction of yield factors as a function of the relative flexibility and load level [Poulos, 1988].

Kuhlemeyer [1979] and Randolph [1981] presented analogous solutions based on the finite element method (FEM, discussed in detail in Section 3.1.2), which led to expressions for the pile's critical length and ground-level deformations similar to (2.9) (2.10) and (2.11), but allowing for arbitrary distributions of soil stiffness. For that purpose, Randolph [1981] introduced a characteristic shear modulus G_C, as the average shear stiffness over the active length of the pile, and presented a solution in terms of an equivalent solid pile with the same flexural stiffness and cross sectional area as the actual pile in the following form

$$y = \frac{\left(E_P / G_C\right)^{1/7}}{\rho_C G_C}\left[0.27\,H\left(\frac{L_C}{2}\right)^{-1} + 0.30M\left(\frac{L_C}{2}\right)^{-2}\right] \tag{2.18}$$

$$\theta = \frac{\left(E_P / G_C\right)^{1/7}}{\rho_C G_C}\left[0.3\,H\left(\frac{L_C}{2}\right)^{-2} + 0.80\sqrt{\rho_C}M\left(\frac{L_C}{2}\right)^{-3}\right] \tag{2.19}$$

$$L_C = d\left(E_P / G_C\right)^{2/7} \tag{2.20}$$

where for the case of a circular hollow cross section with wall thickness t, the diameter d and Young's modulus E_P of the equivalent solid pile can be obtained from

$$d = \sqrt{4Dt - 4t^2} \tag{2.21}$$

$$E_P = \frac{(EI)_P}{\pi d^4 / 64} \tag{2.22}$$

being $(EI)_P$ the flexural stiffness of the actual pile.

For a soil where the shear modulus grows linearly with depth, and with a given Poisson's ratio ν, the characteristic modulus G_C and the stiffness homogeneity parameter ρ_C were conveniently defined as

$$G_C = G^*_{L_C/2} \tag{2.23}$$

$$\rho_C = \frac{G^*_{L_C/4}}{G^*_{L_C/2}} = \frac{G^*_{L_C/4}}{G_C} \tag{2.24}$$

$$G^* = G(1 + 3\nu/4) \tag{2.25}$$

which is sketched in Figure 2.7.

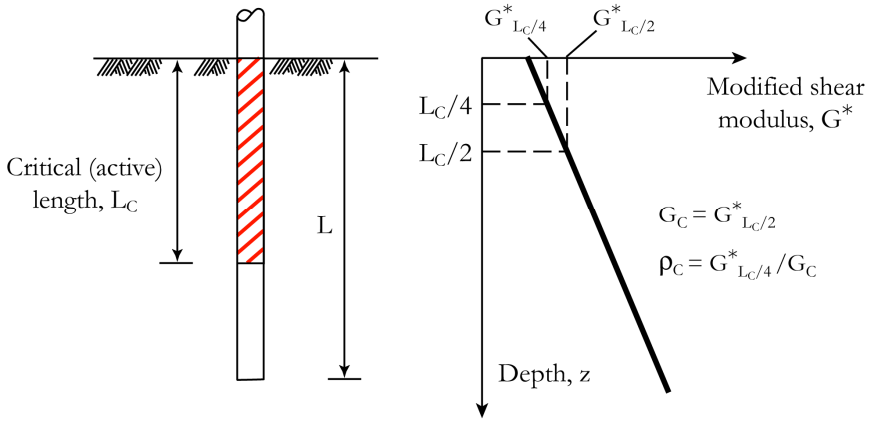

Figure 2.7 Definition of characteristic shear modulus G_C and homogeneity parameter ρ_C, after [Randolph, 1981]

Since the definitions of G_C and L_C are mutually dependent, in practice they may be estimated iteratively, starting with an initial guess for the critical length (say, ten times the pile diameter).

Similar expressions have been proposed for piles with fixed head-rotation (e.g. piles within a group) and for short broad piles (i.e. piles where $L/d < 0.05(E_P/G_C)^{1/2}$), and may be found for instance in [Fleming *et al.*, 2009] and [Poulos & Davis, 1980].

To conclude this section, it must be noted that although the design methods presented so far have often been the choice of preference for offshore pile analysis [Swane, 1983; Poulos, 1988], a number of further static design methods have been proposed, such as the Strain Wedge Method (SWM), the Characteristic Load Method (CLM) or the Equivalent Cantilever idealization, which have been profusely described and discussed in a number of publications, e.g. in [Norris, 1986; Ashour & Norris, 2000; Evans & Duncan, 1982; Duncan *et al.*, 1994; Russo & Viggiani, 2008; Fleming *et al.*, 2009].

2.2 Effects of Cyclic Loading. Considerations in Design

It is not the intent of this section to give account of the vast amount of studies on the effects of cyclic loading on the behaviour of piles and soil elements (recent works in that direction can be found for instance in [Wang, 2000], [Wichtmann, 2005], [Kuo, 2008] or [Hinz, 2009]), but rather to summarise the main effects identified in the literature and particularly their consideration in design. In this respect, two main trends may be observed in lateral pile design:

- Either a completely unspecific cyclic design approach, aiming to provide a lower bound or "envelope" to the cyclic behaviour. Such approaches are characterised by a static design with some form of degrading constant factor, which is the same for all forms, types and magnitudes of cyclic loading.
- Or models and formulas focusing on certain aspects of cyclic loading (for instance the number of applied cycles or the load level), in order to predict more accurately the evolution of the pile behaviour.

Given its over-the-board generality, the first type of methods intends to be overly conservative, but the ease of its application has often made it the choice of preference in the practice, for instance in the API or DNV standards. They are briefly discussed in the next sub-section.

2.2.1 General cyclic behaviour. Lower bound design methods

It appears that in general, the most salient effect of cyclic lateral loading on a pile foundation, in comparison to its static behaviour, is an increase of the deflection and rotation. This has traditionally been explained on the basis of two main phenomena, namely a "structural shakedown" (i.e. an accumulation of deformations without a change in the soil properties) and a material degradation of the soil leading to a decrease of its strength and stiffness, being the latter the dominant effect [Swane, 1983; Poulos, 1988].

However, both the rate of accumulation of permanent deformations and the displacement cyclic amplitude tend normally to diminish, which implies that the reloading stiffness has to be higher than the virgin stiffness, and also grow with every cycle (see for instance [Hinz, 2009]).

This apparent contradiction of material degradation versus cyclic stiffening probably stems from the inconsistency of terminology employed in the literature, where all too often the term "stiffness" is employed without specifying whether the absolute secant, the tangent or the cyclic secant stiffness is meant (see Figure 2.8), or used to designate different things such as the foundation stiffness (i.e. the macromechanical load-displacement relationship), the subgrade modulus (the ratio of earth pressure to pile displacement at each depth) and the soil elementary stiffness (normally the shear modulus).

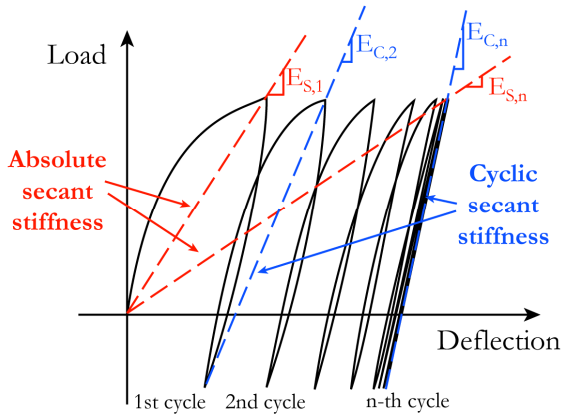

Figure 2.8 Cyclic response of a laterally loaded pile with a decreasing secant stiffness and an increasing cyclic stiffness.

In this respect, the (absolute) secant stiffness, defined as the ratio of applied load to absolute displacement, will always have a decreasing (or degrading) character, noting that such "apparent degradation" in general has no physical meaning whatsoever. On the other hand, the cyclic stiff-

ness, which may reflect better the actual state of the soil and foundation, will in general tend to increase with cycling (at least for the case of drained cohesionless soils) [LeBlanc, 2009]. Such pattern of stiffness evolution was observed and discussed for instance in [Verdure *et al.*, 2003] and [Rosquoët *et al.*, 2007] on the basis of a series of centrifuge tests.

In a set of more than 50 model tests with cyclic loading, Grabe and Dührkop [2008] also observed a permanent accumulation of pile-head displacements, while both the cyclic amplitude and accumulation rate showed a progressive attenuation, i.e. the elastic displacements decreased while the total and plastic components increased with every cycle. This supports the idea expressed before that the bedding tends to "soften" in absolute terms (relative to the initial position) but hardens effectively within every cycle, which may have important consequences for the dynamic behaviour of the foundation in the long term (a shift of the pile's eigenfrequencies and resonance phenomena may occur).

Making use of the idea that the absolute secant stiffness shows always a degrading tendency, the early design approaches for the consideration of cyclic effects proposed to conduct simply a static calculation with a reduced subgrade reaction coefficient (for instance in [Davisson & Prakash, 1963] [Broms, 1964] [Verdeyen & Gillet, 1968] or [Davisson & Salley, 1970]), which would provide in a rather unspecific way a lower bound (or "worst case") for the pile lateral behaviour after cycling.

In the same philosophy but in the frame of the p-y method, some authors (e.g. [Matlock, 1970] or Reese *et al.* [1974]) and most notoriously the API standard [API, 2007], have proposed a lower bound for the cyclic ultimate soil resistance, in the case of the API by prescribing a global correction factor of 0.9 at all depths (see Eqs. 2.14 and 2.15), thus enforcing the use of softer p-y relationships at shallow depths. Since this approach abstains from taking explicit account of important factors such as the cyclic load level or the number of load cycles, it should also be seen as a mere envelope to the cyclic behaviour of laterally loaded piles. In any case, given that the API approach is mainly based on the results from tests with less than 200 load cycles [Achmus *et al.*, 2009], such lower bound may not cover the effects of further load repetitions.

The assumption that for flexible piles only the upper part of the pile-soil system is somehow affected by the cyclic loading has been confirmed by several authors on the basis of model and centrifuge tests (e.g. [Verdure *et al.*, 2003; Rosquoët *et al.*, 2007; Dührkop, 2010]).

2.2.2 Particular aspects of cycling

The second type of design approaches usually makes explicit use of some kind of relationships observed in field, model or elementary tests*), or derived from analytical models. They are often generalised in a normalised or dimensionless form and through the explicit consideration of some aspects of cycling can be particularised (at least to some extent) to the characteristics of the expected loading.

In general, the different factors bearing influence on the cyclic behaviour of the pile can be classified in the following manner, in analogy to the distinctions made at element level in [Sagaseta *et al.*, 1991]:

- Effects of cyclic load level
- Number of load repetitions
- Type of cyclic loading (uniform or irregular, one-way vs. two-way, ...)
- Rate (or frequency) of loading
- Other factors relevant for cyclic behaviour (material, boundaries, etc...)

Cyclic load level

In general, the pile response to cyclic loading will heavily depend on the load level, particularly on both the mean and cyclic amplitude load levels, and as such has often been classified according to the following categories (see for instance [Swane, 1983; Levy *et al.*, 2009]):

1) *Purely elastic*. If the induced soil reaction at all depths is below the yielding threshold, then the pile displacements during the first cycle will remain the same for all subsequent cycles and no displacement accumulation nor hysteretic energy dissipation will occur.
2) *Shakedown*. In this case, the loading level is high enough to produce plastic deformations in the soil at some depths, but after a finite number of cycles the pile response stabilizes and from then on only elastic deformations occur.

3) *Alternating plasticity (or plastic shakedown)*. Under certain loading conditions and after a certain number of cycles, the pile may reach a stable steady state where energy dissipation still occurs, but only at a constant rate and without further accumulation of pile displacements. In this case, plastic deformations still take place during each cycle, but are equal in the two directions and therefore form a closed (hysteretic) loop.

4) *Ratcheting*. If the pile displacements fail to stabilize at any depth but continue to increase with every cycle, then the cyclic loads may lead eventually to a global failure of the system, either as a mechanical collapse or simply as a serviceability failure rendering the structure useless. The terminology employed for this type of behaviour in the literature is quite diverse (and sometimes contradicting) but in general the following subcategories can be identified:

    a. *Attenuation*. In this case, the rate of displacement accumulation will decrease continuously but never be zero, as for instance in a logarithmic evolution with the number of cycles. This was observed experimentally e.g. by Hettler [1981] although there he referred to it as "shakedown" evolution.

    b. *Incremental collapse*. For higher loads the pile displacements may increase at a constant rate with every cycle or even in an over-linear way leading to the eventual failure of the foundation.

The evolution of pile displacements for the different categories and a theoretical cyclic interaction diagram are sketched in Figure 2.9. Some authors have proposed theoretical limiting values for such domains (e.g. [Swane, 1983], [Haldar *et al.*, 1990], or [Levy *et al.*, 2009]), usually based on optimization methods and Melan's static shakedown theorem combined with linear programming techniques. Alternatively, an extrapolation method can be employed to determine whether the plastic work within the soil will be zero or constant after a finite number of loads [Swane, 1983; Levy *et al.*, 2009]. However, most of these techniques have been applied to cohesive soils, while for the case of cohesionless sands the elastic threshold seems to be extremely low (or in some cases even not existing at all) and the pile will usually fail to shakedown completely.

Abundant experimental evidence from triaxial tests with cohesionless soils, for instance those carried out by Festag [2003] and Helm *et al.* [2000], have shown no load level leading to an elastic response, so for this type of soils it is in general accepted that just an attenuating evolution but no pure shakedown may be expected [Goldscheider & Gudehus, 1976]. Similar conclusions have

*) A comprehensive summary of well documented field and model tests available in the literature for cyclic laterally loaded piles is given for instance in [Swane, 1983] [Turner *et al.*, 1987] [Kuo, 2008] and [Hinz, 2009].

been analytically drawn by Alonso-Marroquin and Herrmann [2004; 2005] based on the results from discrete element models under different levels of cyclic loading.

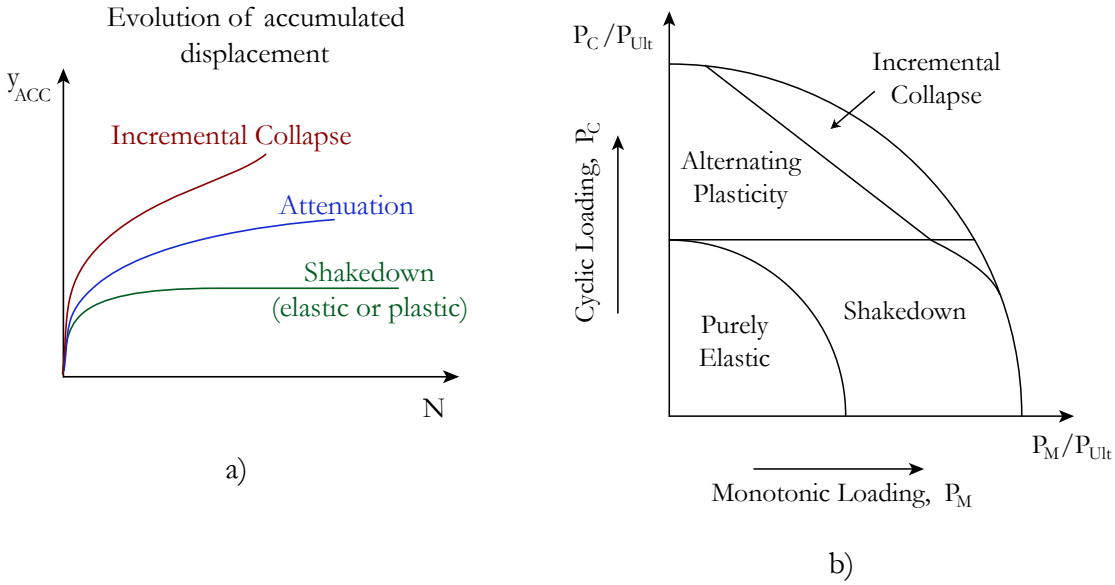

Figure 2.9 Categories of pile response to cyclic lateral loading. a) Evolution of permanent pile displacements, and b) theoretical cyclic interaction diagram after [Levy *et al.*, 2009].

Based on results from cyclic triaxial tests on North Sea sands, Marr and Christian [1981] were able to derive empirical charts of cumulative soil strains in order to estimate the permanent displacements of marine structures, and observed that the mean shear stress level had a direct effect on the magnitude of the residual strain, while the cyclic stress ratio and mean confining stress were only included as part of empirical coefficients within a power-law function of the number of applied load cycles.

Another interesting fact common to both element and foundation behaviour is that for a given level of maximum cyclic load $\boldsymbol{H_{MAX}}$, higher levels of minimum load $\boldsymbol{H_{MIN}}$ will involve lower levels of cyclic degradation, so in this respect the cyclic amplitude $\boldsymbol{\Delta H}=(\boldsymbol{H_{MAX}}-\boldsymbol{H_{MIN}})$ is the governing agent of degradation. The smaller the cyclic amplitude $\boldsymbol{\Delta H}$, the higher the cyclic stiffness, which may be explained by the lower amount of energy being lost in the hysteretic cycles [Rosquoët *et al.*, 2007].

Regarding the higher levels of maximum load, it must be noted that for stress levels above 1 MPa, grain breakage in the soil may take place and cyclic abrasion and elastic compression of the grains may play a significant role [Hettler, 1983]. However, such stress levels are not to be expected in general around the pile foundation, especially in the shallow layers of soil which are the most significant for the pile's lateral resistance.

Another potential issue for flexible piles under very high cyclic lateral loads is that the pile may work its way upwards [Dietrich, 1966; Hettler, 1981], which may be explained by the slight vertical component of the resultant of soil reaction when the pile is deflected.

Number of load cycles

Just as for cohesionless soils there does not seem to exist a purely elastic domain, the lateral cyclic load on piles embedded in sands will in general not produce a complete shakedown, but rather a progressive accumulation of plastic deformations. This accumulation may be described initially with a logarithmic function of the number of cycles (as for instance in [Hettler, 1981; Rosquoët *et al.*, 2004; Lin & Liao, 1999]), and eventually followed by an over-logarithmic accumulation stage for higher numbers of cycles (usually $N>10^4$), which may be approximated for instance with power laws or log-linear functions of the number of load repetitions [Long & Vanneste, 1994; Dührkop, 2010].

However, in this respect only small numbers of cycles have normally been investigated (in field tests only seldom over a hundred [Hinz, 2009]), especially when compared to the amount of cycles that can be expected during the service lifetime of an offshore turbine ($\sim 10^9$ cycles), so as mentioned before, the common cyclic design approaches would need to be validated with long term experimental data, and if possible with full-scale field tests or *in situ* observations.

Furthermore, the analysis of offshore piles poses the additional problem of the *definition* of the number cycles itself, given the irregular and stochastic nature inherent to the offshore loading. For this matter, a common practice in fatigue analysis is to resort to some form of Rychlik's rainflow counting procedure (some implications are discussed in the Appendix A.5), although for the case of geomaterials some alternative counting techniques have been proposed, for instance in [Liu & Carter, 2001] where the value of N is associated to the variations of a pseudo-yield surface, thereby implicitly taking into account the order effects. In the context of liquefaction analysis, the most popular cycle counting methods may have been the "range-mean count“ or the "peak-between-mean crossing count" techniques [Dowling, 1971], although as observed by Green and Terri, this aspect is only very seldom explicitly stated in the literature [Green & Terri, 2005].

Type of cyclic loading

Considering that the typical storm is an irregular pattern of waves with varying amplitudes, Marr and Christian [1981] observed that the different levels of cyclic shear stress and mean normal

stress could be transformed into a reference value of each parameter by means of a suitable definition of an equivalent number of load cycles. A similar approach for the equivalence of cyclic effects using isolines of cumulative strain (or alternatively pore pressure) has also been explored for instance by Andersen *et al.* [1978; 1992] for the analysis of offshore foundations under irregular cyclic loading. However, in order to investigate the effects of the order of loading, Marr & Christian [1981] acknowledge that a finer subdivision of a storm and a separate examination of the different parcels of waves would be required, and propose to keep the cumulative residual strains as a measure of the cyclic damage caused by earlier parcels.

Of central relevance as to whether the so-called "order effects" (Figure 2.10) must be considered or not is the question of whether the cyclic damage (however it may be defined) does accumulate linearly, as assumed in the well-known Palmgren-Miner (P-M) superposition rule developed originally for the analysis of fatigue in metals [Palmgren, 1924; Miner, 1945]. Two particularly elucidating reviews on the conditions that allow the use of the P-M rule are given in [Green & Terri, 2005] and especially in [Allotey & El Naggar, 2008], where it is shown that even scenarios with nonlinear damage evolution are allowed as long as the damage function can be showed to be independent of the stress level.

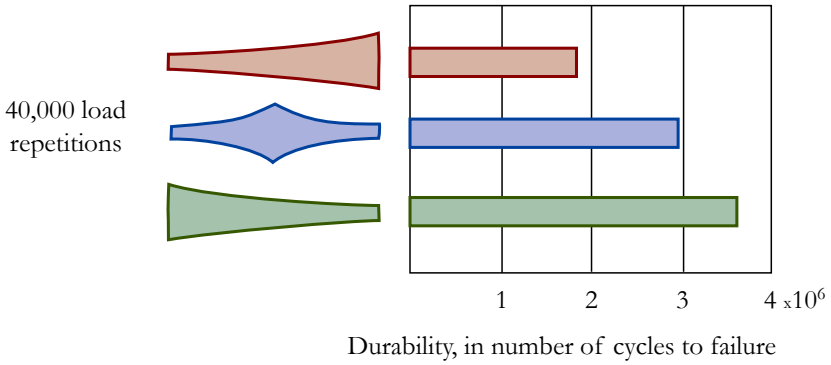

Figure 2.10 Influence of the order effect on the durability of a structural component subject to cyclic loading with irregular amplitude, after qualitative sketch shown in [Wellmann Jelic, 2007].

At the soil element level, results from many investigations seem to show that the order effects for sands may be moderate (e.g. in [Annaki & Lee, 1977; Stewart, 1986; Kaggwa *et al.*, 1991; Wichtmann, 2005]), particularly when a large enough number of cycles at each load level is applied [Hinz, 2009], so that the application of Miner's rule or the concept of equivalent cycles of uniform load may be acceptable in such cases. However, in a boundary value problem at macromechanical (multi-element) level every cycle will in general change the system and the boundary

conditions for every soil element to some extent, so the order effect may not always be negligible, especially if transient effects such as pore pressure accumulation are involved.

Tests on model piles by Hettler [1981] appear to contradict this by showing no order effect, but it must be noted that only few irregular cycles were applied there, followed by a large number of cycles with constant amplitude. In fact, the relevance of the past loading history seems to decrease with the number of cycles, so that the "soil memory" may be erased after a large enough number of cycles [Grabe & Dührkop, 2008; Dührkop, 2010]. The results from model tests with dry sand presented in [Achmus *et al.*, 2007] did show some minor discrepancies depending on the order of application of the loads, while the relevance of the order effects were there observed to increase with the relative density of the sand, which seems to agree with the higher sensitivity of the denser sands to order effects observed by Shen *et al.* [1978] in their cyclic triaxial tests.

Regarding the symmetry and character of the load reversals (either one-way or two-way), in general higher soil stresses and strains have been observed under one-way cyclic loading, while the two-way lateral loading, particularly under service conditions, tends to improve the soil characteristics [Rosquoët *et al.*, 2007]. In this respect, perfectly symmetrical stress reversals allow particles to form denser packings compared to asymmetric stress reversals [Swane, 1983], which in turn may imply that if the soil conditions are close to undrained, the increased compacting tendency of symmetrical loading leads to a faster PWP accumulation and therefore to an increased liquefaction potential.

To this matter, the observations of LeBlanc [2009] out of model tests with one-way and two-way cyclic loads featuring different degrees of symmetry showed two interesting phenomena: (i) all of the tests irrespective of their nature produced an increase of the foundation stiffness, and (ii) the two-way tests with an asymmetry character of 0.6 (i.e. maximum loads in one direction equal to 60% of the maximum loads in the opposed direction) produced the highest amounts of cumulative deformation, in fact up to four times the deformation caused by the one-way test.

Rate and frequency of cyclic loading

In the offshore practice, cyclic loading has often been presumed capable of producing both adverse and beneficial effects on the pile capacity, the latter being normally associated to rate effects assuming that the soil tends to behave stiffer at higher loading rates [Kagawa, 1986; Poulos, 1988]. However, for dry sands, frequency effects seem to be negligible in the range under consideration here (loading frequencies below 1 Hz), as shown for instance in [Wichtmann, 2005; Gotschol, 2002].

In the presence of water, the sand permeability and drainage conditions will determine the influence of the loading frequency on the cyclic behaviour, which is mainly related to the possible accumulation of PWP with every cycle, and shall be discussed in Section 2.3.1.

Poulos [1982] found reasonable to assume that whenever undrained conditions in the soil were to be expected, both the soil stiffness and the ultimate subgrade reaction could vary with the loading rate in a similar fashion as the soil's undrained strength, and therefore proposed the use of a consequent degradation factor for such parameters in design.

In a theoretical analysis by means of a modified subgrade reaction model, Kagawa [1986] decoupled the loading rate effects from the pore pressure accumulation and observed an increasing tendency of the pile-head spring constants (hence a stiffening) with the rate of loading. However, such increase was found to be relatively small and also independent of the number of load cycles.

Other factors relevant for cyclic behaviour

In a set of model tests with varying loading directions Dührkop [2010] observed that the pile-soil system would "forget" its loading history to some extent when a change in loading direction happened. This is an effect that has also been observed at element level when a change in the polarization of the load cycles is introduced, with the magnitude of the "memory loss" increasing with the angle of departure from the original loading direction [Yamada & Ishihara, 1982; Wichtmann, 2005]. Further effects of a change in loading direction may be a considerable increase of total displacements and a progressive drift of the pile away from the main loading axis (see Figure 2.11) [Dührkop & Grabe, 2008; Grabe & Rudolph, 2010].

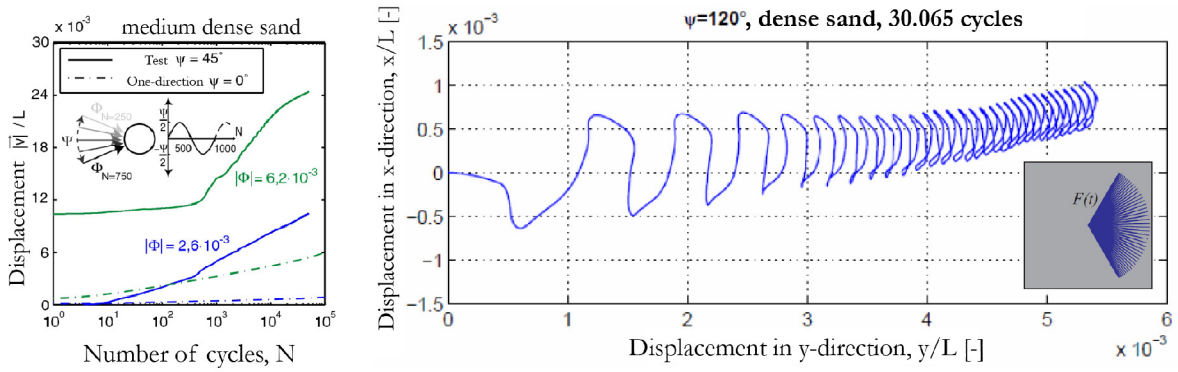

a) b)

Figure 2.11 Experimental observations of the effects of changes in the direction of cyclic lateral loading on the pile's displacement evolution: a) increased accumulation of total displacements with the number of cycles, and b) pile drift in the horizontal plane [Grabe & Rudolph, 2010].

Regarding the soil's density and dilatancy, at the elementary level there's a marked difference between monotonic and cyclic behaviour: while under monotonic loads, the sand can be dilatant or contractant depending on its initial state of stress and density (typically, loose states are contractant, and dense are dilatant), the cyclic behaviour of drained sand elements is generally contractant and striving the maximum density, which is approached asymptotically in the long term [Wang, 2000; Gudehus, 2000]. However, at the general level of the pile's boundary value problem, the sand may experience some dilatancy and softening at shallow depths, at least during the initial stages of cycling, as shown by [Verdure *et al.*, 2003] with their centrifuge tests. Whether such initial softening could be reversed and compensated later by the densification of the sand in the long term, was not investigated there and remains unclear.

Besides, for any given initial density the cyclic tendency to contract decreases with higher confining stresses, which incidentally calls for caution when extrapolating model tests to full-scale or field conditions [Swane, 1983].

Concerning the different pile installation methods, their influence on the pile's cyclic behaviour appears to be mainly related to the degree of densification that they cause in the surrounding soil. In their extensive compilation of field tests, Long & Vanneste [1994] analysed the influence of the installation method on the cyclic deformations of laterally loaded piles, and as expected, vibrated piles showed the lowest rates of deformation accumulation, while the drilled piles were found to be the most sensitive to cycling. The same conclusion can be drawn for a cyclic preloading of the piles, that densifies the soil and makes it less sensitive to further cyclic loading, although the effects of the pre-loading will tend to vanish as the cycling progresses [Grabe & Dührkop, 2008].

Other factors that can bear some influence on the cyclic behaviour of laterally loaded piles but lie out of the scope of this review are, for instance, the material of the pile itself, particularly its ability to develop cracks (thereby reducing progressively its flexural stiffness) or its permeability in the case of wooden or concrete piles (as investigated by Randolph and Carter [1979]), the soil mineralogy and granulometry (sands with higher non-uniformity coefficients tend to densify faster [Wichtmann & Triantafyllidis, 2005]), the presence of clayey contents or embedded layers, the soil's plasticity and geologic age, the possible cementation of the grains (particularly for calcareous sands) and the initial state of stress and consolidation history.

2.2.3 Explicit considerations in design

Hettler derived semi-empirical formulae for the prediction of cyclic pile-head displacements by performing a dimensional analysis of model tests, yielding an expression for static loads in terms of a power law of the load level, and a cyclic evolution dependent on the logarithm of the number of cycles [Hettler & Gudehus, 1980; Hettler, 1981; 1986]. However, their applicability is restricted to the conditions of the tests, i.e. moderate (service) loads on piles embedded in homogeneous sand. For the case of irregular load histories Hettler proposes to calculate an "upper bound" of pile displacement by simple linear summation of the displacement that each load level would cause in a "virgin pile", hence disregarding any possible order effects. This way, for a load history composed of i blocks of different uniform load levels, an upper bound for the total pile-head displacement y_{TOT} at the end of the loading could be calculated as

$$\left(y_1\right)_i = A \cdot L \cdot \left(\frac{H_i}{\gamma L^2 L_E} \right)^B \tag{2.26}$$

$$\left(y_N\right)_i = \left(y_1\right)_i \cdot \left(1 + C \cdot \ln N_i\right) \tag{2.27}$$

$$y_{TOT} = \sum_i \left(y_N\right)_i \tag{2.28}$$

where A, B are empirical constants to be obtained from model tests and C would be a simple function of the cyclic load ratio [Hettler, 1986].

Poulos [1982] presented a solution based on a modified boundary element analysis, where the effects of cyclic loading were conveniently introduced by means of several explicit degradation factors D relating the states of both soil modulus E and ultimate soil resistance p_y before and after the application of the load cycles. This way, the soil parameters for the BEM analysis would be determined from

$$D_E = \frac{E_C}{E_S} \tag{2.29}$$

$$D_P = \frac{p_{y\,C}}{p_{y\,S}} \tag{2.30}$$

$$D_E = D_P = N^{-t} \tag{2.31}$$

where the subscripts S and C denote the original (static) and degraded (cyclic) states of the parameters respectively, N is the number of applied cycles and t is a degradation parameter dependent on the cyclic strains. For cases where undrained conditions prevail, a further degradation factor D_R to account for the effects of the loading rate was proposed in the following form:

$$D_R = 1 - F_P \log \frac{\lambda_R}{\lambda} \tag{2.32}$$

in which F_P is a rate coefficient and λ_R and λ are the loading rates for a reference and the actual cases respectively. However, and although such approach may in general be suitable for a wide range of soils, the data and solution charts given in [Poulos, 1982] only apply to cohesive soils.

Employing a discrete subgrade reaction approach, Swane [1983] proposed to consider the load repetitions on a cycle-by-cycle basis (i.e. calculating the full transient event), where a p-y model with springs and friction slider-blocks would include some material degradation models as well as reflect explicitly the effects of "structural shakedown" (adhesion, gap opening and sand-flow into the gap).

In contrast, Long and Vanneste [1994] proposed a power-law of the number of cycles for the reduction of initial subgrade reaction coefficient k_1, see equations (2.33) and (2.34), with a degradation coefficient in the exponent dependent on the load type (F_L), pile installation method (F_I) and initial density of the soil (F_D). However, in view of the database used to calibrate the method, its validity may be restricted to long flexible piles in sand and loaded only with up to 50 cycles.

$$k_N = k_1 N^{-t} \tag{2.33}$$

$$t = 0.17 \cdot F_L \cdot F_I \cdot F_D \tag{2.34}$$

Including a degrading factor t analogous to that of Long and Vanneste (dependencies on load type, installation method and soil density), Lin and Liao [1999] have proposed a logarithmic evolution of soil deformation instead, and define the soil strain at every depth as a constant proportion of the pile's lateral displacement. The consideration of load cycles with different amplitude is there made through the strain superposition method advocated by Stewart [1986]. There, the strains are accumulated in a curve-hopping procedure (Figure 2.12) by using different characteristic accumulation curves for the different load levels and preserving the strains caused by previous events as a measure of damage. This way, Lin and Liao were employing implicitly a linear superposition method for the pile displacements, with which they were able to reproduce the field-test

results from the database of Long and Vanneste. Its validity would in principle also be restricted to just a few tens of cycles.

Assuming a power-law accumulation of strains in the soil, Hinz and coworkers [Hinz *et al.*, 2007; Hinz, 2009] propose a semi-empirical approach combining the results of cyclic triaxial tests with either static FEM or SWM models. This way, for the FEM approach, the elastic stiffness modulus of the soil down to a certain critical depth would be degraded by considering the total amount of deformation caused by the cyclic loading being applied. Such deformation would be obtained from triaxial tests and generalised to any irregular load combination by means of a consequent form of Miner's rule of linear damage accumulation, in this context defined through the plastic strain. Alternatively, a modified SWM model is proposed there, where the plastic deformation derived from the triaxial tests could be simply added to the reference strain needed for the SWM calculation.

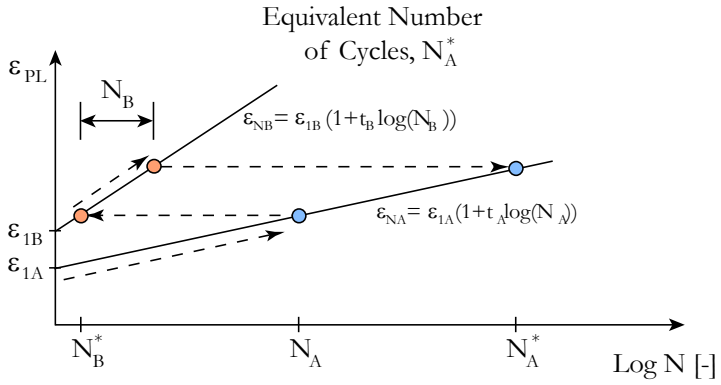

Figure 2.12 Procedure for the superposition of strains caused by load cycles with different amplitude, after [Stewart, 1986] and [Lin & Liao, 1999]

In the same line of thought, Kuo [2008] and Achmus *et al.* [2009] propose to carry out static FEM calculations with a degraded elastic modulus, also following a power-law function of the number of cycles. However, a key difference is that now the exponent for the material degradation at every point depends on a stress ratio that takes into account the different stress states at rest and under monotonic load (thus considering to some extent the effect of rotation of principal stresses). Furthermore, for the application of irregular cyclic loads they resort to the same superposition technique used by Lin and Liao [1999]. On the basis of such calculations, Achmus *et al.* [2009] presented dimensionless charts for a preliminary design of large-diameter monopiles that would provide the pile-head displacement as a function of the number of cycles.

A perhaps more sophisticated approach is advocated by Wichtmann *et al.* [2008], who performed a FE analysis of an offshore monopile under the effects of one million load cycles using a hypop-

lastic constitutive model upgraded with the so-called explicit high-cycle accumulation model (HCA) introduced by Niemunis and Wichtmann [Niemunis *et al.*, 2005; Wichtmann, 2005]. There, the first two load cycles are calculated "implicitly" (i.e. fully captured as a transient event) and serve as a basis for the extrapolation of the following cycles as a package using the HCA model (see Figure 2.13).

The HCA model, also referred to as the Bochum accumulation model in [Wichtmann, 2005], has been derived on the basis of multiple element tests with up to 10^6 cycles and provides a detailed description of the strain accumulation rate within a soil element in dependence of the load history (number and magnitude of previous cycles), load polarization, cyclic strain amplitude, void ratio, confining pressure and stress ratio in the following multiplicative form

$$\dot{\varepsilon}_{ACC} = \dot{f}_N \cdot f_\Pi \cdot f_{AMP} \cdot f_e \cdot f_p \cdot f_Y \tag{2.35}$$

where the different factors consider respectively the dependencies mentioned before and can be calibrated by means of cyclic triaxial tests. In particular the integral of the historiotropic rate function, f_N, takes the following log-linear*) form

$$f_N = C_1\left[\ln\left(1 + C_2 N\right) + C_3 N\right] \tag{2.36}$$

where C_1, C_2 and C_3 would be constants.

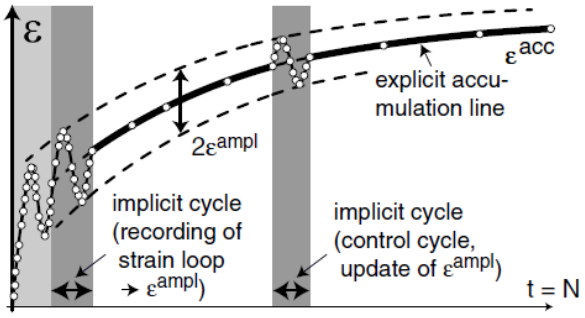

Figure 2.13 Explicit model for high-cycle accumulation of deformations [Wichtmann, 2005]

Having observed that an analogous function (i.e. log-linear) describes well the evolution of pile-head displacements in a set of model tests with up to 10^5 cycles, Dührkop [2010] proposes to use it for design either directly as a prognosis of pile-head displacements in the following form

$$y_N = y_1 f_N = y_1\left(1 + B_1\left[\ln\left(1 + B_2 N\right) + B_3 N\right]\right) \tag{2.37}$$

*) Here and throughout this thesis, log-linear only implies an algebraic function with logarithmic and linear addends, not to be confused with the log-linear models for multivariate statistics

where B_1 would depend on the initial density and B_2 and B_3 are constants to be calibrated by means of model tests, or within a subgrade reaction approach being part of a reduction coefficient for the subgrade modulus at shallow depths (e.g. down to z/L = 0.5, as illustrated in Figure 2.14-a)

$$k_N = \begin{cases} k_1 f_N^{-1} & \textit{for rigid piles in sand} \\ k_1 f_N^{-5/3} & \textit{for flexible piles in sand} \end{cases} \tag{2.38}$$

where k_1 and k_N are the subgrade reaction coefficients for the first and n-th cycles respectively.

Alternatively, and whenever results from model tests were not available, Dührkop [2010] proposes to adopt for service cyclic loads a more restrictive reduction profile for the long-term ultimate soil resistance in the frame of the p-y curves (Figure 2.14-b), judging that the API proposal of A=0.9 is only valid for the first hundred cycles.

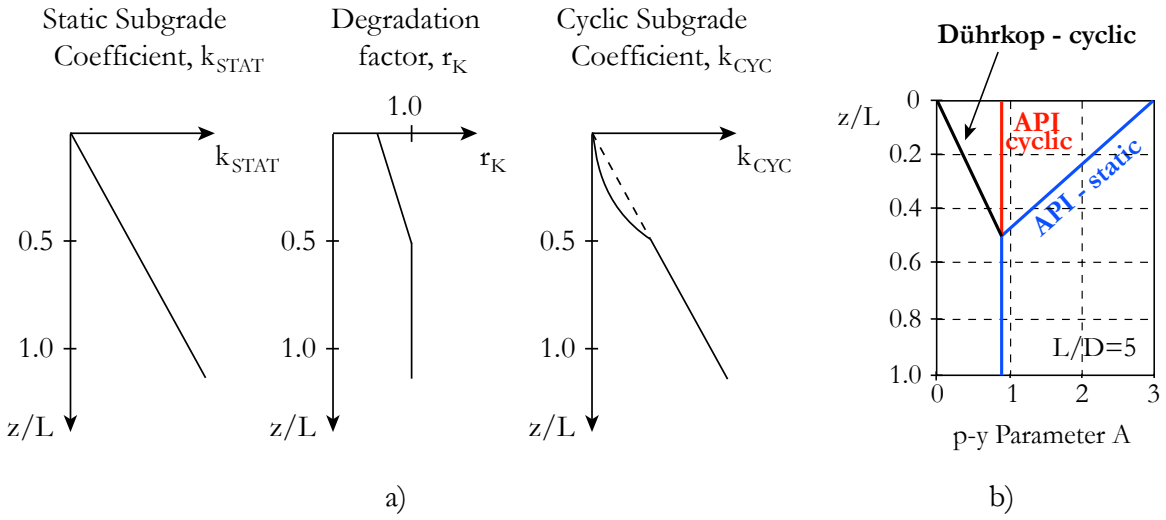

Figure 2.14 Consideration of cyclic loading in pile design, after [Dührkop, 2010]. a) Depth-dependent reduction of coefficient of subgrade reaction. b) Profile of correction factor A for the adjustment of ultimate soil resistance in the p-y method.

2.3 Open Issues for the Large-Diameter Offshore Piles

In any case, independently of the calculation procedure for cyclic loads, for which there's still no unanimously accepted or dominant approach, there's currently also a lack of consensus for the design criteria, i.e. for the conditions that the calculated pile should fulfill. In this respect, the

German GL offshore guideline [2005] prescribes limits for the maximum tolerable deformations (displacement and rotation) at pile-head level during the whole service lifetime of the offshore turbine, as well as its dynamic stability (no significant shift of its eigenfrequencies) and particularly the zero toe-kick or the attainment of a vertical tangent at some point of the deflected shape of the pile under maximum load. The latter conditions have been criticised by Achmus *et al.* [2009], who consider such criteria as inappropriate and overly conservative for a large-diameter offshore pile, and propose instead a simple design criterion for the accumulated pile-head displacement after 100 cycles, with a tolerable limit of 0.3% of the pile's embedded length.

But further than the design criteria for the offshore piles, there seems to be two particular aspects of their behaviour that are still not well understood and for which there exists no design procedure in the offshore guidelines and standards, namely:

- The generation and transient evolution of excess pore pressure around the pile during a storm (a short term cyclic event), and their consequences regarding the pile capacity and stability.
- The very long term behaviour of the pile after millions of load cycles have taken place upon the structure, in particular their cumulative effect on the pile's embedment and progressive inclination.

Concerning the development of excess pore pressure, in general there are only few studies that investigate on a cycle-by-cycle basis the behaviour of offshore structures, especially for the case of large-diameter piles, probably due to technical difficulties of performing direct on-site measurements and the high computational cost of a detailed numerical modeling. In this respect, most of the studies perform a simplified analysis of the foundation including semi-empirical relations of pore pressure generation and dissipation obtained from undrained elementary tests, and usually discretise the irregular storm loading as consecutive packages of load cycles with constant amplitude (e.g. in [Rahman *et al.*, 1977; Kagawa, 1986; Taiebat & Carter, 2000; Taiebat, 1999]).

2.3.1 Short-term. Pore pressure accumulation during a storm

From a phenomenological point of view, the problem of the possible accumulation of PWP around offshore piles during cyclic lateral loading has been well summarised by Swane [1983]:

"Conditions which inhibit the dissipation of PWP around a laterally loaded pile during cyclic loading can have a significant influence on the soil and hence on the pile response. Some of these conditions are: (i) large pile diameters (ii) piles closely spaced in a group (iii) high frequency of loading and (iv) low permeability. (...) Increasing pile diameter increases the effective length of the dissipation path, thereby reducing the degree of pore pressure dissipation during a given time interval. (...) The more frequent the load, the greater is the rate of degradation in the soil due to accumulation of PWP. (...) The permeability of the soil is of fundamental importance to the potential of soil to accumulate and redistribute PWPs during cyclic loading. The grading of the sand has a direct influence on it."

Swane also observed that in this respect a preloading of the pile could have a beneficial effect, since the preshearing of sand causing compaction prior to the undrained cyclic loading would make the soil less sensitive to possible accumulations of PWP [Swane, 1983]. However, he did not investigate such implications further, and only made reference to the analytical study of the influence of PWP on soil-pile interaction under seismic motion by Martin *et al.* [1980].

Riechwien *et al.* [2005] also acknowledge the fact that for short drainage paths, high permeabilities and low loading frequencies, the transient increases of PWP may be able to dissipate within each cycle, leading to no accumulation, but they provide no further orientation nor quantitative values. They performed some tentative transient coupled simulations of a laterally loaded offshore pile, but due to the limitations of the constitutive model (a simple elastic-perfectly-plastic model), they were not able to reproduce any accumulation of pore pressure.

At soil element level, comprehensive descriptions of the sand liquefaction phenomena and cyclic behaviour have been provided elsewhere (for instance in [Ishihara *et al.*, 1975], [Castro & Poulos, 1977], or more recently in [Triantafyllidis, 2003] and [Seed *et al.*, 2003]) and shall not be discussed here. In any case, the main relevant aspects will be introduced later, in Section 3.1.3.1.

However, and despite the vast amount of information on liquefaction behaviour of sands obtained in the past from elementary tests, no laboratory data completely covers the complex stress conditions that exist in the field and hence the need for full three-dimensional "boundary value investigations". As Taiebat [1999] clearly put it, the distribution of total stresses caused by the external loads may be changing continuously due to transient reductions of soil stiffness when the pore pressures increases and the stress redistributes inside the "multi-element" soil body. Therefore, and since the effective stress paths will not necessarily move horizontally towards the failure envelope, the stress states for the onset of failure cannot be determined from the initial conditions at the beginning of a phase of cyclic loading.

One of the few quantitative three-dimensional analyses that has been published on this topic is precisely that of Taiebat [1999], although there the pile (of small dimensions) was attached to a footing, thus constraining its movements and preventing a free drainage at the pile head, and no parametric study was carried out. Nevertheless, the method of analysis is of interest, particularly due to its reduced computational cost. There, the employed strategy, based on the method proposed by Rahman *et al.* [1977] for the analysis of the Ekofisk tank in the North Sea, consisted in dividing the transient loading into parcels of load cycles with constant amplitude and analyse the effects of each parcel in a multi-step procedure, thereby considering the phenomena of pore pressure generation and dissipation separately (see Figure 2.15).

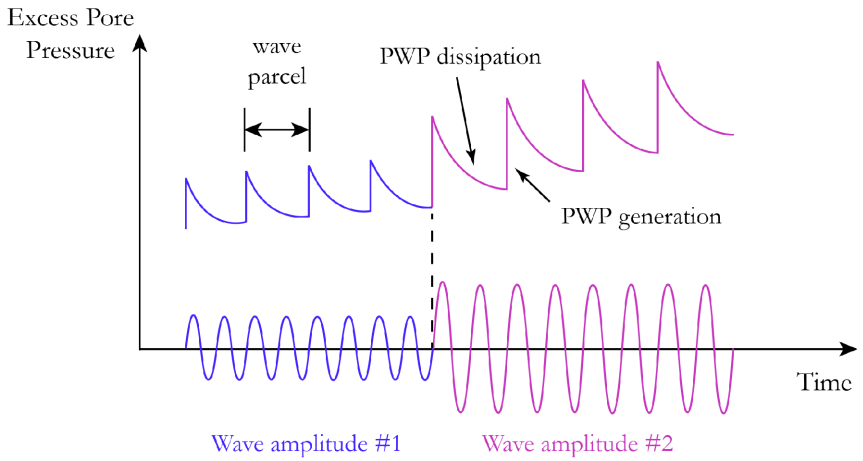

Figure 2.15 Simplified strategy for the analysis of pore pressure evolution: Division of loading in parcels of constant amplitude, and separate consideration of pore pressure generation and dissipation phenomena, after [Taiebat, 1999].

In order to be able to use a simple constitutive model for the soil (simple elastic-perfectly-plastic with Mohr-Coulomb yield criterion), the increase in pore pressure would be calculated using Seed's empirical formula [Seed *et al.*, 1975] on the basis of an initial static FE calculation, and a subsequent drainage stage in the form of a transient consolidation analysis would be then performed for the rest of the parcel's duration. The main shortcoming of such procedure is its limited predictive capability arising from the assumption of an elastic-perfectly-plastic soil, as already pointed out by the author [Taiebat, 1999].

From the empirical side, only results from model tests in reduced scale have generally been published, such as those presented by Stahlmann *et al.* [2007] where the soil around a pile under dynamic lateral loading appears to show a momentary liquefaction in the shallow depths of the foundation. The pore pressure exceeded the initial effective stress at those depths, which was defined by the authors as a liquefaction event.

Kluge [2007] performed further tests and compared them with numerical FD calculations, where, again, due to the limitations of the constitutive model the increases of PWP had to be introduced artificially through an empirical PWP generation formula dependent on a measure of the shear and volumetric strains of the soil. An important drawback of the investigation was its restriction to two-dimensional conditions, which certainly prevents the flow and drainage of pore pressure around the pile and hence is only representative of the plane strain case of an infinite wall. But further than that, and independently of the spatial dimensions of the analysis, the suitability and predictive capabilities of such procedure are not clear, since the drainage conditions of the soil needed to be changed arbitrarily during a simulation. A satisfactory comparison with the empirical results was only possible if the initial stages of the test were assumed fully undrained, and then switched to fully drained at certain arbitrary moment of the cyclic loading. Although such procedure may be conveniently tuned to match *a posteriori* the results from a given loading event by switching on and off the drainage conditions of the soil, its arbitrariness seems to preclude in general any class-A prediction of pore pressure evolution.

Grabe and coworkers also have performed model tests on a small scale and particularly some three-dimensional numerical investigations using a coupled FE model with a hypoplastic constitutive model for the soil [Grabe *et al.*, 2004; Grabe, 2008], which spared them the need to resort to an additional PWP generation formula. Upon examination of 5 different cyclic loading scenarios, there they confirmed that not only the load characteristics (amplitude, frequency and type) but also the soil properties (permeability, density and drainage conditions) bear an influence on the generation of excess pore pressure, which would tend to dissipate not only towards the soil surface but also flowing around the pile. However, no detailed parametric study was made nor specific design recommendations were given there.

Further model tests but in a bigger scale are being performed by Savidis and coworkers [2004; 2007], also complemented with fully coupled FE numerical investigations featuring a hypoplastic constitutive model. Out of those investigations, all of them in the frame of the doctoral research by Tasan and parallel to the work presented here, the to-date most comprehensive parametrical study of the main factors that influence the accumulation of PWP around the pile has been recently published [Tasan *et al.*, 2010b; Tasan, 2011]. Due to the analogies with the work presented here and the special interest of a comparison (and eventual validation) of the two different models (different FE implementations and different constitutive models), its results and conclusions will be introduced and commented later, in Chapter 3.

Finally, it must also be pointed out that apart from the excess pore pressure generated by the wave-induced displacements of the foundation, the change in water-level itself as the wave prop-

agates over the seafloor may also result in a net pore pressure accumulation within the soil (see for instance [Martin *et al.*, 1980], [Siddharthan, 1987], [Tsotsos *et al.*, 1989] or [Pastor *et al.*, 2006]).

2.3.2 Long-term. Incremental collapse and embedment stiffening

Regarding the long-term behaviour of the offshore piles, two particular issues seem to demand a significant deal on further research. Firstly, and from a phenomenological point of view, it appears that the existing empirical knowledge about lateral pile behaviour is restricted to the very short term, since most studies (either model tests or in field-scale) included at the most a few hundred or thousand load cycles, and in no case go beyond the first million of load cycles. Therefore, not only the theoretical calculation models for the high-cycle range need empirical validation, but also the experimental formulae for the description of the cyclic displacement evolution and pile incremental collapse have to be verified for their extrapolation to the very long-term range.

The second issue is related to the physical properties of the pile's embedment itself, especially regarding its dynamic behaviour in the long-term. Due to the proximity of the operational frequencies of the wind turbines to those of the fundamental modes of vibration of the offshore towers (see Figure 2.16), the German GL offshore certification guideline prescribes that for the 10^9 load cycles expected in a turbine's lifetime there can be no significant shift of eigenfrequencies [GL WIND, 2005].

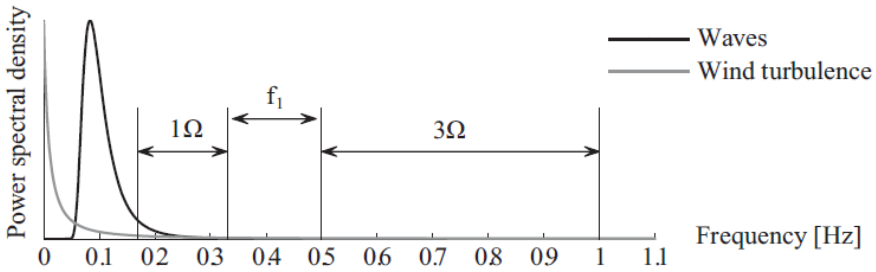

Figure 2.16 Available range for the first eigenfrequency f_1 of an offshore wind turbine, between the operational excitation frequencies 1Ω and 3Ω (full revolution and blade-passing, respectively), from [LeBlanc, 2009].

On the other hand, Grabe and coworkers have illustrated the importance of the correct assessment of the embedment stiffness and how the eigenfrequencies could be shifted with an increase of the subgrade reaction modulus [Grabe & Mahutka, 2005; Grabe, 2008]. However, to the

knowledge of the author currently there exists no particular method for the assessment of the long-term effective changes in the embedment stiffness and soil density around the pile.

It must be stressed that in this respect, most pile design procedures for cyclic loads only estimate a fictitious degraded "secant" stiffness to provide the absolute pile displacement after the cyclic event, and hence do not reflect the actual state of the soil nor its real dynamic properties.

The only tentative approach to this matter that the author is aware of is that of LeBlanc [2009] where, on the basis of results from model tests with up to 60,000 load cycles, an empirical logarithmic formula for the evolution of the cyclic stiffness of the whole foundation is derived (the stiffness being defined there as the cyclic secant ratio of applied moment and pile-head rotation between maximum and minimum loaded states). However, the relationship of the so-defined stiffness to the actual soil and embedment dynamic stiffnesses at every depth was not clarified there, while the suitability of the approximation for the high-cycle range beyond 10^4 cycles still has to be validated.

3 SHORT TERM BEHAVIOUR: NUMERICAL INVESTIGATIONS

The numerical simulation offers an insight into the fundamental behaviour of the system that is normally not available by means of experimental investigations. For instance, the stress-path followed by the soil elements surrounding the pile and the pore pressure evolution along the pile's embedded depth, in particular the possibility of reaching the liquefaction condition at some point, are some of the key aspects that can be studied with a numerical model but are hardly traceable in model tests or in-situ conditions.

However, the quality of the calculations and their ability to reproduce the real behaviour of the foundation will depend on several factors. In analogy to a chain, which is only as strong as the weakest of its links, the accuracy of the numerical model will never be higher than that of the worst of its components. For instance, it might be of little use to implement a very complex and accurate constitutive model for the soil if one does not employ at the same time the appropriate techniques to avoid numerical instabilities, or to use an extremely detailed geometrical representation of the problem (e.g. a really fine mesh with millions of elements) if one does not provide the appropriate mathematical model to describe the physics of the system. In this respect, there's a certain need to find a compromise between model complexity (or accuracy) and computational cost, and this balance should be kept for all of the components of the analytical model.

In the first sections of this chapter, the different components of a rational model for the 3D coupled analysis of the offshore pile foundation will be presented. Then, several important issues that can be potentially critical for the coupled simulations, such as the element technology to avoid spurious pore-pressure oscillations or the adoption of efficient solution strategies, will be discussed and an insight into the time consumption and the possible ways to alleviate it will be given. In connection to this, the implications of a partial parallelization of the FE code for a high-performance computing will be explored and an outlook on current trends and functional software will also be presented.

In the second part of the chapter, the capabilities of the model shall be demonstrated by means of a case study and the relevance of different factors for the accumulation of pore water pressure during the cyclic loading shall be analysed. Finally, a practical case with the irregular loading of a storm realisation will be investigated.

The academic finite element code GeHoMadrid, originally developed by Pastor and coworkers in the polytechnical universities of Madrid and Hohai, has later been enhanced and extended by,

a.o., Mira and Fernandez Merodo in the frame of their respective doctoral works [Mira, 2001; Fernandez Merodo, 2001]. In the course of the investigations presented here, it has been further adapted in order to meet the specific requirements for the simulation of the offshore pile.

3.1 Model Description

In general, the analytical models used nowadays to solve engineering problems include three main ingredients: (i) a mathematical model, to express by means of equations the physical processes that take place in the system to be studied, (ii) a constitutive model, to describe the behaviour of the materials, in particular the relationship between their internal stresses and strains, and (iii) a numerical model, to discretize all the equations so they can be solved efficiently with a calculation program.

3.1.1 Mathematical model: The u-p_W formulation

In order to achieve a realistic representation of the offshore pile behaviour, the first requisite is to use a suitable mathematical model to describe the main physical processes taking place within the saturated soil, in particular the interaction between the solid skeleton (the soil grains) and the pore fluid (the sea water).

The equations of dynamic poroelasticity originally due to Biot [1941; 1955; 1956] were implemented for the first time into a numerical model by Ghaboussi and Wilson [1972], who used a mixed formulation in terms of the displacements $\boldsymbol{u}_i$ of the solid matrix and $\boldsymbol{w}_i$ of the pore fluid relative to the solid. That model was later reformulated and simplified by Zienkiewicz and Bettess [1982] to ease its numerical implementation using as independent variables of the system the displacements $\boldsymbol{u}_i$ of the solid phase and the pressures $\boldsymbol{p}_w$ of the pore fluid. Further extensions to this model by Zienkiewicz and coworkers (e.g. in [Zienkiewicz *et al.*, 1980; Zienkiewicz & Shiomi, 1984] and [Zienkiewicz *et al.*, 1990b]) broadened its scope to include geometrical and material non-linearities as well as the non-saturated condition [Mira, 2001].

Generally, the complete representation of a partially saturated porous geomaterial would require the consideration of a mixture of three different phases, namely the solid particles and the two pore fluids (i.e. gas and liquid), where the pressure of the gaseous phase must also be taken into account. The aggregated system can then be analyzed as a continuum for instance by means of averaging techniques or considering the Theory of Mixtures, originally proposed by Truesdell [1957]. In general, the averaging methods aim at calculating the effective properties of a representative elementary volume of the mixture from the known behaviour of the single components, and then use the effective properties to derive appropriate constitutive relations for the mixture. On the other hand, the theory of mixtures considers the aggregate as dense enough so that the properties of each constituent can be averaged individually, and then assumes that all constituents fill the same infinitesimal volume separately. This way, the mixture is represented by the coexistence of the homogenized constituents in the same volume, where every single point does not consist of a single particle, but of a particle of every constituent [Temizer, 2004].

Given the scope of the present work, it may suffice to assume a fully saturated soil with no air bubbles occluded between the soil grains and consider only the liquid and solid phases. In any case, the presence of gas bubbles and dissolved air within the fluid can also be taken into account indirectly by means of the compressibility of the fluid [Fernandez Merodo, 2001]. Figure 3.1 shows a representation of the saturated soil and the idealized model being used in the present work.

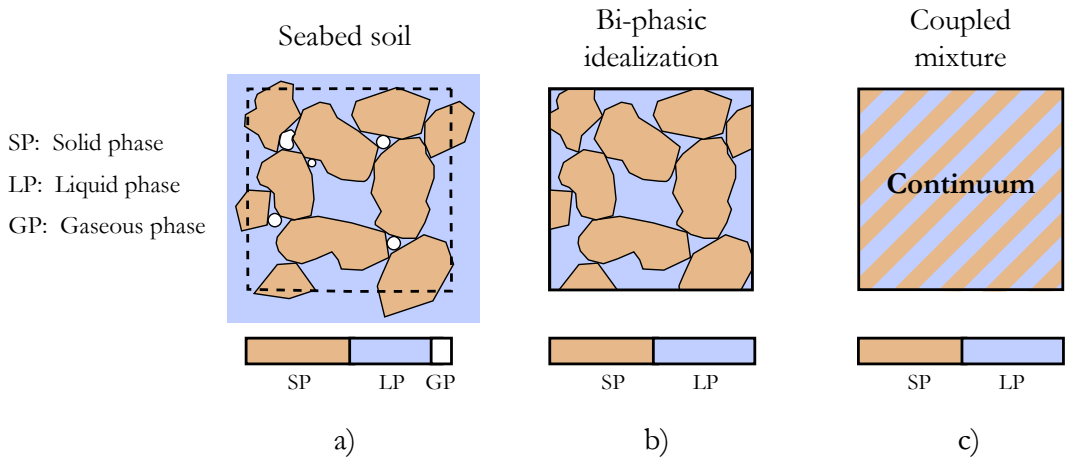

Figure 3.1 a) General case of porous geomaterial saturated with water and gas bubbles. b) Simplified bi-phasic consideration of saturated soil. c) Idealized model of the mixture as a continuum

This way, considering the soil as a mixture of a solid skeleton and a single fluid phase, the general form of the governing equations will include (i) the mass balances for both the liquid and solid phases, (ii) the conservation of linear momentum for the pore fluid and for the mixture, and (iii) constitutive and kinematic equations.

For the mathematical formulation of these equations, the following hypotheses have been adopted:

- The solid skeleton is deformable.
- The pores are fully saturated with a liquid phase*).
- The components of the mixture are supposed immiscible (i.e. the liquid cannot penetrate into the solid particles).
- The temperature is constant and the thermodynamical balance is kept in the whole domain. There are no phase transformations in the mixture (evaporation, condensation, etc…) due to changes in temperature or pressure.
- There are no chemical reactions between the mixture components.
- Both liquid and solid phases are compressible.
- The solid skeleton only experiences small deformations and negligible rotations.

As a starting point for this formulation, it is convenient to express the total stresses within the soil as the sum of the partial stresses acting on the different phases, $\boldsymbol{\sigma_{(s)}}$ on the solid skeleton and $\boldsymbol{\sigma_{(w)}}$ on the pore water:

$$\sigma = \sigma_{(S)} + \sigma_{(W)} \tag{3.1}$$

Then, introducing the concept of porosity $\boldsymbol{n}$ as the ratio of the pore volume relative to the total volume of mixture, and disregarding any shear stresses within the fluid, this expression can be rewritten as:

$$\sigma = (1-n)\sigma_S - np_W I \tag{3.2}$$

where $\boldsymbol{\sigma_s}$ is the stress of the solid phase, $\boldsymbol{p_w}$ is the pore water pressure and $\boldsymbol{I}$ represents the second order unitary tensor (i.e. Kronecker's delta). Note that the sign convention adopted here implies that tractions in the soil are positive. Furthermore, the definition of an effective stress $\boldsymbol{\sigma'}$ in the following form:

$$\sigma' = (1-n)(\sigma_S + p_W I) \tag{3.3}$$

*) For the interested reader, a detailed description of the mathematical model for a partially saturated soil can be found, for instance in [Zienkiewicz *et al.*, 1990b], [Sanavia & Schrefler, 2002], [Mira, 2001] and [Fernandez Merodo, 2001].

leads to the well known decomposition of total stress into effective stress and pore water pressure originally proposed by Terzaghi [1943]:

$$\sigma = \sigma' - p_W I \tag{3.4}$$

A strict definition of the effective stress should also to take into account the volumetric deformations of the solid grains due to the interstitial pressure as proposed in [Biot & Willis, 1957; Zienkiewicz & Bettess, 1982], introducing for this purpose an additional factor α:

$$\sigma' = \sigma + \alpha p_W I \tag{3.5}$$

but in practice, this coefficient can be approximated as:

$$\alpha \approx I - \frac{K_T}{K_S} \tag{3.6}$$

where K_T is the volumetric stiffness of the solid skeleton and K_S is that of the solid grains [Fernandez Merodo, 2001; Mira, 2001]. Since the latter can be orders of magnitude higher than the former, for most soils the coefficient α will assume values close to unity*), thus returning back to the classical Terzaghi expression of effective stress shown in equation (3.4).

On the other hand, the effective stresses can be related to the strains in the soil through a suitable constitutive dependency, such as the one described below in Section 3.1.3, which in general can be expressed in the following terms:

$$d\sigma' = D_{EP} (d\varepsilon - d\varepsilon_V^S - d\varepsilon_0) \tag{3.7}$$

where D_{EP} is the elastoplastic constitutive tensor, $d\varepsilon$ is the total strain tensor, $d\varepsilon^S_v$ represents the volumetric deformation of the solid grains due to uniform compression, and $d\varepsilon_0$ represents the rest of *initial* deformations in the soil that cannot be directly attributed to the effective stress (for instance, the strains due to changes in temperature). Since the volumetric compression of the grains due to the interstitial pressure is assumed to be negligible for the type of soils considered in this study ($\alpha \approx 1$), and the initial deformations will henceforth be disregarded, the constitutive relation in (3.7) may take the following simplified form:

$$d\sigma' = D_{EP} d\varepsilon \tag{3.8}$$

The corresponding constitutive relation for the pore fluid can be written in terms of the pore pressure p_w and water volumetric stiffness K_W as:

*) Certain kinds of rocks and concretes with small porosity can show values of α as low as 0.5 [Zienkiewicz & Shiomi, 1984; Zienkiewicz *et al.*, 1999], and special soils as calcareous sands with collapsible grains might also require the consideration of the volumetric deformations of the grains due to the pore pressure.

$$\varepsilon_V^W = -\frac{p_W}{3K_W} \tag{3.9}$$

And finally, the strain field will be related to the displacements $\boldsymbol{u}$ of the solid skeleton through a kinematic relationship:

$$\varepsilon_{ij} = \frac{1}{2}\left(\frac{\partial u_i}{\partial x_j} + \frac{\partial u_j}{\partial x_i}\right) \tag{3.10}$$

where the subscripts *i* and *j* refer to the coordinate directions. The incremental form of the kinematic relationship may also be expressed as:

$$d\varepsilon = Sdu \tag{3.11}$$

where $\boldsymbol{S}$ is the so-called strain operator in this context.

$$S = \begin{bmatrix} \frac{\partial}{\partial x_1} & 0 & 0 \\ 0 & \frac{\partial}{\partial x_2} & 0 \\ 0 & 0 & \frac{\partial}{\partial x_3} \\ \frac{\partial}{\partial x_2} & \frac{\partial}{\partial x_1} & 0 \\ 0 & \frac{\partial}{\partial x_3} & \frac{\partial}{\partial x_2} \\ \frac{\partial}{\partial x_3} & 0 & \frac{\partial}{\partial x_1} \end{bmatrix} \tag{3.12}$$

With this background, now it is possible to define the governing equations in the following manner. The first equation to consider is the overall equilibrium or equation of motion for the total system (i.e. the conservation of linear momentum for the soil-fluid mixture) which, in a Lagrangian formulation with $\boldsymbol{u^S_i}$ and $\boldsymbol{u^W_i}$ as the absolute displacements of the solid and fluid phases respectively, reads:

$$\frac{\partial \sigma_{ij}}{\partial x_j} + \rho b_i = \frac{D^S\left[(1-n)\rho_S \dot{u}_i^S\right]}{Dt} + \frac{D^W\left[n\rho_W \dot{u}_i^W\right]}{Dt} \tag{3.13}$$

where $\boldsymbol{\sigma_{ij}}$ is the total stress, $\boldsymbol{b_i}$ represents the acceleration of the body forces (generally gravity), and $\boldsymbol{\rho_s}$ and $\boldsymbol{\rho_w}$ are the densities of the solid and fluid phases respectively. Here, the density $\boldsymbol{\rho}$ of the mixture can be defined simply as:

$$\rho = (1-n)\rho_S + n\rho_W \tag{3.14}$$

and the total derivatives $\boldsymbol{D^S}$ and $\boldsymbol{D^W}$, often also referred to as balance operators or material derivatives, represent the following expressions:

$$\frac{D^S(*)}{Dt} \equiv \frac{\partial(*)}{\partial t} + \frac{\partial\left(* \dot{u}_i^S\right)}{\partial x_i} \tag{3.15}$$

$$\frac{D^W(*)}{Dt} \equiv \frac{\partial(*)}{\partial t} + \frac{\partial\left(* \dot{u}_i^W\right)}{\partial x_i} \tag{3.16}$$

Then, the second equilibrium equation describes the conservation of linear momentum in the pore fluid:

$$n\frac{\partial p_W}{\partial x_i} + \frac{D^W\left[n\rho_W \dot{u}_i^W\right]}{Dt} + nR_i = n\rho_W b_i \tag{3.17}$$

where $\boldsymbol{R_i}$ represents the viscous drag forces arising between the pore fluid and the solid matrix as the former flows through the latter. According to Darcy's law [Darcy, 1856], the drag forces are related to the relative velocity w_i of the fluid with respect to the solid (often referred to as Darcy's velocity) through the permeability tensor $\boldsymbol{k_{ij}}$ as follows:

$$k_{ij}R_j = n\left(\dot{u}_i^W - \dot{u}_i^S\right) = w_i \tag{3.18}$$

This way, isolating the drag forces in (3.18) and substituting back into (3.17), we obtain

$$n\frac{\partial p_W}{\partial x_i} + \frac{D^W\left[\rho_W w_i + n\rho_W \dot{u}_i^S\right]}{Dt} + n\frac{w_i}{k_{ij}} = n\rho_W b_i \tag{3.19}$$

And finally, the consideration of the mass balance equations for each of the phases, solid and fluid, completes the description of the physical system under examination. These equations can be expressed respectively as:

$$\frac{D^S\left[(1-n)\rho_S\right]}{Dt} = 0 \tag{3.20}$$

$$\frac{D^W\left[n\rho_W\right]}{Dt} = 0 \tag{3.21}$$

These two equations can be reformulated in terms of the absolute displacements of the solid skeleton $\boldsymbol{u_i}$ (now omitting the superscript s) and of the Darcy's velocity w, yielding the following expressions:

$$\frac{(1-n)}{\rho_S}\frac{D(\rho_S)}{Dt} - \frac{D(n)}{Dt} + (1-n)\frac{\partial \dot{u}_i}{\partial x_i} = 0 \tag{3.22}$$

$$\frac{n}{\rho_W}\frac{D(\rho_W)}{Dt}+\frac{D(n)}{Dt}+n\frac{\partial \dot{u}_i}{\partial x_i}+\frac{\partial \dot{w}_i}{\partial x_i}+\frac{1}{\rho_W}\frac{\partial \dot{w}_i}{\partial x_i}\frac{\partial \rho_W}{\partial x_i}=0 \tag{3.23}$$

where the balance operator is now defined as:

$$\frac{D(*)}{Dt}\equiv\frac{\partial(*)}{\partial t}+\frac{\partial(*)}{\partial x_i}\dot{u}_i \tag{3.24}$$

Since the equations (3.22) and (3.23) above are not independent, they can be combined to eliminate the material derivative of the porosity, yielding a single mass balance equation as follows:

$$\frac{(1-n)}{\rho_S}\frac{D(\rho_S)}{Dt}+\frac{n}{\rho_W}\frac{D(\rho_W)}{Dt}+\frac{\partial \dot{u}_i}{\partial x_i}+\frac{\partial \dot{w}_i}{\partial x_i}+\frac{1}{\rho_W}\frac{\partial \dot{w}_i}{\partial x_i}\frac{\partial \rho_W}{\partial x_i}=0 \tag{3.25}$$

On the other hand, the balance equations of the two phases can also be expressed as

$$\frac{D(\rho_S V_S)}{Dt}=\frac{1}{\rho_S}\frac{D(\rho_S)}{Dt}+\frac{1}{V_S}\frac{D(V_S)}{Dt}=0 \tag{3.26}$$

$$\frac{D(\rho_W V_W)}{Dt}=\frac{1}{\rho_W}\frac{D(\rho_W)}{Dt}+\frac{1}{V_W}\frac{D(V_W)}{Dt}=0 \tag{3.27}$$

where $\boldsymbol{V_S}$ and $\boldsymbol{V_W}$ are the volumes of the solid and liquid phases respectively. These two equations (3.26) and (3.27) can be combined with the volumetric constitutive relations in order to obtain the material derivatives of the phase densities:

$$\frac{1}{\rho_S}\frac{D(\rho_S)}{Dt}=-\frac{1}{V_S}\frac{D(V_S)}{Dt}=-\frac{1}{3K_S}\frac{D(\sigma_{S\,ii})}{Dt}=$$

$$=\frac{1}{1-n}\left[\frac{\alpha-n}{K_S}\frac{D(p_W)}{Dt}-(1-\alpha)\frac{D(\varepsilon_V)}{Dt}\right]\cong\frac{1}{K_S}\frac{D(p_W)}{Dt} \tag{3.28}$$

$$\frac{1}{\rho_W}\frac{D(\rho_W)}{Dt}=-\frac{1}{V_W}\frac{D(V_W)}{Dt}=\frac{1}{K_W}\frac{D(p_W)}{Dt} \tag{3.29}$$

which then can be introduced into equation (3.25) to obtain the final expression of the mass balance:

$$\left[\frac{(1-n)}{K_S}+\frac{n}{K_W}\right]\frac{D(p_W)}{Dt}+\frac{\partial \dot{u}_i}{\partial x_i}+\frac{\partial \dot{w}_i}{\partial x_i}+\frac{1}{\rho_W}\frac{\partial \dot{w}_i}{\partial x_i}\frac{\partial \rho_W}{\partial x_i}=0 \tag{3.30}$$

This way, the system of equations (3.13), (3.19) and (3.30), along with the kinematic and constitutive equations and an appropriate set of boundary conditions, describes the behaviour of the coupled problem. However, the solution of this system of partial differential equations is com-

plex and further simplifications may be pursued. In this respect, since the relative acceleration of the fluid with respect to the solid skeleton is generally small, particularly for the low loading frequencies involved in the problems under consideration, it will henceforth be omitted. Additionally, the convective terms of the linear momentum equation and the gradient of fluid density in the mass balance equation will also be assumed negligible from now on. Under these premises*), the Darcy velocity w in equation (3.19) can be isolated and introduced into the balance equation (3.30) to obtain finally the following expression:

$$\left[\frac{(1-n)}{K_S}+\frac{n}{K_W}\right]\frac{D(p_W)}{Dt}+\frac{\partial \dot{u}_i}{\partial x_i}+\frac{\partial}{\partial x_i}\left(k_{ij}\left(\rho_W b_i-\frac{\partial p_W}{\partial x_i}\right)\right)=0 \tag{3.31}$$

where the term of dynamic filtration $\partial(k\rho_w\ddot{u})/\partial x_i$ has been omitted for simplicity, since it only has some relevance in the range of high frequencies, where this formulation is no longer valid [Mira, 2001].

Similarly, now equation (3.13) can be reformulated as:

$$\frac{\partial(\sigma'_{ij}-p_W\delta_{ij})}{\partial x_j}+\rho b_i=\rho\ddot{u}_i \tag{3.32}$$

It is worth to mention that now the Darcy velocity $\dot{w}$ has vanished from both equations (3.31) and (3.32), therefore leaving a formulation with only $\boldsymbol{u}$ and $\boldsymbol{p_W}$ as independent variables.

A summary of this formulation is shown in
Table 3.1, where the vectorial notation has been employed and the following symbol conventions have been adopted:

$$\frac{1}{Q^*}=\frac{(1-n)}{K_S}+\frac{n}{K_W} \tag{3.33}$$

$$\nabla^T=\left\{\partial/\partial x_1 \quad \partial/\partial x_2 \quad \partial/\partial x_3\right\} \tag{3.34}$$

$$m^T=\{1 \quad 1 \quad 1 \quad 0 \quad 0 \quad 0\} \tag{3.35}$$

*) The validity of these assumptions has been studied in detail in [Zienkiewicz *et al.*, 1980; Zienkiewicz *et al.*, 1999], where the various approximations are compared to the complete formulation for the full range of frequencies. There it is concluded that the u-p_W approximation is valid for all frequencies for most soils (permeabilities up to $k=10^{-3}$ m/s). Soils with higher permeabilities (up to $k=10^{-1}$ m/s) are also well described for frequencies below a few Hz, and only shock phenomena and very high frequencies might require the full formulation.

Table 3.1 Summary of the general dynamic u-p_W formulation for saturated soils

Physical law	**Mathematical expression**	**Eq.**
Momentum balance for the solid-liquid mixture	$S(\sigma' - mp_W) + \rho b - \rho \ddot{u} = 0$	(3.32)
Momentum balance for the fluid + Mass conservation	$m^T S\dot{u} + \nabla^T \left(k(\rho_W b - \nabla p_W)\right) + \frac{\dot{p}_W}{Q^*} = 0$	(3.31)
Soil's internal constitution	$d\sigma' = D_{EP} d\varepsilon$	(3.8)
Kinematic compatibility	$d\varepsilon = Sdu$	(3.11)

A particular case of this formulation is that of the saturated consolidation, valid to describe systems where the loads are applied only gradually and in such a smooth fashion that the accelerations of the solid skeleton can be considered negligible and the terms associated to them omitted from the equations above.

3.1.2 Numerical model: The Finite Element approach

The analytical solution of the equations presented so far is in general quite complex, even for the 1-dimensional case, and in practice it is customary to resort to numerical techniques such as the Finite Element (FE) or the Finite Differences (FD) methods.

The FD approach, based on replacing the partial derivatives of the equations by suitable differential quotients at discrete points (both in time and in space), might not be the choice of preference for this particular case, mainly due to the complex geometry and the fact that in order to achieve a certain accuracy level it usually requires a much higher number of numerical grid points than other spatial discretisation techniques, which becomes even more important in three dimensional simulations [Frehner *et al.*, 2008]. For this type of problems, the FE approach seems to be the most appropriate and widely used [Zienkiewicz *et al.*, 1999; Fernandez Merodo, 2001].

In the FE method, the process of discretisation is normally divided into two consecutive stages, first for the spatial domain and then for the temporal one. In this process, the boundary value problem (i.e. the partial differential equations plus the set of additional restraints) is firstly reformulated in its variational or weak form, which is then discretised in a finite dimensional space.

Afterwards, a finite differences scheme (typically of the Newmark type) is applied to obtain the expressions discretised in time. More details about the general basis of these procedures can be found, for instance, in [Zienkiewicz & Taylor, 2000; Bathe & Wilson, 1976; Knothe & Wessels, 1999].

3.1.2.1 Discretization in space

The boundary value problem for the case under study is composed by the equations summarised in

Table 3.1 plus the following set of boundary conditions:

- Prescribed displacements:

$$u = \widetilde{u} \qquad \text{in } \Gamma_u \tag{3.36}$$

- Prescribed stresses:

$$t = \sigma' n - p_W n = \widetilde{t} \qquad \text{in } \Gamma_t \tag{3.37}$$

- Prescribed pore pressures:

$$p_W = \widetilde{p}_W \qquad \text{in } \Gamma_p \tag{3.38}$$

- Prescribed water flux:

$$q = k(\rho_W b - \nabla p_W) n = \widetilde{q} \qquad \text{in } \Gamma_q \tag{3.39}$$

The weak formulation of the problem states that, for any two arbitrary functions $\boldsymbol{\delta u}$ and $\boldsymbol{\delta p_w}$ contained in the fields of admissible displacements and pressures respectively, the following residual equations must hold true*):

*) The weighted residual equations are more "permissive" than the original differential equations, since they admit discontinuous first derivatives of the variables which is not permitted in the differential form, and they "only" require that the integral over the whole domain of the residuum times a weight function be zero, not demanding the exact fulfilment of the differential equations in every single point. They are therefore usually referred to as "weak form".

$$\int_\Omega \delta u^T \left(S(\sigma' - m p_W) + \rho b - \rho \ddot{u} \right) d\Omega = 0 \tag{3.40}$$

$$\int_\Omega \delta p_W \left(m^T S \dot{u} + \nabla^T \left(k(\rho_W b - \nabla p_W) \right) + \frac{\dot{p}_W}{Q^*} \right) d\Omega = 0 \tag{3.41}$$

Then, integrating by parts, making use of Gauss's divergence theorem and rearranging the terms, the equations transform into

$$\begin{aligned} &\int_\Omega \delta u^T S^T \sigma' d\Omega - \int_\Omega \delta u^T S^T m p_W d\Omega + \int_\Omega \delta u^T \rho \ddot{u} d\Omega = \\ &= \int_\Omega \delta u^T \rho b d\Omega + \int_{\Gamma_t} \delta u^T t d\Gamma_t \end{aligned} \tag{3.42}$$

$$\begin{aligned} &\int_\Omega \delta p_W m^T S \dot{u} d\Omega + \int_\Omega \nabla^T \delta p_W k \nabla p_W d\Omega + \int_\Omega \delta p_W \frac{\dot{p}_W}{Q^*} d\Omega = \\ &= \int_\Omega \nabla^T \delta p_W k \rho_W b d\Omega - \int_{\Gamma_q} \delta p_W q d\Gamma_q \end{aligned} \tag{3.43}$$

For the interested reader, a detailed description of this transformation is included in the appendix A.1.

If now, the spatial domain $\boldsymbol{\Omega}$ is discretised and the unknown fields $\boldsymbol{u}$ and $\boldsymbol{p_w}$ are approximated by a finite set of nodal variables, $\boldsymbol{u^e_i}$ and $\boldsymbol{p_w}^e_j$ respectively, and shape functions $\boldsymbol{N_{ui}}$ and $\boldsymbol{N_{pj}}$, so that

$$u \cong \tilde{u} = \sum_i N_{u\,i} u_i^e \tag{3.44}$$

$$p_W \cong \tilde{p}_W = \sum_j N_{p\,j} {p_W}^e_j \tag{3.45}$$

or simply, in vectorial form,

$$u \cong N_u \bar{u} \tag{3.46}$$

$$p_W \cong N_p \bar{p}_W \tag{3.47}$$

and since equations (3.42) and (3.43) must hold for any two arbitrary functions $\boldsymbol{\delta u}$ and $\boldsymbol{\delta p_w}$, it is possible to choose the trial functions to be precisely the shape functions $\boldsymbol{N_u}$ and $\boldsymbol{N_p}$,*) finally transforming the residual equations into

*) The choice of the weighting functions to be the same as the shape functions is know as the Galerkin method, and is in fact optimal for accuracy in the so called self-adjoint differential equations [Zienkiewicz & Taylor, 2000; Zienkiewicz *et al.*, 1999].

$$\int_\Omega B^T \sigma' d\Omega - \int_\Omega B^T m N_p \bar{p}_W d\Omega + \int_\Omega {N_u}^T \rho N_u \ddot{u} d\Omega = \\ = \int_\Omega {N_u}^T \rho b d\Omega + \int_\Gamma {N_u}^T t d\Gamma \tag{3.48}$$

$$\int_\Omega {N_p}^T m^T B \dot{u} d\Omega + \int_\Omega (\nabla N_p)^T k \nabla N_p \bar{p}_W d\Omega + \int_\Omega {N_p}^T \frac{1}{Q^*} N_p \dot{\bar{p}}_W d\Omega = \\ = \int_\Omega (\nabla N_p)^T k \rho_W b d\Omega - \int_\Gamma {N_p}^T q d\Gamma \tag{3.49}$$

which are now ordinary differential equations (i.e. now only time derivatives of the variables appear), where the matrix $\boldsymbol{B}$ stands for the product of the divergence (or strain) operator and the displacement shape functions.

$$B \equiv S N_u \tag{3.50}$$

The discretised ordinary differential equations can now be reformulated as

$$M\ddot{\bar{u}} + \int_\Omega B^T \sigma' d\Omega - Q\bar{p}_W = f_u \tag{3.51}$$

$$Q^T \dot{\bar{u}} + H\bar{p}_W + C\dot{\bar{p}}_W = f_p \tag{3.52}$$

where the naming conventions are summarised in Table 3.2.

Table 3.2 Matrix definition for the discrete problem

Term in eq. (3.51) and (3.52)	**Mathematical expression**	**Eq.**
Mass matrix, $\boldsymbol{M}$	$M = \int_\Omega {N_u}^T \rho N_u d\Omega$	(3.53)
Coupling matrix, $\boldsymbol{Q}$	$Q = \int_\Omega B^T m N_p d\Omega$	(3.54)
Permeability matrix, $\boldsymbol{H}$	$H = \int_\Omega (\nabla N_p)^T k (\nabla N_p) d\Omega$	(3.55)
Compressibility matrix, $\boldsymbol{C}$	$C = \int_\Omega {N_p}^T \frac{1}{Q^*} N_p d\Omega$	(3.56)
Load vector in displacements, $\boldsymbol{f_u}$	$f_u = \int_\Omega {N_u}^T \rho b d\Omega + \int_\Gamma {N_u}^T t d\Gamma$	(3.57)
Load vector in pressures, $\boldsymbol{f_p}$	$f_p = \int_\Omega (\nabla N_p)^T k \rho_W b d\Omega - \int_\Gamma {N_p}^T q d\Gamma$	(3.58)

At this point it is worth to mention that the interpolation (shape) functions for the two fields, $\boldsymbol{N_u}$ for the displacements and $\boldsymbol{N_p}$ for the pressures, need not be the same. In fact, when the permeability of the soil is low and the compressibility of the fluid tends to zero, numerical oscillations of the pressure field and spurious locking phenomena may appear if both $\boldsymbol{N_u}$ and $\boldsymbol{N_p}$ use the same order of interpolation. These problems, which are associated to the so called Babuska-Brezzi restriction [Babuska, 1973; Brezzi, 1974; Brezzi & Pitkaranta, 1984; Zienkiewicz & Shiomi, 1984], can be avoided, or at least mitigated, just by using a higher order of interpolation for displacements as for pressures, or alternatively by employing special numerical techniques. These issues are explained and dealt with below, in section 3.2.

3.1.2.2 Discretization in time

Now, in order to complete the numerical solution, the ordinary differential equations need to be integrated in time. For this purpose there exist many different procedures which can be adopted and readily implemented into a calculation program, as the so called multi-step methods (see, for instance, [Wood, 1990]), or the single-step schemes based on the weighted residual concept (e.g., in [Zienkiewicz *et al.*, 1990a]). A further group of time integration schemes is composed by those based on the Newmark method and employ the finite differences concept, i.e. a truncated Taylor series approximation, to advance the solution in single steps [Zienkiewicz & Taylor, 2000].

In general, all the time stepping techniques are based on the division of time in some finite intervals and provide a recurrence expression that relates the known value $\boldsymbol{\Phi_N}$ of a variable $\boldsymbol{\Phi}$ (and its derivatives) at the time station $\boldsymbol{t_N}$ with the values of $\boldsymbol{\Phi_{N+1}}$ and its respective derivatives at time $\boldsymbol{t_{N+1}}$, which are the unknowns.

Considering that the ordinary differential equations have to be satisfied at every discrete moment in the time line, and in particular at the discrete time point $\boldsymbol{t_{N+1}}$, the equations (3.51) and (3.52) obtained so far can now be particularised as

$$M\ddot{\bar{u}}_{N+1} + \int_{\Omega} B^T \sigma'_{N+1} d\Omega - Q\bar{p}_{N+1} = f^U{}_{N+1} \tag{3.59}$$

$$Q^T \dot{\bar{u}}_{N+1} + H\bar{p}_{N+1} + C\dot{\bar{p}}_{N+1} = f^P{}_{N+1} \tag{3.60}$$

where the subscript of the variables indicates the time station to which they refer.

Now, adopting the recurrence relations provided by the Generalized Newmark method (GNpj, where p is the order of the scheme, and j the order of the differential equation) [Katona & Zienkiewicz, 1985; Zienkiewicz & Taylor, 2000], it is possible to express the variables and their derivatives as a function of their values in the previous time station t_N. The simplest relation for the displacements would be the GN22, which reads

$$\dot{\bar{u}}_{N+1} = \dot{\bar{u}}_N + \Delta t \ddot{\bar{u}}_N + \beta_1 \Delta t \Delta \ddot{\bar{u}}_N \tag{3.61}$$

$$\bar{u}_{N+1} = \bar{u}_N + \Delta t \dot{\bar{u}}_N + \frac{1}{2}\Delta t^2 \ddot{\bar{u}}_N + \frac{1}{2}\beta_2 \Delta t^2 \Delta \ddot{\bar{u}}_N \tag{3.62}$$

where

$$\Delta \ddot{\bar{u}}_N = \ddot{\bar{u}}_{N+1} - \ddot{\bar{u}}_N \tag{3.63}$$

Similarly, the recurrence expression for the pressure field may take the following form using the GN11 scheme

$$\bar{p}_{N+1} = \bar{p}_N + \Delta t \dot{\bar{p}}_N + \theta \Delta t \Delta \dot{\bar{p}}_N \tag{3.64}$$

where

$$\Delta \dot{\bar{p}}_N = \dot{\bar{p}}_{N+1} - \dot{\bar{p}}_N \tag{3.65}$$

Additionally, in order to ensure the unconditional stability of the algorithm, the parameters β_1, β_2, and θ of the Newmark scheme must comply with the following restrictions [Chan, 1988; Zienkiewicz & Taylor, 2000]

$$\beta_2 \geq \beta_1 \geq \frac{1}{2} \quad \text{and} \quad \theta \geq \frac{1}{2} \tag{3.66}$$

Now, introducing the expressions (3.61) through (3.65) into (3.59) and (3.60), the final system of non-linear equations arises [Mira, 2001]

$$G^U{}_{N+1} = M \Delta \ddot{\bar{u}}_N + \int_\Omega B^T \sigma'_{N+1} d\Omega - Q \theta \Delta t \Delta \dot{\bar{p}}_N - F^U{}_{N+1} = 0 \tag{3.67}$$

$$G^P{}_{N+1} = Q^T \beta_1 \Delta t \Delta \ddot{\bar{u}}_N + H \theta \Delta t \Delta \dot{\bar{p}}_N + C \Delta \dot{\bar{p}}_N - F^P{}_{N+1} = 0 \tag{3.68}$$

where

$$F^U{}_{N+1} = f^U{}_{N+1} - M \ddot{\bar{u}}_N + Q\left(\bar{p}_N + \Delta t \dot{\bar{p}}_N\right) \tag{3.69}$$

$$F^P{}_{N+1} = f^P{}_{N+1} - Q^T\left(\dot{\bar{u}}_N + \Delta t \ddot{\bar{u}}_N\right) - H\left(\bar{p}_N + \Delta t \dot{\bar{p}}_N\right) - C \dot{\bar{p}}_N \tag{3.70}$$

It should be noted that $\boldsymbol{\sigma'_{N+1}}$ in equation (3.67) can in general be evaluated by means of the constitutive relation (3.8) in incremental form as follows*)

$$\sigma'_{N+1} = \sigma'_N + D\Delta\varepsilon_{N+1} = \sigma'_N + DB\Delta\bar{u}_{N+1} \tag{3.71}$$

3.1.2.3 Solution of the non-linear system

Since the tangent constitutive matrix $\boldsymbol{D}$ is in general not constant (it is in fact "stress-history dependent" for most geomaterials), the system of equations will have to be solved using an appropriate iterative non-linear solution technique, typically of the Newton-Raphson family. For this purpose, it is convenient to express the system of equations in the following form

$$G(x) = 0 \tag{3.72}$$

where

$$x = \begin{Bmatrix} \Delta\ddot{\bar{u}} \\ \Delta\dot{\bar{p}} \end{Bmatrix} \quad \text{and} \quad G = \begin{Bmatrix} G^U \\ G^P \end{Bmatrix} \tag{3.73}$$

Now, starting from the known solution $\boldsymbol{x_i}$ corresponding to the iteration $\boldsymbol{i}$, which does not meet the required tolerance criteria, a new solution $\boldsymbol{x_{i+1} = x_i + dx_i}$ that satisfies (3.72) will be pursued.
If the Taylor series of equation (3.72), evaluated at the point $\boldsymbol{x_i}$, is considered and disregarding the terms of second and higher order, the system is now expressed as

$$G(x_i) + \left.\frac{\partial G}{\partial x}\right|_{x=x_i} dx_i = 0 \tag{3.74}$$

which can be reformulated, taking the first term to the right-hand side, as

$$J dx_i = -G(x_i) \tag{3.75}$$

*) This equation corresponds to an explicit scheme of stress integration, where the stress increment is *directly* calculated through the strain increment. Such explicit method is in general only conditionally stable depending on the time step and in the plastic case introduces a systematic error with each load increment, since the calculated stresses will lie *outside* the yield surface. These problems can be mitigated by including an algorithm for the return to the yield surface or by using sub-stepping techniques [Zienkiewicz & Taylor, 2000]. An alternative implicit scheme using a consistent tangent elastoplastic matrix is described, for instance, in [Fernandez Merodo, 2001; Tamagnini *et al.*, 2002].

where $\boldsymbol{J}$ is the Jacobian matrix, defined in this case as

$$J = \begin{bmatrix} \partial G^U / \partial \Delta \ddot{\boldsymbol{u}} & \partial G^U / \partial \Delta \dot{\boldsymbol{p}} \\ \partial G^P / \partial \Delta \ddot{\boldsymbol{u}} & \partial G^P / \partial \Delta \dot{\boldsymbol{p}} \end{bmatrix} \tag{3.76}$$

This matrix may be approximated as

$$J \approx \begin{bmatrix} M + K_T \frac{1}{2} \beta_2 \Delta t^2 & -Q\theta\Delta t \\ Q^T \beta_1 \Delta t & H\theta\Delta t + C \end{bmatrix} \tag{3.77}$$

where the tangent matrix $\boldsymbol{K_T}$ is the standard stiffness matrix defined as

$$K_T = \int_\Omega B^T D^{EP} B d\Omega \tag{3.78}$$

Now, introducing the approximation of the Jacobian (3.77) back into (3.75), the system of equations is finally written as

$$\begin{bmatrix} M + K_T \frac{1}{2} \beta_2 \Delta t^2 & -Q\theta\Delta t \\ Q^T \beta_1 \Delta t & H\theta\Delta t + C \end{bmatrix} \begin{Bmatrix} d(\Delta \ddot{\boldsymbol{u}}_N) \\ d(\Delta \dot{\boldsymbol{p}}_N) \end{Bmatrix} = - \begin{Bmatrix} G^U \\ G^P \end{Bmatrix} \tag{3.79}$$

which is a *linear* system of equations that provides the iterative correction to the incremental solution according to

$$\begin{Bmatrix} \Delta \ddot{\boldsymbol{u}}_N \\ \Delta \dot{\boldsymbol{p}}_N \end{Bmatrix}_{i+1} = \begin{Bmatrix} \Delta \ddot{\boldsymbol{u}}_N \\ \Delta \dot{\boldsymbol{p}}_N \end{Bmatrix}_i + \begin{Bmatrix} d(\Delta \ddot{\boldsymbol{u}}_N) \\ d(\Delta \dot{\boldsymbol{p}}_N) \end{Bmatrix} \tag{3.80}$$

The iterative process is to be repeated until a suitable tolerance criterion, based both on the residuals as well as on the magnitudes of the variables' increments, is fulfilled. Some details on the convergence rate of the non-linear solver and a description of the tolerance criteria implemented in the calculation program GeHoMadrid can be found in the Appendix A.2.

As a closure to this section, it may be worth to make the following remarks:

- The linear system of equations shown in (3.79) is non-symmetric. Although the second set of equations can be multiplied by a scalar in order to achieve symmetry in the coupling terms, the overall symmetry of the linear system of equations will ultimately depend on the symmetry of the stiffness matrix $\boldsymbol{K_T}$. This matrix will, in general, be unsymmetric whenever a non-associative constitutive law is used, as is normally the case for modeling cohesionless soils. As it will be shown later in Section 3.3.1, the

lack of symmetry of the linear system of equations carries important consequences for the choice of a solution strategy.

- On deriving the approximation of the Jacobian $\boldsymbol{J}$ shown in equation (3.77), the matrices $\boldsymbol{M}$, $\boldsymbol{Q}$, $\boldsymbol{H}$ and $\boldsymbol{C}$ have been assumed to remain constant with respect to both $\boldsymbol{u}$ and $\boldsymbol{p_w}$. However, for the unsaturated case they are no longer constant and may vary with the degree of saturation (and hence with the pore pressure). In such cases, an exact calculation of the Jacobian as shown in [Fernandez Merodo, 2001] will be required in order to improve the convergence rate.
- As mentioned in Section 3.1.1, a particular case of this formulation is that of the saturated consolidation, where the accelerations of the solid skeleton are small and the terms associated to them can be neglected. For this case, it will suffice to use a Newmark scheme of the type GN11 for the time discretisation of the displacement field, and the resulting system of equations is consequently simplified. Details of this particular case are given in the Appendix A.3.

3.1.3 Constitutive model

Along with the mathematical and numerical models described so far, the third main ingredient for the numerical investigations is the choice of an appropriate constitutive model for the soil that can replicate with sufficient accuracy the real stress behaviour of the material in dependence of the imposed deformations (or *vice versa*).

3.1.3.1 Sand behaviour and the Generalized Plasticity Theory

One of the particular features of cohesionless soils, regardless of their initial state of density, is their general tendency to contract when they are subject to cyclic loading (see, for instance, [Youd, 1972; Tatsuoka & Ishihara, 1974; Cuéllar *et al.*, 1977; Sagaseta *et al.*, 1991; Jefferies & Been, 2006]). In saturated soils, this cyclic densification can lead to an increment of the pore pressure if the permeability of the soil is low or the drainage of pore water is somehow inhibited.

Such increments in pore pressure will reduce the effective stress within the soil skeleton and eventually can lead to a total loss of resistance (the so-called liquefaction) with potential catastrophic consequences [Zienkiewicz *et al.*, 1999; Pastor *et al.*, 2009; Jefferies & Been, 2006]. It is therefore essential that the constitutive model can reproduce the real behaviour of sand. The main aspects of sand behaviour can be broadly summarized as follows [Pastor *et al.*, 2008]:

- When subject to loading and before reaching failure, the soil crosses a stress state at which no volumetric deformations occur, and then returns to it at ultimate (residual) conditions. This state is characterized by a specific stress ratio $\eta=q/p'$ that lies on the so-called Characteristic or Critical State Line, which also marks the point where the behaviour of the soil changes from contractive to dilatant [Tatsuoka & Ishihara, 1974; Ishihara *et al.*, 1975; Sagaseta *et al.*, 1991].

- When the loading is characterized by a drained monotonic shearing, loose sands experience a compaction that reduces their volume (contractive behaviour), while dense sands tend to expand once they have crossed the CSL line (dilatant behaviour). Dilation causes softening, i.e. the strength of the soil features a peak and then decreases [Muir Wood, 2004; Pastor *et al.*, 1990].

- When the soil is not fully drained, any reductions in volume do increase the pore pressure. In the limit, this can lead to liquefaction.

- Under cyclic loading, the same patterns of compaction and dilation occur, but cyclic plastic deformations appear, causing a progressive compaction of the sand regardless of its initial density [Goldscheider & Gudehus, 1976]. When the conditions are undrained, a progressive accumulation of pore pressure is caused instead, which in loose sands can lead to a cyclic liquefaction failure.

- Medium dense sands do not experience cyclic liquefaction, but rather a special behaviour denominated 'cyclic mobility', which also features large shear deformations but leaves some degree of strength in the soil (i.e. the soil is not totally fluidized and can hold some stress). The main difference with the cyclic liquefaction is that when dilation appears, it produces a decrease in the pore pressure, hence causing some hardening of the sand.

In order to reproduce these features within the frame of elasto-plasticity, three key issues need to be considered, namely, a non-associative flow rule, a hardening law not only dependent on the soil density, and the possibility of plastic strains upon unloading [Pastor *et al.*, 1999]. The Generalized Theory of Plasticity, initially proposed by Zienkiewicz and Mroz [1984] and later extended

to soils by Pastor and Zienkiewicz [1986; Pastor *et al.*, 1990] offers a convenient framework for the consideration of such features. In its basic form, it relates the increments of stress $\boldsymbol{d\sigma}$ and strain $\boldsymbol{d\varepsilon}$ in a material as follows

$$d\boldsymbol{\varepsilon} = C_{EP} \cdot d\boldsymbol{\sigma} = C_E \cdot d\boldsymbol{\sigma} + \frac{\boldsymbol{n}_{gL/U}\boldsymbol{n}^T \cdot d\boldsymbol{\sigma}}{H_{L/U}} \tag{3.81}$$

where the first summand provides the elastic strain through the use of an elastic constitutive tensor $\boldsymbol{C_E}$, inverse of the elastic matrix $\boldsymbol{D^E}$, and the second term introduces the plastic strain in dependence of a scalar $\boldsymbol{H}$ (the plastic modulus) and the product of two directions $\boldsymbol{n}$ and $\boldsymbol{n}_G$. The inverse relationship defines the elastoplastic tangent matrix $\boldsymbol{D^{EP}}$ and can be written as

$$d\boldsymbol{\sigma} = D^{EP} \cdot d\boldsymbol{\varepsilon} = \left(D^E - \frac{D^E \boldsymbol{n}_{gL/U} \boldsymbol{n}^T D^E}{H_{L/U} + \boldsymbol{n}^T D^E \boldsymbol{n}_{gL/U}} \right) \cdot d\boldsymbol{\varepsilon} \tag{3.82}$$

In (3.81) and (3.82), the loading direction $\boldsymbol{n}$ discriminates the stress increments between loading and unloading in the following manner

$$d\boldsymbol{\sigma}^T \cdot \boldsymbol{n} > 0 \quad \Rightarrow \quad \textit{Loading} \tag{3.83}$$

$$d\boldsymbol{\sigma}^T \cdot \boldsymbol{n} < 0 \quad \Rightarrow \quad \textit{Unloading} \tag{3.84}$$

$$d\boldsymbol{\sigma}^T \cdot \boldsymbol{n} = 0 \quad \Rightarrow \quad \textit{Neutral (elastic) loading} \tag{3.85}$$

and the plastic flow direction $\boldsymbol{n}_G$ defines the orientation of the plastic strains. The values of $\boldsymbol{n}_G$ may be defined arbitrarily in any suitable manner that is convenient to the problem at hand. Whenever the directions $\boldsymbol{n}$ and $\boldsymbol{n}_G$ are different, the plastic flow is said to be non-associative and, as it can be seen from equation (3.82), the tangent matrix $\boldsymbol{D^{EP}}$ will be non-symmetric. As mentioned previously, this is the main factor that conditions the overall symmetry of the system of equations.

It can be shown that if irreversible plastic deformations are to be achieved within a closed stress cycle, $\boldsymbol{H}$ and $\boldsymbol{n}_G$ need to be defined differently for the loading and unloading states, and hence the subscript L or U in equations (3.81) and (3.82) (see for instance [Zienkiewicz *et al.*, 1999]).

At this point it must be noted that, although the *classical* plasticity models (like those due to Mohr-Coulomb, Drucker-Prager, Tresca, etc…) can be shown to be particular cases of the Generalized Plasticity (e.g., in [Zienkiewicz *et al.*, 1999]), this generalized formulation avoids the need for an explicit definition of the yield and plastic potential surfaces or the introduction of a pure elastic domain, which in the case of sands and in light of empirical evidence seems to be extremely small

or even not to exist at all (see for instance [Gudehus *et al.*, 1984], [Tobita, 1996] or the recent micro-mechanical investigations in [Alonso-Marroquin & Herrmann, 2005; 2004]). As shown in [Zienkiewicz *et al.*, 1999], the classical elasto-plastic models, are basically unable to reproduce either the behaviour of overconsolidated soils or phenomena like the cyclic densification, which are key aspects for the development of liquefaction and cyclic mobility. Such limitations can be overcome for instance within the frame of the Generalized Plasticity (see the Pastor-Zienkiewicz model below) as well as within the frame of Hypoplasticity (e.g. in [Kolymbas, 1991], [Kolymbas *et al.*, 1995] or [Wu *et al.*, 1996]). The latter additionally considers the continuous nonlinear dependence of the tangent stiffness tensor on the direction of the strain rate, which is not possible with the plasticity-type models and might be required for modelling certain complex loading paths. However, there is probably no single constitutive model that can give optimal results for all possible cases and hence the choice of it might be better done on a case-dependent basis. Extensive descriptions of the main available constitutive models, as well as their relevance for geotechnical engineering, have been provided, for instance, in [Desai & Siriwardane, 1984], [Kolymbas, 1993], [Cambou & Di Prisco, 2000], [Heeres, 2001] or [Tamagnini & Viggiani, 2002].

3.1.3.2 The Pastor-Zienkiewicz model for sands

The Pastor-Zienkiewicz Mark III model (in the following referred to as PZ model) suitably defines the three directions $\boldsymbol{n}$, $\boldsymbol{n}_{G,L}$ and $\boldsymbol{n}_{G,U}$ and the scalar functions $\boldsymbol{H_L}$ and $\boldsymbol{H_U}$ in (3.81) to reproduce the main aspects of the sand behaviour.

For the definition of the model, it is convenient to adopt the usual notation of soil mechanics based on the stress invariant magnitudes $\boldsymbol{p'}$, $\boldsymbol{q}$ and $\boldsymbol{\theta}$, which for completeness are described in the Appendix A.4.

Starting with the definition of the elastic components of the strain increment, now expressed in the space of invariants, the model introduces two elastic moduli $\boldsymbol{K^e}$ and $\boldsymbol{G^e}$ dependent on the confining pressure as

$$d\boldsymbol{\varepsilon}^e{}_V = \frac{dp'}{K^e} \qquad \text{where} \qquad K^e = K_0^e \frac{p'}{p'_0} \tag{3.86}$$

$$d\boldsymbol{\varepsilon}^{e}{}_{S} = \frac{dq}{3G^{e}} \qquad \text{where} \qquad G^{e} = G_{0}^{e}\,\frac{p'}{p'_{0}} \tag{3.87}$$

Similarly, the volumetric and deviatoric plastic strain increments can be defined in the space of invariants according to

$$d\boldsymbol{\varepsilon}^{p}{}_{V} = \frac{1}{H_{L/U}}\,\boldsymbol{n}_{g,V}\left(\boldsymbol{n}_{V}\cdot dp' + \boldsymbol{n}_{S}\cdot dq\right) \tag{3.88}$$

$$d\boldsymbol{\varepsilon}^{p}{}_{S} = \frac{1}{H_{L/U}}\,\boldsymbol{n}_{g,S}\left(\boldsymbol{n}_{V}\cdot dp' + \boldsymbol{n}_{S}\cdot dq\right) \tag{3.89}$$

which are additionally related through the dilatance $\boldsymbol{d_G}$ as

$$d_{g} = \frac{d\boldsymbol{\varepsilon}^{p}{}_{V}}{d\boldsymbol{\varepsilon}^{p}{}_{S}} \tag{3.90}$$

A suitable expression for the dilatance proposed by Pastor *et al.* [1985] based on the experimental results obtained by Frossard [1983] takes the following form

$$d_{g} = \frac{d\boldsymbol{\varepsilon}^{p}{}_{V}}{d\boldsymbol{\varepsilon}^{p}{}_{S}} = \left(1+\alpha_{g}\right)\left(M_{g}-\eta\right) \tag{3.91}$$

in dependence of both the stress ratio $\boldsymbol{\eta=q/p'}$ and the slope $\boldsymbol{M_g}$ of the CSL in the $\boldsymbol{p'}$-$\boldsymbol{q}$ plane. The parameter $\boldsymbol{\alpha_g}$ is a constant of the material that can be obtained for instance from experimental diagrams of dilatance versus stress ratio. It can be easily verified that the above expression makes the dilatance zero for all stress states where the stress ratio equals $\boldsymbol{M_g}$, thus fulfilling one of the basic premises of the Critical State Theory.

Strictly speaking, the equations presented above have been defined merely in the triaxial plane, where it will suffice with the consideration of just the first two stress invariants. A generalization to three-dimensional conditions in order to consider any stress path can be achieved by adopting a suitable law for the dependency of $\boldsymbol{M_g}$ on the third stress invariant or Lode's angle $\boldsymbol{\theta}$. Such a dependency can for instance take the form proposed by Zienkiewicz and Pande [1977], which reads

$$M_{g} = \frac{6\,\sin\varphi'}{3-\sin\varphi'\,\sin 3\theta} \tag{3.92}$$

where $\boldsymbol{\varphi'}$ is the residual friction angle of the material.

Now, the plastic flow vector $\boldsymbol{n_g}$ can be simply expressed in terms of the dilatance as

$$n_g = \begin{Bmatrix} n_{g,V} \\ n_{g,S} \\ n_{g,\theta} \end{Bmatrix} \tag{3.93}$$

$$n_{g,V} = \frac{d_g}{\sqrt{1 + d_g^{\,2}}} \tag{3.94}$$

$$n_{g,S} = \frac{1}{\sqrt{1 + d_g^{\,2}}} \tag{3.95}$$

$$n_{g,\theta} = \frac{-q\, M_g \cos 3\theta}{2\sqrt{1 + d_g^{\,2}}} \tag{3.96}$$

For the unloading case, i.e. whenever (3.84) holds true, the plastic flow direction can be similarly defined, but this time imposing that the plastic strains be of contractive nature, which can be written as

$$n_{gU} = \begin{Bmatrix} -\left| n_{g,V} \right| \\ n_{g,S} \\ n_{g,\theta} \end{Bmatrix} \tag{3.97}$$

It can be shown, as for instance in [Pastor *et al.*, 1990; Zienkiewicz *et al.*, 1999]), that there exists a unique surface $\boldsymbol{g}$ such that

$$n_g = \frac{\partial g}{\partial \sigma} \tag{3.98}$$

which makes $\boldsymbol{n_g}$ normal to it in every point of the surface. This surface can be interpreted as the plastic potential surface of the classical plasticity models, but needs not be explicitly defined and therefore will not be further described here.

Since, as stated before, the use of a non-associative flow rule is needed in order to model the unstable behaviour of sand in the hardening region (i.e. below the CSL), the direction $\boldsymbol{n}$ has to be different from $\boldsymbol{n_g}$, but it can nevertheless be specified in a similar way:

$$n = \begin{Bmatrix} n_{,V} \\ n_{,S} \\ n_{,\theta} \end{Bmatrix} \tag{3.99}$$

$$n_{,V} = \frac{d_f}{\sqrt{1 + d_f^{\,2}}} \tag{3.100}$$

$$n_{,S} = \frac{1}{\sqrt{1 + d_f^{\,2}}} \tag{3.101}$$

$$n_{,\theta} = \frac{-q\, M_f \cos 3\theta}{2\sqrt{1 + d_f^{\,2}}} \tag{3.102}$$

along with a definition of $\boldsymbol{d_f}$ as

$$d_f = (1 + \alpha_f)(M_f - \eta) \tag{3.103}$$

where $\boldsymbol{\alpha_f}$ and $\boldsymbol{M_f}$ are parameters of the PZ model. This way, the performance of the model is strongly conditioned by the ratio $\boldsymbol{M_f / M_g}$ which is related to the initial density of the sand so that low values of the ratio correspond to "loose" samples and high values to "dense" conditions [Pastor *et al.*, 1985].

Similarly as for the case of $\boldsymbol{n_g}$, there is also a surface $\boldsymbol{f}$ implicitly defined with the load vector $\boldsymbol{n}$ that could be understood as the yield surface of the classical plasticity models. Figure 3.2 illustrates exemplarily these concepts for the particular case of a loose sand.

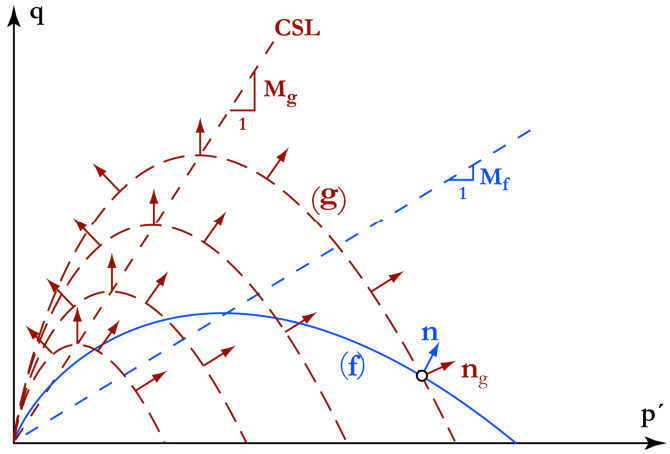

Figure 3.2 Loading and plastic flow directions and their associated surfaces for a loose sand (after [Pastor *et al.*, 1985]).

And now, a hierarchical definition of the plastic modulus $\boldsymbol{H_L}$, here shown in eq. (3.104), permits the consideration of single aspects of sand behaviour, like for instance the existence of a critical

line where all the residual stress states lie or the fact that failure does not necessarily occur when this line is first crossed.

$$H_L = H_0 \cdot p' \cdot H_f \cdot \left(H_v + H_s\right) \cdot H_{DM} \tag{3.104}$$

This way, $\boldsymbol{H_L}$ incorporates the following ingredients: (i) a pressure dependence through the effective confining stress $\boldsymbol{p'}$, (ii) an isotropic compression plastic modulus $\boldsymbol{H_0}$, (iii) a "frictional" factor $\boldsymbol{H_f}$ that limits the possible stress states within the sand, (iv) a volumetric strain hardening function $\boldsymbol{H_v}$ with a dependence on the mobilized stress ratio which makes it zero at the critical state line, (v) a deviatoric strain hardening $\boldsymbol{H_s}$, which models the material degradation by accumulated strains and permits the crossing of the critical state line without causing immediate failure, and finally (vi) a discrete memory factor $\boldsymbol{H_{DM}}$ that accounts for the effects of past events upon cyclic reloading.

Pastor and Zienkiewicz proposed the following expressions for the components of the plastic modulus [Pastor & Zienkiewicz, 1986]:

$$H_f = \left(1 - \frac{\eta}{\eta_f}\right)^4 \qquad \text{where} \qquad \eta_f = \left(1 + \frac{1}{\alpha_f}\right) M_f \tag{3.105}$$

$$H_V = \left(1 - \frac{\eta}{M_g}\right) \tag{3.106}$$

$$H_S = \beta_0 \beta_1 \, exp(-\beta_0 \xi) \tag{3.107}$$

$$H_{DM} = \left(\frac{\zeta_{max}}{\zeta}\right)^{\gamma} \tag{3.108}$$

where ξ is the accumulated shear plastic deformation, also referred to as "variable of continuous memory" [Garcia Nuñez, 2007], and is given by

$$\xi = \int \left| d\varepsilon^p{}_S \right| \tag{3.109}$$

and ζ is the variable of mobilized stress level, or "discrete memory", used to introduce a hardening effect that takes into account past loading events in a similar manner as the bounding surface models, i.e. interpolating with the maximal value ζ_{max} of ζ reached during the loading history.

$$\zeta = p'\left(1 - \frac{\eta}{\eta_f}\right)^{-\frac{1}{\alpha_f}} \tag{3.110}$$

And finally, for the unloading case, the plastic modulus can be defined with a simple expression dependent on the point where the load reversal takes place, as proposed in [Pastor *et al.*, 1990]

$$H_U = H_{U,0}\left(\frac{M_g}{\eta_U}\right)^{\gamma_U} \qquad \text{for} \quad \left|\frac{M_g}{\eta_U}\right| > 1 \tag{3.111}$$

$$H_U = H_{U,0} \qquad \text{for} \quad \left|\frac{M_g}{\eta_U}\right| \leq 1 \tag{3.112}$$

where η_U is the stress ratio at the point where the unloading begins.

Altogether, a set of 12 parameters needs to be determined in order to fully characterize the sand at a given initial pressure and density and is summarized in Table 3.3.

Table 3.3 Parameters of the Pastor-Zienkiewicz constitutive model

Parameter	Description	Units
K^e_0	Elastic volumetric modulus	N / m²
G^e_0	Elastic shear modulus	N / m²
M_g	Slope of the Critical State Line	-
α_g	Slope of the dilatance vs. stress ratio diagram	-
M_f	Shape parameter, function of CSL slope and relative density	-
α_f	Shape parameter, usually taken equal to α_g	-
H_0	Plastic modulus of isotropic compression	N / m²
β_0	Deviatoric strain hardening parameter	-
β_1	Deviatoric strain hardening parameter	-
γ	Discrete memory interpolation parameter	-
$H_{U,0}$	Modulus of plastic unloading	N / m²
γ_U	Plastic unloading parameter	-

A useful extension to the model has been recently proposed by Manzanal [2008; Manzanal *et al.*, 2010] based on the state parameter of Been and Jefferies [1985], introducing two parameters that take into account the dependency on the initial conditions of confining stress and density respec-

tively. In contrast to the original PZ model, the extended model permits a unified definition of the material parameters valid for the full range of pressures and densities. It has however not been used in the present work and its consideration has been left for future investigations.

In any case, the general validity of the original PZ model to reproduce the main features of the monotonic and cyclic response of sands has been abundantly demonstrated in the literature, as for instance in [Pastor *et al.*, 1990; Zienkiewicz *et al.*, 1999; Fernandez Merodo, 2001; Garcia Nuñez, 2007; Manzanal *et al.*, 2010].

Figure 3.3 shows exemplarily the simulated results reproducing the well-known monotonic triaxial tests on Banding sand carried out by Castro [1969], while on Figure 3.4 the results corresponding to the cyclic triaxial tests of Tatsuoka [1972] with the Niigata sand can be seen.

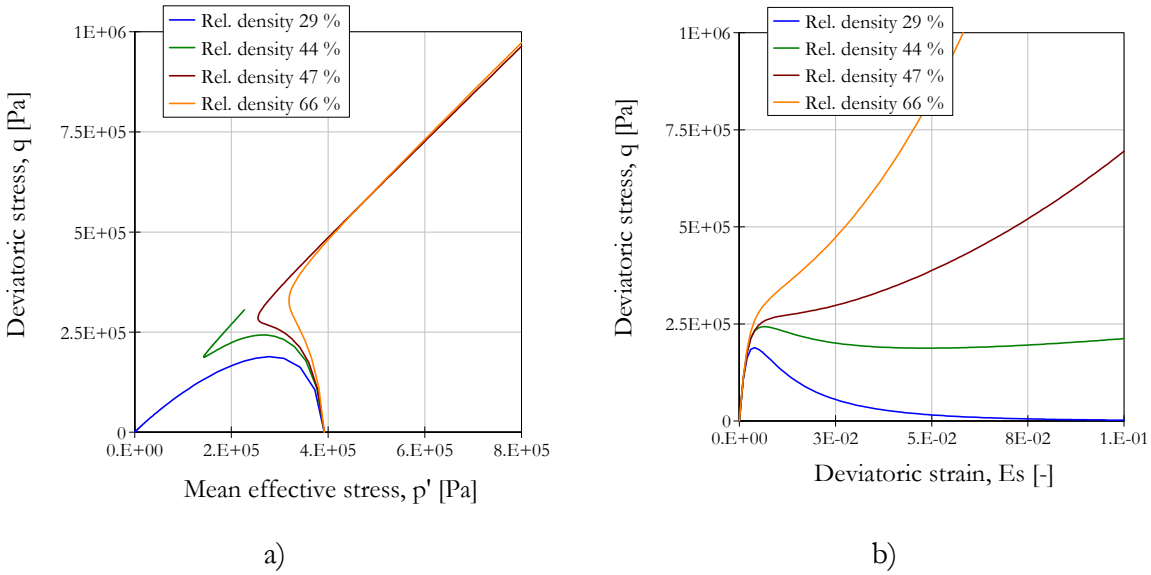

Figure 3.3 Computed behaviour of Banding sand under monotonic triaxial loading, after the empirical results of [Castro, 1969]. a) Stress paths on the triaxial plane. b) Deformational behaviour.

The FE code GeHoMadrid includes a Fortran-90 module with the PZ model, which has been extended in the frame of this work in order to consider three-dimensional conditions. Previous versions of the PZ implementation in GeHoMadrid were aimed at two-dimensional, plane strain or axially symmetric conditions, and were therefore unsuitable for the problem under consideration here.

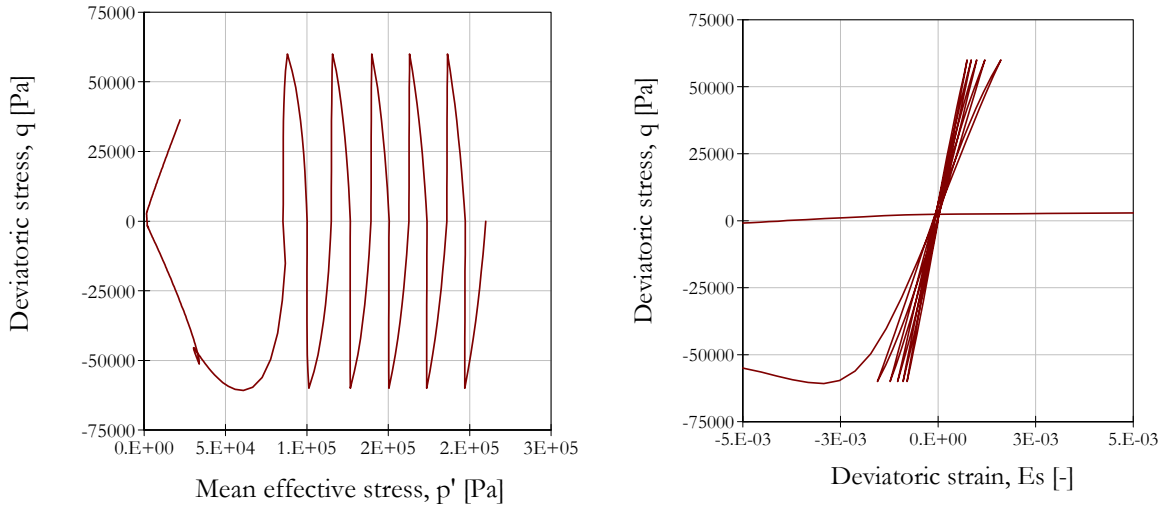

a) b)

Figure 3.4 Computed behaviour of loose Niigata sand under cyclic triaxial loading, after the empirical results of [Tatsuoka, 1972]. a) Stress path on the triaxial plane. b) Deformational behaviour.

3.1.3.3 Parameter calibration

The general procedure for the calibration of the material parameters to reproduce the behaviour of a particular sand has been described for instance in [Pastor *et al.*, 1985; Chan, 1988; Zienkiewicz *et al.*, 1999; Manzanal, 2008] and is based on the analysis and curve fitting (through trial and error) of conventional triaxial test results. The main lines of the calibration process can be summarized as follows:

- H_0 is the plastic modulus when the stress path is isotropic, so it can be estimated by adjustment of isotropic compression tests.
- The slope of the critical line M_g can be obtained from undrained triaxial tests at the point of the stress path where no change in p' is produced, i.e. at the point with vertical tangent. It can also be obtained from conventional drained triaxial tests at the point where the dilatancy changes its sign (from contractive to dilatant) or identified as the stress ratio at residual conditions.
- The parameter α_g can be obtained from the dilatancy vs. stress ratio plot of a drained triaxial test and usually ranges between 0.4 and 0.5 (most authors recommend using $\alpha_g = 0.45$). It is also a general practice to adopt $\alpha_f = \alpha_g$.

- The parameter M_f can be estimated as a proportion of M_g depending on the relative density Dr of the soil. A first estimation can be $M_f \approx Dr \cdot M_g$.
- The strain hardening parameters β_0 and β_1 are normally obtained through curve fitting (trial and error), and they usually take values around 4.2 and 0.2 respectively. Their recommended ranges are 1.5-5.0 and 0.1-0.2 [Garcia Nuñez, 2007].
- The unloading parameters $H_{U,0}$ and γ_U can be identified by curve fitting of cyclic triaxial tests at different stress levels. Specific details about the matching process are given in [Zienkiewicz *et al.*, 1999] and [Chan, 1988].
- The elastic moduli K^e_0 and G^e_0 can be obtained by matching the initial slopes of stress-strain plots of undrained tests.
- The discrete memory parameter γ affects the number of cycles before liquefaction occurs and can be obtained by matching the slope of the first reloading curve or by matching the number of cycles in an undrained test.

For the purposes of the present work, and given the frame of the project for the investigation of wind turbines in the North Sea, a special focus has been placed on the sands that can be found in the German Bight of the North Sea, which can in general be represented by the soil profiles at the Alpha-Ventus site (see for instance [FINO-Offshore]). However, a sand that can be obtained from quarries north of Berlin features very similar properties and geological origin and it has been adopted for the investigations presented here. This sand will henceforth be termed here as Berliner Sand and is described later in Section 4.2.2.

The calibration of the PZ model to reproduce the behaviour of the Berliner sand under triaxial loading is shown exemplarily in Figure 3.5 and Figure 3.6, where the experimental results have been taken from [Rackwitz, 2003]. The characteristics of the triaxial tests and their respective calibrated material parameter sets for the PZ model are given in Table 3.4 and Table 3.5 respectively.

Since no experimental data from cyclic triaxial tests with Berliner Sand have been published yet, the values for the cyclic parameters of a different sand had to be employed for the calculations, and were taken from the literature. For this purpose, the cyclic parameters calibrated for the tests by Tatsuoka [1972] with the Niigata sand have been used. The set of assumed parameters is given in Table 3.6.

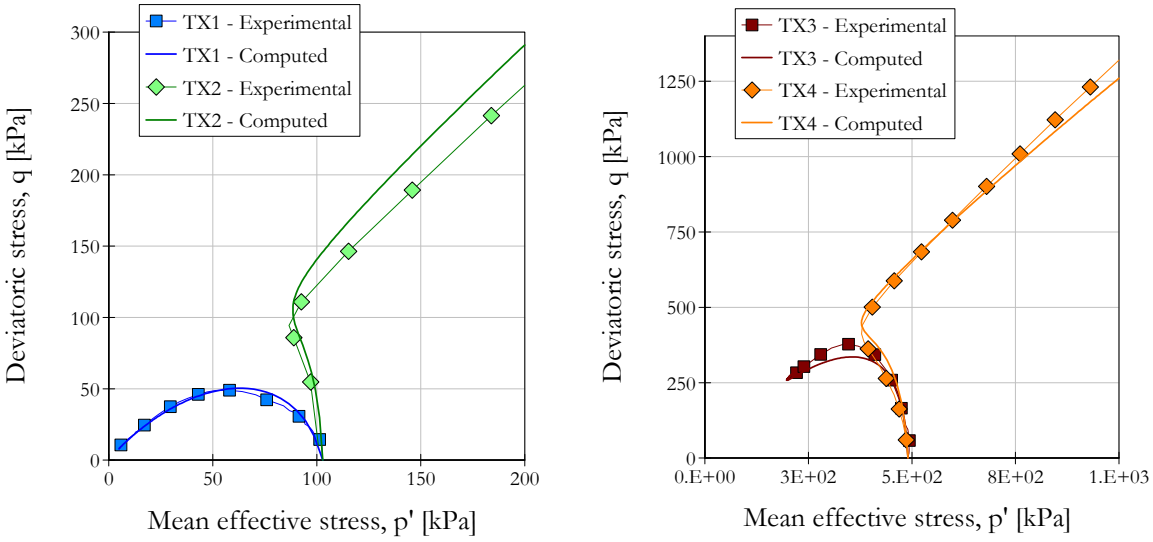

a) b)

Figure 3.5 Calibration results for Berliner sand under monotonic triaxial loading. Stress paths on the triaxial plane with a) samples at 100 kPa of initial confining pressure, and b) samples at 491 kPa of initial confining pressure.

Table 3.4 Experimental data for the calibration of the monotonic parameters of PZ model for Berliner Sand.

Case	***Confining pressure, p'0***	***Soil density, D_R***	***Data source in [Rackwitz, 2003]***
Fig. 3.5 - TX1	100 kPa	1 %	tx558 - CU
Fig. 3.5 - TX2	100 kPa	28 %	tx552 - CU
Fig. 3.5 - TX3	491 kPa	12 %	tx559 - CU
Fig. 3.5 - TX4	491 kPa	42 %	tx554 - CU
NOTE: Soil density according to German convention (Lagerungsdichte), $D_R = (\rho - \rho_{MIN}) / (\rho_{MAX} - \rho_{MIN})$			

Table 3.5 Adjustment of PZ model for Berliner Sand. Calibrated monotonic parameters.

Case	K^e_0 *[kPa]*	G^e_0 *[kPa]*	M_g *[-]*	α_g *[-]*	M_f *[-]*	α_f *[-]*	H_0 *[kPa]*	β_0 *[-]*	β_1 *[-]*
Fig. 3.5 - TX1	5500	10000	1.85	0.45	0.58	0.45	65	4.2	0.2
Fig. 3.5 - TX2	5500	10000	1.18	0.45	0.77	0.45	65	17.2	0.43
Fig. 3.5 - TX3	25000	27000	1.31	0.45	0.52	0.45	300	4.2	0.2
Fig. 3.5 - TX4	45000	27000	1.18	0.45	0.65	0.45	300	23.2	0.08

Table 3.6 Adjustment of PZ model for Berliner Sand. Assumed cyclic parameters.

Case	γ *[-]*	$H_{U,0}$ *[kPa]*	γ_U *[-]*
Cyclic TX - Berliner Sand	1	250	5

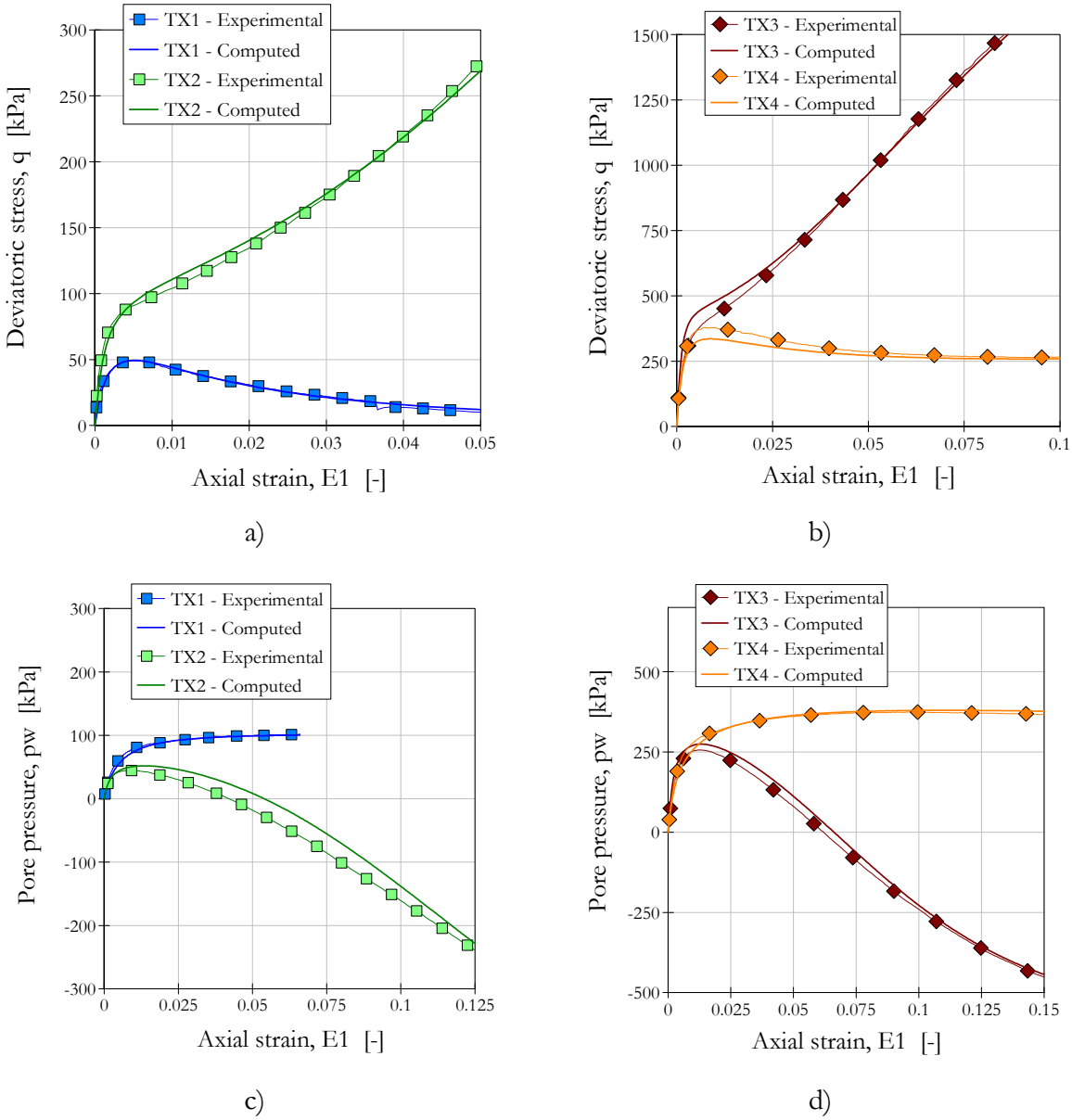

Figure 3.6 Calibration results for Berliner sand under monotonic triaxial loading. Deformational behaviour of a) samples at 100 kPa of initial confining pressure, and b) samples at 491 kPa of initial confining pressure. Pore pressure evolution in c) samples at 100 kPa of initial confining pressure, and d) samples at 491 kPa of initial confining pressure.

As a final remark to this section, it may be worth to stress the importance for the simulation of the general boundary value problem of the use of an adequate calibration set, in terms of the conditions of density and pressure. In contrast to the case of elementary tests, the offshore foundation normally features a soil with varying densities and confining pressures, which implies a material with varying parameters unless an appropriate state parameter is incorporated.

In the course of these investigations, that was found to have indeed a certain impact on the numerical stability of the PZ model. Calculations with a set of parameters calibrated for high pressures tended to present stability problems at points in the shallow layers of the soil, i.e. at low confining pressures, while the model seemed to respond "better", i.e. more stable, when the parameter set calibrated for the low pressures was used. This is probably due to the fact that whenever problems arise, they tend to appear in the low pressure regions (shallow soil layers) and hence a good calibration for lower pressures might work better. In any case, the use of the extended PZ model with state parameter [Manzanal *et al.*, 2010] seems very promising and it might mitigate these problems to some extent.

3.2 Element Technology

The set of mathematical, numerical and constitutive models described so far provides in essence the basic requirements for the numerical analysis of the foundation. However, there are certain practical aspects and restrictions that need to be observed in order to avoid the appearance of spurious (unphysical) or wrong solutions. In this respect, the particular case of the offshore pile brings about some further requirements that will be discussed in the following sections.

In principle, due to the high computational cost of the three-dimensional modeling, it appears desirable to use finite elements with low-order interpolations, like the classical 8-node hexahedron, in order to keep the total number of degrees of freedom within affordable margins. However, the use of such elements entails some limitations, as poor bending behaviour or locking phenomena under certain conditions (see for instance [Zienkiewicz & Taylor, 2000] or [Pastor *et al.*, 2002]).

Conventional first-order elements (i.e. elements with linear shape functions) subject to bending conditions suffer from shear stiffening, often termed also as shear locking, and will show spurious shear strains [Andelfinger & Ramm, 1993; Cerioni *et al.*, 1995; Pastor *et al.*, 2002].

In order to overcome this problem, an efficient alternative to the use of higher-order elements was proposed in the early seventies by Wilson *et al.* [1973] with the introduction of the element with incompatible displacement modes, which was later extended and generalized by several authors (Taylor *et al.* [1976] and Ibrahimbegovic & Wilson [1991] among others) and especially by Simo and Rifai with their enhanced-strain element [Simo & Rifai, 1990].

A further limitation of the classical elements is that in conditions of near incompressibility they tend to show a volumetric locking that affects the quality of the results, often leading to wrong limit loads, inadequate failure mechanisms or even to a "blocked" system where the nodes cannot move at all (see for instance [Zienkiewicz & Taylor, 2000], [Pastor *et al.*, 2002], and [Mira, 2001]).

It must be noted, that the condition of near-incompressibility (i.e. where values of the Poisson ratio are close to 0.5) can also be given in problems with saturated soils and fast loading or undrained conditions, or in elastoplastic problems involving plastic flow at constant volume [Pastor *et al.*, 2002; Mira, 2001]. Furthermore, since this problem affects all kinds of displacement-based finite elements to some extent, the locking phenomena should in general not be discarded a priori and awareness of this problem should always be exercised.

The most popular methods to mitigate the volumetric locking are the use of higher-order elements, the reduced integration elements*), the enhanced-strain elements of Simo and Rifai, and the mixed displacement-pressure formulations [Zienkiewicz & Taylor, 2000], being the last two the best choices according to Pastor *et al.* [2002].

In this work, a special implementation of the Simo-Rifai element due to Mira *et al.* [2003], which also features pressure stability in coupled problems, has been employed. Such implementation is described in the next section along with the so-called Babuska-Brezzi restriction.

3.2.1 Special issues for the transient simulation of an offshore pile

In order to model adequately the laterally loaded offshore pile, several additional requisites must be met. Apart from the fact that only a full 3D model can be used, since the axial symmetry is no longer valid due to the lateral loading**), special care has to be taken when modeling the pile-soil interface. An important feature of laterally loaded piles is the possible formation of a gap behind the pile as the loading progresses, and, therefore, the ability to model a discontinuous interface has to be somehow included. A natural way to do this is to define the interaction between pile and soil as a multi-body contact problem, as described for instance in [Wriggers & Simo, 1985; Wriggers & Imhof, 1993; Belytschko *et al.*, 2000], with the introduction of the "master-slave" surface concepts and an efficient contact detection algorithm.

*) The reduced integration methods employ an integration rule of lower degree than the one required for the exact integration of the polynomials existing in the stiffness matrix, and have the advantages of lower computational cost and improved incompressibility performance, but in some cases with ill conditioning they can show spurious bending modes, the non rigid-body zero-energy deformation modes, also known as "hourglass modes". This problem can be mitigated by using appropriate control methods (hourglass control) and selective integration (see for instance [Zienkiewicz & Taylor, 2000]).

**) The inherent axial symmetry of the pile foundation's geometry can in general not be exploited for the problem at hand due to the lateral loading and non-linear soil behaviour. However, the Fourier Series Aided Finite Element Method (FSAFEM) has been proposed as a means to overcome this limitation (see for instance [Ganendra, 1993], [Potts & Zdravkovic, 1999] or [Hardy, 2003]). It generally employs a 2D geometry and assumes that the out-of-plane displacements can be represented by a Fourier series. Extensions of the method for nonlinear analysis have been proposed, but they are in general restricted to cases where the constitutive tangent stiffness matrix D is constant in the out-of-plane direction θ. Otherwise, special iterative solution techniques must be adopted [Potts & Zdravkovic, 1999], with a consequent increase in computational cost and/or loss of accuracy.

An alternative approach, which can be conveniently implemented into a FE code without major changes, is the use of special interface "joint" elements to allow for differential movement (slip and separation) between pile and soil [Potts & Zdravkovic, 1999]. The isoparametric joint element, described e.g. by Carol and Alonso [1983], can be suitably adapted to reproduce no-tension conditions (i.e. gap opening) by simply defining a non-linear normal stiffness (discontinuous in this case) with different values for tension and compression. However, joint elements might present problems of numerical instability and ill-conditioning and should be handled with care (see e.g. [Day & Potts, 1994]). The no-tension joint element implemented and used for this work is described below, in Section 3.2.3.

On the other hand, the coupling with pore water pressure brings about an additional restriction, namely the so-called Babuska-Brezzi condition [Babuska, 1973; Brezzi, 1974], which implies that the order of interpolation for the displacement field must be higher than that for the pressure field if the permeability is very low (nearing undrained incompressible conditions). In such cases, both the permeability and compressibility matrices H and C in equation (3.79) tend to zero, producing a system of equations in the form of

$$\begin{bmatrix} A & B \\ C & 0 \end{bmatrix} \begin{bmatrix} \xi \\ \varphi \end{bmatrix} = \begin{bmatrix} f_\xi \\ f_\varphi \end{bmatrix} \tag{3.113}$$

which will be singular and present pore pressure oscillations unless the number of variables in ξ is greater than in φ or special stabilization techniques are employed [Fernandez Merodo & Pastor, 2002].

This leads to the dilemma of either using the "expensive" quadratic interpolation for displacements (e.g. the 20-node hexahedron with 8 nodes for the pressure field h20p8), or resorting to some special techniques, like the stabilized elements from fluid mechanics (see the divergence, fractional-step or alpha methods, e.g. in [Brezzi & Pitkaranta, 1984; Chorin, 1968; Pastor *et al.*, 1996; Hughes *et al.*, 1986; Oñate, 2000]) or special implementations of enhanced-strain elements as shown in [Mira *et al.*, 2003; Mira *et al.*, 2004]. The latter provide the additional advantages inherent to the enhanced-strain elements, namely a better performance in bending and the prevention of locking [Mira, 2001]. This is the option that has been used for the present investigations, and is described in the next section.

At this point it is important to stress that the term "very low permeability" is a relative one, in particular relative to the element size. From the author´s experience, even high permeability values typical of clean sands (around 10^{-4} m/s) may cause pore pressure instabilities if the element size is big enough, like for instance when modeling real offshore prototypes which might incor-

porate element dimensions of half a meter or bigger. Therefore, the possibility of pressure oscillations should not be excluded "a priori", regardless of the soil permeability. In this respect, the use of high-order or special element implementations might be unavoidable for the particular case of real-size offshore foundation prototypes.

3.2.2 The stabilized enhanced strain Simo-Rifai formulation

The enhanced assumed strain (EAS) formulation basically consists in expanding the field of compatible strains*), normally obtained through the kinematic relationship (3.10), with an additional field of strains $\tilde{\varepsilon}$, which is not bound to continuity restrictions between elements (see [Simo & Rifai, 1990]). This way, the enriched strain field can in general be expressed as

$$\varepsilon = Su + \tilde{\varepsilon} \tag{3.114}$$

where now, for the finite element formulation, the new additional field variable $\tilde{\varepsilon}$ can be approximated through a corresponding vector of (internal) degrees of freedom $\bar{\alpha}$ and a suitable matrix of (internal) shape functions $\boldsymbol{G}$ in the following form:

$$\tilde{\varepsilon} = G\,\bar{\alpha} \tag{3.115}$$

where the interpolation matrix $\boldsymbol{G}$ is the analogous to the discrete strain operator $\boldsymbol{B}$ expressed in (3.50), but applied to the local enhanced strain parameters $\bar{\alpha}$, and takes the following general form:

$$G = g(\xi,\eta,\zeta)\,E(\xi,\eta,\zeta) \tag{3.116}$$

Here, ξ, η and ζ are the isoparametric coordinates of the finite element and the matrix $\boldsymbol{E(\xi,\eta,\zeta)}$ contains the polynomial shape functions for the new field $\tilde{\varepsilon}$ in the isoparametric space, while $\boldsymbol{g(\xi,\eta,\zeta)}$ defines their transformation into the global frame (see [Simo & Rifai, 1990] or [Andelfinger & Ramm, 1993] for more details). In general, many different sets of functions can be chosen for the interpolation of the additional strains, but as shown in [Andelfinger & Ramm, 1993], the simplest expansion which is free of volumetric locking for an 8-node element is given by

*) Strain compatibility implies here just consistency with the compatible (continuous) displacement field through the kinematic relationship. However, strictly speaking both strain terms in the r.h.s. of (3.114) are incompatible (strain fields are never compatible, only displacements are), as pointed out by Mira [2010].

$$E(\xi,\eta,\zeta) =$$

$$= \begin{bmatrix} \xi & 0 & 0 & 0 & 0 & 0 & 0 & 0 & 0 & 0 & 0 & 0 & 0 & 0 & 0 & \xi\eta & \xi\zeta & 0 & 0 & 0 & 0 \\ 0 & \eta & 0 & 0 & 0 & 0 & 0 & 0 & 0 & 0 & 0 & 0 & 0 & 0 & 0 & 0 & 0 & \xi\eta & \eta\zeta & 0 & 0 \\ 0 & 0 & \zeta & 0 & 0 & 0 & 0 & 0 & 0 & 0 & 0 & 0 & 0 & 0 & 0 & 0 & 0 & 0 & 0 & \xi\zeta & \eta\zeta \\ 0 & 0 & 0 & \xi & \eta & 0 & 0 & 0 & 0 & \xi\zeta & \eta\zeta & 0 & 0 & 0 & 0 & 0 & 0 & 0 & 0 & 0 & 0 \\ 0 & 0 & 0 & 0 & 0 & \xi & \zeta & 0 & 0 & 0 & 0 & \xi\eta & \eta\zeta & 0 & 0 & 0 & 0 & 0 & 0 & 0 & 0 \\ 0 & 0 & 0 & 0 & 0 & 0 & 0 & \eta & \zeta & 0 & 0 & 0 & 0 & \xi\eta & \xi\zeta & 0 & 0 & 0 & 0 & 0 & 0 \end{bmatrix} \tag{3.117}$$

which expands the expressions of the compatible strains with 21 additional polynomial terms in the isoparametric space (i.e. it includes 21 additional deformation modes). In principle, simpler expansions with only 9 or 15 additional terms could be used in order to improve the bending capabilities of the 8-node element, but as shown in [Mira *et al.*, 2003] for an analogous element in 2D, those kinds of formulations are not stable in the Babuska-Brezzi sense.

Now introducing the enriched strain field into the corresponding places of the governing equations, the processes of spatial and temporal discretisation can proceed in exactly the same fashion as before (i.e. firstly a Galerkin weighted residual formulation and then a Generalized Newmark temporal recurrence relation, both applied as well to the new internal variable $\overline{\alpha}$, and linearized with a Newton-Raphson scheme). As shown in [Mira *et al.*, 2003] for the consolidation case, where the accelerations are disregarded, this leads to the following system of linear equations

$$\begin{bmatrix} {K_T}^* \beta\Delta t & -Q^* \theta\Delta t \\ (Q^*)^T & H\theta\Delta t + C^* \end{bmatrix} \begin{Bmatrix} d(\Delta\dot{\overline{u}}_N) \\ d(\Delta\dot{\overline{p}}_N) \end{Bmatrix} = -\begin{Bmatrix} {F_U}^* \\ {F_P}^* \end{Bmatrix} \tag{3.118}$$

where now

$${K_T}^* = K - \Gamma^T {H_\alpha}^{-1} \Gamma \tag{3.119}$$

$$Q^* = Q - \Gamma^T {H_\alpha}^{-1} Q_\alpha \tag{3.120}$$

$$C^* = C + \frac{\theta}{\beta} {Q_\alpha}^T {H_\alpha}^{-1} Q_\alpha \tag{3.121}$$

$${F_U}^* = F_U - \Gamma^T {H_\alpha}^{-1} F_\alpha \tag{3.122}$$

$${F_P}^* = F_P - \frac{1}{\beta\Delta t} \Gamma^T {H_\alpha}^{-1} F_\alpha \tag{3.123}$$

Here, $\boldsymbol{K}$, $\boldsymbol{Q}$, $\boldsymbol{C}$ and $\boldsymbol{H}$ are the same as in the standard formulation and $\boldsymbol{\Gamma}$, $\boldsymbol{Q_\alpha}$ and $\boldsymbol{H_\alpha}$ are defined as

$$\Gamma = \int_\Omega G^T D^{EP} B d\Omega \tag{3.124}$$

$$Q_\alpha = \int_\Omega G^T m N_P d\Omega \tag{3.125}$$

$$H_\alpha = \int_\Omega G^T D^{EP} G d\Omega \tag{3.126}$$

and the corresponding residuals can be evaluated at element level through the following advancing relations

$$F_U{}^{n+1} = f_U{}^{n+1} - K\left(\overline{u}^n + \Delta t\dot{\overline{u}}^n\right) - \Gamma\left(\overline{\alpha}^{n+1} + \Delta t\dot{\overline{\alpha}}^n\right) + Q\left(\overline{p}^n + \Delta t\dot{\overline{p}}^n\right) \tag{3.127}$$

$$F_\alpha{}^{n+1} = -\Gamma\left(\overline{u}^n + \Delta t\dot{\overline{u}}^n\right) - H_\alpha\left(\overline{\alpha}^{n+1} + \Delta t\dot{\overline{\alpha}}^n\right) + Q_\alpha\left(\overline{p}^n + \Delta t\dot{\overline{p}}^n\right) \tag{3.128}$$

$$F_P{}^{n+1} = f_P{}^{n+1} - Q^T\dot{\overline{u}}^n - C\dot{\overline{p}}^n - H\left(\overline{p}^n + \Delta t\dot{\overline{p}}^n\right) \tag{3.129}$$

At this point, the following remarks can be made:

- The new expressions in (3.118) have exactly the same form as in the standard formulation but with different values for the stiffness, permeability and coupling matrices (compare it for instance with the saturated consolidation formulation in the Appendix A.3).
- This stabilized element has similar precision as the expensive 20-node hexahedron h20p8, i.e. quadratic precision in displacements and linear precision in pressures.
- In conditions nearing undrained incompressibility, no spurious pressure oscillations appear, despite H and C tending to zero.
- The local enhanced strain parameters $\overline{\alpha}$ do not appear explicitly in the linear system (they have been eliminated from the equations by static condensation). This means that the number of global degrees of freedom is exactly the same as before. Therefore, at the global level, the computational cost of this element is comparable to the standard first-order h8p8 element, and significantly lower than for the quadratic h20p8 element.
- With respect to the first-order (unstable) h8p8 element, the new formulation only requires additional computations at the element level stemming from the static con-

densation of the local strain parameters $\overline{\alpha}$. This additional cost may be roughly proportional to the number of elements in the mesh (see [Mira *et al.*, 2003]).

3.2.3 Pile soil interface and contact problem

The sharp discontinuity of physical and mechanical properties arising at the pile-soil interface can in principle be introduced into the analytical model in many different ways. From a topological point of view, the different methods to do this may be classified into three main groups:

i. Models with no explicit interface, where the neighbouring materials share a certain set of nodes and element faces, which implicitly constitutes the interface.

ii. Models with explicit interface elements, where a specific entity (be it a continuum model, a set of springs between nodes, or the so called joint elements) is assigned with the particular properties of the interface. In general, the interface entity connects the neighbouring bodies in a predefined way, and hence the connectivity between elements and nodes at both sides of the interface is fixed (i.e. every node or element of the pile boundary can only interact with a certain node or element of the soil boundary).

iii. Multi-body problems with contact constraints, where the interacting bodies are modelled separately (i.e. the contacting meshes don't need to match) and the compatibility of forces and displacements at the interface is ensured through constraint equations.

It seems clear that the first option is in general not suitable for the analysis of laterally loaded piles, where the possibility of differential displacements at the interface (slip and/or separation) usually plays a relevant role. However, an improvement of this type of models is the so-called "discrete crack" approach, as proposed for instance in [Skrikerud & Bachmann, 1986], where upon fulfillment of a certain condition (e.g. the average stress at the neighbouring elements exceeding a given value), the shared nodes are split into pairs of new nodes and then the elements are allowed to separate [Tzamtzis & Asteris, 2004]. But even so, this approach presents several inconvenients, as for instance the problem of a strong mesh dependency or the variable number of nodes, which implies sudden changes in the size and bandwidth of the assembled Jacobian matrix. A further option, which can replicate well the macroscopic response of a continuum intercepted by a discontinuity, is the smeared crack approach (e.g. in [Norman & Anderson, 1985;

Mlakar, 1987; Pietruszczak, 1999]). These methods are based on a suitable averaging of the material properties at the integration points of regular continuum elements in order to account for the discontinuity. This way, the formation of a crack doesn't involve a remeshing or new degrees of freedom and the topology of the interface does not need to be known beforehand. These approaches are very suitable for cases where the discontinuities are indeed "smeared out" within the failing material, as in reinforced concrete or bonded masonry applications (see e.g. [Shieh-Beygi & Pietruszczak, 2008]), and they also have been used for modelling the opening of discrete joints (e.g. in [Kuo, 1982]) but in any case they have only limited ability to model sharp discontinuities and in general they present difficulties to reproduce the local topology and material behaviour in the immediate vicinity of the crack [Tzamtzis & Asteris, 2004].

The second main group of methods encloses a wide range of techniques, including for instance the simple discrete springs between opposite nodes (e.g. in [Herrmann, 1978; Frank *et al.*, 1982]), the thin continuum interface elements (e.g. in [Pande & Sharma, 1979; Griffiths, 1985]), and especially, the so called joint elements, firstly introduced by Goodman *et al.* [1968] in rock mechanics for jointed rock masses and later reformulated and extended by many authors for particular features as zero thickness and isoparametric formulations (see for instance [Mahtab & Goodman, 1970; Ghaboussi *et al.*, 1973; Beer, 1985; Carol *et al.*, 1986; Boulon *et al.*, 1995]). The first two options (the discrete springs and the standard continuum elements) are very easy to implement but only offer a very limited representation of the interface and shall not be considered further here. On the other hand, the isoparametric zero-thickness joint element seems to be particularly well suited for a wide range of engineering problems (as the laterally loaded pile problem) due to the simplicity and flexibility of its formulation, and is probably the most commonly used approach for geotechnical applications [Potts & Zdravkovic, 1999].

The third group of methods, which generally involve the introduction of the "master-slave" surface concepts and an efficient kinematic constraint algorithm (usually the node-to-segment or node-to-surface approaches), probably offers the most realistic description of the interface, since here the pairs of contacting points are not univocally defined a priori and any kind of frictional relation may be defined between the surfaces (see for instance [Zavarise *et al.*, 1992], [Wriggers & Imhof, 1993], [Zavarise *et al.*, 1998] or the recent [Haraldsson, 2003] where a detailed description of the frictional behaviour between soil and concrete has been introduced). However, in general they are computationally more expensive, they still present problems of ill-conditioning (they often use a penalty method and very high contact stiffnesses to minimize the body interpenetrations) and their implementation into pre-existing FE codes is not straightforward.

Since in the problem at hand the contact topology is fairly simple (the pile just moves back and forth and the contact element couplings in principle do not change much) and given that the interest of this numerical study lies on the evolution of pore pressure within the soil mass rather than on the mechanical processes at the interface, the potential benefits of a complex interface description did not justify the implementation and computational costs of a full contact problem. Hence, a no-tension joint element formulation with slip and separation capabilities has been implemented and used for this work instead.

The formulation originally implemented in GeHoMadrid is based on the isoparametric joint element of Zienkiewicz *et al.* [1970], where the stresses and strains along the natural coordinates of the interface element are related through a linear elastic constitutive relationship as follows:

$$\begin{Bmatrix} \tau_\xi \\ \tau_\zeta \\ \sigma_\eta \end{Bmatrix} = \begin{bmatrix} G_S & 0 & 0 \\ 0 & G_S & 0 \\ 0 & 0 & E_N \end{bmatrix} \begin{Bmatrix} \gamma_\xi \\ \gamma_\zeta \\ \varepsilon_\eta \end{Bmatrix} \tag{3.130}$$

where $\boldsymbol{G_S}$ and $\boldsymbol{E_N}$ are the elastic shear and normal stiffnesses respectively and the interface stresses are oriented as shown in Figure 3.7. The interface strains are simply defined as the relative displacements of the top and bottom surfaces along the natural coordinates.

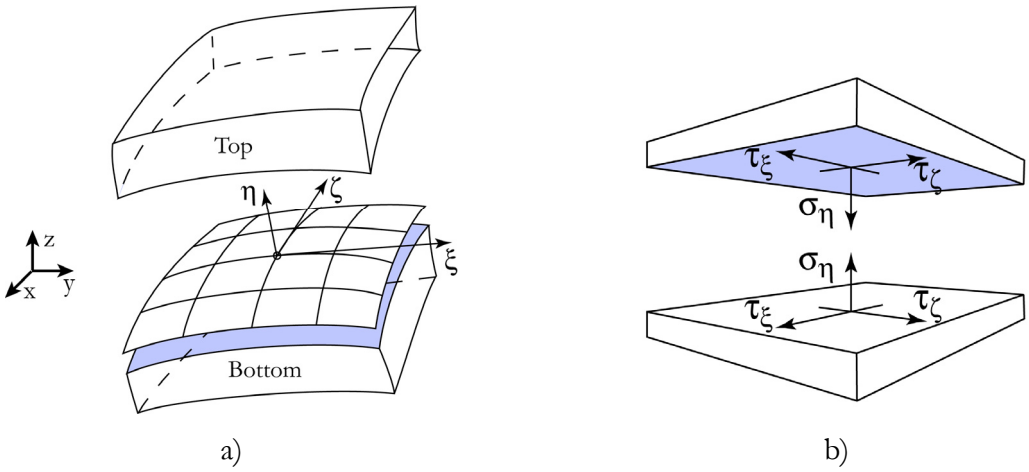

Figure 3.7 a) Three-dimensional isoparametric joint element. b) Definition of interface stresses (after [Carol *et al.*, 1986])

The no-tension condition can be easily implemented by monitoring the normal strain and keeping the interface stresses set to zero whenever the normal strain is positive (i.e. when a gap opens at the interface), so that the residual tensile stresses are redistributed to the neighbouring elements via the nonlinear algorithm.

However, such bilinear nature of the stiffness will in general lead to convergence problems at points where the joint state changes (mainly when the joint is closing) and especially if an initial state of stress is assumed in the boundary-value problem, since that implies an offset of strains and displacements while keeping the initial stresses. In such cases, the amount of offset initial strain needs to be recorded and used for the proper definition of the "breaking point" where the normal stiffness changes from $\boldsymbol{E_N}$ to zero.

In any case, a second alternative formulation has been introduced in order to alleviate the abrupt nonlinearity of the "no-tension" element during the transitions between tension and compression (between open and closed states of the joint). The regularisation consists in the substitution of the abrupt bilinear stiffness law by a "smoother" function with continuous derivative in the origin, which is the problematic point. For such purpose, an exponential law with horizontal asymptote in tension and tangent to the linear elastic law in compression can be suitable.

On the other hand, the adoption of a regularisation implies the introduction of "undesired effects", as shown in Figure 3.8. There, the linear elastic law is shown in discontinuous line and three possible regularisations are drawn in solid lines. The smoothed function will be then in one of the following situations: 1) either not passing through the origin of stresses and strains (blue line in the figure), or 2) implying a state of residual stresses in tension (red line), or 3) shifted in compression with respect to the linear law (green line). The severity of these problems grows with the degree of regularisation, so the smoother the function, the bigger the offsets, either in stresses or strains.

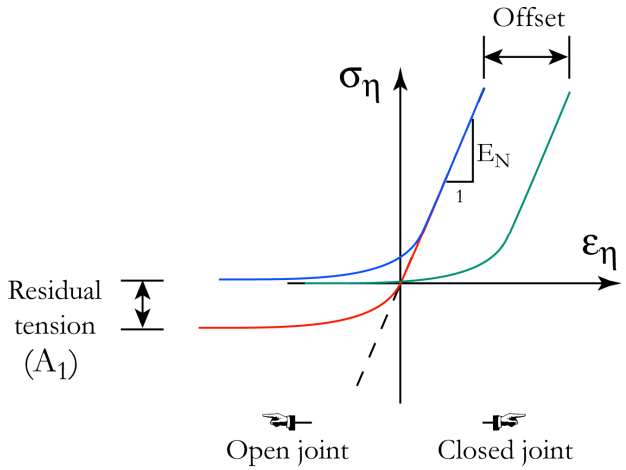

Figure 3.8 No-tension contact stiffness laws with exponential regularisation at the origin of stresses and strains.

Therefore, a trade-off between speed of convergence and undesired effects will be inevitable. In this respect, a combination of low values of the residual tension and big values of normal stiff-

ness, as in principle would be desirable, implies that the slope of the function changes dramatically in a very narrow region close to the origin, although it does so in a continuous way.

For these calculations, a function with residual state of stress in tension was chosen. With the sign convention assuming positive normal stress in tension and positive normal strains when the joint opens, the function can be described piecewise in the following manner:

$$\begin{cases} \sigma_\eta = A_1 \cdot \left(1 - e^{-A_2 \cdot \varepsilon_\eta}\right) & whenever \quad \varepsilon_\eta > 0 \\ \sigma_\eta = E_N \cdot \varepsilon_\eta & whenever \quad \varepsilon_\eta \le 0 \end{cases} \tag{3.131}$$

where $\boldsymbol{E_N}$ is the normal stiffness in compression (assumed constant), $\boldsymbol{A_1}$ is the value of the residual tension to be allowed, and $\boldsymbol{A_2}$ can be easily calculated as $\boldsymbol{E_N}$ divided by $\boldsymbol{A_1}$. This way, the tangent normal stiffness at any point of the tensile region $\boldsymbol{K_N}$ would be defined as:

$$K_{N,TENSION} = \frac{\partial \sigma_\eta}{\partial \varepsilon_\eta} = A_1 A_2 \cdot e^{-A_2 \varepsilon_\eta} = E_N \cdot e^{-A_2 \varepsilon_\eta} \tag{3.132}$$

which tends to zero as the normal strain grows and is regular at the origin, where it tends to the compressive stiffness value $\boldsymbol{E_N}$.

Additionally, the interface shear stresses can also be limited through any suitable failure condition, usually of the Mohr-Coulomb or Drucker-Prager type, and may be expressed as

$$F = \sqrt{\tau_\xi^{\,2} + \tau_\zeta^{\,2}} + \sigma_\eta \, tan\,\varphi' - c \tag{3.133}$$

where $\boldsymbol{\varphi'}$ is the maximum angle of shearing resistance and $\boldsymbol{c}$ the allowed cohesion, which equals to the residual normal tensile threshold $\boldsymbol{A_1}$ times *tan(**φ'**)*.

To conclude this section, the following remarks can be made:

- The assumption of a diagonal constitutive matrix in (3.130) implies that there is no coupling between shear and normal components and therefore the behaviour of the joint is non-dilatant.
- The interface strains are not dimensionless but have length dimensions, and therefore now the shear and normal stiffness moduli are expressed in units of (force/length^3).
- Independently of the convergence problems when the contact state changes, the joint element may still present problems of numerical instability in cases where the contact stiffnesses are very different from those of the adjacent elements (ill-conditioning) and therefore should be handled with care. Guidelines for the choice

of the stiffness values can be found for instance in [Day & Potts, 1994; Potts & Zdravkovic, 1999].

- The joint element described so far is not coupled with the pore pressure field and hence constitutes a non-permeable boundary, even when the joint is open. The drainage condition in the open interface may be defined by enforcing that the pore pressure be equal to a hydrostatic reference pressure whenever the normal contact strain is positive (i.e. when a gap opens). However, such procedure may aggravate the convergence difficulties, since it may imply an abrupt change in the pressure field at the opening boundary. In any case, since the problem at hand involves a cohesionless soil where in general only slip but not separation may occur at the pile-soil interface (see Figure 3.9), such drainage capability has not been considered necessary and thus not been implemented yet.

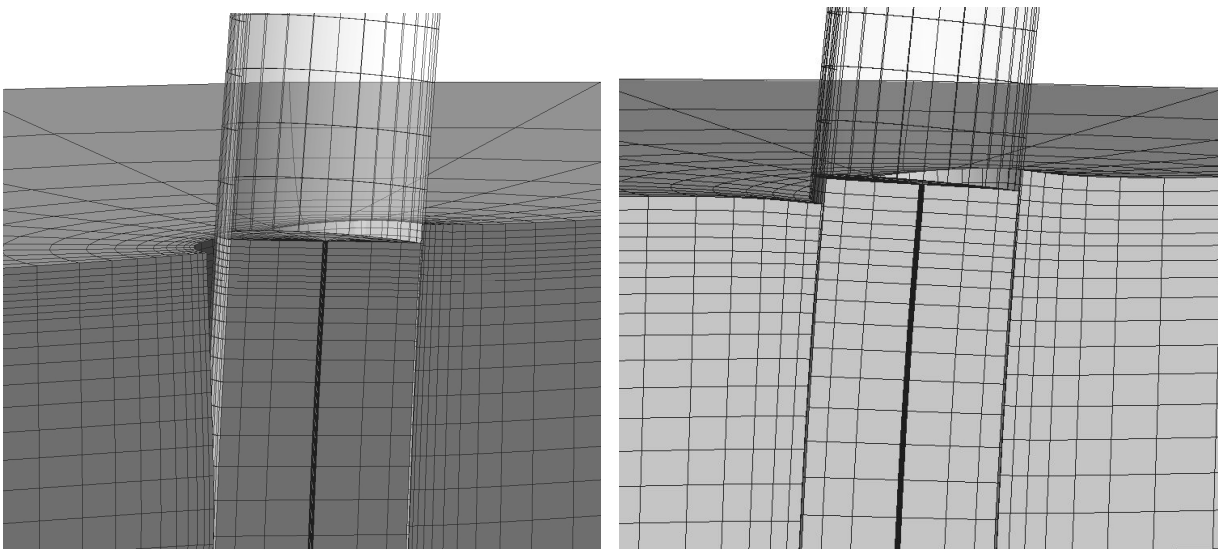

Figure 3.9 Simulated pile-soil interface contact behaviour in dependence of the soil nature. a) Gap opening in a cohesive soil. b) Tangential slip but no surface separation for a pile in cohesionless soil.

3.3 Optimization of the Computational Cost

The motivation for this section is the critical issue of the computational cost and the imperious necessity to optimize it, for instance through the choice of an appropriate solution strategy, an efficient handling of the sparse matrices and specially a parallel computation. Without such optimizations, the cost of the calculations proposed in this chapter would have been simply unaffordable.

As it is often the case, the main drawback of 3D modeling stems from the large amount of degrees of freedom being considered, where in a typical case the assembled Jacobian matrix can easily include tens or hundreds of thousands of rows and columns (i.e. billions of entries). Moreover, the transient problem at hand involves a highly nonlinear constitutive model and requires a low error tolerance criterion in order to preserve the numerical stability of the solution and keep the accumulated error as low as possible, which in turn increases the number of iterations required for convergence per time step. Consequently, a linear system in the order of 10^5 equations will have to be solved from 10^3 to 10^4 times for the computation of every single load cycle, which highlights the importance of the choice of an appropriate solution strategy.

3.3.1 Solution strategies

A crude and rather inefficient method for solving the sparse linear system Ax=b when A is square and nonsingular is to compute the inverse A^{-1}. This is numerically unstable when A is ill-conditioned and also very costly, since normally the inverse of a sparse matrix has no zero entries at all [Davis, 2006].

In principle, iterative solvers like the preconditioned conjugate gradient or the Jacobi methods, are adequate choices for large problems and can be programmed easily using Fortran or C [Pastor *et al.*, 2002]. However, they are only conditionally convergent and in general cannot deal with non-symmetric matrices, which makes them unsuitable for problems with non-associative materials like sand. In order to solve non-symmetric systems of equations, special schemes such as the generalized minimum residual (GMRES) will be required, which are considerably more complex

and costly than their symmetric counterparts (see for instance [Barrett *et al.*, 1994] or [Gutknecht, 2005] for comprehensive reviews of the main options).

On the other hand, direct solvers like the Gaussian elimination method are in principle unconditionally stable and require relatively few changes to deal with non-symmetric systems, but as the size of the system grows their computational and storage cost can become prohibitive. As shown in [Dongarra *et al.*, 1998], the direct solution of a system of order n requires $O(n^2)$ storage and $O(n^3)$ floating-point operations. To alleviate this problem, the sparsity of the matrix can be exploited in order to reduce the storage and number of operations, for instance with special storage schemes (like the skyline or the compressed-column, as described in the next section) or by additionally performing suitable row and column permutations to reduce the amount of fill-in during factorization [Davis, 2006]. The aim of the sparse algorithms is to perform the solution in a number of operations proportional to $O(n) + O(\tau)$, being τ the number of non-zero entries of the matrix.

But then, "hybrid" approaches that combine the advantages of both types of solvers have been recently proposed (see for instance [Schenk & Gärtner, 2004], [Manguoglu *et al.*, 2009] or [Hartmann *et al.*, 2009]) where the LU decomposition (direct Gaussian solver) is only performed at the first step of the simulation and then for the following steps the algorithm resorts to an iterative scheme preconditioned with the previous LU decomposition. Whenever the convergence of the iterative scheme fails or if the convergence rate gets below a predefined threshold, the hybrid solver switches back to a direct scheme and performs an update of the LU decomposition. Such approach seems particularly well suited for transient FE calculations as the ones proposed here, since the progressive and rather smooth nature of the wave loading implies that the changes in the system, and thus the changes in the assembled matrix, are not abrupt and, hence, a single LU decomposition can be stored and used for many steps without having to update it too frequently.

In any case, regardless of the type of solver to be used, the management of data traffic and memory locality can have a decisive impact on the overall efficiency of the algorithms. The performance of a solver can indeed be dominated by the amount of data traffic rather than the number of operations involved [Dongarra *et al.*, 1998]. Most computers nowadays include temporary fast-access blocks of memory called caches, where frequently-used data is stored. Since the data flow from the main memory is very expensive (has a much longer access time), an efficient use of the caches can be critical for the performance.

This way, when the processor requests some data, it first checks whether that data is already contained in the caches. If that is the case (a so-called cache hit), it fetches the data directly from there, and otherwise (a cache miss), it has to get it from the main memory, which takes normally

around 10 times longer than from the cache. When data is obtained from the main memory, a copy is stored in the cache. By exploiting the spatial and temporal locality of data access, i.e. trying to make all references to an area of stored data consecutively, it is possible achieve a high percentage of cache-hits and therefore speed up the data transfer considerably.

This has motivated a restructuring of existing algorithms and new methods that minimize the data movement have arisen. Among these, the BLAS (Basic Linear Algebra Subprograms) and the LAPACK (Linear Algebra PACKage) constitute a key building block that provides efficient subroutines for basic vectorial and matrix operations. This way, it can very advantageous to organize the calculations so that the matrices are partitioned into small blocks that fit in the caches and then perform the computations by matrix-matrix operations on the blocks. This constitutes the basis for the so-called supernodal and multifrontal approaches for the LU factorization, which can obtain very high performances and have been thoroughly described in [Davis, 2006].

In the author's experience, the use of a solver with BLAS and LAPACK subroutines, along with the efficient sparse strategies described in the next section, was the main source of savings in computational time, specially for smaller problems (say, with up to ~10^4 degrees of freedom). Bigger cases did require some degree of computing parallelism (see Section 3.3.3), but in any case the importance of the cache efficiency and sparse strategies was always considerable.

3.3.2 Handling of the sparse matrices

As it is well known, in FE calculations the storage of the full assembled Jacobian matrix is often extremely inefficient since that matrix is usually very sparse (i.e. with only few non-zero components). A popular and widely used storage method is the so-called skyline (or profile) format, which employs two arrays for saving the data and their location (see for instance [Marques, 1993]) and typically reduces the storage requirements to a 10% of the original full size matrix. However, such format is still inefficient since it stores all zero components between the matrix diagonal and the skyline, which may still outnumber the non-zeros in a proportion of 70 to 1 in a typical case, and therefore renumbering techniques might be needed in order to reduce the diagonal bandwidth of the matrix. Figure 3.10 illustrates this problem for the typical assembled matrix used in these investigations.

In contrast, modern solution algorithms tend to use the so-called compressed (or Harwell-Boeing) storage formats [Duff *et al.*, 1992; Demmel *et al.*, 2009; Schenk & Gärtner, 2009], which

by using three data arrays disregard all zero components of the matrix. As shown in [Dongarra *et al.*, 1998], just by disregarding all zero components of the matrix, not only the storage requirements but also the number of floating point operations needed for the solution of the linear system is reduced dramatically.

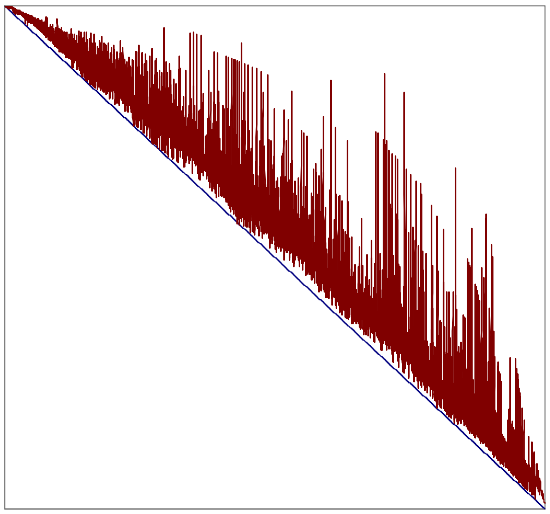

Figure 3.10 Skyline profile of the typical assembled Jacobian matrix used in this work

Additionally, if a direct solution scheme is being used, the rows and columns of the matrix can be permuted in what is normally termed a reordering stage, so that the sparsity is preserved throughout the solution process (the LU factorization normally "fills" many zero components with non-zero values, making the L and U factors denser than the original matrix). A suitable permutation of rows and columns can minimize the amount of fill-in and consequently reduce the storage and computational cost. This can be particularly interesting for FE problems such as the ones presented here, where the "connectivity" of nodes (and variables) is in principle fixed*), which implies that the structure of zeros and non-zeros of the assembled Jacobian matrix will not change during the simulation. In such cases, the reordering analysis only needs to be performed once and then the permutation matrix can be stored and reused for the rest of the calculations.

The most popular filling-reducing permutation procedures are the Minimum Degree algorithms (e.g. in [George & Liu, 1987]), which are derived from the Markowitz method for non-symmetric linear programming problems [Markowitz, 1957], and the Multilevel methods based on the theories for graph partitioning (e.g. in [Karypis & Kumar, 1998]), the latter being in general more effi-

*) The contact problem at the pile-soil interface may alter the connectivity of nodes if a general "master-slave" approach is used, since the elements in contact are a priori not know and may change, but in this work the no-tension joint elements have been used, which by definition always connect the same couples of elements.

cient for parallel computing since during factorization they show a higher level of concurrency [Karypis & Kumar, 1995].

For this work, the storage of the sparse matrices has been adapted to the Compressed Column format and a Multilevel reordering (the Nested Dissection algorithm from the METIS package [Karypis & Kumar, 1998]) has been performed on the assembled Jacobian before the solution of the linear system.

3.3.3 Parallelism and super-computing

For practical purposes and considering the high cost of the transient calculations proposed here, the computational savings obtained by adopting the strategies described so far might not be enough. Further reductions in computational time may then be achieved through the use of multi-processor parallel computing.

The basic idea behind the parallelization is to divide a big computational job into smaller *independent* tasks that can be assigned to different processors that work concurrently, thereby reducing the total calculation time (Figure 3.11). Since in general it will not be possible to divide the whole job into completely independent groups of tasks of equal size, the processors will need to communicate with each other or even wait for the results being computed elsewhere. Therefore, a *master* processor (or master thread) is normally assigned with the distribution of tasks and the gathering of results from the rest of processors (the *slaves*) and an efficient communication protocol (when and how to communicate) will have to be established.

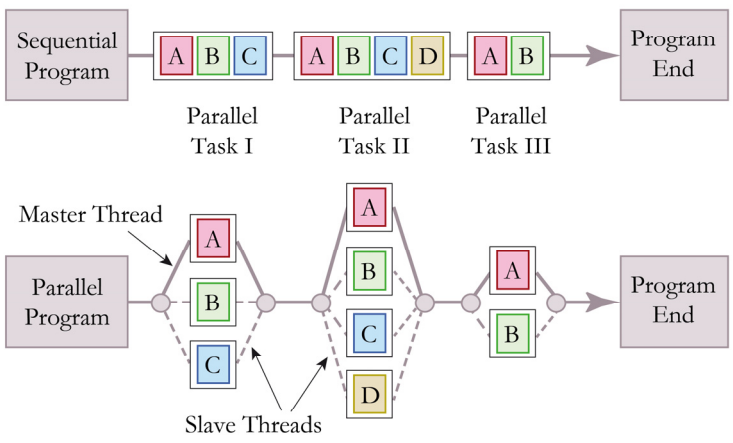

Figure 3.11 Paradigm of multi-processor parallel computation

In this respect, a couple of *de facto* standards have emerged for the implementation of parallel algorithms into computer applications, namely the OpenMP (Open Multi-Processing) and the MPI (Message Passing Interface) standards. Although in some cases they can be seen as complementary, the OpenMP is mainly oriented to shared-memory systems (i.e. multi-processor workstations), while the MPI has been introduced for the communications in distributed-memory systems (high-performance computing clusters). They provide a robust framework for parallelization that can be suitably incorporated into Fortran and C codes, and they have been extensively described in a number of publications, for instance in [Chandra *et al.*, 2001] and [Gropp *et al.*, 1999] respectively. For the interested reader, some guidelines comparing their advantages and disadvantages for Finite Element analysis have been provided in [Bane *et al.*, 2000].

In any case, a careful planning of the task division will be required since parallel processing does not necessarily imply fast and efficient computing. For instance, in a typical FE calculation with tens of thousands of degrees of freedom, more than 97% of the computing time can be spent in a single loop for the dot product, which is required for the LU factorization of the linear system, but a direct parallelization of that loop will surely be counterproductive, since the workload of each dot product hardly justifies the associated overhead (i.e. the time spent in creating the threads, synchronizing the jobs and gathering the results at the end). As the function for the dot product is constantly being called, the total overhead will by far overshadow any parallel gains in performance. Therefore, instead of local parallelization of key loops (fine grain parallelization), a more general division of computational tasks should be pursued (coarse grain parallelism).

In general, the sparse linear system of equations can show three inherent levels of parallelism: (a) Parallelism at a *system level*, where the underlying problem (for instance the partial differential equations or the physical structure) can be divided into a set of small subproblems through domain decomposition or substructuring, (b) parallelism at *matrix level*, where sparsity can lead to simultaneous operations taking place in *independent* parts of the matrix, and (c) parallelism at *submatrix level*, where the dense submatrices of the overall sparse system can be treated with the parallel techniques of the dense linear algebra (level 3 BLAS) [Dongarra *et al.*, 1998].

Parallelization at the system level has normally the greatest potential for performance gains but is problem-dependent and usually involves major *pre-processing* tasks in order to achieve an efficient division of the system. An overview on the techniques for domain decomposition and parallel meshing can be obtained for instance from [Chrisochoides, 2005; Barrett *et al.*, 1994; Bitzarakis *et al.*, 1997; Farhat *et al.*, 1987], while interesting examples applied to geotechnical FE calculations are provided for instance in [Lu, 2006].

On the other hand, parallelization at the matrix and submatrix levels can be costly and involve complex algorithms, but in the past years it has been subject of extensive research and now there exists a number of efficient packages that can be used as external libraries for the solution of the linear system (see [Davis, 2006] for a comprehensive summary of parallel packages with direct solvers for sparse linear systems).

The level of parallelism employed for these investigations has been kept at matrix and submatrix level in the frame provided by the external solver PARDISO, which is described in the next section. Since the computations were performed in a workstation with 8 processors, the implementation for shared-memory systems based on the OpenMP directives was chosen. An extension to high-performance computing clusters (based on MPI) and the higher levels of parallelism (substructuring and domain decomposition techniques) has been left for future work.

3.3.4 Functional software: external solver libraries

From the non-commercial software packages available up to date for the solution of linear systems of equations, the external libraries PARDISO [Schenk & Gärtner, 2009], SuperLU [Demmel *et al.*, 2009] and MUMPS [Amestoy *et al.*, 2009] are probably the most robust and widely used*). They include both sequential and parallel algorithms for an efficient LU factorization of non-symmetric matrices (supernodal or multifrontal methods) and the subsequent solution of the linear system. Provided that the matrices are issued in the appropriate format (the Harwell-Boeing compressed-column or compressed-row formats), these libraries can be readily incorporated to any Fortran or C code through suitable bridge subroutines.

But further than that, the PARDISO package offers the possibility of combining the direct solver with an iterative scheme of the Krylov-subspace type (the so-called CGS solver), in a hybrid approach of the kind explained before in Section 3.3.1, and for that reason it was the choice of preference for this work.

The way it works can be summarized as follows:

*) For the interested reader, a comparison of the mainstream single-thread (i.e. non-parallel) direct and iterative sparse solvers can be found for instance in [Gould *et al.*] and [Hartmann *et al.*, 2009] respectively.

- The library firstly performs a *symbolic* factorization, dependent only on the sparsity structure of the assembled Jacobian matrix. During this phase, a fill-in reducing permutation is calculated and stored for later use.
- Then, the proper *numerical* LU factorization is performed. Since this is computationally the most expensive part, the algorithm has been designed to exploit the vector and matrix block multiplications (the BLAS level 3 subroutines), which are cache-efficient and can profit from low-level parallelism (sub-matrix level). Additionally, the factorization proceeds here using the so-called left-right looking supernodal technique [Schenk & Gärtner, 2009], which benefits from pipelining (matrix level) parallelism by working on "independent" parts of the whole Jacobian matrix.
- If the direct approach is used, then the solution is obtained by the usual forward and backward substitution with the LU factors. If a hybrid approach is used instead, the LU factors are stored and in the subsequent steps used as preconditioners for the iterative scheme, in the expectation that the iterations will converge in less than half of the factorization time. Whenever that is not the case, the numerical factorization is repeated and the LU factors updated.

The implementation of PARDISO into GeHoMadrid was done through a bridge subroutine that converts the matrices into the sparse compressed-column format, issues them to the external library and then reintroduces the results back into the non-linear solution scheme (the Newton-Raphson iterative cycle). Once such a subroutine is written, the external library only needs to be added to the linker-line of the compiler program being used.

As an order of magnitude, by employing all the optimizations described so far the author was able to speed up the calculations from an original (projected) time of around 30 days per load cycle to about a day per load cycle. In any case, the convergence rate and computational time for each case depended very much on the model characteristics (particularly the loading conditions), which will be illustrated in Section 3.6 on the basis of different examples.

3.4 Validation

While the general performance and validity of the GeHoMadrid FE code have been broadly demonstrated in the literature (e.g. in [Mira, 2001; Fernandez Merodo, 2001; Mira *et al.*, 2004; Pastor *et al.*, 2006; Pastor *et al.*, 2009]), the four main changes introduced to the code in the frame

of this doctoral work, namely (i) the extension of the PZ constitutive subroutine to three-dimensional conditions, (ii) the 3D version of the Simo-Rifai coupled element, (iii) the no-tension interface element and (iv) the optimization and partial parallelization of the non-linear solver routine, needed to be validated against reference solutions.

Concerning the constitutive subroutine, the validation was performed by means of the classical reference results from Castro's and Tatsuoka's triaxial tests, as shown previously in Section 3.1.3.2., as well as by the successful reproduction of the behaviour of the Berliner Sand from the triaxial tests presented in [Rackwitz, 2003].

Regarding the changes for the optimization of the calculation time, they were validated during their implementation simply by ensuring that the Jacobian matrices and solution vectors of simple elementary cases remained essentially the same with and without the optimization, their only difference being the time to compute them.

The other two novel aspects in the code were validated as briefly described in the following subsections.

3.4.1 Stabilized coupled element

In order to validate the stabilization technique, the benchmark problem of a flexible footing on saturated soil studied for the 2D case in [Mira *et al.*, 2003] has been analyzed in three-dimensional conditions for this work. The problem, which consists of a square flexible foundation lying on a saturated soil stratum with material properties listed in Table 3.7, is sketched in Figure 3.12. The figure also shows the reference solution in 2D for a consolidation time of $t = 1$ s, which was already introduced in [Mira *et al.*, 2003] using quadratic elements q8p4 (quadratic interpolation in displacements and linear in pressures, hence fulfilling the Babuska-Brezzi condition), and the computed values in 3D using the two alternative first-order formulations considered here.

As it is evident from the figure, the standard first order formulation h8p8 produces an unphysical solution with spurious pressure oscillations, while the result obtained from the stabilized Simo-Rifai elements shows the same pressure pattern as the reference solution.

Here it can be noted that the computed values of the pore pressure are not strictly comparable quantitatively, since the 2D calculation had been performed in plane strain conditions, hence representing a strip foundation, while the 3D model represents a fourth of a square foundation.

Therefore the pore pressures in the 3D model can be expected to be a bit lower, as shown in the figure.

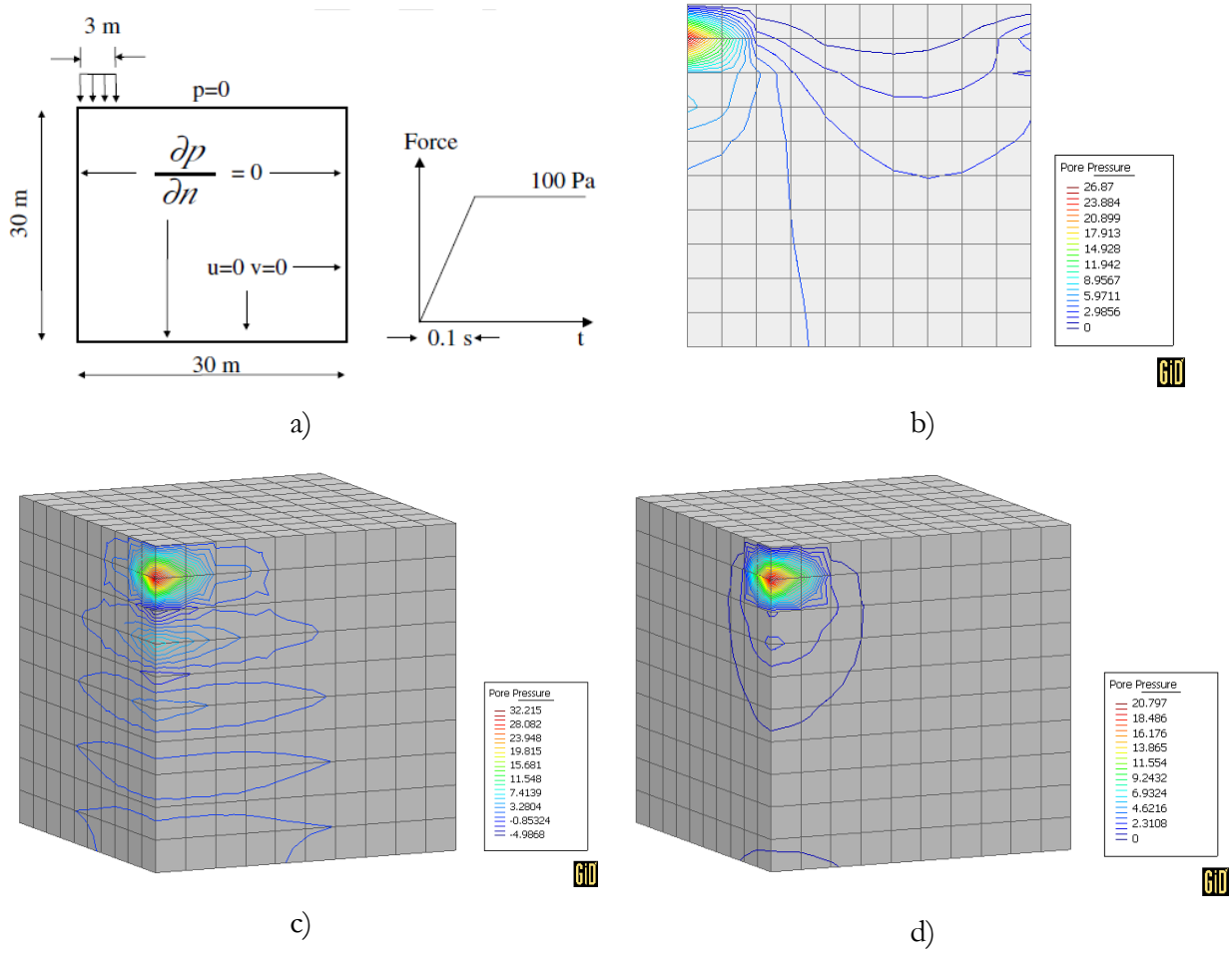

Figure 3.12 Validation of the stabilized element: Pore pressure oscillations in a flexible foundation problem. a) Sketch of geometry, loads and boundary conditions [Mira *et al.*, 2003]. b) Reference results in 2D for t=1s with quadratic elements q8p4. c) Computed result in 3D with first-order elements h8p8, featuring pressure oscillations d) Computed result in 3D with the stabilized Simo-Rifai 8-node element.

Table 3.7 Material parameters for the validation problem "Flexible foundation on a saturated soil stratum"

Material parameter	**Value**	**Units**
Young's modulus, E	$2.5 \cdot 10^{7}$	Pa
Poisson's ratio, ν	0.3	-
Soil's specific weight, ϱ_S	$2.667 \cdot 10^{3}$	N / m^3
Porosity, n	0.25	-
Permeability, k	$1.0 \cdot 10^{-7}$	m / s
Compressibility of the mixture, $1/Q^*$	$1.0 \cdot 10^{-10}$	1 / Pa

3.4.2 No-tension joint element

The performance of the no-tension joint element has been validated with the simple case of an inclined joint under static compression used in [Carol & Alonso, 1983], but extended symmetrically so that a second joint works in tension at the same time (hence it should open the contact and not transmit any stresses). The geometry and data for this problem are sketched in Figure 3.13, and the stresses and displacements can be computed directly as

$$\tau = \frac{100/\sqrt{2}}{\sqrt{2}} = 50\ Pa \tag{3.134}$$

$$\gamma = \frac{\tau}{G_S} = 1.35 \cdot 10^{-4}\ m \tag{3.135}$$

$$u_Z = \frac{\gamma}{\sqrt{2}} = 9.5555 \cdot 10^{-5}\ m \tag{3.136}$$

where the normal component of the deformation has been neglected, since the ratio of normal to shear stiffness is $\boldsymbol{E_N / G_S}$ = 2.7e4. Again it must be noted that here the interface strains have dimensions of length.

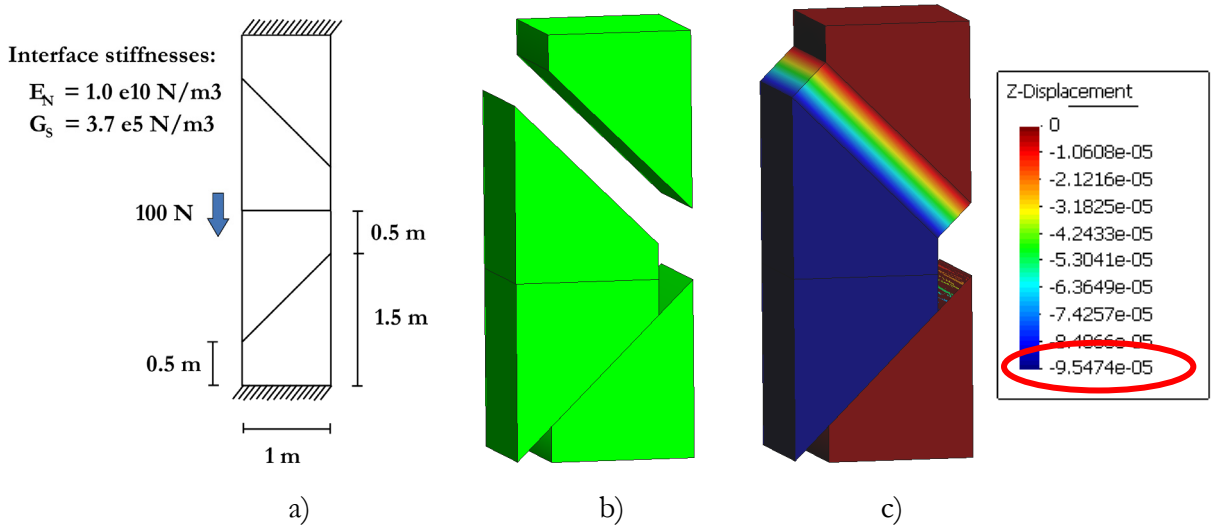

Figure 3.13 a) Validation problem of jointed rigid blocks under vertical static compression. b) Expected contact behaviour. c) Computed result of vertical displacement, in metres.

As shown in Figure 3.13-c, the computed vertical displacements agree very well with the analytical solution (eq. 3.136), hence validating the numerical implementation of the element.

3.5 A Case Study

This section aims to demonstrate the predictive capabilities of the model and at the same time assess the influence of pore pressure accumulation on the behaviour of an offshore monopile under extremal cyclic lateral loading. For that purpose, all of the issues presented in the previous sections had to be dealt with. The particular choices for the study cases discussed here are summarized in Table 3.8.

Table 3.8 Summary of model features employed for the case studies

Model feature	Description
Constitutive model	P-Z Mark III model, calibrated for Berliner Sand (TX2 Sample)
Mathematical model	Biot-Zienkiewicz u-p formulation. Saturated consolidation case
Coupled soil elements	Stabilized Simo-Rifai 8-node hexahedric elements
Pile-soil interface	No-tension isoparametric joint element
Matrix storage	Compressed-column (Harwell-Boeing) format
Model size	Approximately 60,000 degrees of freedom
Solution strategy	Direct (LU), hybrid (CGS Krylov-subspace iterations)
Level of parallelism	Matrix and sub-matrix level
External solver library	PARDISO
Computing system	Shared-memory, 8-processors (Intel Xeon) Workstation.

In order to disregard the possible constraining effects of the model boundaries, a sea-bed extension of 100 metres (from 12 to 25 times the pile diameters discussed here) and 40 metres in depth was considered. Taking advantage of the symmetry of the system under lateral loading on a single direction, only one half of the pile-soil system was modelled and therefore the transversal displacements within the symmetry plane were set to be zero.

The model pile was in all cases an open-ended steel pipe-pile with a wall thickness of 60 mm and discretised with 8-node volume elements, which, as reported in [Wiemann, 2007] and [Wichtmann *et al.*, 2008], perform as well as the shell elements for such cases. In any case, in order improve the aspect ratio of the elements and disregard any shear locking (i.e. stiffening) of the pile, thicker elements (100 mm thick) were employed, making use of an equivalent reduced Young's

modulus for the steel so that the flexural stiffness of the pile remained unchanged with respect to the 60 mm thick original pile.

Concerning the soil plug inside the pile, consideration has been made that the driven offshore large-diameter piles often behave as unplugged during driving but then form a rigid basal plug and show a closed-ended behaviour under static and quasi-static loading, developing end-bearing resistance all over the full cross section and not only under the steel ring (see for instance [Jardine *et al.*, 2005; Lehane *et al.*, 2005]). Therefore, the last meter of the soil plug was modelled as a stiff basal plug moving solidarily with the pile but featuring the same permeability as the sand so as to permit the drainage of excesses of pore pressure through it.

As reported in [Bachmann & Overbeck, 2008] on the basis of geophysical investigations, the upper layers (up to 6 m in thickness) of the sea-bed in the North Sea locations of future German wind farms are composed of loose sediments of irregular consistency which provide no load-bearing capacity whatsoever. Considering the effective weight and lack of resistance of a 3 m thick layer of such sediments on the sea floor, a distributed load of 34 kPa was applied to the soil surface in the model. Such preloading of the soil did prove quite beneficial for the overall convergence rate of the numerical model.

A first study case, illustrated in Figure 3.14, consisted of a monopile with 8 meters in diameter and 30 meters of embedded length under the effects of a few load cycles of extreme magnitude (50-year return period). Therefore, a symmetrical two-way lateral load with an amplitude of 5 MN and sinusoidal character (0.1 Hz in frequency) was applied to the pile 30 meters above the soil surface. The relevance and representativity of such magnitudes with respect to the foundations of real offshore wind turbines is discussed later, in Section 4.1.3.

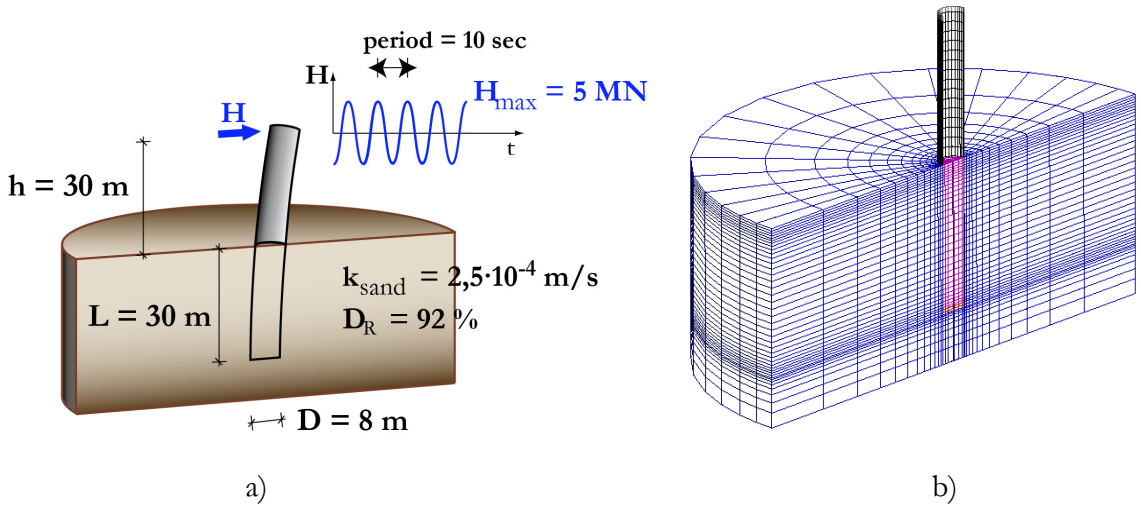

Figure 3.14 a) Selected geometry and parameters for the study case. b) Finite element mesh with 60,000 degrees of freedom.

The element size and degree of refinement of the FE mesh, which is shown in Figure 3.14-b, were chosen small enough to provide a stable and smooth solution of the pressure field and minimise the possibility of locking phenomena. The use of a finer mesh was discarded on regard of the high computational cost of the transient loading event, which remained an important conditioning issue for the calculations despite the implemented optimizations. In this respect, the extreme loading conditions and the sensitivity of the constitutive model demanded in average around one thousand time steps per load cycle and ten Newton-Raphson iterations per time step. A relative error tolerance of 10^{-7} as defined in the Appendix A.2 was adopted.

The soil was modelled as a dense sand (relative density $\boldsymbol{D_R}$ = 92%) with the material parameters calibrated for the Berliner sand (see Table 3.9), which as mentioned before is very similar to the cohesionless geomaterials present in the German part of the North Sea. The hydraulic permeability of the soil was set in this case to $2.5 \cdot 10^{-4}$ m/s.

Table 3.9 Soil constitutive parameters for the study case.

K^e_0 [kPa]	G^e_0 [kPa]	M_g [-]	α_g [-]	M_f [-]	α_f [-]	H_0 [kPa]	β_0 [-]	β_1 [-]	γ [-]	$H_{U,0}$ [kPa]	γ_U [-]
5500	10000	1.18	0.45	0.77	0.45	65	17.2	0.43	1	250	5

3.5.1 Evolution of Pore Water Pressure

The computed variations of pore-water pressure around the monopile during the cyclic loading peaks are depicted in Figure 3.15, where the maximum overpressures can be observed taking place in the passive side of the soil at a depth around 7 meters under the soil surface. On the contrary, the active side of the soil experiences transitorily a certain decrease of pore pressure under the hydrostatic value, particularly at depths between 8 and 12 meters, but such underpressures are mitigated progressively by the following load cycles. By the end of the 4th cycle, almost no underpressure can be seen in the active side as the pile advances, but rather a remanent overpressure accumulated from the previous cycles.

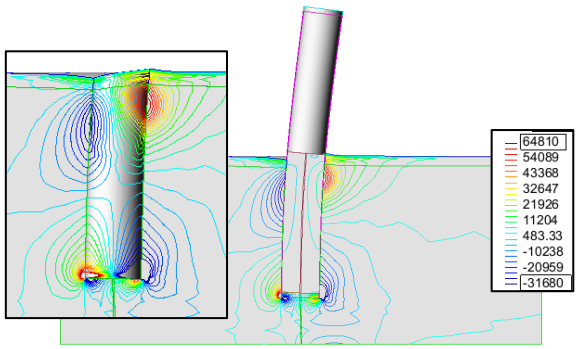

1st cycle - forth

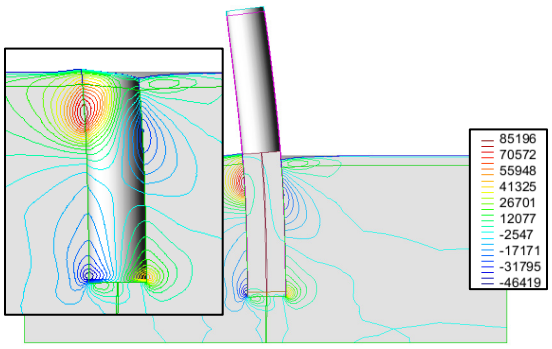

1st cycle - back

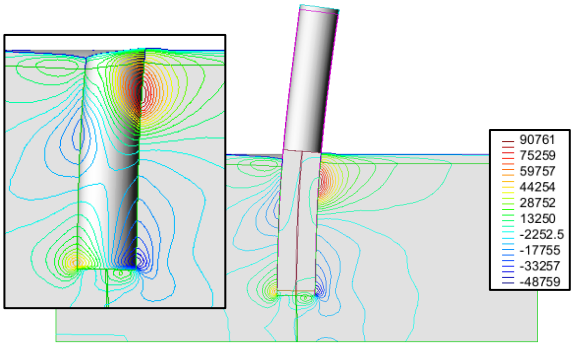

2nd cycle - forth

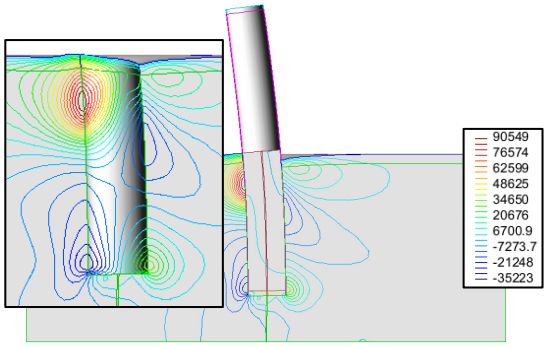

2nd cycle - back

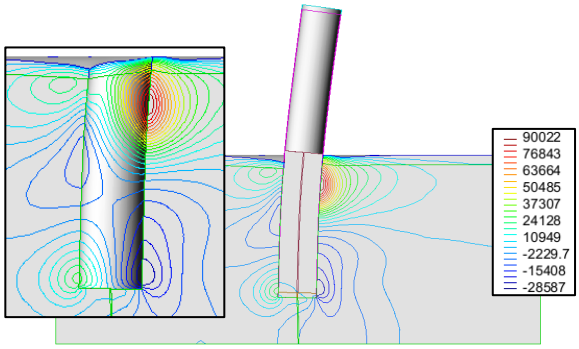

3rd cycle - forth

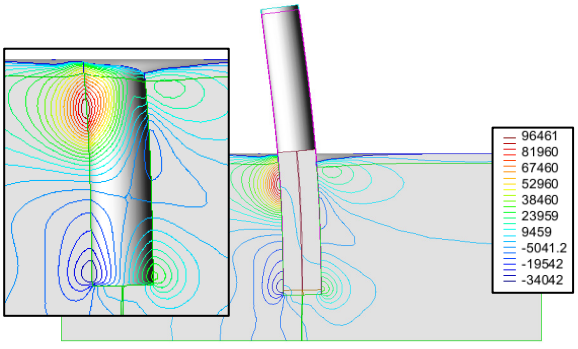

3rd cycle - back

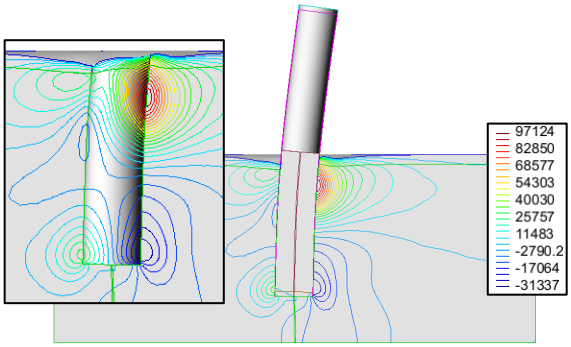

4th cycle - forth

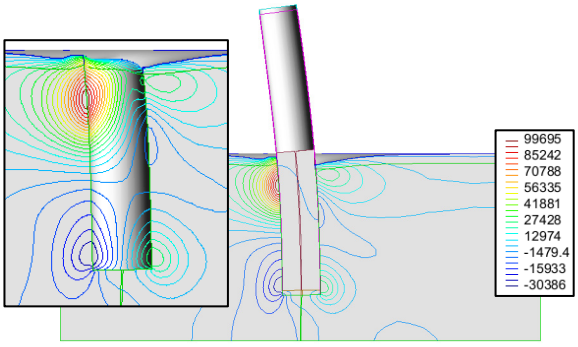

4th cycle - back

Figure 3.15 Contour lines of excess of pore water pressure, in kPa, around the pile during the extremes of cyclic lateral loading. Displacements and deformations magnified 50 times. Pile and soil-plug omitted in the image sections.

Such trend of pore pressure evolution agrees very well with the one presented in [Tasan *et al.*, 2010a], although the results are not strictly comparable since there only the evolution for cyclic loads with one-way character was shown, in contrast to the two-way loads being discussed here.

In this case, the maximum generated overpressure reaches 65 kPa already during the first loading peak, and then steadily increases with every cycle until the onset of liquefaction (or more precisely, cyclic mobility for such dense sand). In fact, in this case the calculations were not able to proceed beyond the 5th load cycle due to the loss of resistance and excessive plastic deformations at the shallow layers of soil.

The evolution of the generated pore pressures at different depths from the soil surface and at different distances from the pile is illustrated in Figure 3.16 and Figure 3.17. It shows that underpressures generated behind the pile in the initial cycles are eventually compensated and reverted into overpressures already by the third load cycle.

The exceptionally high values of pore pressure supported by the soil during the load peaks, eventually exceeding the initial vertical stress at rest, can be attributed to the extraordinary levels of total stress exerted by the pile on the soil at the moments of peak displacement. However, this does not necessarily mean that the soil is liquefied at those moments, since then the effective stresses need not be necessarily zero, as shall be shown in the following section. In this respect, the levels of PWP are just a measure of the difference between the total and the effective stress at each moment.

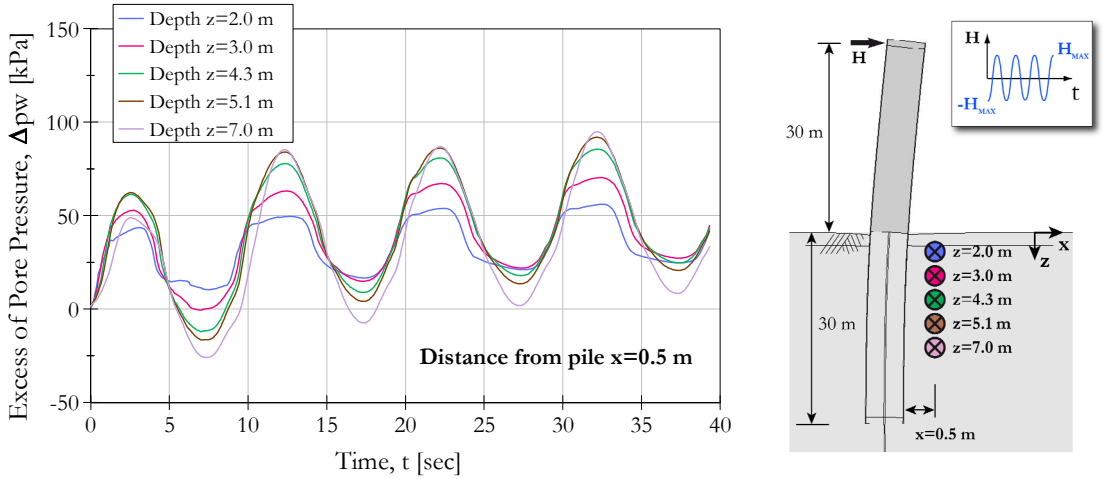

Figure 3.16 Evolution of excess of pore pressure within the soil at selected depths in front of the pile

Incidentally, some significant overpressure and underpressure are developed near the pile base as well, caused by the rigid-body motion of such a "short" stiff pile (the so-called "toe-kick"), but

both of them are mitigated progressively during the following cycles, while in any case their relevance is minor due to the high confining stresses at the soil depths where they take place (See Figure 3.15).

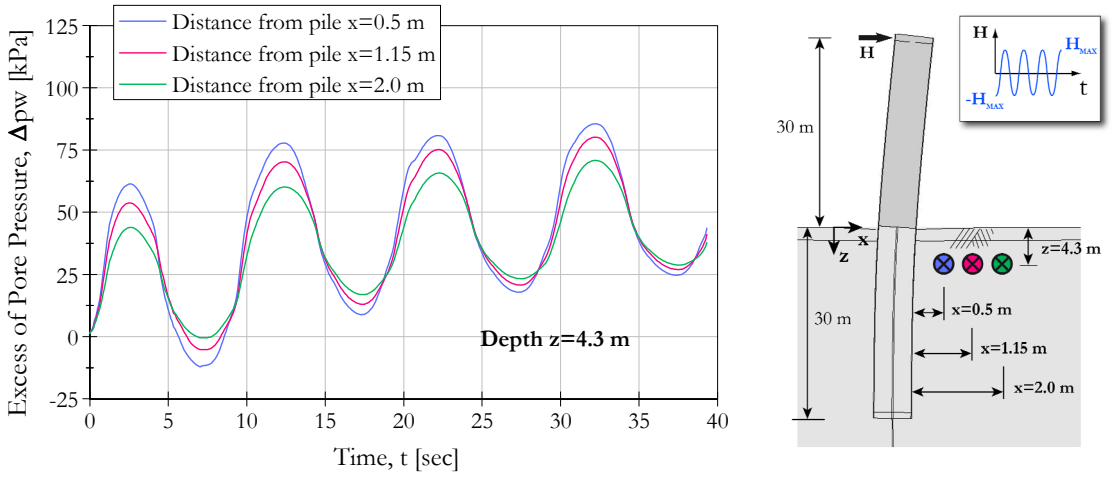

Figure 3.17 Evolution of excess of pore pressure within the soil at selected distances from the pile

The origin of the pore pressure accumulation can be attributed to the cyclic compression of the soil (and hence reduction of pore volume) as the pile advances and the inability of the soil to dissipate the overpressure completely between two consecutive cycles. The former is enhanced by the overall contractive tendency of the sand under cyclic loading, while the latter is mainly due to the relatively high loading speed, the low permeability and the large drainage path imposed by the large pile diameter. The particular relevance of the different factors is discussed in Section 3.6.

3.5.2 Soil stresses and strains. Cyclic mobility

In Figure 3.18, the stress state and plastic shear strains are depicted for selected soil elements in front of the pile at different depths. The clear accumulating trend of excess of pore pressure observed in the sand is reflected in the stress path and deformational behaviour, both characteristic of a cyclic mobility event. There, the stress path is shifted with every cycle towards regions of lower confining pressures until the critical state surface is eventually reached, producing then a considerable plastic flow of the sand and a certain dilatancy marked by the transitory increase in mean effective stress.

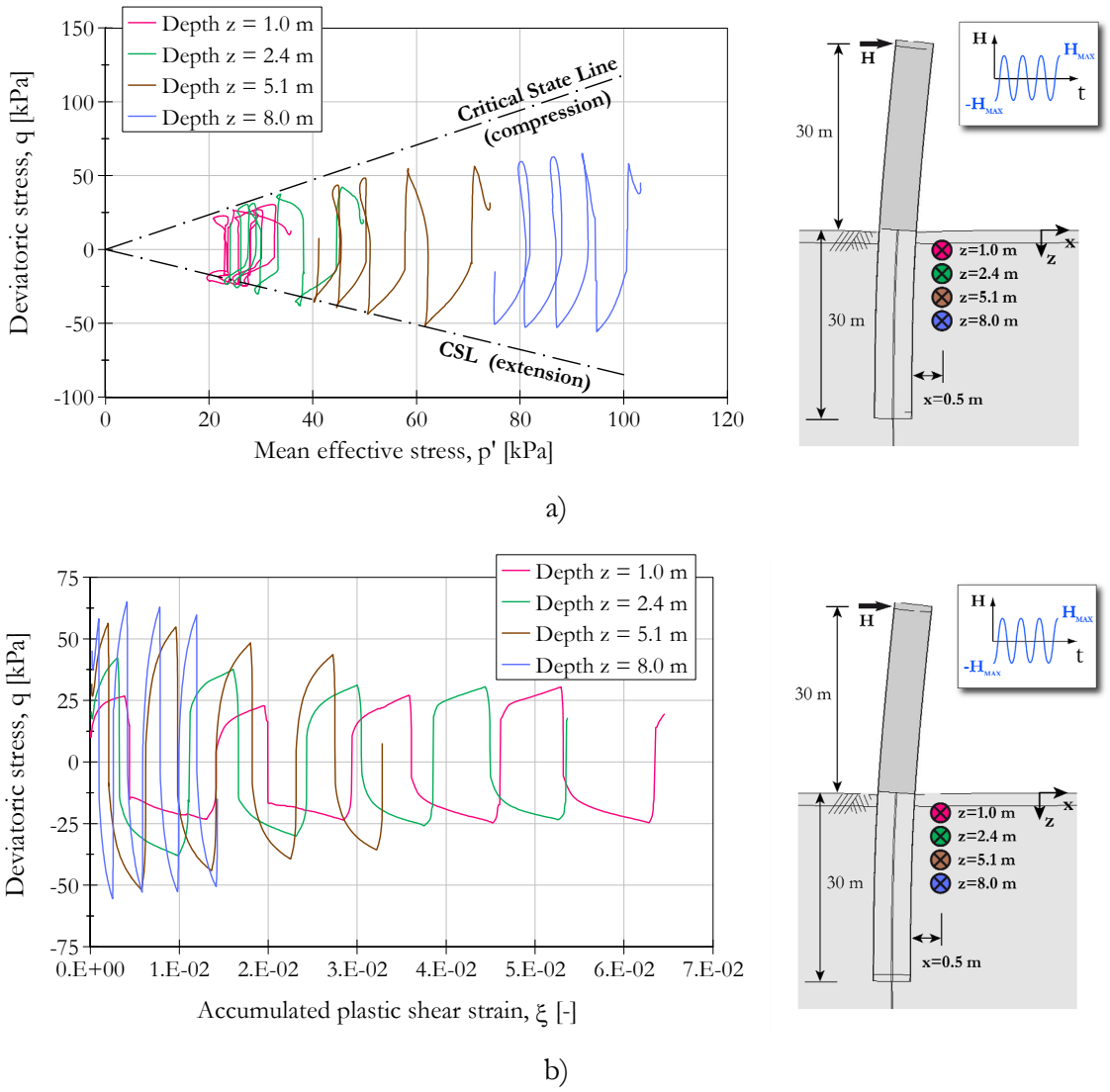

Figure 3.18 Cyclic behaviour of selected soil elements in front of the pile. (a) Stress paths in the triaxial plane. (b) Shear plastic flow of the soil at different depths.

3.5.3 Pile deflection and soil settlement

The discussed cyclic mobility of the sand is also reflected in the general softening experienced by the foundation. A plot of the pile-head displacement versus the applied load (Figure 3.19) shows the progressive inclination of the hysteretic loops, with the pile head displacement increasing at all load levels with every subsequent cycle. A comparison of the deflected shape of the pile during the first and fourth load cycles shows an almost proportional increase of pile displacement at each depth (Figure 3.19-b).

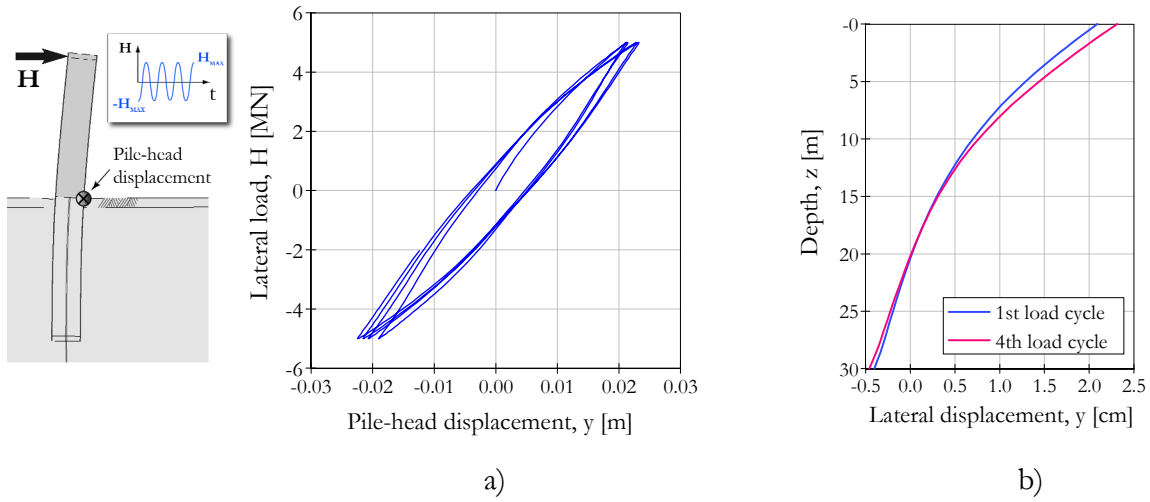

Figure 3.19 Lateral deflection of the pile. a) Evolution of the pile's load-displacement hysteretic cycles. b) Deflected shape of the pile during the first and fourth loading maxima.

A closer examination of the evolution of pile-head displacement shows that the increasing tendency affects both directions of the two-way loading, and hence an increase in the displacement cyclic amplitude as well, which can be attributed to the cyclic softening of the soil rather than to a mere plastic drift of the pile. Figure 3.20 illustrates the increasing tendency in both directions, as well as that of the cyclic displacement amplitude, in comparison to the evolution predicted with the empirical approach of Long and Vanneste [1994] discussed in Chapter 2, which does not consider the possible effects of pore pressure accumulation.

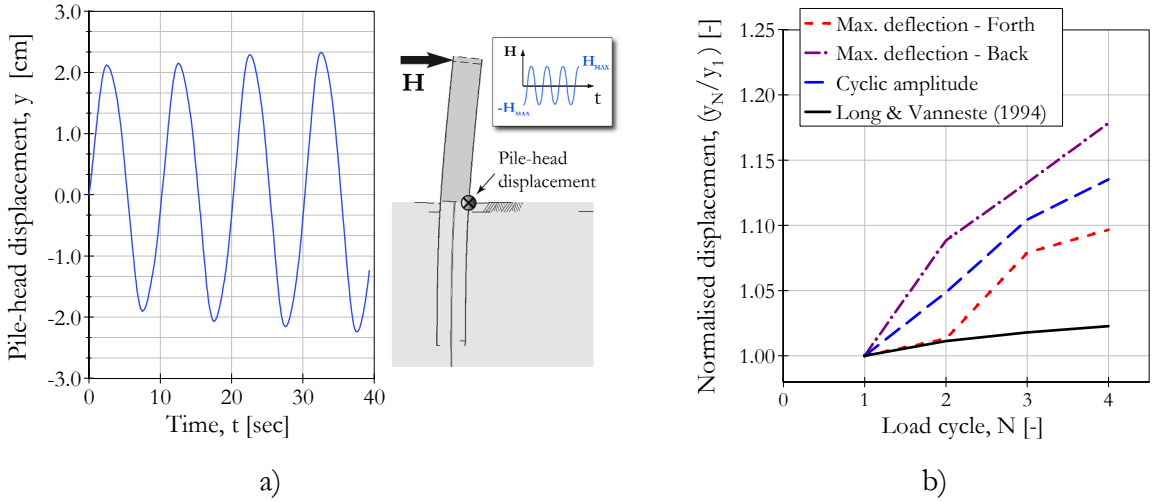

Figure 3.20 Pile-head lateral displacement. a) Temporal evolution. b) Normalised trend of cyclic amplitude and of the cyclic maxima in both directions of the two-way loading, compared to the trend predicted with the empirical approach of Long & Vanneste (1994).

The considerable difference between the results from these two approaches already by the fourth cycle could be partly attributed to the different slenderness and flexibility of the piles in the database employed by Long & Vanneste, but also, and perhaps more importantly, to the fact that those piles did not accumulate any excess of PWP. The severity of such comparison was also observed by Tasan *et al.* [2010a] on the basis of their numerical investigations, which seems to highlight the importance of taking into account the coupling with the pore fluid in the foundation design.

Another aspect relevant for the offshore foundation may be the progressive subsidence of the soil around the pile, which is illustrated in Figure 3.21. There it can be seen that both the cyclic and permanent settlements of the soil increase considerably with every cycle, reflecting the general tendency of the sand to contract when subject to full cycles of shearing.

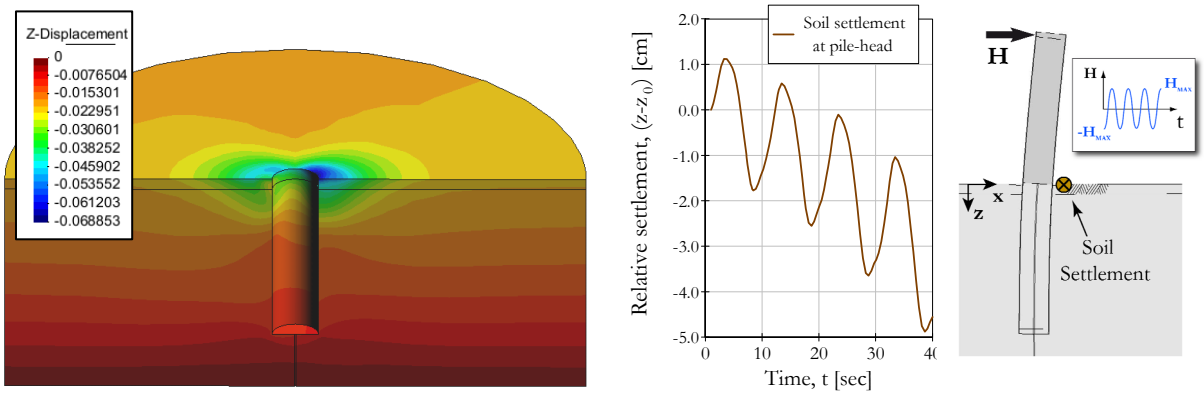

a) b)

Figure 3.21 Soil subsidence around the pile due to cyclic lateral loading. a) Permanent soil subsidence (in metres) at the end of the 4th cycle, with the pile at rest. b) Evolution of soil settlement at pile-head relative to state prior to cyclic loading.

3.6 Parameter Relevance for the Accumulation of PWP

In order to assess the influence and relative relevance of the main factors that have traditionally been identified as playing a significant role in the accumulation of PWP (see Chapter 2), a parametrical study has been carried out, where a basic case was chosen and then the different parameters were varied, one at a time, within the ranges shown in Table 3.10.

In this respect, due to the high calculation cost of every case, for the moment only a dense state of the soil has been investigated, being this state probably the most common and relevant for the

German Bight of the North Sea. However, the sand density is very likely to play a relevant role in the magnitude and rate of pore pressure accumulation around the pile, as already shown by Tasan *et al.* [2010b]. Furthermore, for a given sand the initial density along with the confining stress will in general determine which one of the extreme cases of PWP accumulation could possibly happen, either liquefaction or cyclic mobility, both being very damaging in terms of plastic deformations but featuring different degrees of softening in the soil (in principle, in the liquefied state the soil cannot hold any stress, which is not the case for the cyclic mobility). Such implications shall therefore be analysed in forthcoming investigations.

The rest of model characteristics and boundary conditions are the same as in the study case shown in the previous section, except for the distributed load caused by the effective weight of the sediment layer, which in order to improve the convergence rate and computational time for the parametric study, was set in this case to 54 kPa.

Table 3.10 Investigated cases for the parametrical study.

Parameter variation	**BASIC CASE**	**#2**	**#3**	**#4**	**#5**	**#6**
Load Level, H_{MAX} [kN]	**2500**	250	500	750	1250	3500
Load Frequency, f [Hz]	**0.1**	0.001	0.01	0.15	0.2	-
Soil Permeability, k [m/s]	**2.5 E-4**	1.25 E-4	7.5 E-4	2.5 E-2	2.5 E-1	7.5 E-1
Pile Diameter, D [m]	**6**	4	8	4-DC (*)	8-DC (*)	-
Load Amplitude Pattern	**constant**	increasing	decreasing	irregular	Full storm	-
NOTE: (*) = Displacement controlled, with the pile-head displacement prescribed to that of the basic case.						

As a matter of clarity and consistency, the investigation of PWP evolution was focused on three single control points in front of the pile at a distance of 0.5 m from the pile border. The different control points, at depths of 2.4 m, 4.3 m and 7 m, shall be termed henceforth ***CP#1***, ***CP#2*** and ***CP#3*** respectively.

However, for the sake of concision most of the results shall be presented here only as computed in ***CP#2***, while the values for the other control points will be included only wherever relevant or whenever a significant deviation from the pattern shown in ***CP#2*** appears.

Assuming that the amplitude of the cyclic variations of PWP is known and remains roughly constant (as will be shown here), then the evolution of PWP could be described in terms of the evolution of residual PWP alone, which tentatively could take the following form considering the different factors investigated in this parametric study:

$$\Delta p_{W,RES} = C_0 \cdot f_N \cdot f_L \cdot f_K \cdot f_F \cdot f_D \tag{3.137}$$

where

$$\begin{aligned} f_N &: \textit{ Explicit accumulation function} \\ f_L &: \textit{ Influence of load level} \\ f_K &: \textit{ Influence of soil permeability} \\ f_F &: \textit{ Influence of load frequency} \\ f_D &: \textit{ Influence of pile diameter} \end{aligned} \tag{3.138}$$

The following sections will attempt to address the form of these functions, while the rest of influencing factors, such as the soil density or the type of loading (one-way or two-way), will be here lumped into the system constant $\boldsymbol{C_0}$.

At this moment, the analysis of PWP evolution in such a multiplicative form is convenient for this parametrical study, since in this case only one parameter at a time has been investigated, while the rest were set to be constant (i.e. those of the reference case). However, this way the mutual inter-dependencies between the different factors are not being captured and will have to be addressed in future investigations.

3.6.1 Influence of load level

Starting from the reference case of the loading produced by an extremal storm with a 50 years return period, which here and for the case of a 6 m diameter monopile is assumed as causing loading peaks of 2.5 MN with a resultant lever arm of 30 m, and in a sinusoidal two-way fashion, the influence of the load level on the generation of excess of PWP is depicted in Figure 3.22.

There, it can be observed that the higher levels of loading produce not only higher transient levels of PWP, but also an increasing trend of PWP accumulation. Such is so, that the calculations for the highest level of loading could not proceed further than the third load cycle due to excessive softening and soil plastic deformations at the pile-head level.

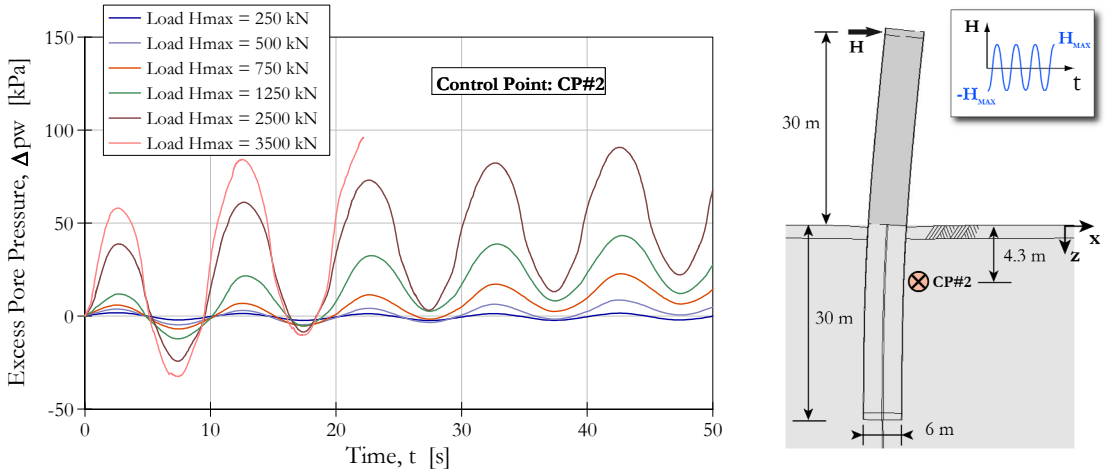

Figure 3.22 Time history of excess of PWP at control point CP#2 for different levels of cyclic loading.

However, instead of comparing the absolute values of PWP of the different cases, it may be more elucidating to examine them in relation to the load levels to which they pertain. For that purpose, it is useful to adopt a normalisation with the averaged subgrade reaction pressure Π, conveniently defined here as the maximum applied load H_{MAX} divided by the product of the pile diameter D and elastic length L_e (in a way, a measure of the reacting soil surface), which may be written as:

$$\Pi = \frac{H_{MAX}}{D\,L_e} \qquad where \quad L_e = \sqrt[4]{\frac{EI}{\gamma' L}} \tag{3.139}$$

In the light of the normalised results, illustrated in Figure 3.23, the following conclusions may be drawn:

- As it can be observed from the first load cycle, the generated PWP is in general not proportional to the applied load (otherwise the curves would be identical), which can be explained by the general nonlinear nature of the sand response and the different levels of plastic volumetric strains produced in the different cases.
- For this particular system, loads equal or below 500 kN originate irrelevant levels of permanent volumetric strains, and hence in such cases the generated excess of PWP is proportional to the applied load, at least during the first two cycles.
- There appears to exist a threshold load level, in this case 250 kN, below which the generated variations of PWP will dissipate completely between consecutive cycles,

and hence no accumulation of residual pressure will occur. In the following, this shall be termed “drained threshold”.

- There also appears to exist an upper bound for the normalised values and rates of accumulation of PWP, to which all the "accumulating cases" tend to strive. The lowest load within this bound shall be referred to as “undrained threshold” from now on.
- In consequence, the computed solutions can be interpreted to be bound by two attractors: a "safe" lower bound, where the generated PWP is proportional to the applied load and no accumulation takes place, and an upper bound "potentially unsafe", in which the accumulation rate appears to be a constant proportion of the loading magnitude.
- For the cases in between these two thresholds, neither the excess PWP nor its accumulation rate seem to be proportional to the applied loads. However, they appear to approach gradually the upper bound.

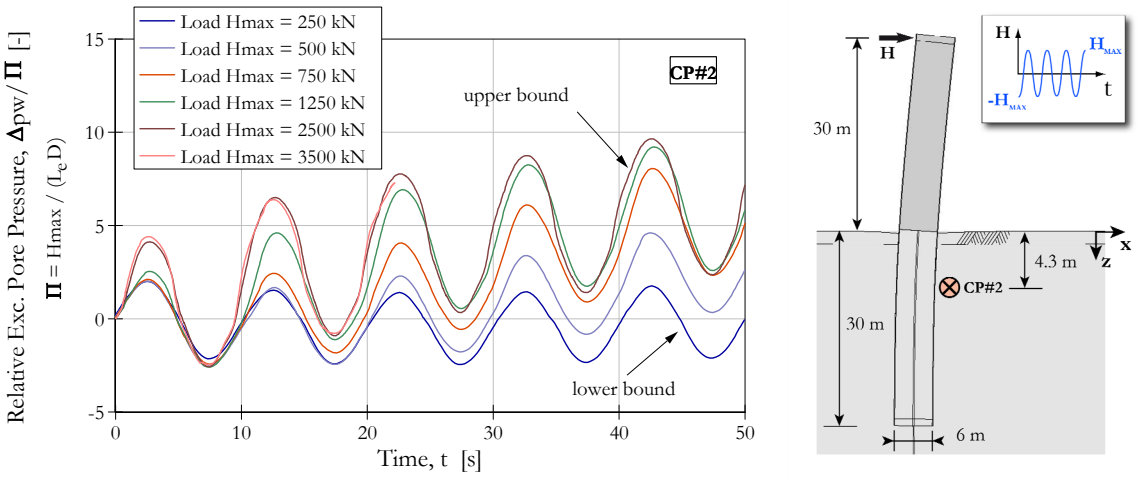

Figure 3.23 Normalised values of excess of PWP relative to the maximum applied load, at control point #2 for different levels of cyclic loading.

Such conclusions may be visualised more clearly by inspecting the extremal values (maxima and minima) of the normalised excess of PWP, as well as its cyclic amplitude (difference between cyclic maxima and minima) and residual values, as shown in Figure 3.24.

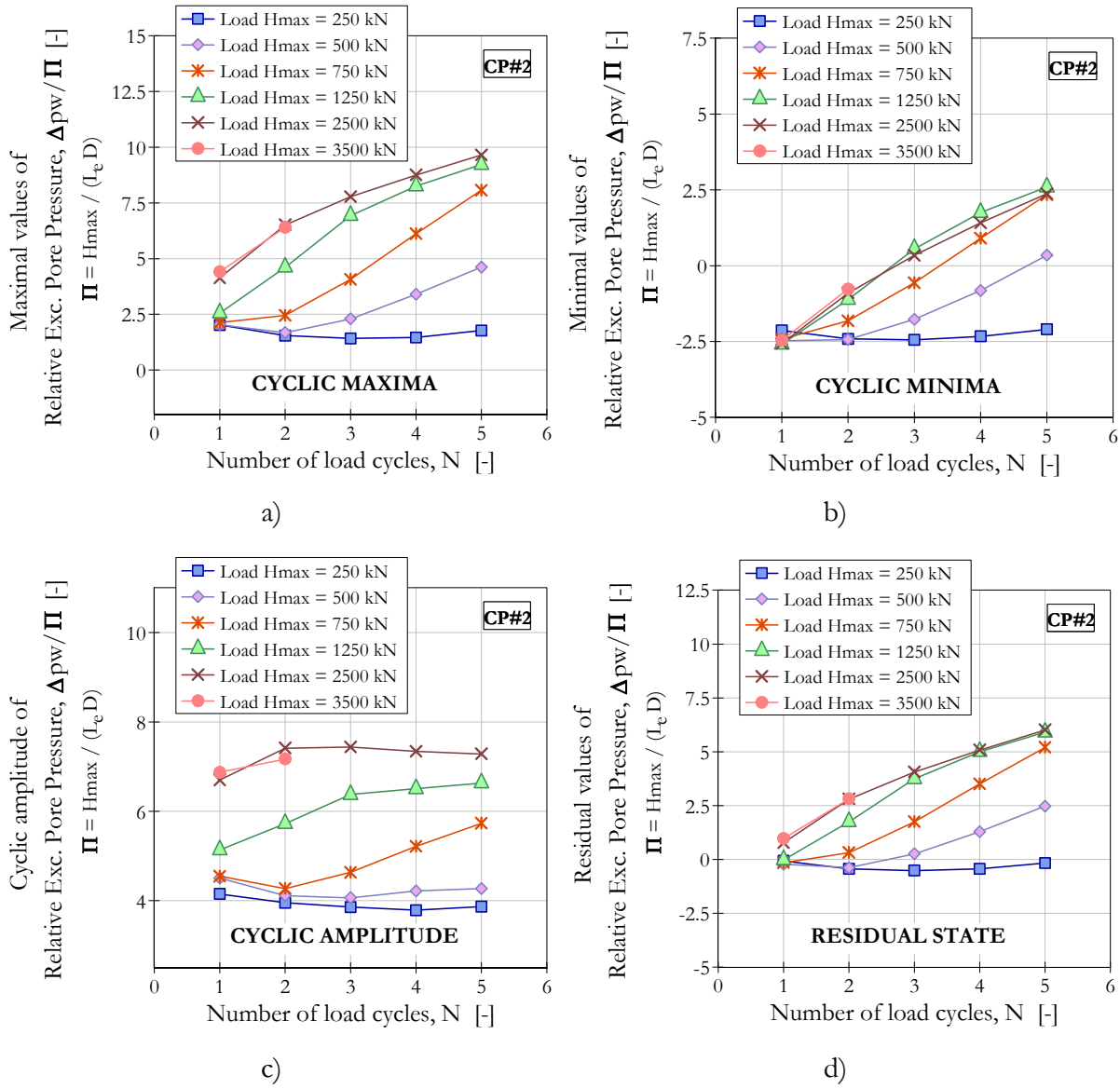

Figure 3.24 Cyclic extremal normalised values and residual state of excess of PWP at control point #2 for different levels of cyclic loading. a) Cyclic maxima. b) Cyclic minima. c) Cyclic amplitude, as direct difference between cyclic maxima and minima. d) Residual state after cycling.

Incidentally, these numerical results seem to agree well with those shown by Tasan *et al.* [2010b]. There, a pile with 7 m in diameter was investigated under one-way cyclic loading, and a load level of H_{MAX}=500 kN was found to produce no PWP accumulation, while by increasing the loading magnitude up to 1500 kN a clear accumulating trend could be observed, which fits well with the orders of magnitude presented here.

Another interesting feature is that the amplitude of the PWP cycles is load dependent but not proportional to the applied load, and also seems to remain constant throughout the cycling, irrespective of the accumulation trend, which implies that for all cases the cyclic maxima and minima increase at the same rate.

On the other hand it appears that for those cases that fall into the so-called upper bound (here the load levels equal or above the threshold of 1.25 MN, or in other words, averaged subgrade pressures Π above the undrained threshold of Π_{UT} = 1250 / (L_e D) = 4.7 kPa), the rate of accumulation of residual PWP is the same for all cases, which can be expressed as

$$\frac{\partial\left(\frac{\Delta p_w}{\Pi}\right)}{\partial N} \approx C_0 \qquad \textit{for loads such that} \quad \Pi > \Pi_{UT} \tag{3.140}$$

being C_0 a "system constant", and hence, recalling Eq. 3.139, for every load level in the upper bound

$$\left(\Delta p_{W,RES}\right)_{\substack{LOAD \\ VARIATION}} \approx C_0 \cdot \Pi \cdot N = C_0 \cdot \frac{H_{MAX}}{L_e D} N \tag{3.141}$$

For those cases where the load level lies in between the two thresholds, the evolution of residual pressures appears to be more complex and definitely not linear, so due to the scarce data available at the moment, an analytical description will not be attempted yet.

3.6.2 Influence of soil permeability

Concerning the influence of the soil permeability, it appears reasonable to assume that lower values of permeability will be associated with higher levels of transient variations of PWP since the drainage and flow of pore water will then be inhibited to a higher degree. However, as Figure 3.25 shows, for a given system (i.e. for a given pile diameter, load level and frequency, among other factors) there also seems to exist an "undrained threshold“ for the permeability beyond which the system remains essentially undrained and further decreases in permeability do not alter the system response.

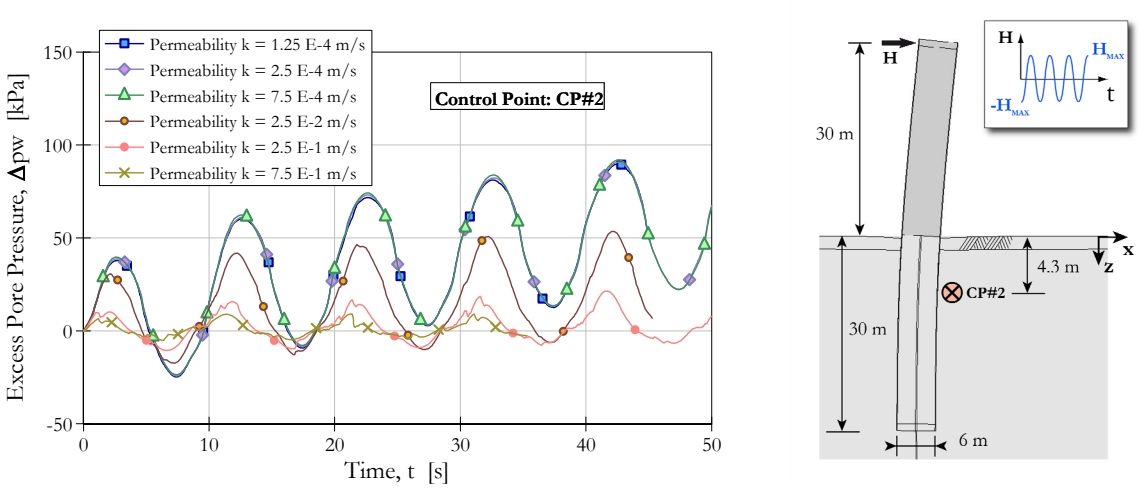

Figure 3.25 Time history of excess of PWP at control point #2 for different values of soil permeability.

In this particular case, for soil permeabilities equal or below the threshold of k=7.5 E-4 m/s the response was almost identical, showing a constant cyclic amplitude and rate of accumulation, as depicted in Figure 3.26. For higher values of permeability, the accumulation of PWP also takes place, but at lower (constant) rates, and only for the extreme case of k=7.5 E-1 m/s the rate can be assumed to be zero and the residual values of excess of PWP negligible.

A plot of the soil settlement at the pile-head (Figure 3.27) supports the idea of the undrained threshold, since the undrained behaviour will preclude in general any changes in soil volume. In this respect, the cases with permeability below the undrained threshold show almost no permanent settlement of the soil, while for the cases with higher permeability the drainage of pore water allows a progressive reduction of the pore volume and a consequent soil compaction and subsidence.

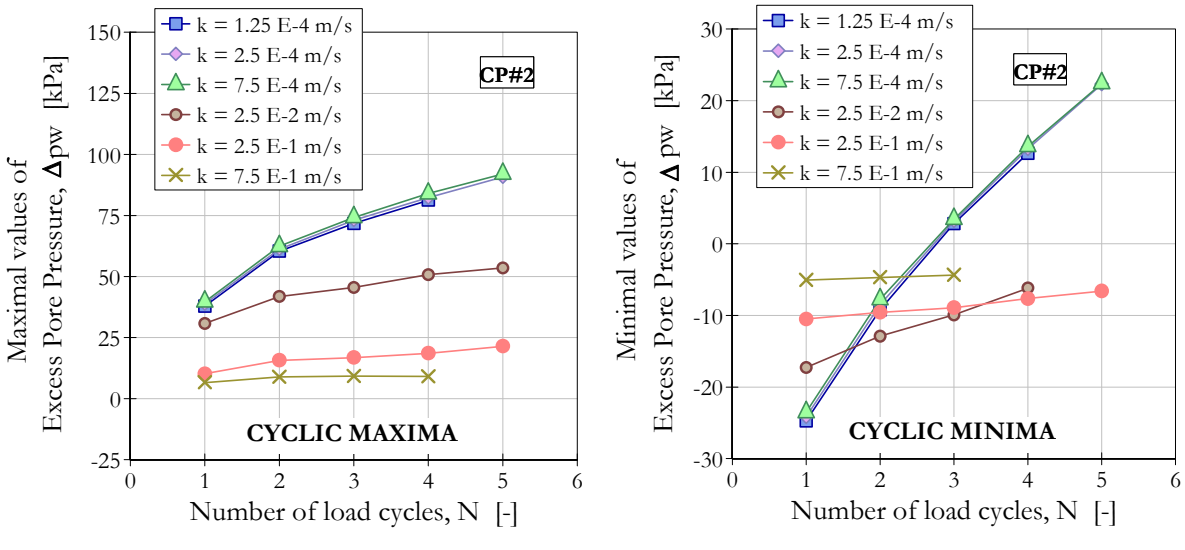

a) b)

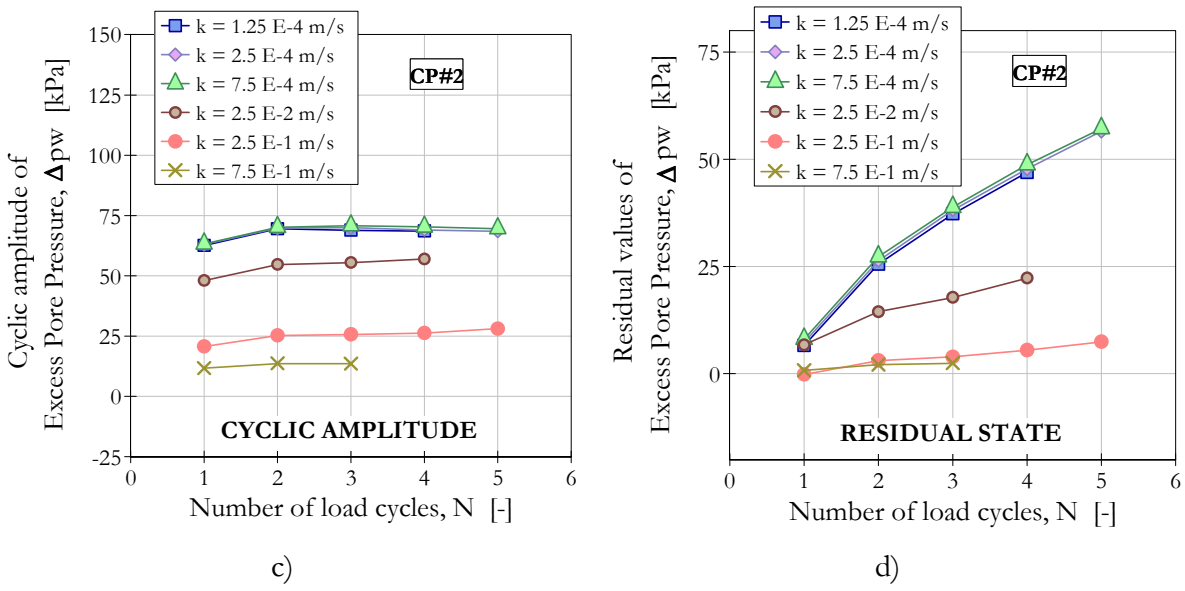

Figure 3.26 Cyclic extremal values and residual state of excess of PWP at control point #2 for different values of soil permeability. a) Cyclic maxima. b) Cyclic minima. c) Cyclic amplitude, as direct difference between cyclic maxima and minima. d) Residual state after cycling.

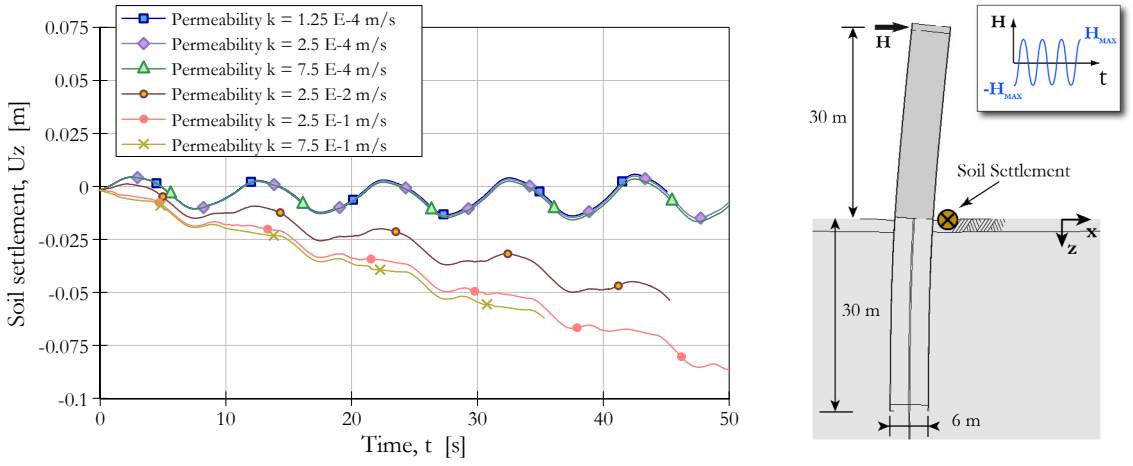

Figure 3.27 Time history of soil settlement at pile-head for different values of soil permeability.

Finally, the following additional conclusions may be outlined:

- For this particular system configuration and load level, the soil behaviour close to the pile is essentially undrained for the kind of sands typical of the North Sea (permeabilities in the order of magnitude of 10^{-4} m/s).
- The "drained threshold" above which the high permeability ensures a fully drained behaviour and no accumulation of PWP seems to be three orders of magnitude higher than the typical permeability values of clean North Sea sands.

- The magnitudes of the permeability thresholds are very likely to be load level dependent, as it can be deduced from the previous section, and in principle also sensitive to the rest of system characteristics (load frequency and pile diameter, among others).
- A function f_K suitable to describe the influence of soil permeability on the evolution of residual excess of PWP in the frame of Eq. 3.137 could take the following form:

$$f_K = \begin{cases} 1.0 & for\ permeabilities\ k \le undrained\ threshold\ k_{UT} \\ 0.0 & for\ permeabilities\ k \ge drained\ threshold\ k_{DT} \\ 0.0 < f_K < 1.0 & whenever \quad k_{UT} < k < k_{DT} \end{cases} \tag{3.142}$$

A suitable function to fulfill such criteria could be for instance the following

$$f_K = \begin{cases} 1.0 & for\ permeabilities\ k \le k_{UT} \\ e^{\frac{(k_{UT}-k)}{k_{DT}}C_1} & whenever \quad k_{UT} < k < k_{DT} \\ 0.0 & for\ permeabilities\ k \ge k_{DT} \end{cases} \tag{3.143}$$

where C_1 would be a system constant. Such function is exemplarily illustrated in Figure 3.28 for the thresholds observed here and $C_1 = 20$.

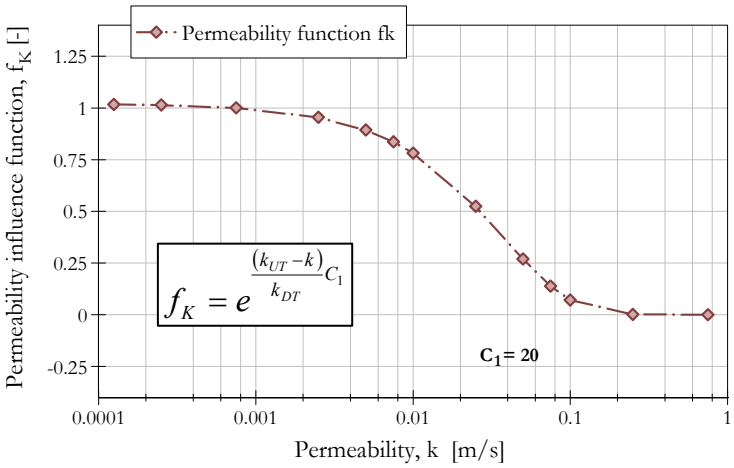

Figure 3.28 Permeability influence function f_K for the interpolation of excess PWP for soil permeabilities in between thresholds.

Concerning the analogous investigations by Tasan *et al.* [2010b], there the existence of an undrained threshold was not addressed, but a limiting permeability for which no accumulation of PWP would occur (hence corresponding to the drained threshold proposed here) was also re-

ported. For the system investigated there, the permeability threshold was observed at $k=6\cdot10^{-2}$ m/s.

3.6.3 Influence of loading frequency

A seemingly surprising result out of the simulations with regards to the loading frequency, is that at least for the initial stages of loading it appears to have absolutely no influence on the evolution of the excess of PWP for the frequencies that might be practically expected from a storm event (see Figure 3.29 and Figure 3.30). In this respect, only some minor deviation could be observed for the investigated frequency of 0.001 Hz.

This seems to agree for instance with the observations made by Lee and Focht [1975] on the basis of their cyclic triaxial tests with the North Sea sands from the Ekofisk site, where the loading frequency had almost no effect on the cyclic strength of the sand, and also with the numerical investigations of Tasan *et al.* [2010b] for the offshore monopiles, where the initial stages of cycling were completely insensitive to the frequency and only after the 6th loading cycle there were some minor deviations in the evolution of pile-head displacements (and presumably of PWP as well).

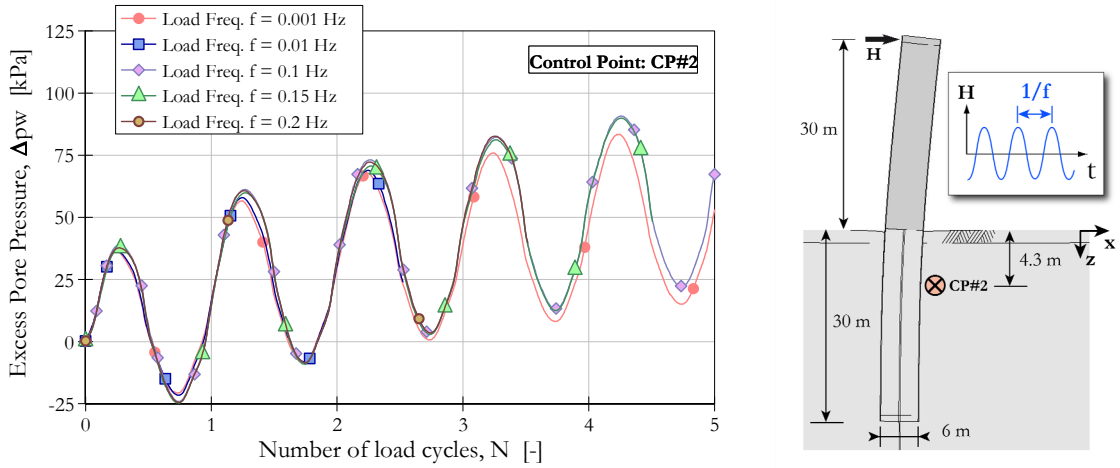

Figure 3.29 Time history of excess of PWP at control point #2 for different frequencies of cyclic loading.

This also seems to support the observation made before, that this particular system and loads are characterised by an essentially undrained behaviour of the soil, where therefore the loading frequency is irrelevant.

Consequently in this case, and for the range of frequencies typical of the offshore storm loading events (frequencies between 0.01 Hz and 0.2 Hz), the function f_F to take into account the influence of frequency into the frame of Eq. 3.137 could be

$$f_F = 1.0 \qquad for\ load\ \ frequencies\ f \in [0.01\,Hz, 0.2\,Hz] \tag{3.144}$$

However, this might not be necessarily true for other load levels, especially for soils with a different permeability. In fact, since for this parametric study only one parameter at a time has been investigated, the mutual inter-dependence between the different factors are not being captured, so they remain unclear and will have to be addressed in forthcoming investigations.

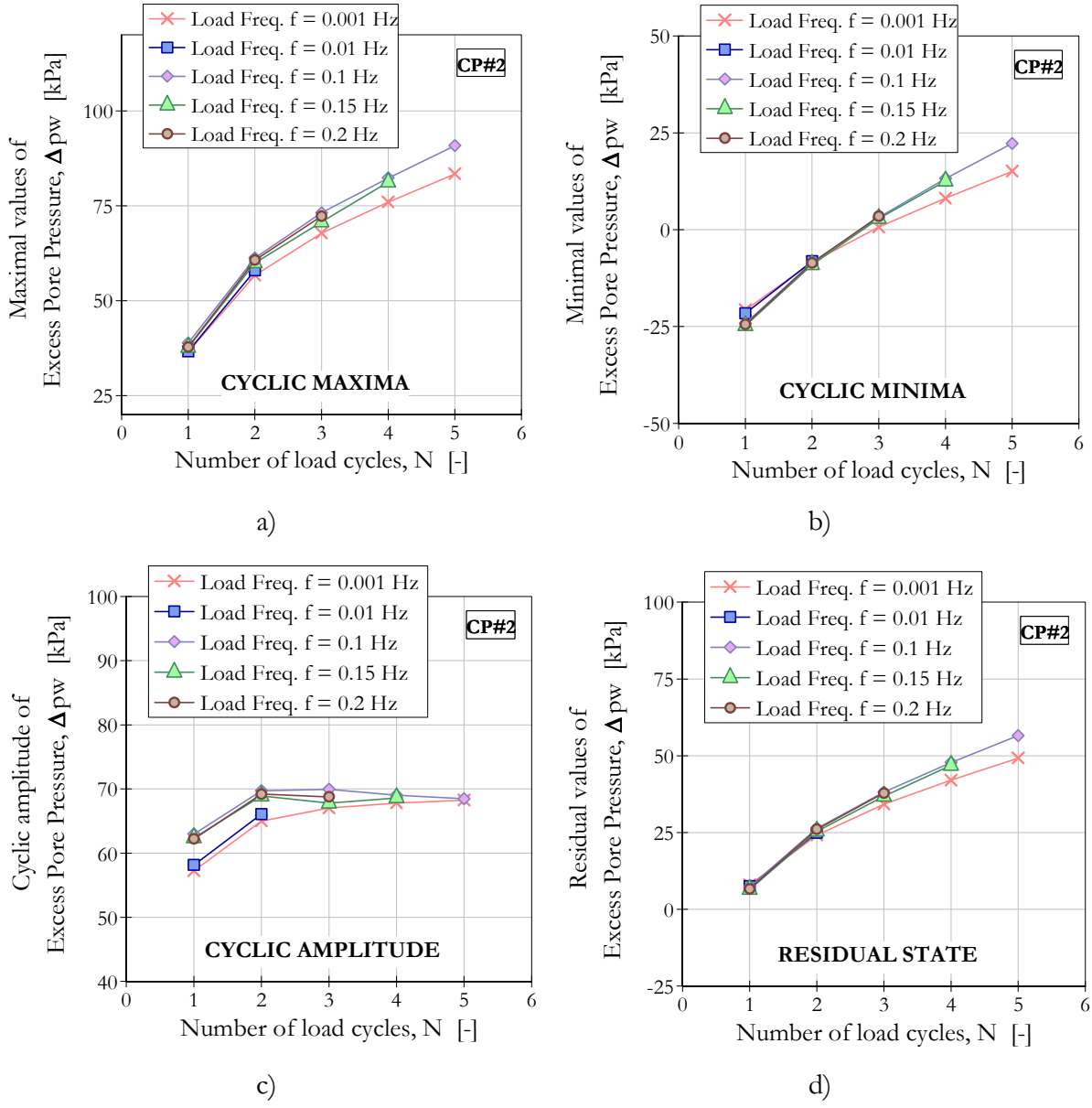

Figure 3.30 Cyclic extremal values and residual state of excess of PWP at control point #2 for different frequencies of cyclic loading. a) Cyclic maxima. b) Cyclic minima. c) Cyclic amplitude, as direct difference between cyclic maxima and minima. d) Residual state after cycling.

Incidentally, the only significant effect of a variation in the loading frequency that could be observed was a slight increase of soil settlement at the pile-head level, but only for the very low frequencies (see Figure 3.31). This can be explained by the fact that at low frequencies, the soil at shallow depths has the chance to drain partially some of the excess PWP towards the soil surface, hence allowing for some compaction and subsidence.

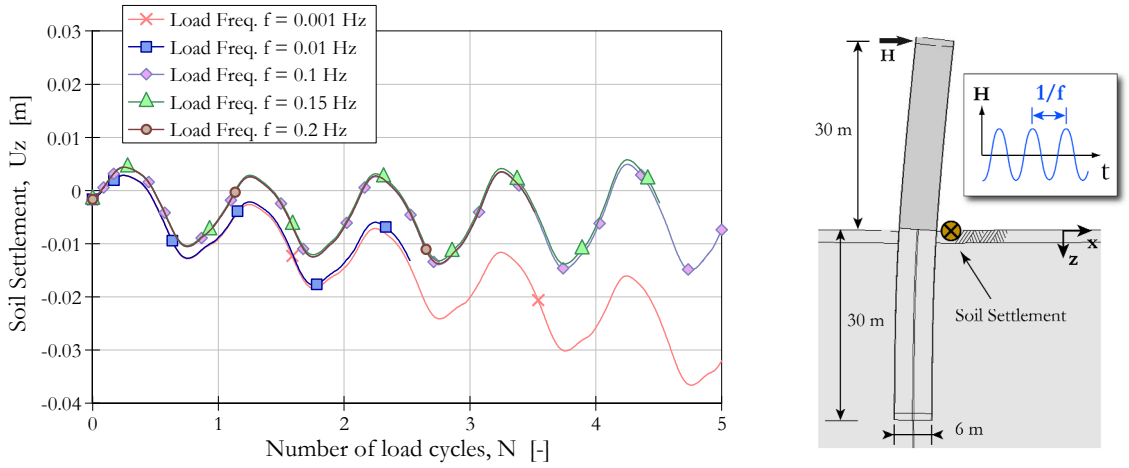

Figure 3.31 Time history of soil settlement at pile-head for different frequencies of cyclic loading.

3.6.4 Influence of pile diameter

As will be shown here, the magnitude of the pile diameter has in general two opposed effects on generation and evolution of excess PWP, which depending on the loading conditions can compensate each other to some extent:

- On the one hand, for a given load magnitude, bigger pile diameters will imply a better load transfer and stress distribution into the soil and lower levels of pile-head displacement and soil deformation, hence causing lower transient levels of excess PWP.
- On the other hand, for a given soil deformation in front of the pile, the longer drainage paths imposed by the bigger pile diameters will inhibit to a higher extent the drainage of pore water around the pile, hence causing higher transient levels of excess PWP.

This is illustrated in Figure 3.32, where two different sets of results are shown, respectively for load-controlled and displacement-controlled conditions. For the first case, three monopiles with

different pile diameters were subject to cyclic loading with the same maximum dimensionless load $\boldsymbol{\Phi}$ (as defined previously in Eq. 1.5 in Chapter 1). In this case, the piles with smaller diameter distribute the load over a smaller "subgrade reaction surface" and hence show greater pile displacements and higher absolute levels of excess PWP.

Quite the contrary, when the pile displacements are prescribed to those of the reference case as shown in Figure 3.32-b, then the single soil element in front of the pile experiences similar levels of compression for all cases, so then the longer drainage path of the bigger piles plays a dominant role, which is translated into higher absolute levels of PWP. In this case, the PWP levels generated by the 8 m diameter pile are only marginally higher than those of the 6 m diameter pile, which suggests the existence of a critical diameter beyond which further increments of diameter do not change the magnitude of generated PWP in front of the pile for a displacement controlled loading (i.e. the pile diameter beyond which the soil element "experiences" the pile as an infinite wall).

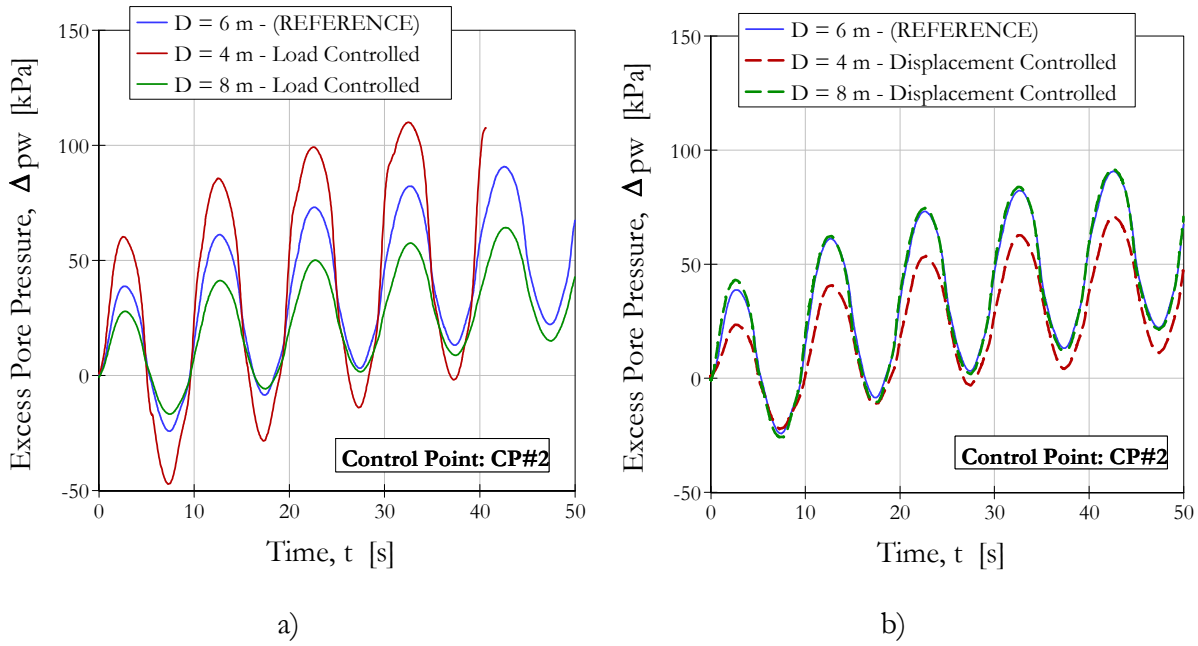

Figure 3.32 Influence of pile diameter on the time history of excess of PWP at control point #2. Comparison between cases under load control (maximum dimensionless load $\boldsymbol{\Phi}$=7.0 E-3) and displacement control (pile-head displacement prescribed to that of the reference case), shown in a) and b) respectively.

It seems important to note that for practical design purposes, the choice of a pile diameter in general is done in a "load control" manner with the prescription of a certain "storm magnitude". However, strictly speaking this does not imply constant loading conditions, since for a given sea state and design storm, the applied loads will also depend on the pile diameter, in particular through the Morison equation. Nevertheless, the conclusions out of the load-controlled analysis performed here might still be valid, since the employed dimensionless load $\boldsymbol{\Phi}$ also includes a

dependency on the pile diameter, so in absolute values the loads applied to the different piles were also somehow proportional.

In any case, in order to derive conclusions consistent with the previous sections, it is helpful to "remove" the dependence on the loading conditions and analyse the results in a normalised fashion relative to the applied pressure, for instance by means of the averaged subgrade reaction pressure $\boldsymbol{\Pi}$ introduced before (eq. 3.139). As Figure 3.33 shows, this way the results collapse roughly into one single curve, which again means that PWP is proportional to $\boldsymbol{\Pi}$ and hence inversely proportional to the pile diameter and elastic length.

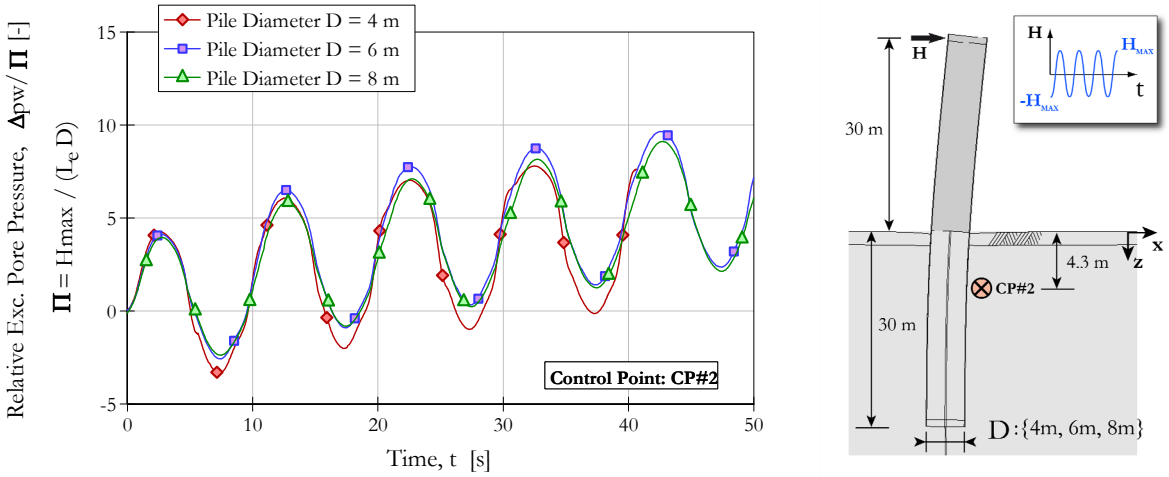

Figure 3.33 Influence of pile diameter on the evolution of normalised excess of PWP at control point #2.

Therefore this seems to indicate that at least for this system the first effect is somehow dominant while the second effect plays only a subordinate role, which appears to make sense for such extreme cases where the soil behaviour is essentially undrained, since by definition in undrained conditions the length of the drainage path is irrelevant.

Nevertheless, for cases with lower load levels and high permeabilities, it appears reasonable that the soil behaviour in front of the pile will be more sensitive to the second effect.

With respect to the evolution of the residual excess of PWP, here the rate of accumulation seems to be again rather constant, and therefore Eq. 3.141 could also apply here

$$\left(\Delta p_{W,RES}\right)_{\substack{DIAMETER\\VARIATION}} \approx C_0 \cdot \frac{H_{MAX}}{L_e D} N \tag{3.145}$$

The validity of this expression to describe also the displacement-controlled phenomena stems from the fact that by increasing the pile diameter, the denominator in (3.145) increases, but so does the numerator as well, and in a greater magnitude*).

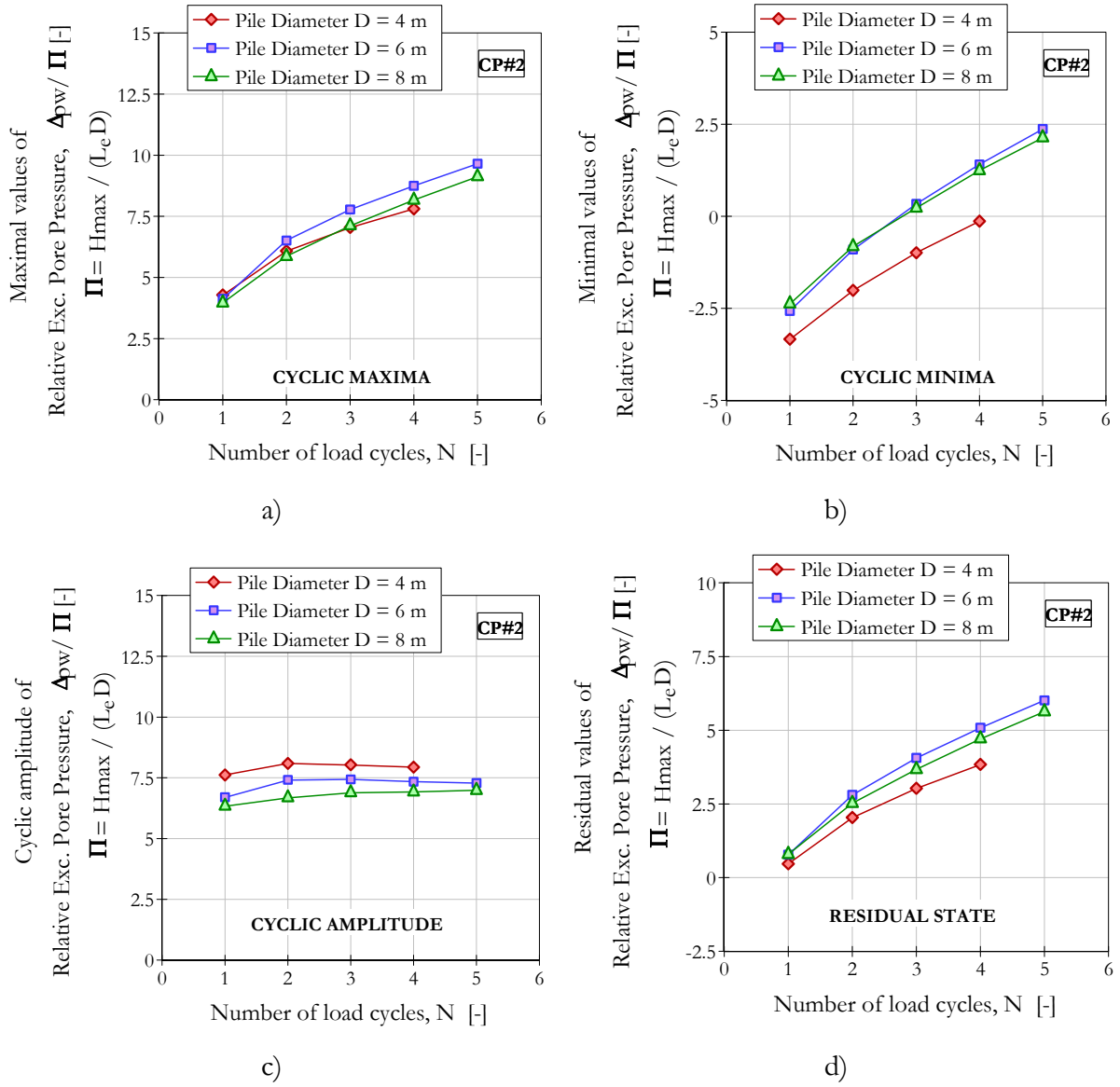

Figure 3.34 Influence of pile diameter on the normalised extremal values and residual state of excess of PWP at control point #2. a) Cyclic maxima. b) Cyclic minima. c) Cyclic amplitude, as direct difference between cyclic maxima and minima. d) Residual state after cycling.

Concerning the numerical results shown in [Tasan *et al.*, 2010b], there the investigations were focused on the displacement-controlled cases, and as a consequence they captured the second of

*) As discussed in Chapter 2 and shown for instance by Terzaghi (1945), the pile displacement and pile diameter are not related by a directly inverse proportion, so doubling the pile diameter will in general reduce the displacement by a factor greater than 2.

the effects discussed here, namely that under displacement control an increase of pile diameter increases the levels of excess PWP. Interestingly, they also investigated the spatial distribution of excess of PWP along the pile embedded length, showing that the location at which the maximum variation of PWP is generated moves downwards as the pile diameter is increased.

As a closure to this section, it is also interesting to highlight the potential similarities between the large-diameter piles and the new concepts for piles with wings, which are currently starting being considered for the foundation of offshore wind turbines (see e.g. [Grabe, 2008; Dührkop, 2010]). In this respect, and although the introduction of the wings implies an elongation of the drainage path in shallow layers (the water may not flow easily around the pile at those depths), the better distribution of loads and lower soil stress levels in front of the pile will probably imply lower transient levels of excess PWP, just as seems to happen with the large diameter piles studied here. In any case, detailed numerical studies in this direction should provide more information not only about the levels of excess PWP but also about the accumulation rates.

3.6.5 Comprehensive PWP accumulation trend

On the basis of the results shown so far, the global description of PWP accumulation pattern introduced in Eq. 3.137 could take the following tentative form:

$$\Delta p_{W,RES} = C_0 \cdot \frac{H_{MAX}}{L_e D} \cdot e^{\frac{(k_{UT}-k)}{k_{DT}} C_1} \cdot N \qquad for \begin{cases} \Pi > \Pi_{UT} \\ and \\ k \in (k_{UT}, k_{DT}) \end{cases} \tag{3.146}$$

$$\Delta p_{W,RES} = C_0 \cdot \frac{H_{MAX}}{L_e D} \cdot N \qquad for\ k \le k_{UT} \tag{3.147}$$

$$\Delta p_{W,RES} = 0 \qquad for \begin{cases} \Pi \le \Pi_{DT} \\ or \\ k \ge k_{DT} \end{cases} \tag{3.148}$$

where C_0 is a system constant, and k_{UT}, k_{DT}, Π_{UT} and Π_{DT} are the thresholds for permeability and averaged subgrade pressure respectively, as investigated in the previous sections.

As mentioned previously, for those cases where the load level lies in between the upper and lower thresholds, the evolution of residual pressures appears to be more complex and definitely not

linear, so due to the scarce data available at the moment, an analytical formulation for those cases has not been attempted here and just be left for future investigations. However, for a preliminary conservative evaluation, the undrained load threshold can be taken as low as the drained one (i.e. $\Pi_{UT} = \Pi_{DT}$) so that all load levels above Π_{DT} are calculated through (3.146) and (3.147).

As can be seen in Figure 3.35 and Figure 3.36, where the proposed approximation has been used to describe the results of the parametric study, a single set of thresholds and system constants can reproduce fairly well the PWP accumulation trend of most of the studied cases. For all the approximations shown in the figures, the following constants were used:

Table 3.11 System constants for the synthetical approximation of numerical results of PWP accumulation.

Parameter in (3.146)	**C_0**	**C_1**	**Π_{UT}**	**Π_{DT}**	**k_{UT}**	**k_{DT}**
Value	1.2	20	0.94 kPa	0.94 kPa	7.5E-4 m/s	7.5E-1 m/s

It is important to stress again that this way the mutual inter-dependencies between the different factors are not being captured, so in this respect, the different thresholds discussed here are also very likely to be related to each of the other variables.

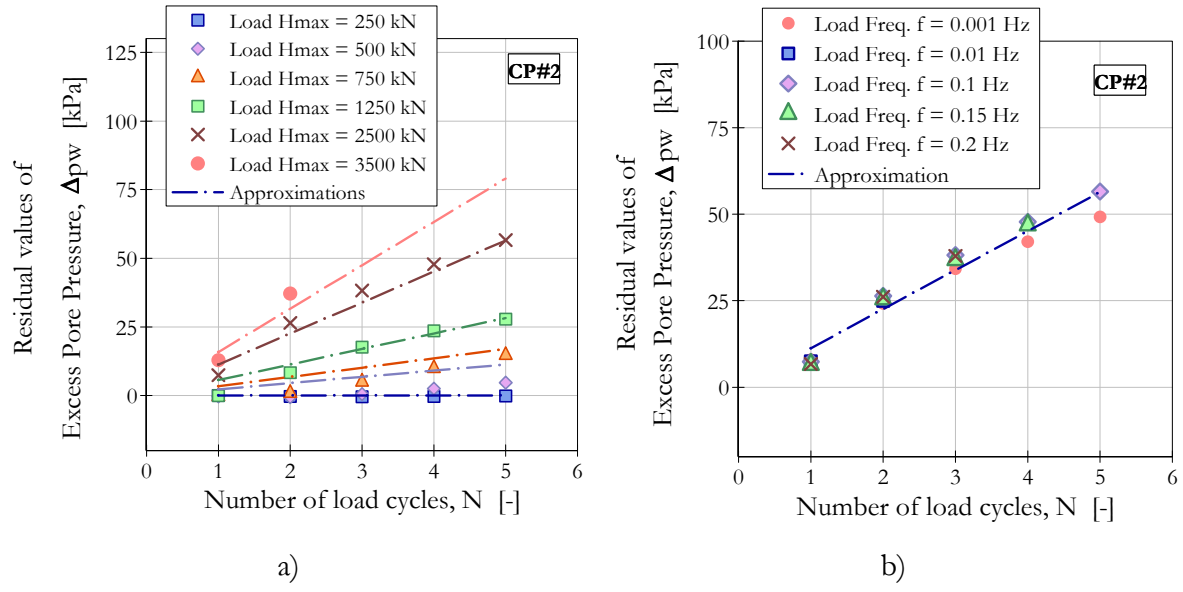

Figure 3.35 Synthetical approximation of PWP accumulation trends from the numerical results of the parametrical study. Approximation including variations of a) Load level and b) Frequency.

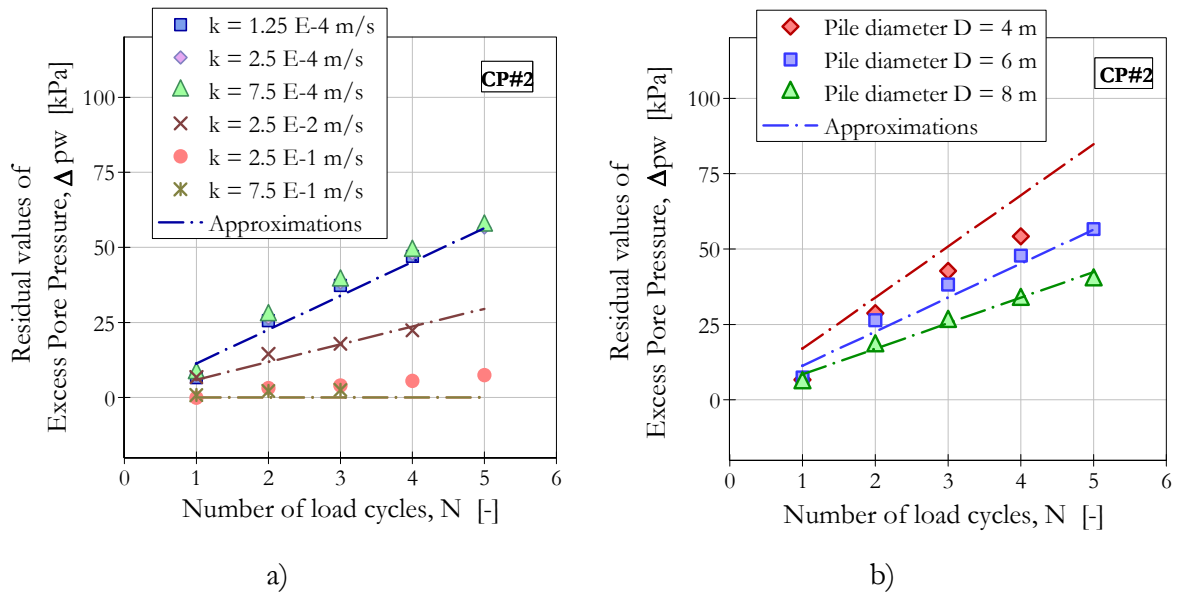

Figure 3.36 Synthetical approximation of PWP accumulation trends from the numerical results of the parametrical study. Approximation including variations of a) Permeability and b) Pile diameter.

As a final remark, it can be pointed out that the linear evolution observed for the first 5 cycles is very likely to change with higher numbers of cycles, in particular as the excess of PWP approaches the "saturation level" where it cannot increase further. Also significant changes in the amplitude of the cyclic variations may occur for higher numbers of cycles, as shown for instance by Tasan *et al.* [2010b] for the cyclic one-way loads. In any case, the linear increase of PWP adopted here might be for most of the cases a conservative assumption, since probably a logarithmic or power law evolution with the number of cycles would be more close to the reality.

3.6.6 A note on irregular loading and order effects

The effects of an irregular loading and specially the influence of the system's historiotropy (i.e. its dependence on the past loading history) are probably quite significant and complex, and therefore their detailed investigation shall be left for future investigations. Nevertheless, it is possible to obtain some useful information about these topics just by considering simple cases, as shown in this section.

First of all, the particular case where the system is subject to two sinusoidal load signals with variable amplitude, linearly increasing and linearly decreasing respectively, has been considered, and illustrates the fact that the order effects can play a relevant role, even under moderate load levels

and few cycles. For such purpose, the load signals shown in Figure 3.37-a have been employed, which feature the same number of cycles and identical load amplitudes but just in inverse order.

A direct plot of the pile-head displacements and their residual values (i.e. the values at the moments when the applied load ***H*** equals zero) as shown in Figure 3.37-b might not reveal many differences after so few cycles, although there it is already possible to observe a different displacement amplitude during the extreme cycle, pointing to a softer response of the pile under the increasing load pattern.

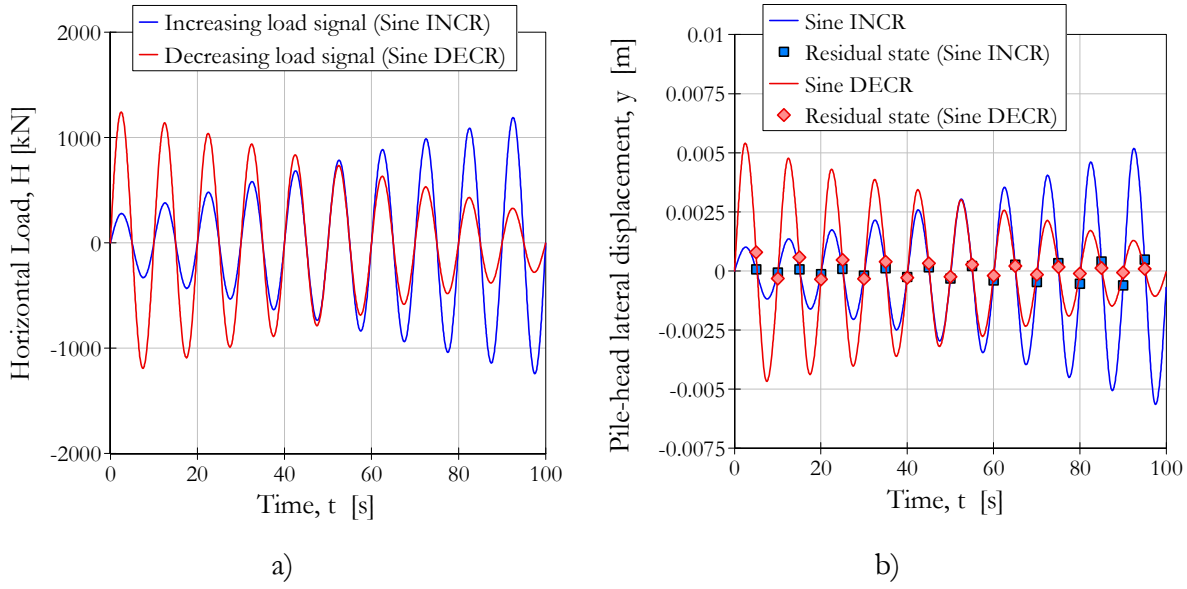

Figure 3.37 Increasing and decreasing sinusoidal load signals for the investigation of the order effects. b) Time history and residual states of pile-head displacement.

A plot of the evolution of excess of PWP (Figure 3.38) already shows more distinct deviations, eminently at shallower depths (***CP#1***), where not only the residual values but particularly the cyclic amplitudes are significantly different, just depending on the order of application. Here again it is possible to see that the increasing load signal produces much higher oscillations during the extremal cycles than the decreasing one.

However, the most salient evidence of the sensitivity of the system to the order effects might be observed upon consideration of the global response of the foundation in terms of its actual (tangent) integral stiffness and hysteretic cycles, shown here in Figure 3.39. There, the evolution of the integral stiffness, defined as the increment of external load divided by increment of foundation displacement it produces, shows and confirms that the increasing load signal causes a more remarkable softening than the decreasing one, in both absolute and relative terms. Not only that for the former case the stiffness is reduced by almost 15% of its original value within ten cycles

while for the latter it remains rather stable, but also the final state after cycling is clearly softer for the increasing load pattern, despite showing a stiffer initial response.

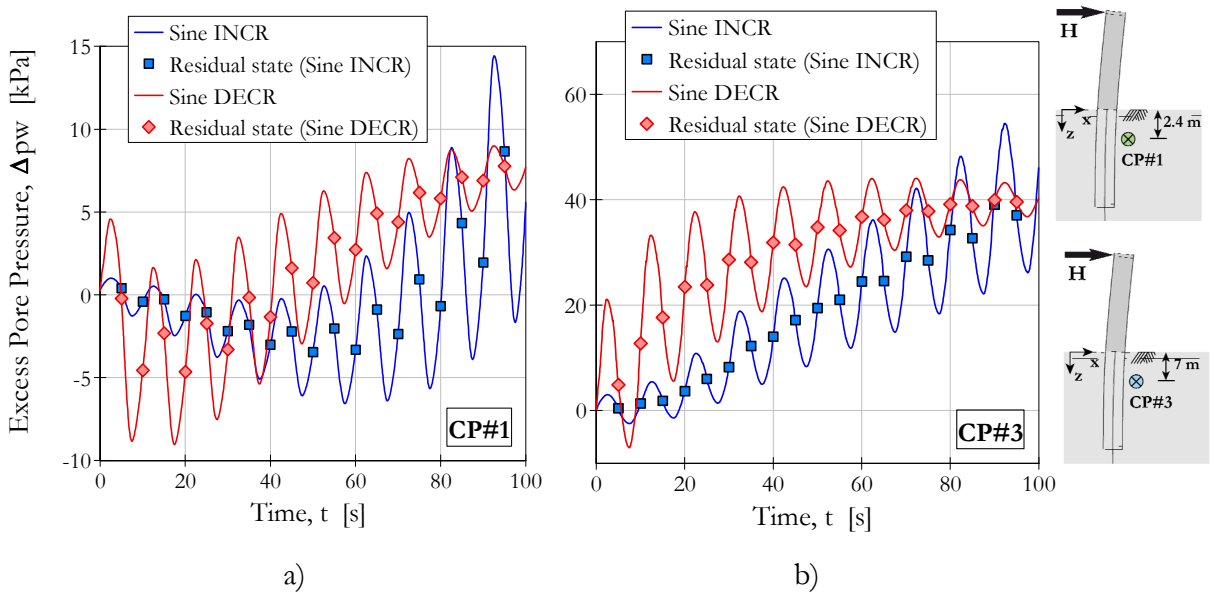

Figure 3.38 a) Time history and residual states of excess of PWP at control point #1 for increasing and decreasing sinusoidal load signals. b) Results at control point #3

Similar conclusions can be drawn from the global load-displacement relationships (see Figure 3.39-b), where the characteristical hysteretic loops are more slanted for the case with increasing load signal than for its decreasing counterpart.

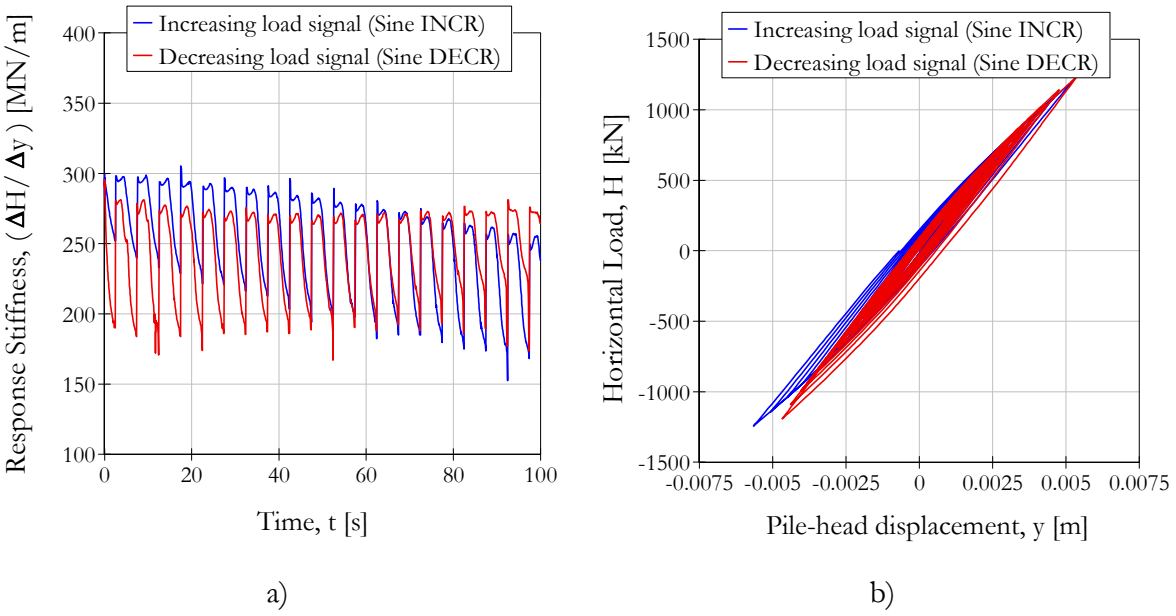

Figure 3.39 Influence of the order effect on the pile's integral response. a) Stiffness evolution for the two different sinusoidal loading schemes. b) Softening of the pile's load-displacement hysteretic cycles.

The second example in this respect features a load signal with the same duration and maximum amplitude as the preceding ones, but this time in an irregular succession of cycles taken out of a real time signal from a storm loading realisation of an actual offshore wind turbine (more details on this are given in Section 3.7). Figure 3.40 shows the employed time signal and the computed pile-head displacements.

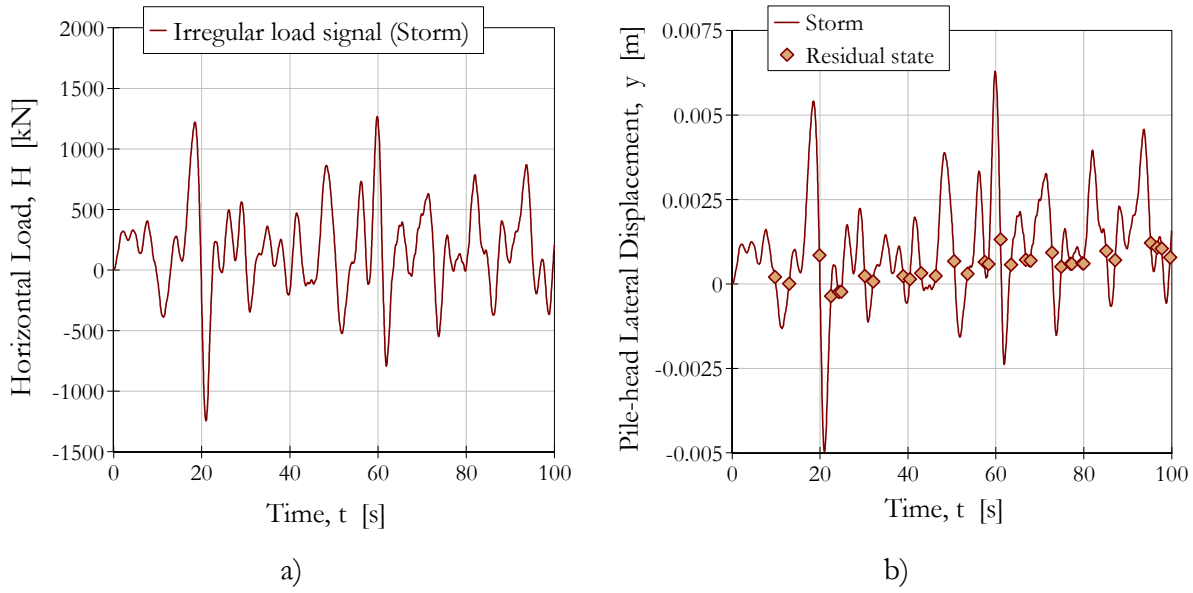

Figure 3.40 Irregular load signal from a storm event. b) Time history and residual states of pile-head displacement.

In this case, the first thing that becomes apparent is the significant increase of residual (permanent) pile-head displacements as compared to the cases under sinusoidal loading, which seems to be reasonable considering that now the loading neither is symmetrical nor has a purely two-way character.

The second relevant feature is that in this case the excess of PWP also increases at all depths as the cycling progresses (Figure 3.41), incidentally to the same orders of magnitude as in the cases with sinusoidal loading. It is also interesting to observe how the first "extreme cycle", taking place after approximately 20 seconds, has a completely opposed effect at the two different control depths. While that load cycle causes at the ***CP#1*** a pronounced underpressure, which is only compensated after the following 30 seconds, the very same cycle produces a steep increase in residual PWP at the ***CP#3***, five meters below. Alone this fact already calls for special caution when extrapolating the results and patterns from a single depth to the whole embedded length of the pile.

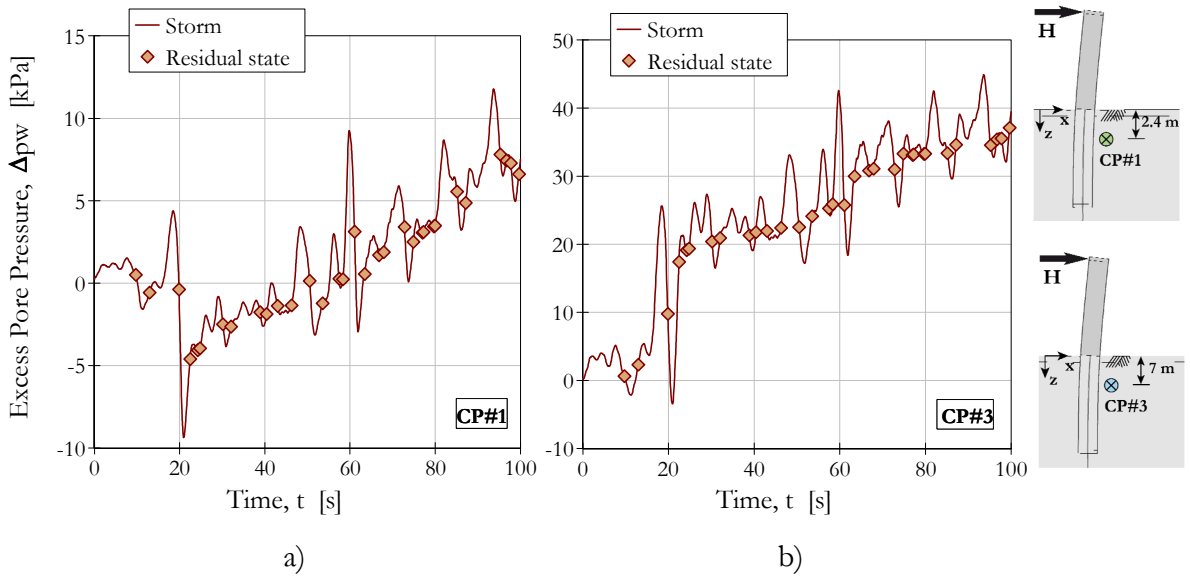

Figure 3.41 a) Time history and residual states of excess of PWP at control point #1 for a storm event. b) Results at control point #3.

Finally, as it was done for the irregular sinusoidal cases, a plot of the response stiffness and hysteretic cycles shows how the global response of the pile becomes softer in general terms, although the latter diagram remains somewhat obscure due to the irregular shape of the cycles.

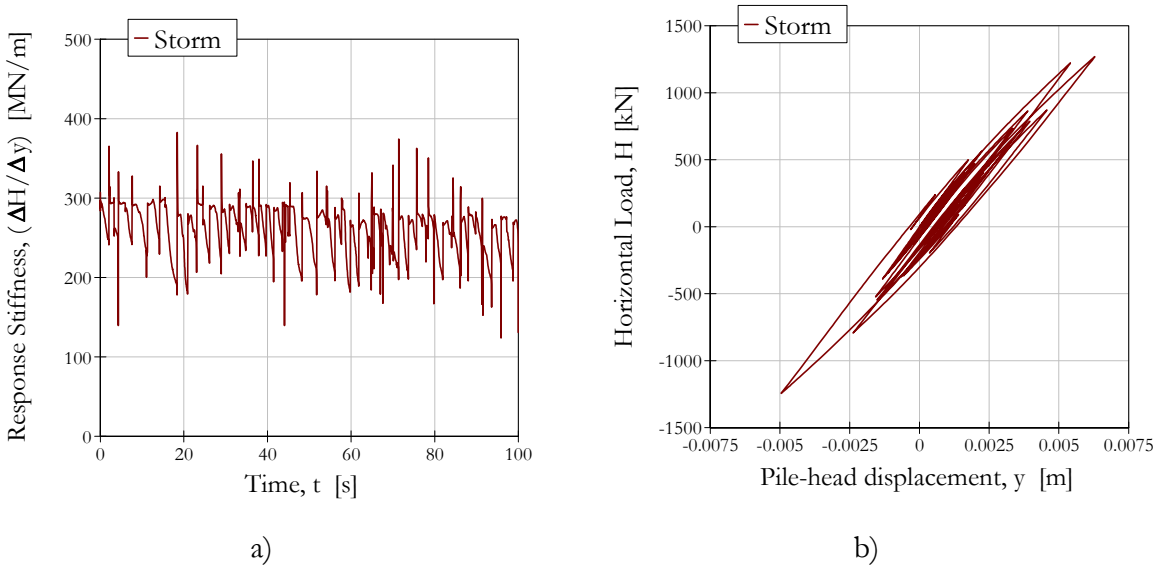

Figure 3.42 Evolution of the pile's integral stiffness. a) Time history of the response stiffness during a storm event. b) Pile's load-displacement hysteretic cycles.

3.6.7 A note on the computational cost

As a complement to Section 3.3 and guidance concerning the computational cost of such investigations, Figure 3.43 illustrates the impact of the different factors on the average number of time steps necessary for the simulation of one single load cycle.

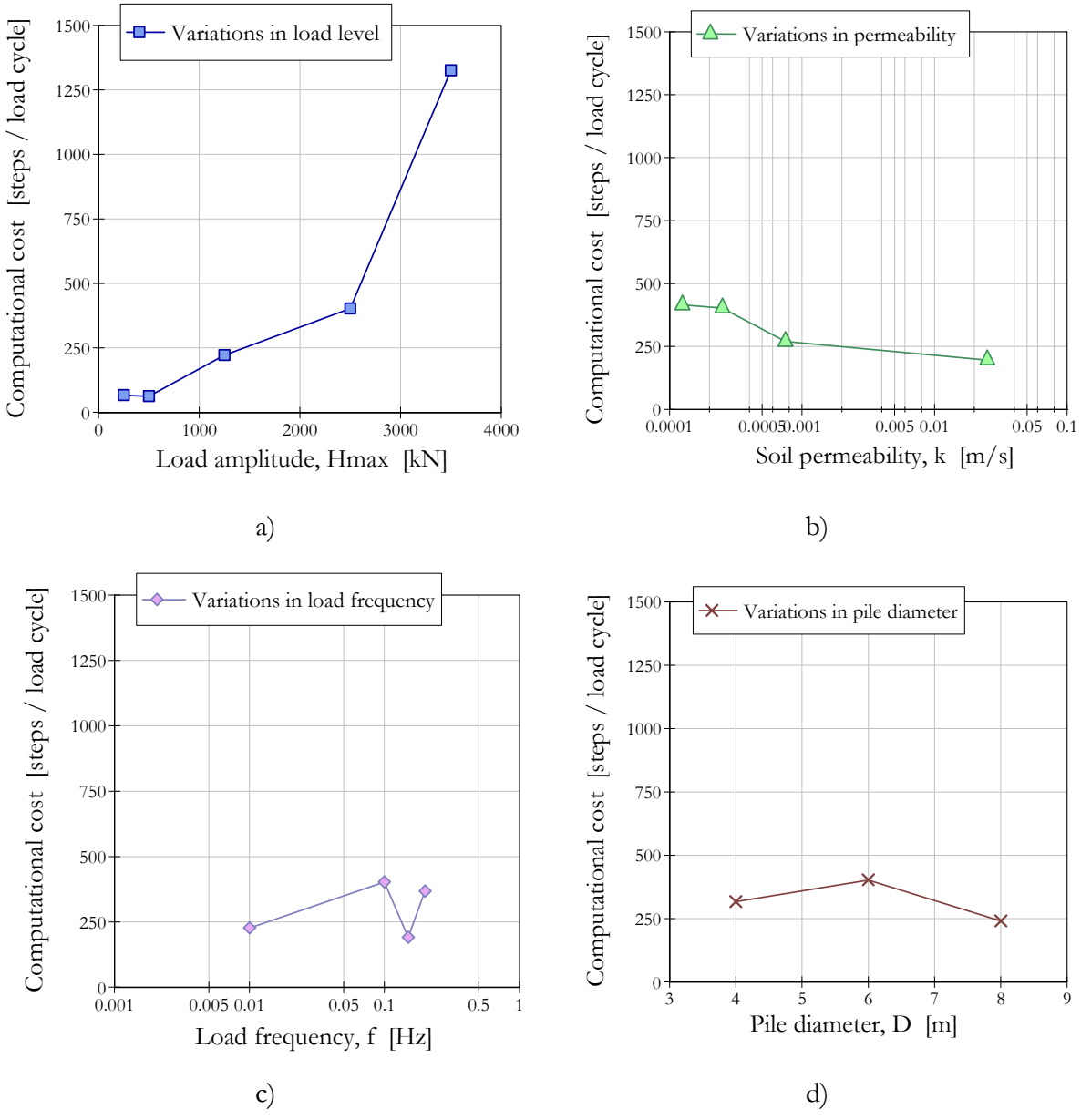

Figure 3.43 Relative measure of the computational cost of the different cases depending on a) load level, b) soil permeability, c) load frequency and d) pile diameter.

For these calculations, an adaptive time-stepping algorithm was employed, in which a maximum number of 20 Newton-Raphson iterations per time step was prescribed. Whenever the calcula-

tions would fail to converge within this limit, the time step size would be automatically reduced, while after 5 consecutive successful steps the time step size would be increased again.

This way, the number of steps per load cycle is a direct measure of the global difficulties to compute a given case. As shown in Figure 3.43, the computational time almost doubled for the cases with low permeability or high loading frequency. However, the most influential factor on the computational cost was by far the load level, which showed an exponential growth as the loading increased.

3.6.8 A note on the choice of constitutive model

The need for an advanced constitutive model in order to simulate the PWP evolution in the soil and the obvious limitations and inadequacy for such purpose of the classical elastic-perfectly-plastic models can be well illustrated with a simple plot of the time history of excess PWP in the soil when using the different models under the same conditions and with comparable material constants (Figure 3.44).

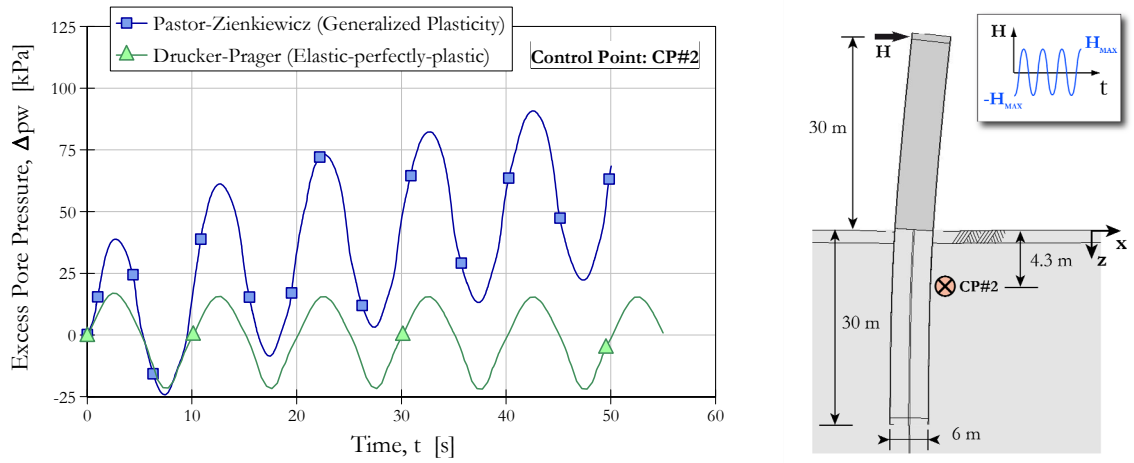

Figure 3.44 Influence of the choice of constitutive model on the computed evolution of excess of PWP.

In this respect, and independently of the yield criterion that they incorporate (Drucker-Prager, Mohr-Coulomb, etc....), the elastic-perfectly-plastic models are only capable of generating transient changes of PWP within a load cycle, but are basically unable to reproduce its accumulation as the cycling progresses. This is mainly due to the assumption of an elastic behaviour for all

stress states inside the yield surface and the inability to produce permanent volumetric strains upon stress reversal.

3.7 Computation of a real storm

In order to demonstrate the suitability of the presented model for its practical application in design, a real time signal from a storm loading realisation of an actual offshore wind turbine in the North Sea has been used as input load signal for the basic foundation model discussed in Section 3.6. The load realisation, shown here in Figure 3.45, has been defined as a 600-seconds time signal, as it is usual in the offshore practice, and corresponds in this case to the maximal storm with a return period of 1 year, which has the local characteristics presented in Table 3.12.

Table 3.12 Local characteristics of a 1-year return period extreme storm in the German bight of the North Sea.

Parameter	Description	Value
$v_{1,RED}$	Extreme 1-minute wind gust speed at hub height	32.5 m/s
TI	Turbulence intensity	9.7 %
H_S	Significant wave height	6.5 m
T_P	Peak wave period	11.2 sec
H_{MAX}	Maximum wave height	12.2 m
-	Turbine's operational mode	Off-load

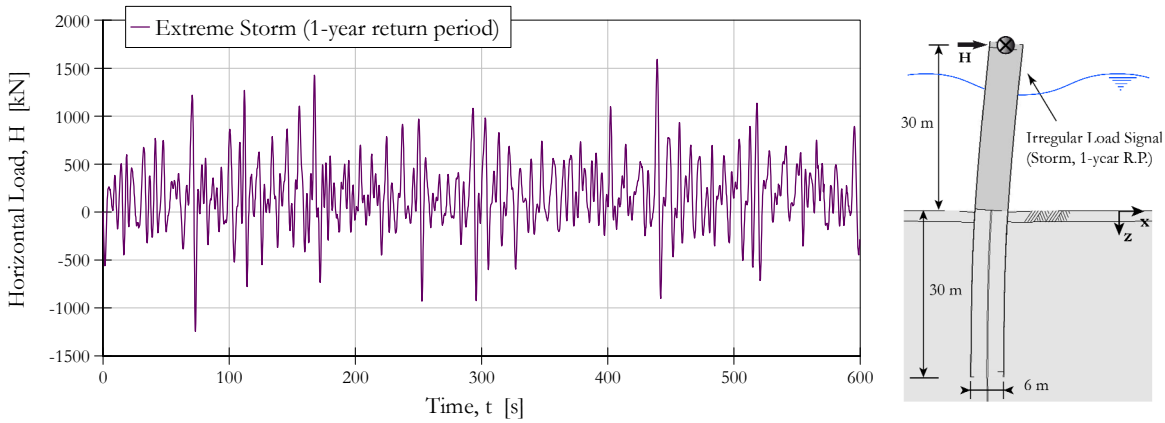

Figure 3.45 Time history of horizontal loading produced by an extreme storm with 1-year return period.

The transient and permanent deformations caused by the storm on the foundation and its surrounding soil are illustrated in Figure 3.46, where the pile-head lateral displacement and soil settlement are shown exemplarily for the initial 400 seconds. While the few centimetres of soil settlement might not be of direct relevance for the foundation design and operation, they already indicate that the passage of such a storm produces changes in the soil with a particular densifying character, which at least for a certain duration might imply a transient softening of the foundation, until the excesses of PWP are dissipated completely after the storm.

Of direct relevance for design are however the several millimetres of permanent pile-head lateral displacement, which, it must be stressed, are produced in only 10 minutes of storm. Even if the rest of the storm were assumed to produce no further permanent deformations, the fact that such storm has a 1-year return period means that during the turbine's life-time (say 20 to 25 years) the accumulated lateral displacement could reach orders of magnitude of tens of centimetres, which can indeed interfere with the turbine's serviceability and normal operation.

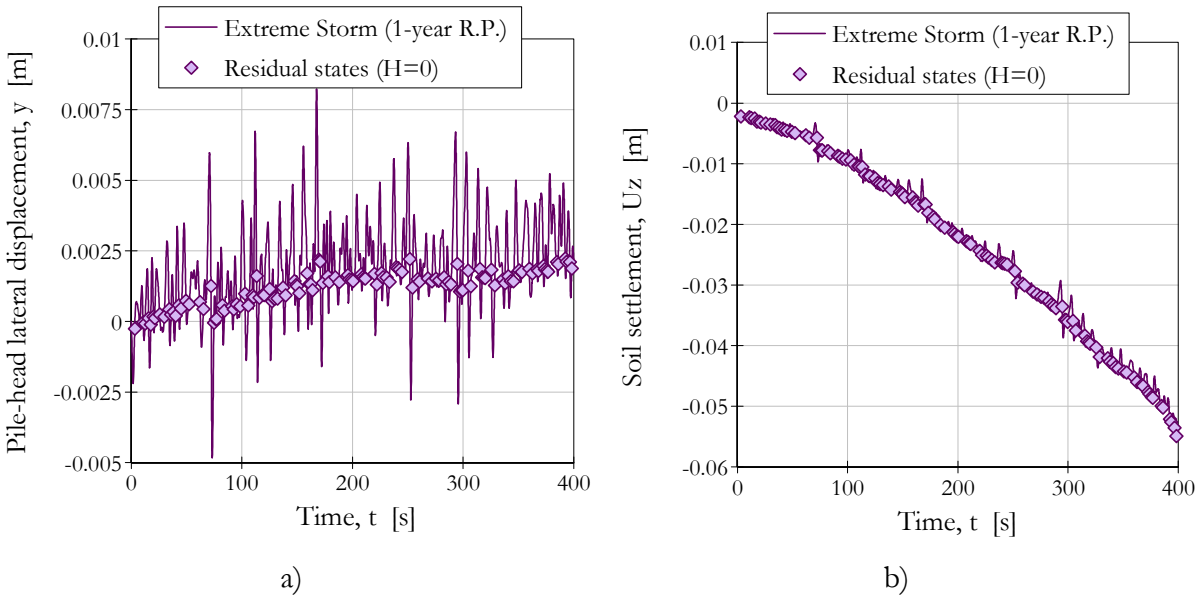

Figure 3.46 Time history and residual states of the displacements produced by a 1-year return period extreme storm. a) Pile-head lateral displacement. b) Soil settlement at pile-head.

An examination of the excess of PWP at the control points reveals again a clear accumulating trend, although with a different character at the different depths (Figure 3.47). In this respect, the residual pressure at the ***CP#1*** only starts to increase after approximately the first 100 seconds of loading, while in the ***CP#3*** the accumulation starts immediately at the beginning of the storm. Nevertheless, in both cases the rate of accumulation does not remain constant and the levels of excess PWP seem to gradually stabilise at all depths at some point (approx. after 300 seconds).

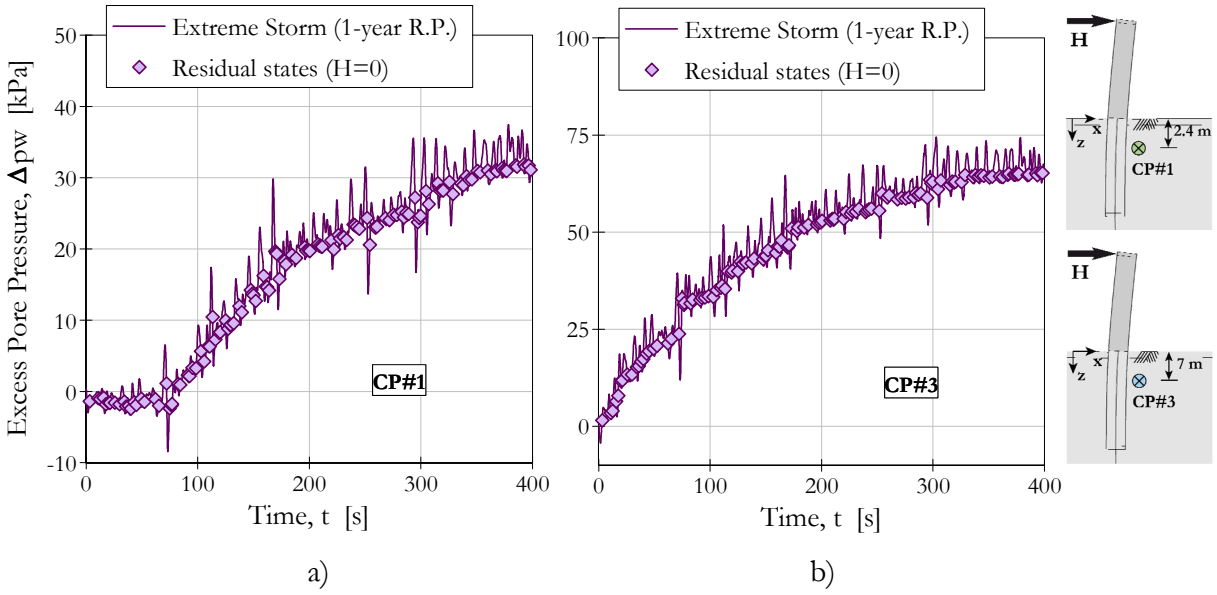

Figure 3.47 Time history and residual states of excess of PWP produced by a 1-year return period extreme storm. a) Computed results at control point #1. b) Computed results at control point #3.

But probably, the most illustrative picture of the effects of the storm on the state of the foundation is obtained by observing the evolution of the tangent integral stiffness of the whole system, as depicted in Figure 3.48. There it is possible to appreciate directly the softening effect produced by the progressive accumulation of excess of PWP at the different depths and, most interestingly, how this transient reduction of global stiffness seems to stabilise at the same time as the levels of residual excess PWP become steady.

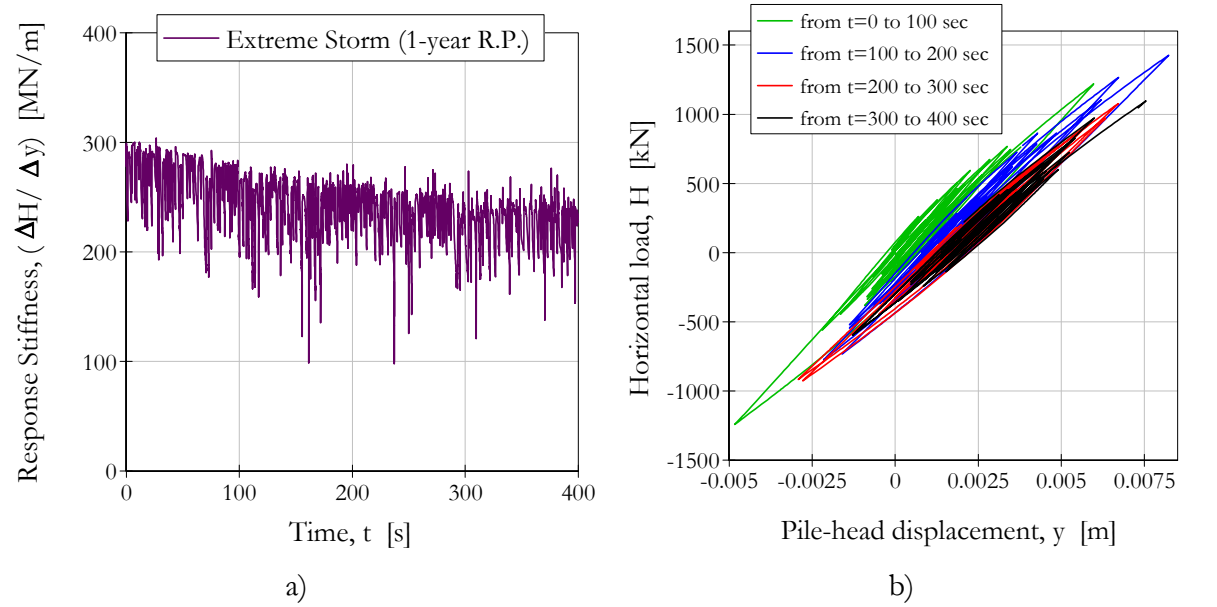

Figure 3.48 Evolution of the pile's integral stiffness during a 1-year return period extreme storm. a) Time history of the response stiffness. b) Pile's load-displacement hysteretic cycles.

It is important to note that although such loss of stiffness might only be transitory and the foundation may be able to regain its original stiffness again once the excesses of PWP are dissipated after the storm (or even higher, due to the soil densification), the general softer behaviour during the storm might give origin to significant levels of permanent displacements, which in general will not be compensated after the storm. This highlights the importance of considering the coupling effects between soil stress and pore water pressure in design, even for those cases (such as the one presented here) where a soil liquefaction could in principle be disregarded on the grounds of the high relative density of the soil.

As a final note on the computational cost of such a storm realisation, the average rate during the calculations using an Intel Xeon 8-processors Workstation was around 10 to 20 real-time seconds per day. For other cases, it must be stressed again that the actual computational cost will heavily depend on the soil and foundation characteristics, but especially on the loading conditions, as discussed previously in Section 3.6.7.

3.8 Recapitulation

In the first part of this chapter, the three basic requirements for the coupled transient analysis of an offshore pile foundation have been introduced, namely a mathematical model that accounts for the interaction between the soil solid skeleton and the pore water, a constitutive model that reproduces the main aspects of sand behaviour and is able to generate residual pore pressures upon cyclic loading, and finally a numerical model that discretises all the equations for their efficient implementation in a calculation program.

Then, the particular conditions to ensure the stability of the pressure field and to provide a suitable pile-soil interface have been addressed and two efficient options have been proposed, namely the coupled form of the Simo-Rifai EAS element due to Mira and the no-tension isoparametric joint element respectively.

Afterwards, the focus has been put on the critical issue of the computational cost and its possible optimization through the choice of an appropriate solution strategy, an efficient handling of the sparse matrices and specially the parallel computation. Without such optimizations, the cost of the calculations presented here would have been simply unaffordable.

Subsequently, the capabilities of the model have been shown by means of a case study, where the instance of an 8 m-diameter pile subject to extreme lateral loading has been examined and the behaviour of the surrounding soil analysed. A clear accumulating trend in the evolution of excess of PWP was observed, which led to local phenomena of cyclic mobility and a general softening of the foundation.

Thereafter, the influence and relevance of some of the main factors that affect the generation of pore pressure have been discussed on the basis of a parametric study and a tentative formulation to describe the results has been derived. As an outcome of the study, the existence of thresholds for the undrained and drained behaviour of the pile has been proposed and a particularly unexpected conclusion drawn, namely that an increase of pile diameter can have an overall beneficial effect on the accumulation of PWP despite the elongation of the drainage paths around the pile.

Then, the so-called order effects and the influence of load irregularities have been briefly discussed by means of two simple examples, whereby a certain significance of the order effects was noticed, particularly for the overall stiffness of the foundation's response.

And finally, the loading case of a realistic storm time signal was examined, which again was observed to produce a general increase of pore pressure in the soil. Interestingly, the excess of PWP did not increase indefinitely during the storm, but at all depths reached a certain "saturation level" where it appeared to stabilise. Nevertheless it can be concluded that, even if a full liquefaction seems unlikely to happen, particularly for the dense sands of the North Sea, a certain softening of the foundation will probably take place during such storms.

Therefore, the main issue with accumulation of PWP around the pile, at least for moderate storms (1-year return period), may not be the full soil liquefaction and collapse of the foundation, but rather the very probable softer behaviour of the foundation during the storm and its possible consequences for serviceability in terms of excessive permanent pile displacements.

4 LONG TERM BEHAVIOUR: EXPERIMENTAL INVESTIGATIONS

Although the numerical simulations are a powerful tool which can provide useful information about the system's behaviour, they also have some inherent limitations. For instance, the usual representation of the geomaterials as continua in the FE approaches may give an adequate description of their behaviour at macro-mechanical level, but by definition will fail to reproduce the micro-mechanical phenomena occurring at the granular level, even if their effects are included *artificially* into the constitutive model. On the other hand, the discrete numerical approaches, which aim at the consideration of every single particle as a separate body, are usually restricted by the shape and number of the particles in the model so that their applicability to real-size foundations is at present still quite limited.

In any case, regardless of the mechanical scope of the numerical model (either macro or micro), the transient simulations will always face at some point the constraints imposed by the *chronological* time (in addition to the computational time). No matter how simple the constitutive models are, the transient simulations will always imply a division of time into discrete steps or time stations and, hence, a progressive accumulation of the residual errors which eventually renders the calculations useless after certain number of steps. This is especially true for the case of geomaterials, where the complex non-linear and path-dependent constitutive models will usually require a large number of small time steps for the simulation of transient scenarios. In practice, it is generally assumed that the conventional incremental approaches have an upper limit of validity between 50 and a few hundred cycles for common cyclic loading processes [Niemunis, 2000; Wichtmann, 2005; Achmus *et al.*, 2009].

An alternative approach that aims to circumvent this problem is given by the so-called explicit accumulation (or N-dependent) methods*) which, by the use of empirical rules or theoretical simplifications, replace the time variable by some suitable expression of the number of load cycles $\boldsymbol{N}$ [Sagaseta *et al.*, 1991; Niemunis *et al.*, 2004; Wichtmann, 2005]. Although such procedures can usually be calibrated with element tests to replicate the effects of a large number of load cycles, their applicability to more general cases, with for instance irregular transient loading or partially drained saturated conditions, is still not clear.

*) Not to be confused with the explicit methods for the numerical integration of ordinary differential ecuations, like for instance the forward-Euler scheme.

Therefore, an overview on the long-term behaviour of the cyclically loaded piles may be better achieved empirically through suitable physical model tests, even if their representativity may sometimes be only qualitative due to scaling restrictions and other simplifications.

In the first section of this chapter, the two main questions that motivated these experimental investigations, namely the long-term foundation stability and the local phenomena of soil subsidence and grain migration around the pile, are introduced and discussed.

Then, the physical model tests in reduced scale performed at the BAM for the offshore pile under long-lasting cyclic lateral loading are described, and subsequently the results and data gathered from the sensors are presented and analysed.

Afterwards, aiming to study the subsidence and cyclic densification of the soil, some topographic measurements of the soil surface around the pile are introduced and some conclusions are drawn. And finally as a closure to this chapter, new empirical evidence of ratcheting convective cells of sand grains around the laterally loaded piles as well as the practical implications of these experimental findings are brought forward and discussed.

4.1 Motivation and Scope

In principle, the main purpose of the experimental investigations was to study the structural stability of the laterally loaded pile after the application of several millions of load cycles, and specifically to assess whether a brittle failure as in the case of axially loaded piles could take place or not. However, in the course of the first experiments two particular phenomena were observed, namely a soil subsidence around the pile and a permanent grain migration towards the pile. These two effects seemed to be closely related to a densification of the soil around the pile due to the cyclic loading, but the fact that the grain migration never ceased during the application of the 5 million load cycles motivated further experimental investigations.

Other long-term phenomena as the time effects involved in the so-called pile ageing or set-up were out of the scope of these investigations (the interested reader may refer for instance to [Chow *et al.*, 1997], [Bowman, 2002], or [Jardine *et al.*, 2006]) and besides were assumed to be negligible or play a minor role in the scheduled tests, where the loading frequencies were relatively high and the loading program for each test was accomplished within around 8 weeks. In any case, the cyclic densification and embedment stiffening discussed later in Section 4.3 can be re-

garded as a form of ageing effect, indirectly related to the chronological time through the number of applied load cycles.

4.1.1 Long-term stability: cyclic Axial vs. cyclic Lateral loading

Although cyclic loading is only seldom taken into account explicitly during pile design*), it is well known and widely accepted that cyclic axial loading of piles can cause the so-called friction fatigue [White & Lehane, 2004; White, 2005], where the cyclic densification (and hence contraction) of the soil at the pile-soil interface leads to a reduction of the radial stress exerted by the far field on the pile shaft. Such progressive decrease of radial stress at the interface is directly related to a reduction in the shaft bearing capacity of the pile, which eventually can lead to a brittle (sudden) failure of the pile. Figure 4.1 shows exemplarily the cyclic axial load tests performed by Jardine & Standing [2000] and Schwarz [2002], where, despite their initial stable behaviour under cyclic loading, the piles eventually fail abruptly after a certain number of load cycles. It is remarkable that in the latter reference the brittle failure only happens after the application of several tens of thousands of load cycles.

In contrast, the available literature on the cyclic *lateral* loading of piles shows in general a decreasing pattern of the incremental cyclic displacements, which has been usually approximated with a logarithmic or power law function of the number of cycles (see for instance [Alizadeh & Davisson, 1970; Hettler, 1981; Long & Vanneste, 1994; Grabe & Dührkop, 2008; Achmus *et al.*, 2009]). Those observations agree with the common assumption that the cyclic lateral loading of piles generally involves an attenuation ("Beruhigung" in the German literature) of the cyclic displacements and only potential serviceability problems (i.e. excessive pile head displacements or rotations, rendering the structure useless) rather than an eventual loss of mechanical equilibrium (pile failure leading to a dramatic increase in cyclic deflections).

However, such assumptions and approximating descriptions of lateral pile cycling are based mainly on experimental tests with a *low* number of load cycles (e.g. from the mere tens or hundreds of cycles in the early investigations of Alizadeh & Davisson or Cheang & Matlock to the tens of thousands of cycles in the recent works of Achmus *et al.* or Grabe & Dührkop).

*) Offshore standards merely prescribe an across-the-board reduction in the p-y curves for cyclic lateral pile resistance, irrespective of the magnitude and number of repetitions of the load [API, 2007; DNV, 2004].

Since the pile foundations in the offshore environment are exposed to millions of load cycles during their service life-time, the absence in the literature of empirical studies of lateral pile behaviour in such range of number of cycles prompted the performance of the physical model tests presented in this chapter. The loading schedules, each of them including millions of cycles, were therefore aimed at elucidating whether an abrupt failure analogous to those shown in Figure 4.1 could also take place for the laterally loaded pile *after* the usual stabilizing shakedown phase of the first thousands of cycles, and in general at clarifying the long-term lateral behaviour of the piles.

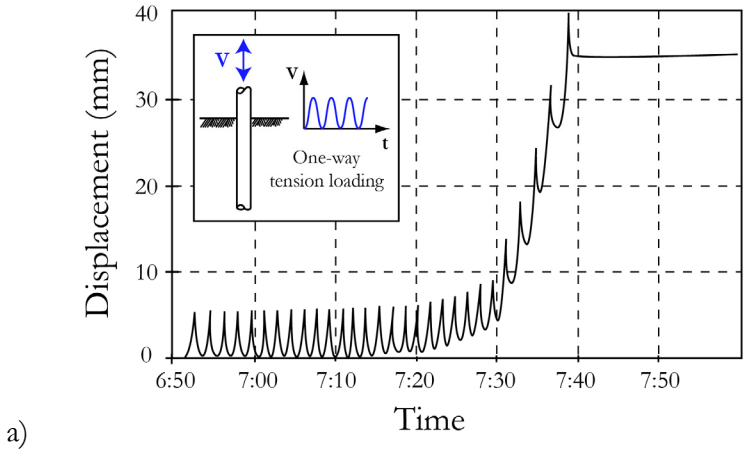

a)

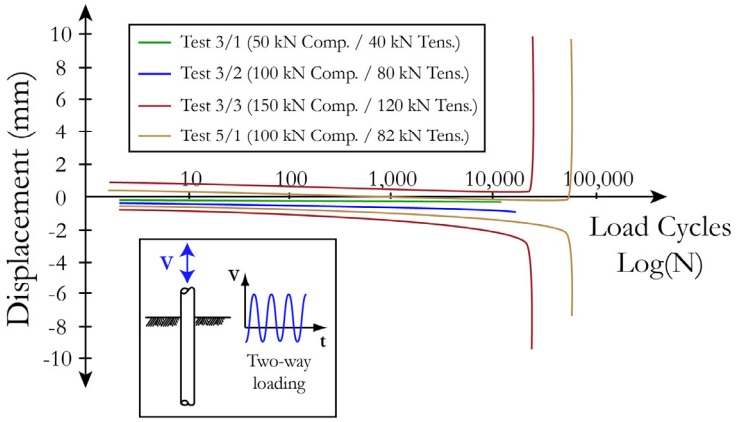

b)

Figure 4.1 Brittle failure of cyclic axially loaded piles a) Displacement vs. time curve during field testing with one-way cyclic loading of tension pile in Dunkirk sand, after [Jardine & Standing, 2000]. b) Displacement vs. number of cycles during two-way cyclic load tests on micropiles, after [Schwarz, 2002].

4.1.2 Soil subsidence and grain migration

The conical soil depression around cyclic laterally loaded piles in sand has been observed and reported in the past, e.g. in [Cheang & Matlock, 1983; Swane, 1983; Brown *et al.*, 1988; Savidis *et*

al., 2004], and soil densification due to the pile-head lateral displacements has also been shown to happen with numerical simulations using advanced constitutive laws (e.g. in [Grabe *et al.*, 2005]). Nevertheless, and despite the abundance of analytical models for the pile-soil interaction under repeated lateral loading (e.g. in [Achmus *et al.*, 2009], [Bentley & El Naggar, 2000] or [Taiebat, 1999]), the references to subsidence or soil densification near the pile head are scarce in the literature, in part due to the inability of the most commonly used constitutive models to take into account the changes in density of the soil under cyclic solicitation.

In their extensive experimental work with cyclic laterally loaded piles on medium dense sands, Cheang and Matlock consider that this local subsidence might be related to some grain migration towards the pile triggered by the repeated compaction of the soil as the pile moves back and forth, and they acknowledge that after a number of cycles the conical depression is fully developed and remains more or less constant [Cheang & Matlock, 1983].

Gudehus proposes the same densifying explanation for the subsidence and grain migration near a cyclically loaded pile or wall, where the cyclic shearing causes a net contraction of the soil near the structure, thereby producing a flow of material towards the latter and downwards "until the maximal density of the soil is reached" [Gudehus, 2000].

In a first set of long-lasting model tests in a reduced scale (1:100) of a pile under cyclic lateral load (up to 5 million load cycles), the author was able to observe the same local subsidence (see Figure 4.2-a), and noticed that within the first thousands of cycles the depression seemed to reach a steady depth and then remain constant. However, during the whole runtime of each test (two months with load cycles at a frequency of 1 Hz), the grain migration towards the pile never ceased nor seemed to slow down significantly.

Given the natural tendency of dense siliceous sands to dilate under shear at low confining pressures [Bolton, 1986], the fact that the tests had been carried out in an already very dense sand (approximately 93% of the Proctor density) appears to contradict the densifying explanation of this continuous grain migration. It seems unlikely that the densification could account for the steady grain migration throughout the whole test since, after all, the soil cyclic densification should have a limit [Gudehus, 2000; Triantafyllidis, 2003], especially for such dense sands at low confining stress where particle overriding (and hence dilation) rather than particle crushing might be expected [Bolton, 1986].

On the other hand, it is widely accepted that the driving of piles into the soil can also cause fines migration, soil contraction and stress relaxation as a result of particle crushing and rearrangement during the pile-driving [Randolph, 2003; White & Bolton, 2004; Lobo-Guerrero & Vallejo, 2005; 2007]. However, such phenomena were ruled out in these model tests, where in fact, the pile

driving didn't produce any appreciable local subsidence of the soil surface, in contrast to that one produced by the subsequent cyclic loading.

Therefore, attempting to find out the final destination of the migrated grains, further tests were devised incorporating bands of coloured sand grains on the soil surface in order to be able to identify them at the end of the loading schedules, upon removal of the upper layers of soil.

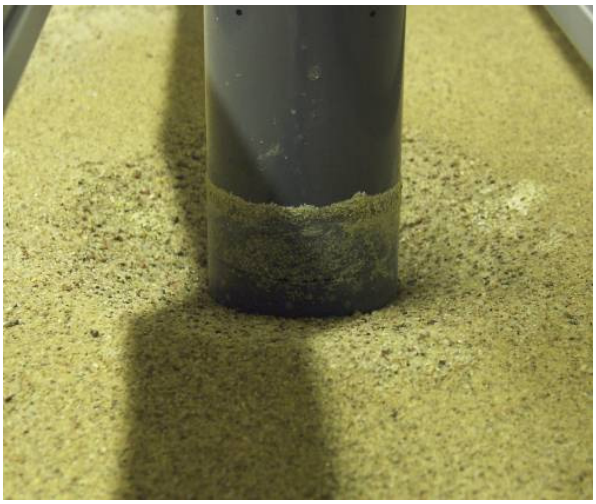

a)

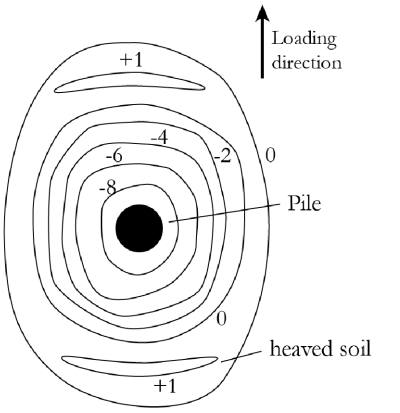

Elevations relative to original sand surface, in inches
(redrawn from Brown et al. 1988)

b)

Figure 4.2 Soil subsidence around a cyclic laterally loaded pile. a) Observed by the author during preliminary model tests. b) Topographic sketch of soil surface around the pile at a field test, after [Brown *et al.*, 1988].

4.1.3 Study object: Large diameter offshore monopile

For representativity of realistic conditions and relevance with respect to the German plans for offshore wind-energy production, the monopile prototype dimensions for this study were chosen to be 7.5 metres in diameter and 30 metres of embedded length, which fall within the ranges proposed by Lesny [2008] and Achmus *et al.* [2008; 2009] for the monopile foundation of the 5-MW wind-turbines to be located in the German bight of the North Sea.

Regarding the magnitude of the loads, the common estimations for an extreme event (maximum wind and waves with 50 years return period) assume horizontal loads on the monopiles in the range of a few megaNewtons. The loads will of course depend on the type and size of the structure, and especially on the specific environmental conditions at the wind farm location, but for the purpose of these investigations the broad estimates provided in the literature, for instance by Byrne and Houlsby [2003] or in Lesny [2008], may suffice to define the range of loads for the

tests. The former reference states that the foundation of a typical 3.5 MW offshore wind turbine could be subject to maximum lateral loads of about 4 MN and overturning moments in the range of 120 MN m, or equivalent to the horizontal load being applied 30 meters above the sea-bed level, while the latter author anticipates that the loads for a 5 MW design in the North Sea could rise up to 15 MN of lateral load and 450 MN m of overturning moment (also equivalent to the application of the single lateral load 30 meters above the pile head).

Interestingly, the equivalent lever arm of around 30 metres seems to be typical for the wind-turbines of the MW-class planned in the North Sea (see the mentioned literature and elsewhere). However, in real conditions it may change very rapidly with time, as the ratio of moment to lateral load will generally depend on the actual conditions of wind and waves (which need not be linearly correlated) and particularly on the operation configuration (the turbine blades are usually rotated around their longitudinal axis depending on the speed of the wind).

Such loading conditions are in sharp contrast to the loading cases for the typical offshore constructions of the oil industry, where the vertical loads may be an order of magnitude higher than the lateral ones and the ratio of moment to horizontal load normally remains rather constant [Byrne & Houlsby, 2003].

Given the general character of these experimental investigations, where no particular offshore location is to be analysed and only general findings about the pile behaviour are pursued, the detailed procedure for the calculation of loads has not been deemed particularly relevant here. In any case, the main lines of the load estimation process have been summarised in the Appendix A.5 of this dissertation.

The characteristics of the selected prototype and loads for this study are summarised in Figure 4.3.

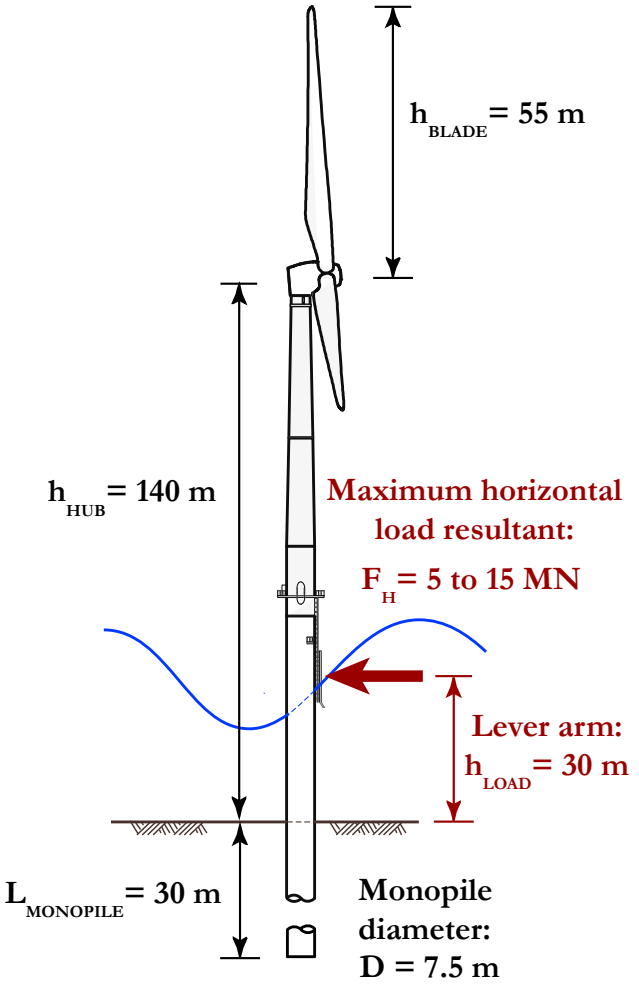

Figure 4.3 Prototype basis for the experimental study. Monopile dimensions and loads.

4.2 Model Tests

Rather than a quantification of the complex phenomena associated to the pile-soil interaction, the main goal for these experiments was the qualitative understanding of the long-term behaviour of the saturated sand around a cyclic laterally loaded pile. Therefore, and for the sake of simplicity and repeatability, the model tests presented in the following sections were performed in 1g conditions and at a geometrical scale of 1:100 relative to the offshore monopile prototype.

4.2.1 Model testing and 1-g scaling laws

In order to be able to relate the results of a model test in a reduced scale with the corresponding variables of the prototype system in real size, there are certain conditions that must be met so that the kinematic and constitutive similarity between the systems is preserved. To this end, it is useful to perform a dimensional analysis of the system and if possible describe it in terms of dimensionless magnitudes, typically by means of Buckingham's Π-Theorem [Buckingham, 1914; 1915]. Such procedure can be outlined as follows:

- Let $\boldsymbol{S}$ be a reference system (the prototype, in this case) where a certain physical relation $\boldsymbol{f(Q)=0}$ holds among a number of dimensional quantities $\boldsymbol{Q}$ which pertain to $\boldsymbol{S}$.
- The Π-Theorem states that any physically meaningful relation $\boldsymbol{f(Q_1,\ldots,Q_n)}$ can be reduced to a relation of the form $\boldsymbol{\Psi(\Pi_1,\ldots,\Pi_{n-r})}$ involving a maximal set of independent dimensionless combinations $\boldsymbol{\Pi}$. The new variables $\boldsymbol{\Pi}$ represent arbitrary dimensionless products of powers of the original quantities $\boldsymbol{Q}$.
- Interestingly, the new relation involves $\boldsymbol{r}$ fewer variables than the original, being $\boldsymbol{r}$ the number of arbitrary fundamental units needed as a basis for the absolute quantities $\boldsymbol{Q}$.
- Now let the reference system $\boldsymbol{S}$ be transformed into another system $\boldsymbol{S'}$ (the reduced scale system, in this case) with dimensional quantities $\boldsymbol{Q'}$ corresponding to the essential quantities $\boldsymbol{Q}$ in $\boldsymbol{S}$. If the original physical relation $\boldsymbol{f(Q)}$ holding in $\boldsymbol{S}$ must also subsist in the transformed system $\boldsymbol{S'}$ among the transformed quantities $\boldsymbol{Q'}$, then it

can also be reduced to an analogous form $\Psi'(\Pi'_1,\ldots,\Pi'_{n-r})$ involving dimensionless products of powers of the transformed quantities Q'.

- The systems S and S' are said to be "physically similar" as regards this relation if the corresponding Πs are equal in the two systems. The procedure of transformation which leaves a system similar to itself is discussed in detail in [Buckingham, 1914].
- The scaling process then hinges on identifying the quantities relevant for the physical relation under consideration and deriving the suitable Πs that need to be equal in both scales. Then, a set of independent ratios of quantities of the same kind is chosen (for instance the ratio of geometrical lengths λ and the ratio of gravitational accelerations $\varkappa$) and, imposing the conservation of Πs across the scales, the scaling factors for the other quantities are obtained.

As mentioned before, the conditions for the present experiments were chosen to be at a geometrical scale of 1:100 and under normal gravity (1-g) conditions, which may be expressed as

$$\lambda = \frac{L_P}{L_M} = 100 \tag{4.1}$$

$$\kappa = \frac{g_P}{g_M} = 1 \tag{4.2}$$

where L_P, g_P, L_M and g_M denote length quantities and gravitational accelerations at the prototype and model scales respectively. The latter expression implies that if the same soil with the same volumetric mass density d_S is being used for both the prototype and scaled systems, then their unit weights γ_S are also directly related through $\varkappa$ equal to 1:

$$\frac{\gamma_{S,P}}{\gamma_{S,M}} = \frac{d_{S,P}}{d_{S,M}} \frac{g_P}{g_M} = \frac{d_{S,P}}{d_{S,M}} \kappa = \kappa = 1 \tag{4.3}$$

Now, having defined the independent ratios λ and $\varkappa$ so far, the choice of dimensionless combinations Π may be carried out by inspecting the dimension matrix of the quantities relevant for the physical problem at hand, as explained for instance in [Hanche-Olsen, 2004] or in [Stieß, 2009], or guided by trial FE calculations (see e.g. [Sedran *et al.*, 2001]) or common practice. In the frame of 1-g model tests with sands, it is often convenient to employ for this purpose the following dimensionless force (as done for instance in [Winter & Hettler, 1983; Holzlöhner, 1983; Walz, 2006; Dührkop, 2010]):

$$\Pi_f = \frac{F}{\gamma_S L^3} \tag{4.4}$$

where $\boldsymbol{F}$ is a dimensional force quantity, $\boldsymbol{\gamma_S}$ is the unit weight of the soil and $\boldsymbol{L}$ is the reference geometrical length taken as a basis for the nondimensionalization. Now, imposing the conservation of $\boldsymbol{\Pi_f}$ across the scaling transformation:

$$\Pi_f = \frac{F_P}{\gamma_{S,P} L_P^{\,3}} = \frac{F_M}{\gamma_{S,M} L_M^{\,3}} = \Pi'_f \tag{4.5}$$

and by introducing the independent ratios defined in (4.1) and (4.3), the scaling law for force quantities is finally obtained:

$$F_M = \frac{F_P}{\left(\frac{\gamma_{S,P}}{\gamma_{S,M}}\right)\left(\frac{L_P}{L_M}\right)^3} = \frac{F_P}{\kappa \lambda^3} = \frac{F_P}{100^3} \tag{4.6}$$

The scaling rules for the rest of relevant physical quantities can be derived in the same way and are summarised in Table 4.1, extracted from [Walz, 2006] and [Pöschel *et al.*, 2001].

Table 4.1 Scaling laws for model tests under 1-g conditions

Physical quantity	**Scaling law**	**Dimensions**
Length, $\boldsymbol{L}$	$\boldsymbol{L_M = L_P / \lambda}$	L [m]
Force, $\boldsymbol{F}$	$\boldsymbol{F_M = F_P / \lambda^3}$	F [N]
Distributed line load, $\boldsymbol{q}$	$\boldsymbol{q_M = q_P / \lambda^2}$	F / L [N/m]
Stress (or Pressure), $\boldsymbol{\sigma}$	$\boldsymbol{\sigma_M = \sigma_P / \lambda}$	F / L^2 [Pa]
Unit weight, $\boldsymbol{\gamma}$	$\boldsymbol{\gamma_M = \gamma_P}$	F / L^3 [N/m^3]
Moment, $\boldsymbol{M}$	$\boldsymbol{M_M = M_P / \lambda^4}$	F x L [N m]
Bending stiffness, $\boldsymbol{EI}$	$\boldsymbol{(EI)_M = (EI)_P / \lambda^5}$	F x L^2 [N m^2]
Time, $\boldsymbol{t}$	$\boldsymbol{t_M = t_P / \lambda^{1/2}}$	T [s]
Frequency, $\boldsymbol{f}$	$\boldsymbol{f_M = f_P / \lambda^{-1/2}}$	1 / T [Hz]

A fact that is often neglected in the literature and is worth to mention here is that the scaling of time is a direct consequence of geometrical scaling under 1-g conditions. In this respect, the scaling rule for the time dimension can be derived upon consideration that all accelerations (not only the gravity) be kept unaffected by the scaling, as proposed in [Pöschel *et al.*, 2001]. This can be expressed as follows:

$$a_P = \frac{d^2 x_P}{dt_P^{\,2}} = \frac{d^2 (\lambda\, x_M)}{dt_P^{\,2}} = \frac{d^2 x_M}{dt_M^{\,2}} = a_M \tag{4.7}$$

and hence

$$t_M = t_P \frac{1}{\sqrt{\lambda}} \tag{4.8}$$

where $\boldsymbol{a}$ and $\boldsymbol{x}$ represent acceleration and displacement quantities respectively and the subscripts $_{\boldsymbol{M}}$ and $_{\boldsymbol{P}}$ denote the scale to which they pertain (either model or prototype).

However, the satisfaction of such scaling laws for similarity in granular systems is in general not a trivial matter (see e.g. [Holzlöhner, 1983; Pöschel *et al.*, 2001; Kuhn, 2005]). Among other technical difficulties of model tests with geomaterials, the 1:100 scaling of the grain dimensions would require clay-size soil particles and hence introduce unwanted cohesive forces into the system.

Furthermore, the pressure dependence of the soil's constitutive nature implies that, under 1-g conditions, homologous points of the soil in the model and prototype will show different deformational behaviour since they are subject to different stress conditions. In order to preserve the constitutive similarity across the scales, special techniques need to be adopted such as the centrifuge testing, the fluid-gradient method or the pressure-vessel confinement, so that the stress levels at homologous points in model and prototype are equal (see for instance [Altaee & Fellenius, 1994; Sedran *et al.*, 2001]).

Nevertheless, for practical purposes and for the sake of simplicity it is often customary to use the very same soil for model and prototype and accept some degree of deviation from the strict constitutive similarity. Hettler advocates the use of normal sand for 1-g model testing without any scaling of the grain-size distribution, provided that the void ratio is also kept the same and based on the assumption that the constitutive behaviour of sand may be described exclusively in terms of dimensionless quantities [Hettler, 1981; 1983]. There, it is recognized that the use of the prototype-size sand for the model tests may inevitably introduce some distortion of the constitutive similarity whenever localized failure or shear bands appear, since these are typically characterised by a band width of about ten to twenty times the average particle diameter (see also [Kuhn, 2005]). Hence, the model tests with prototype sand may show disproportionate shear bands and the mobilisation of higher ultimate loads. However, several studies have shown that the influence of these shear-zones on the overall response of the foundation may be neglected if the applied loads lay well below the failure limit [Hettler, 1981] or if the ratio of foundation diameter to grain size (D/d_{50}) is greater than 30 to 60 [Ovesen, 1980; Franke & Muth, 1985; Remaud, 1999; Sedran *et al.*, 2001; Verdure *et al.*, 2003]. Since both conditions are met for the model tests presented here, a real-size sand has been employed and no further investigations on the possible grain-scale effects have been undertaken.

Regarding the interaction with the pore fluid (water in this case), an appropriate set of scaling laws should in principle also be adopted for the relevant parameters such as fluid unit weight, viscosity or permeability. However, for the practical purposes of this experimental work the transient variations of pore pressure may play a minor role in the overall pile response, so a fully drained condition of the soil has been assumed in the long-term and no scaling considerations have been made for the solid-fluid interaction.

4.2.2 Experimental setup and testing program

Model pile. Given the difficulty to fulfil all the scaling laws and since the direct transfer of the results to the prototype behaviour was not intended, only the pile external dimensions and bending stiffness were properly scaled. For such purpose, an open-ended hollow PVC pile with 75 mm in external diameter, a wall thickness of 5 mm and 30 cm of embedded length was used. The flexural stiffness of this pile is about ten times higher of what it should be according to the scaling laws presented before, but neither a softer material with the appropriate dimensions nor a PVC pile with thinner walls were commercially available within reasonable cost margins. In any case, the distorting effects caused by this extra flexural rigidity may be negligible since the aspect ratio of this pile (ratio of diameter to length) makes it behave as a short rigid pile anyway.

The possibility of a significant viscoplastic creep of the PVC pile during the long-term tests was discarded on the basis of a preliminary test with sustained loading.

Model soil. A real-size sand from a quarry north of Berlin was used for the experiments. This sand, whose grain size distribution can be seen in Figure 4.4, is very similar to the siliceous sands present off the German coasts in the North Sea and shall be termed henceforth "Berliner sand". It is a narrowly graded sand with rounded grains and its granulometric properties are summarised in Figure 4.5.

A sand container 100 cm long, 80 cm wide and 50 cm deep was used for the experiments. This way, a clearance of 5,75D between the pile and the container wall was ensured in the loading direction, which was considered enough to disregard disturbing effects from the wall into the pile-soil interaction. The sand was placed into the container with a 10% water content (in this case the optimal water content) in layers of 20 cm thickness, and then compacted with a vibrating plate until a density of around 93% of the ASTM standard Proctor density was achieved (1.79 g/cm^3

for this sand) [ASTM, 2007]. Then, the pile was pressed into the soil to a final embedment depth of 30 cm.

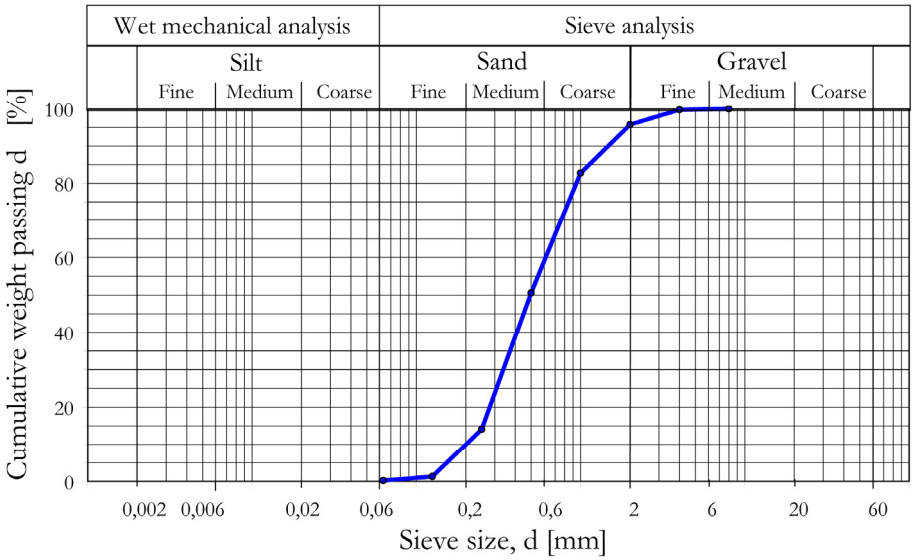

Figure 4.4 Grain size distribution of Berliner sand.

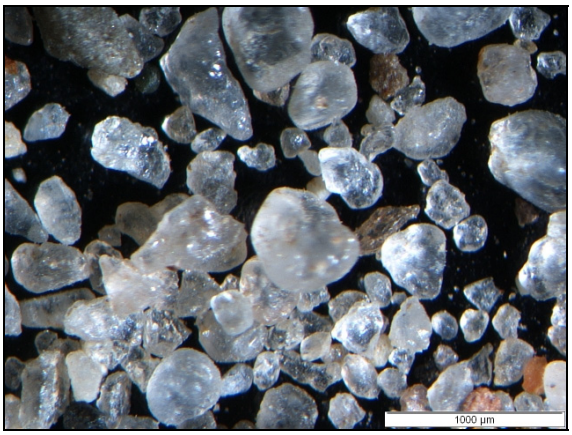

a)

Material Parameter	Value
Internal friction angle, φ'	32 °
Minimum density, $\rho_{d,min}$	1.52 x 10^3 kg/m^3
Maximum density, $\rho_{d,max}$	1.88 x 10^3 kg/m^3
Grain density, ρ_S	2.65 x 10^3 kg/m^3
Coefficient of non-uniformity, $U=d_{60}/d_{10}$	2.95

b)

Figure 4.5 Granulometry of Berliner sand. a) Light-optical micrograph of Berliner sand sample. b) Granulometric parameters

Sand markers. As mentioned in Section 4.1.2, during the first test a continuous grain migration towards the pile was observed, so in order to investigate it a pattern of bands with coloured sand grains was placed on the soil surface for the following tests, as displayed in Figure 4.6. These coloured bands (2 cm thick) were placed along the loading direction and, since an asymmetric two-way cyclic loading program was scheduled, the bands were wider in the soil's side carrying the highest load, covering a 60 degree circular sector, as shown in Figure 4.6. The average size of the coloured grains was about 2 mm.

In order to investigate the grain migration perpendicular to the loading direction, two additional marker lines were placed on the pile's sides. With the additional intent to analyse the influence of grain size and shape on the migration patterns, coarser sand grains (the blue markers in Figure 4.6 with an average size of 7 mm) and ceramic spherical particles (white markers, in average with 1 mm in diameter) were employed for these lateral marker lines.

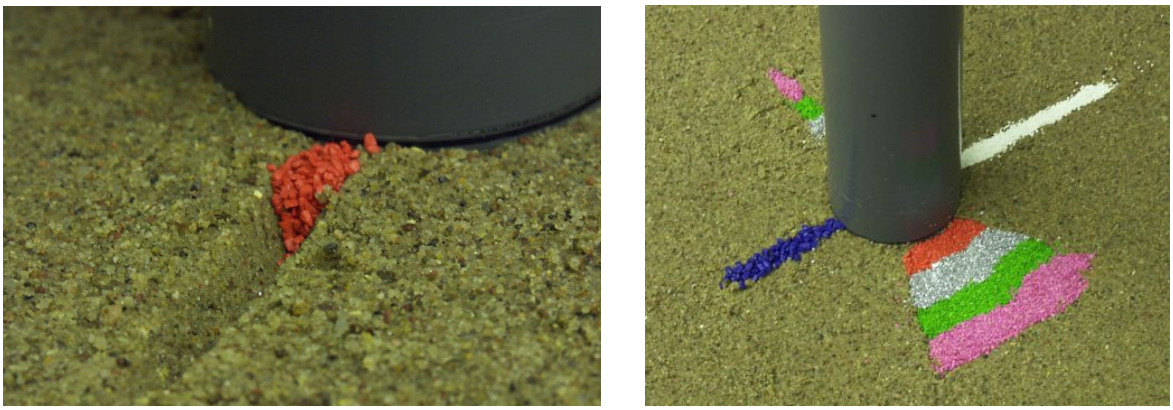

Figure 4.6 Coloured sand markers for the investigation of grain migration.

Model pore fluid. After the installation of the pile and the placement of the sand markers, the container was progressively flooded with water until a full saturation and a water level of 2cm above the soil surface were achieved. The introduction of water was done upwards from a drain at the bottom of the container and very slowly in order to facilitate the expulsion of air occluded between the grains and avoid the disturbance of the soil skeleton.

Model loads. Assuming for simplicity a two-way harmonic (sinusoidal) lateral loading on the foundation, several loading schedules with different amplitudes and average loads have been conducted. With reference to the scaling laws for 1g model tests presented in Table 4.1 and with a geometrical scaling factor of 1:100, the loads applied to the model should be six orders of magnitude smaller than those in the prototype, hence in the range of a few Newtons.

Starting with a two-way purely symmetric loading for the first test, where the load would oscillate sinusoidally between 10 N and -10 N, the subsequent loading programs were increased asymmetrically by raising the peak loads in only one direction, with maximum loads up to 40 N in one direction and the same 10 N in the opposite. Finally, a last one-way cyclic loading program from 0 to 30 N was conducted for a comparison with the two-way loading schemes. A lever arm of 30 cm with respect to the pile-head level (i.e. the mudline) was kept for all the testing programs.

These loads range between 7% and 27% of the static ultimate capacity, which was eventually measured amounting to approximately 150 N at a pile-head displacement of 0.1 D.

The loading frequency was set to 1 Hz, which, considering the scaling laws presented above, corresponds to a prototype loading frequency of 0.1 Hz or a wave period of 10 seconds. Given the relatively high permeability of these clean sands, this frequency and the load magnitudes were considered to be low enough to disregard the possibility of a significant long-term pore pressure accumulation within the soil.

The different loading schedules, which are summarised in Figure 4.7 along with their corresponding dimensionless loads $\boldsymbol{\Phi}$ as defined in Section 1.4, consisted on the application of 5 million load cycles each, which means that, with the frequency of 1 Hz, every test lasted for about 2 months.

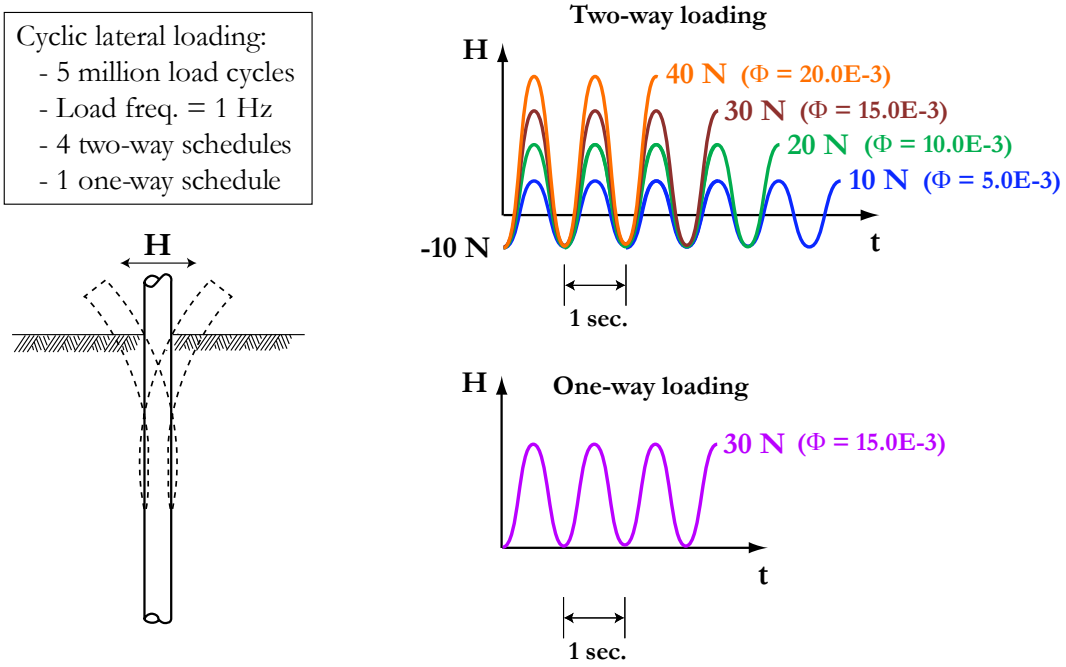

Figure 4.7 Summary of loading schedules for the model tests.

The main characteristics and dimensions of the study object at the prototype and model scales are summarised in Table 4.2.

Arrangement and instrumentation. The loads have been transferred to the pile with a pneumatic actuator on one side and a hanging dead load on the other, both connected to the pile through steel cables at a height of 30 cm above the soil surface and controlled with a pair of load cells. The specific arrangement of the different devices is shown in Figure 4.8.

The pile-head displacements were registered with two laser distance-measuring sensors, placed 20 cm and 47.5 cm above the soil surface respectively, and the soil movements and grain migration on the surface were captured with a digital camera, which additionally produced a continuous

animation with a capture rate of one frame per hour, throughout the whole two months of test duration.

Table 4.2 Magnitudes of studied cases in prototype and model scale

	Physical quantity	Prototype scale	Model scale
PILE	Pile diameter, D	7.5 m	0.075 m
	Pile's embedded length, L	30 m	0.3 m
	Pile's bending stiffness, EI	2.5×10^{12} N m^2	2×10^{3} N m^2
SOIL	Sand grain size, d_{50}	0.5 mm	0.5 mm
	Sand grain unit weight, γ_s	26.5 kN/m^3	26.5 kN/m^3
	Sand permeability, k	2.5×10^{-4} m/s	2.5×10^{-4} m/s
LOADS	Horizontal load, H	15 MN	10 N to 40 N
	Lever arm, h	30 m	0.3 m
	Loading frequency, f	0.1 Hz	1 Hz

For the last two tests (i.e. the 4th and 5th tests), the pile was additionally equipped with six strain gauges arranged in three different levels, with one strain gauge at the front and one at the back of the pile. The strains were measured at the mudline as well as at points 15 cm above and below it. The purpose of measuring the pile strains above the soil level was the validation and re-calibration of the strain gauges, since the moment distribution between the pile head and the point of load application is known a priori. This way, despite of the presence of water and the long-term measurements, the validation of the data with respect to the theoretical values would exclude the possibility of electrical drift in the sensors or in the data-acquisition.

Unfortunately, during the fourth test and after 12 days of testing, a technical malfunction of the data acquisition system prevented the further storage of measured data for that test, so from that moment the measurements got inadvertedly lost. Therefore the results presented in the following section for the 4th test only cover the first million of load cycles, despite the test being carried out for the scheduled five million cycles.

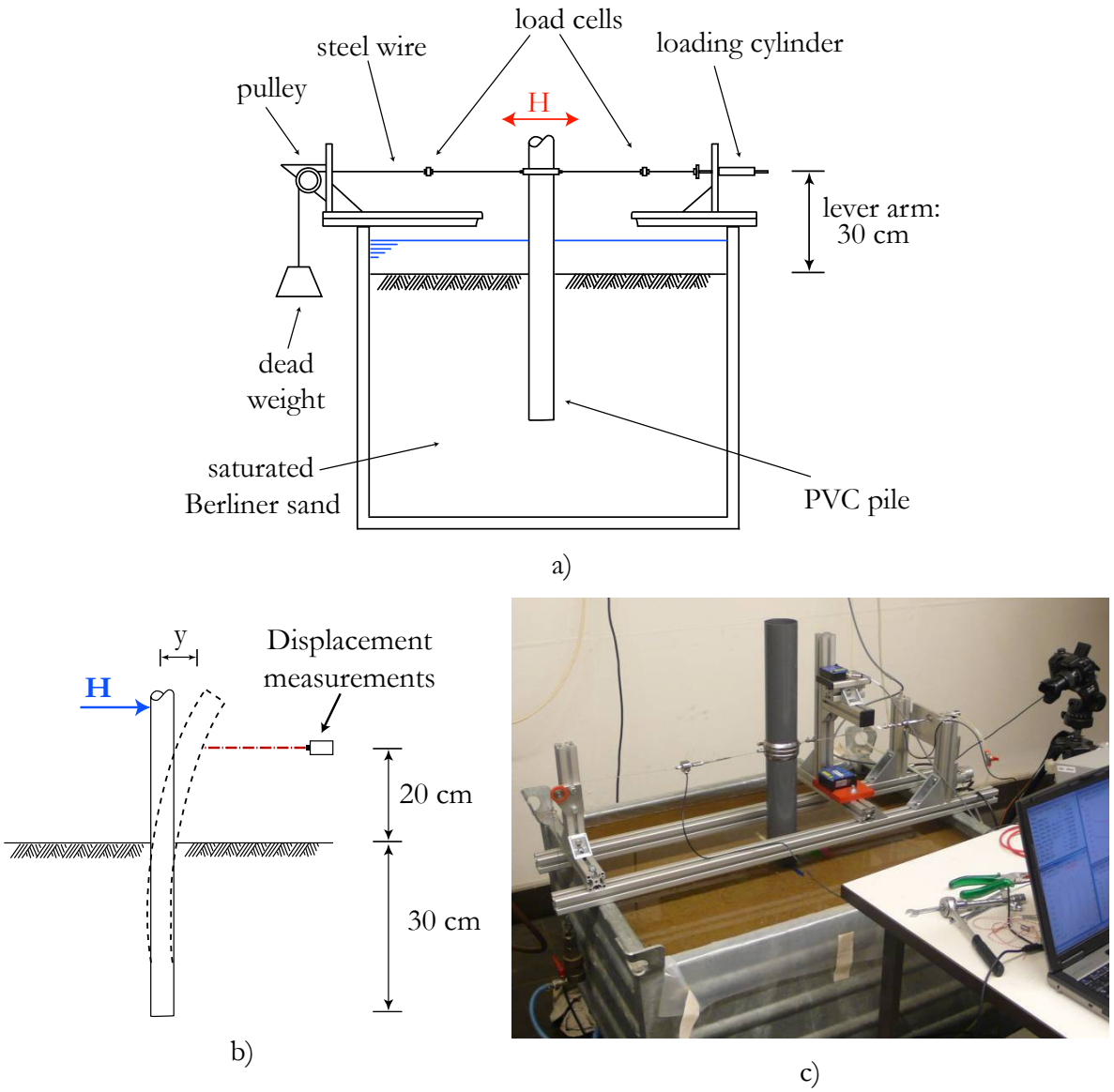

Figure 4.8 Experimental setup. a) Sketch of testing rig and loading actuators. b) Arrangement of distance measuring laser sensor. c) Picture of test setup with the installed devices.

4.2.3 Results of test series. Attenuation of displacement rate

The evolution of the permanent lateral pile-head displacements as measured 20 cm above the soil surface level is shown in Figure 4.9-a for all the tests. As it can be seen, the pile behaviour is quite benign in the sense that during the 5 million cycles no abrupt failure can be observed, but rather a progressive attenuation of the incremental displacements occurs. This feature contrasts with the behaviour that piles under cyclic axial loads can show (for instance in [Jardine & Standing, 2000;

Schwarz, 2002]), where the cyclic degradation of shaft friction can lead to a brittle (sudden) failure as depicted in Figure 4.1.

Here, the measured pile head displacements hint towards a rapid densification (and therefore improvement) of the surrounding soil*) during the first day of loading (i.e. during the first 100,000 load cycles), causing a certain soil depression around the pile and a decrease in the displacement amplitude (see Figure 4.9-b).

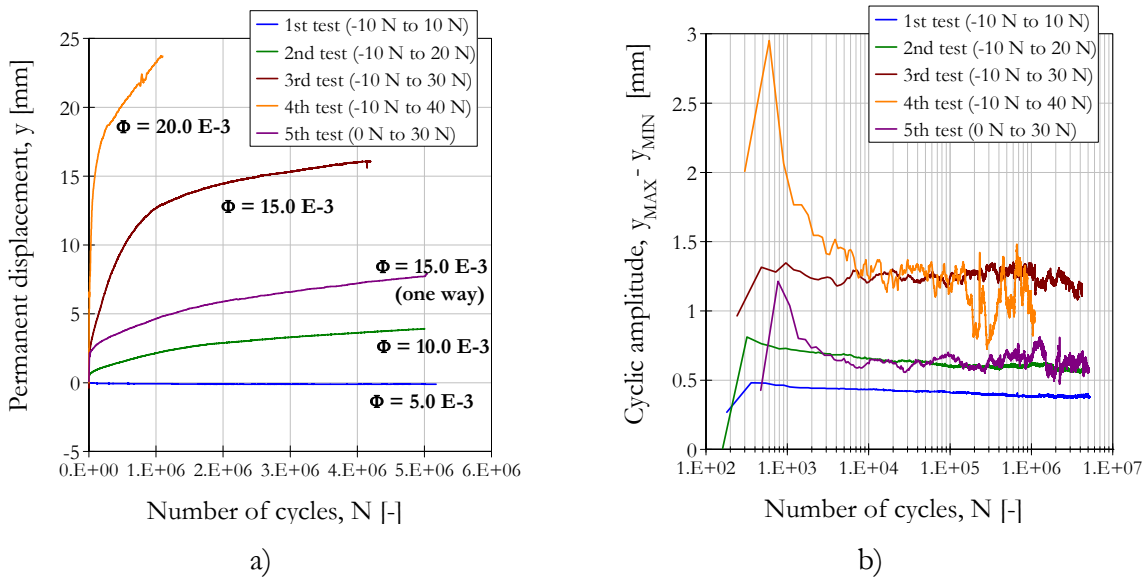

Figure 4.9 Evolution of pile-head displacements. a) Permanent displacements. b) Cyclic amplitude, in log scale of number of cycles.

Then, for the unsymmetric loading series a steady state can be seen where the displacement cyclic amplitude (the difference between cyclic maxima and minima) remains almost constant and only a slow steady drift of the foundation towards the direction of higher loads can be observed. This drift of the pile slows down progressively to a rather stable but slightly decreasing rate, insinuating an incremental collapse evolution (in the sense that it does not show a horizontal asymptote).

It is interesting to observe that the test with the symmetric load program (the first loading series) does not show any significant pile drift but nevertheless features the reduction of cyclic amplitude just as the unsymmetric load cases. This fact supports the idea that the reduction of cyclic amplitude is related to the cyclic densification (which should be expected to happen for both symme-

*) Here, only a soil improvement concerning lateral bedding stiffness is implied. As it is well know, the soil densification around cyclic axially loaded piles causes a net contraction of the soil at the pile-soil interface and thus a reduction of the normal stress acting on the pile shaft, which leads to a deterioration of axial pile capacity (see e.g. [White, 2005]).

tric and unsymmetric loadings), while the pile drift and progressive inclination would mainly be caused by any dissymmetry of the loading.

Another interesting feature which is summarised in Table 4.3 is that the one-way cyclic loading program (i.e. the 5th test) produced twice as much permanent displacement as its two-way counterpart with the same load amplitude (the 2nd test), while their respective cyclic displacement amplitudes tended to stabilise at the same level. However, the two-way loading program with the same maximum load (i.e the 3rd test) caused twice as much permanent displacement as the one-way test, despite having a lower average load. This all seems to indicate that:

- In the long-term (after the soil densification has taken place), the cyclic displacement amplitude only depends on the cyclic load amplitude, regardless of the maximum loads or the character of the loading (one-way or two-way).
- In contrast, the overall cyclic performance (i.e. the permanent displacement) depends on both the average and cyclic loads, as well as on the one-way or two-way character.
- This agrees with the general observations made by Andersen [2009] for the soil performance in triaxial and direct shear tests, which suggests that such behaviour is more intrinsic to sand rather than characteristic of this specific foundation.

Table 4.3 Comparison of the long-term response of two-way cyclic loading tests to the reference one-way test. Results after 5 million cycles

		5th Test ONE-WAY	**2nd Test TWO-WAY**	**3rd Test TWO-WAY**
CYCLIC LOAD	Maximum load, H_{MAX}	***30 N***	⇩ 20 N	⇔ 30 N
	Average load, H_{AVG}	***15 N***	⇩ 5 N	⇩ 10 N
	Load amplitude, $2(H_{MAX} - H_{AVG})$	***30 N***	⇔ 30 N	⇧ 40 N
LONG-TERM RESPONSE	Permanent displacement, y	***7.9 mm***	⇩ 3.9 mm	⇧ ~ 16 mm
	Displ. amplitude, $(y_{MAX} - y_{MIN})$	***0.57 mm***	⇔ 0.56 mm	⇧ 1.11 mm
	Extension of subsidence cone (see next section)	***7/3 D***	⇧ 3 D	⇧ 3 D

The examination of the data measured by the strain gauges during the 4th and 5th tests reinforces again the idea of the initial rapid densification of the soil around the pile and its consequent stiffening of the lateral behaviour. Recalling that the lower strain gauges were installed half-way between the mud-line and the pile-base, Figure 4.10 shows the progressive reduction of bending

moments at that level (and exclusively there), which hints towards the increasing rigidisation (or stiffening) of the upper layers of soil.

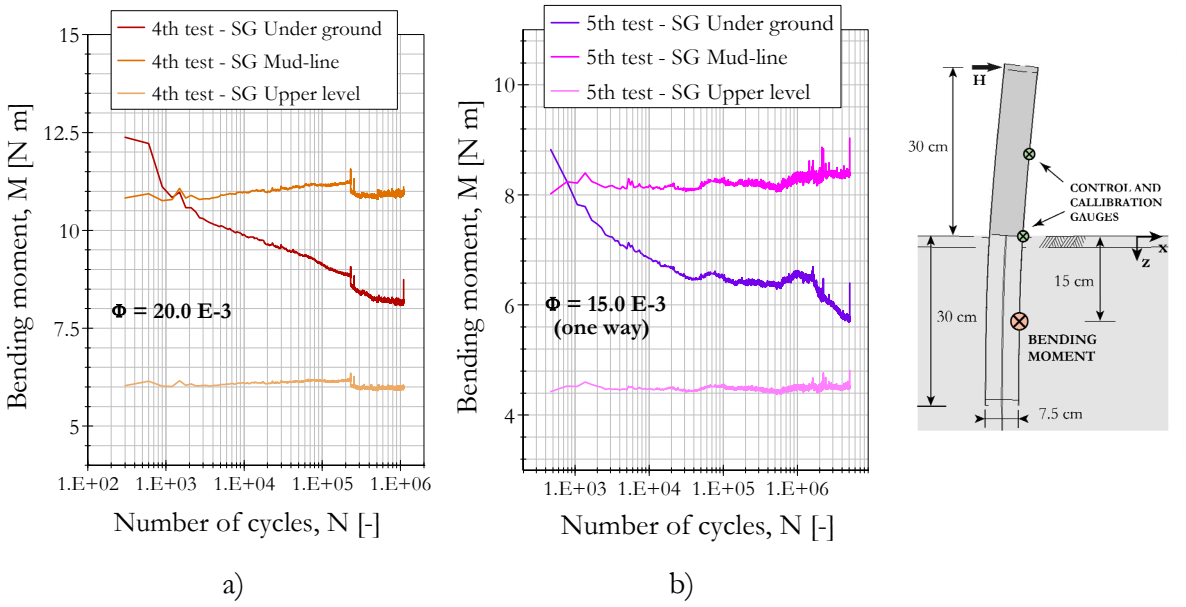

Figure 4.10 Bending moments measured with strain gauges at three different levels, in logarithmic scale. a) Measured during 4th test (two-way, from -10N to 40N). b) Measured during 5th test (one-way, from 0N to 30N).

The other two strain gauges, which were installed for calibration and control during the test and in theory should not be affected by the soil densification, show as expected a fairly constant level of bending moments, hence excluding an electrical drift of the signal as explanation for the reduction in the measured moments.

Such progressive reduction of bending moments in the pile has also been observed for instance in [Swane, 1983], and contrasts with the common assumption that cyclic lateral loading will tend to increase the bending moments (e.g. in [Poulos, 1988]), which may only be appropriate for the case of long flexible piles.

4.2.4 Displacement accumulation pattern

A plot of the pile-head displacements in a double logarithmic scale shows invariably two inflection points, one in the early stages of the cyclic loading (N~$5 \cdot 10^4$ to 10^5) and a second one in the very long-term, when N approaches 10^6 (see Figure 4.11). It is also interesting to note that these

characteristic inflection points appear sooner for higher levels of loading, which indicates that the physical mechanisms responsible for the change in behaviour are stress-level dependent.

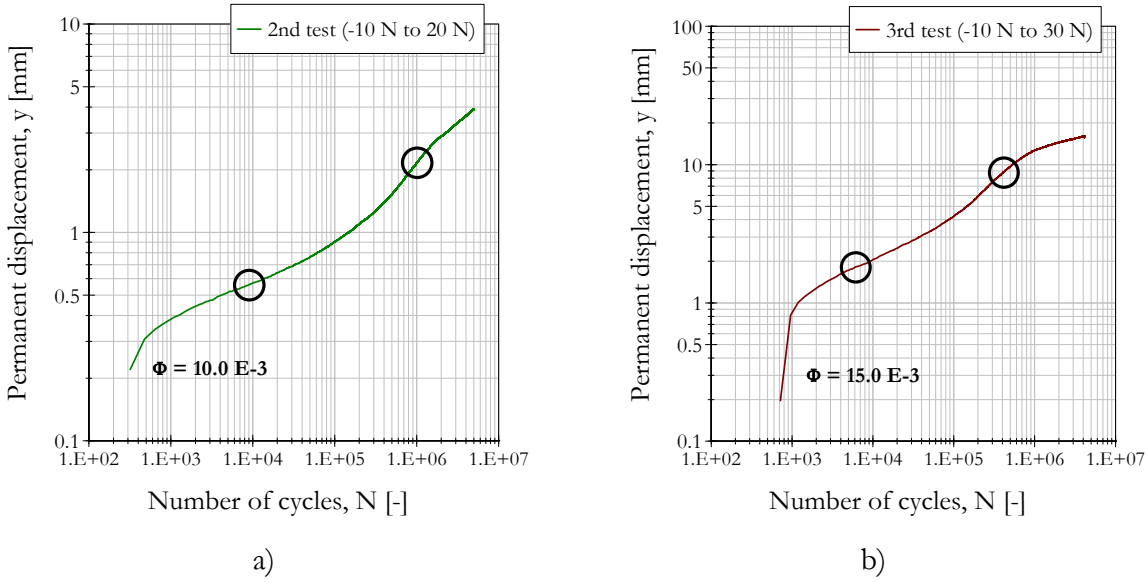

Figure 4.11 Evolution of pile-head lateral displacements in log-log scale. Inflection points in the displacement pattern for unsymmetric two-way cyclic loading tests. a) 2nd testing series. b) 3rd testing series.

This suggests the existence of three distinct phases of pile-head displacement during the cyclic loading: the first one lasting until approximately the first fifty to hundred thousand cycles (incidentally, this is the moment when the soil depression around the pile seems to stabilise), then a transitional phase where the permanent displacements grow rather linearly, and then after the second inflection point (that is, for $N>10^6$) a last phase that characterises the long term behaviour, where the displacement rate decreases progressively and the cyclic amplitude remains almost constant.

The first of the phases is characterised by a fast growth of permanent displacements and may account for most of the densification taking place around the pile since, at the end of it, the cyclic amplitude seems to stabilise (just as the conical depression around the pile). As depicted in Figure 4.12, the accumulated displacements in this phase may be reasonably approximated with a logarithmic function of the number of cycles in the following fashion:

$$y_1 \approx A + B \cdot log(N) \tag{4.9}$$

where $\boldsymbol{A}$ and $\boldsymbol{B}$ would be constants.

On the other hand, the displacements during the transitional second phase can be well described by a linear function of the number of cycles such as

$$y_2 \approx C + D \cdot N \tag{4.10}$$

where $\boldsymbol{C}$ and $\boldsymbol{D}$ would again be constants. Such accumulation pattern with constant rate has been usually referred to as "incremental collapse" ("schrittweises Versagen" in the German literature, for instance in [Hettler, 1981]), or ratcheting behaviour [Levy *et al.*, 2009], and is characterised by a constant increment of energy dissipation at every cycle.

Finally, the third phase, the long term one, seems to fit very well with a power-law of the number of cycles in the following manner

$$y_3 \approx E \cdot N^F \tag{4.11}$$

where $\boldsymbol{E}$ and $\boldsymbol{F}$ would also be constants. In contrast to the previous stage, this last phase is distinguished by a progressive attenuation of the displacement rate. However, this rate never gets down to zero, so the commonly-used term "shakedown effect" does not seem appropriate here, despite their resemblance. The "shakedown" term may be better reserved for those cases where, after a certain number of cycles, only elastic deformations occur and the rate of accumulation of plastic deformations gets down to zero, so that the long-term part of the average displacement curve is horizontal.

The three phases described so far, along with their fittings to the second and third testing series, are exemplarily shown in Figure 4.12.

Such distinction of phases would be consistent with the experimental results presented by Wichtmann [2005], where different sets of long-term cyclic triaxial tests on sands did show a first stage of about 10^4 cycles featuring a logarithmic accumulation of permanent strains. There, the author attributes such deformational regime to the grain re-arrangement at the micro-mechanical level, which could correspond to the densification and subsidence observed in these tests at the macro-mechanical scale.

Then, Wichtmann described the subsequent stage of deformation as being characterised by an over-logarithmic accumulation pattern, which there was credited to the abrasion taking place at the particle contacts [Wichtmann, 2005]. He discussed different possible fitting curves for the over-logarithmic part and acknowledged that a power-law function would provide a good match of the experimental data for the higher-cycle range ($N>10^5$).

Again, it is remarkable that there is such a close similarity in the long-term behaviour of such dissimilar tests (there, elementary triaxial tests, and here, model tests of a boundary value problem), which suggests that the observed long-term evolution and phases are probably an intrinsic characteristic of sand rather than the specific response of a given foundation. Further long-term

tests within a thorough parametric study would be required to confirm such extent, but if that were the case, it would imply that, with the appropriate modifications, the explicit accumulation methods developed at the elementary level might be applicable to describe the behaviour of full foundations in a macro-element fashion.

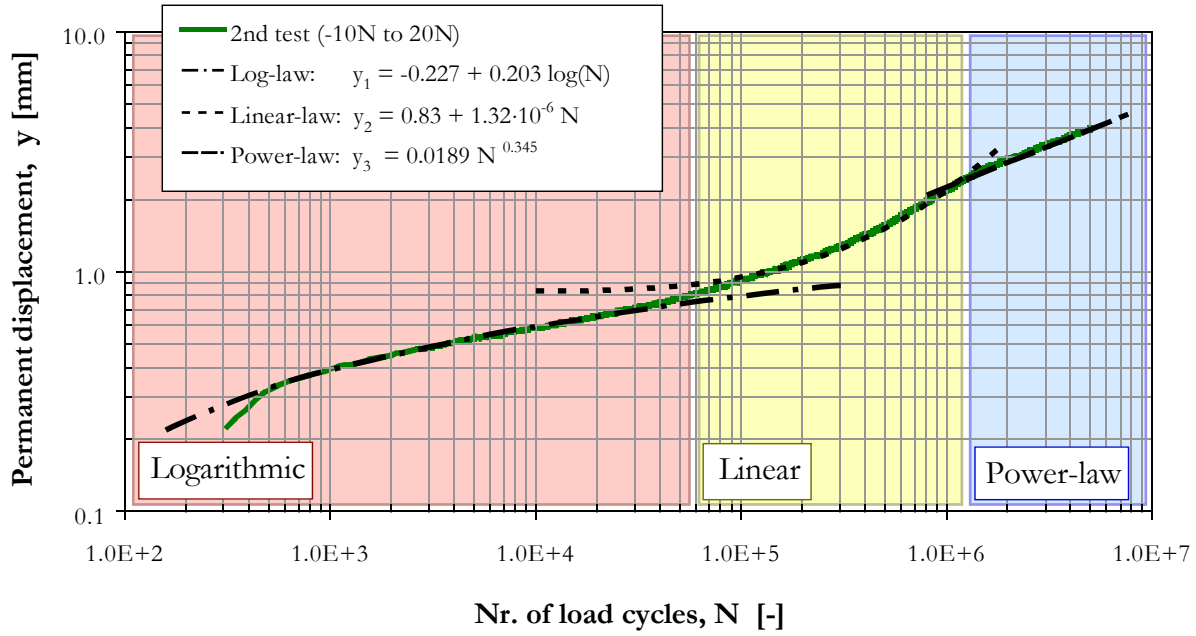

a)

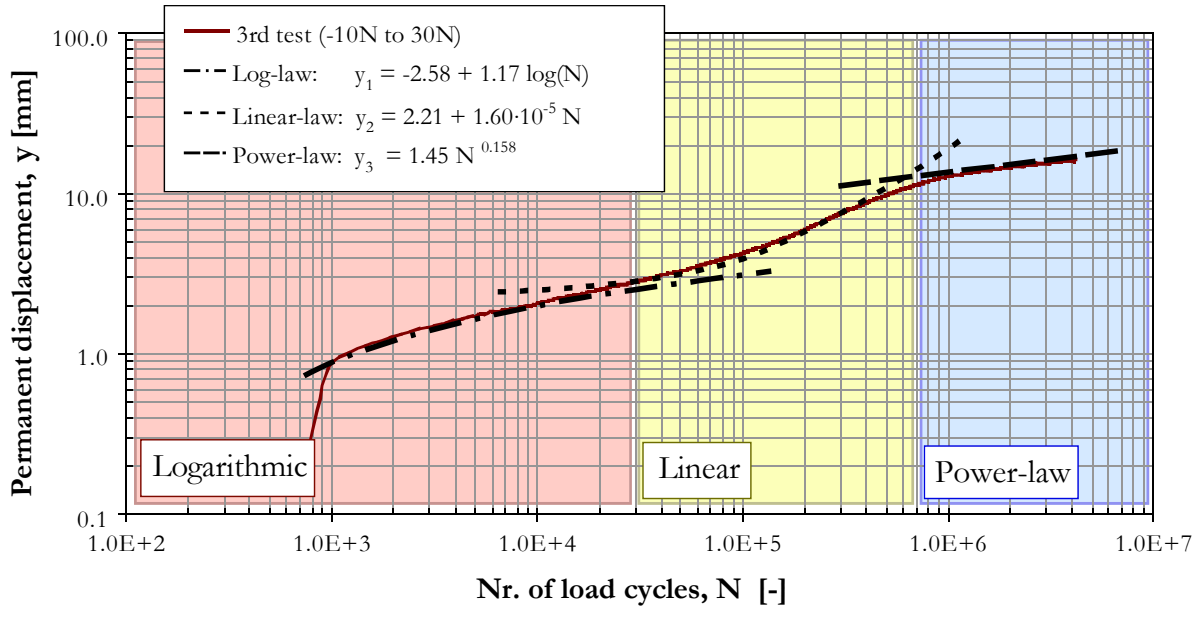

b)

Figure 4.12 Tri-phasic displacement pattern for unsymmetric two-way cyclic loading tests. a) 2nd testing series. b) 3rd testing series.

4.2.4.1 Accumulation laws from the literature

As mentioned in the introduction to this chapter, the accumulation of permanent displacements for a cyclic laterally loaded pile has usually been described either by means of logarithmic laws (e.g. in [Hettler, 1981] or [Verdure *et al.*, 2003]), or power-laws (e.g. in [Long & Vanneste, 1994] or [Little & Briaud, 1988]), or recently by means of log-linear laws (for instance in [Grabe & Dührkop, 2008] and [Dührkop, 2010] based on the general form proposed by [Wichtmann, 2005] for element tests).

A tentative adjustment of such laws to describe the full extent of the experimental data presented here is summarised, exemplarily for the 2nd and 3rd test series, in Table 4.4.

Table 4.4 Adjustment of selected accumulation laws from the literature to the experimental data from the 2nd and 3rd test series on Berliner sand

Accumulation laws for permanent displacements		***2nd test***	***3rd test***	**Other examples in the literature**
$y_N = y_1\left(1 + B_1 ln\left(B_2 N + 1\right)\right)$	B_1	14.375	4.619	[Hettler, 1981] [Verdure *et al.*, 2003]
	B_2	0.075	0.000135	
$y_N = y_1 N^{B_1}$	B_1	0.345	0.172	[Little & Briaud, 1988] [Long & Vanneste, 1994]
$y_N = y_1\left(1 + B_1\left[ln\left(B_2 N + 1\right) + B_3 N\right]\right)$	B_1	1.105	1.95	[Grabe & Dührkop, 2008] [Dührkop, 2010]
	B_2	0.0115	0.002	
	B_3	1.45E-5	2.75E-5	

By inspecting the form of the different adjustments, plotted in Figure 4.13, the following conclusions may be drawn:

- The logarithmic laws may represent well the initial short-term stage of cycling, but tend to underestimate both the rate and the magnitude of the displacements in the long-term.
- The pure power-laws are a too crude representation of the displacement evolution, since they feature a straight line in the log-log plot. They may provide a good estimate of the long term rate of displacement accumulation, but then they largely over-

predict the magnitude of displacements in the mid-term, and might underestimate it in the short-term.

- The log-linear law proposed by Grabe and Dührkop represents very well the accumulation of displacements up to the mid-term range of cycling ($N<10^6$). However, in the long-term stages of cycling the linear term of the law will dominate the behaviour and therefore largely overpredict both the accumulation rate and magnitude of permanent displacements. Hence, the use of such a law beyond the first million of cycles may be overly conservative.

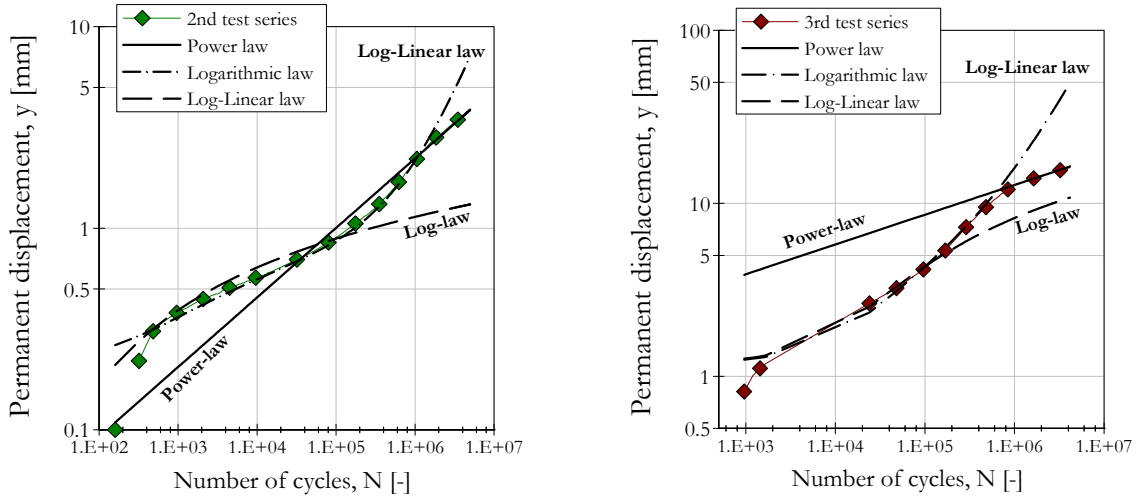

Figure 4.13 Approximation of experimental results with some selected accumulation laws from the literature. a) 2nd test series (-10N to 20N). b) 3rd test series (-10N to 30N).

4.2.4.2 Generalisation of the Log-Linear accumulation law

Bearing all these considerations in mind, the log-linear accumulation law proposed by Grabe and Dührkop, which seems to represent well the short to mid-term ranges of cycling, may be generalised to the full extent of cyclic behaviour by upgrading the linear term to a long-term rate-degradation function $\boldsymbol{\delta_N}$ in the following fashion:

$$y_N = y_1\left(1 + B_1\left[ln\left(B_2 N + 1\right) + B_3\delta_N\right]\right) \tag{4.12}$$

where y_1 and y_N are the permanent pile-head displacements after the first and Nth load cycles respectively, and B_1, B_2 and B_3 are constants. Here, the long-term rate-degradation function δ_N could take the following form

$$\delta_N = N(1 - B_4) - \frac{B_4}{B_5} e^{-N \cdot B_5} + C \tag{4.13}$$

and the integration constant C would be

$$C = B_4 + \frac{B_4}{B_5} e^{-B_5} \tag{4.14}$$

where B_4 and B_5 are also constants.

The derivative of this function, i.e. its contribution to the accumulation rate, then takes the following simple form:

$$\delta_N' = 1 - B_4 \left(1 - e^{-N \cdot B_5}\right) \tag{4.15}$$

which is illustrated in Figure 4.14.

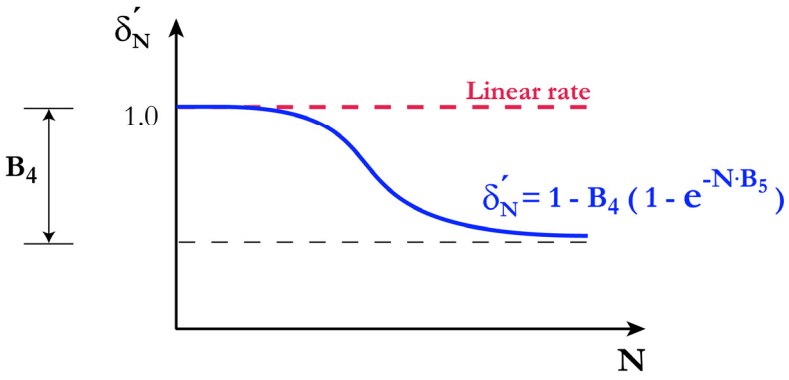

Figure 4.14 Derivative of the function δ_N to model the long-term degradation of the accumulation rate.

Since in the original formulation employed by Wichtmann the linear term was introduced to represent the basic linear rate of accumulation, which would be independent of the number of cycles [Wichtmann, 2005], the new function δ_N introduced here could be considered as the long-term degradation of that basic rate, where the constant B_4 would represent the maximum amount of degradation, and B_5 would control the rate of degradation.

From here it would be straightforward to show that this formulation can be particularised to recover the original form proposed by Grabe and Dührkop simply by setting the rate degradation parameter B_4 equal to zero.

For the estimation of the parameters of the rate degradation function δ_N, consideration can be made that in the long term δ'_N approaches asymptotically the value (1 - B_4), and thus B_4 may be calculated as $B_4 \approx (1 - m / B_3)$, being m the final slope of the graph of accumulation of permanent displacements..

The parameter B_5 controls the rate of degradation of the accumulation rate and may be roughly estimated as $B_5 \approx (1 / N_{REF})$, being N_{REF} the number of cycles at the second inflection point of the log-log plot, mentioned previously and shown in Figure 4.11.

The calibration of the constants of this accumulation law for the different tests presented in this work is illustrated in Figure 4.15 and summarized in the Appendix A.6.

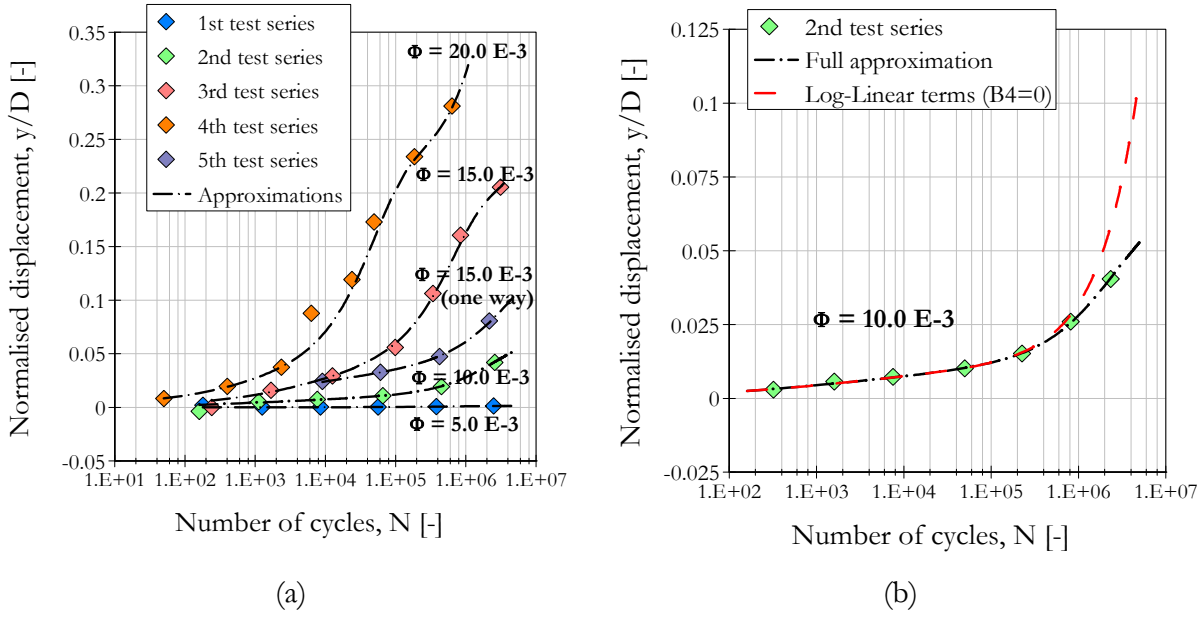

Figure 4.15 Dimensionless horizontal displacements versus number of cycles for different dimensionless loads and their respective approximation with the long-term accumulation law. (a) Summary of the approximations for all tests. (b) Comparison of generalised approximation versus its Log-Linear counterpart obtained by setting B_4 equal to zero, shown exemplarily for the 2nd test series.

To conclude this section the following remarks can be made:

- As shown by Allotey *et al.*, functions similar to δ'_N have already been employed by Grashuis *et al.* [1990] and Matlock [1978] among others, in the context of a strength degradation index for soil-pile load-transfer curves [Allotey & El Naggar, 2008].
- The generalised long-term accumulation law presented so far only takes explicit account of the number of applied load cycles, and in this respect is analogous to the f_N function proposed by Wichtmann to regard the historiotropy and basic rate of strain

accumulation in a soil element, within the frame of the so-called Bochum accumulation model [Wichtmann, 2005].

- The rest of influencing factors, as for instance the dependencies on the load amplitude, average soil density or initial stress state, are here taken into account only indirectly through the permanent displacement caused by the first cycle y_1, as well as through the "system constants" B_i. In this respect, the analogy made here to the Bochum accumulation model could be taken a step further so as to include as well some additional multiplicative functions to replicate such dependencies. However, considering the limited amount of experimental data gathered here such extension lies out of the scope of this work and shall be left for future investigations.
- Another alternative would be to define the permanent displacement caused by the first cycle y_1 as function of the different system parameters (cyclic load ratio, void ratio, etc.), for instance using the same general form as that proposed in [Egglezos & Bouckovalas, 1999] at element level, where the pore pressure and permanent shear strain after the first cycle are computed as the product of powers of the different ratios.

4.3 Soil Densification

The existence and extent of the densification mentioned before were verified by performing topographic measurements of the soil surface before and after the tests with a photogrammetric device called ATOS.

As advanced in the introduction to this chapter, the cyclic lateral loading was observed to cause a pronounced subsidence in the immediate vicinities of the pile, while in the outskirts of the subsided cone the sand would typically emerge, forming two small hills with elongated half-moon shape, similar to those reported by Brown *et al.* in their field tests [Brown *et al.*, 1988] (see Figure 4.2-b).

In this respect, an averaged measure of the densification of the whole system accumulated during the cyclic loading can be computed as the difference between the heaved and subsided volumes, taking as a reference the original soil surface mapped before the test.

4.3.1 Photogrammetry: Structured-light 3D scanning

The optical measuring system ATOS is based on the principle of triangulation and on digital image processing, and has been developed by the Society for Optical Measuring Techniques, GOM (Gesellschaft für Optische Messtechnik). Among the photogrammetric applications, it can be classified as a structured-light 3D scanner, and its purpose is to create a cloud of points of known coordinates on the surface of the subject. These points can then be used to extrapolate the shape of the subject, where any irregular curved surface is reconstructed into a polygonal model by finding and connecting adjacent points with straight lines.

The principle of the structured-light 3D scanners is to project a pattern of narrow light stripes on the subject. The lines of illumination appear distorted from any perspective other than that of the projector, so by using two cameras, offset slightly from the pattern projector, the displacement of the stripes provides the 3D coordinates of any details on the object's surface. This technique is similar to the classical topographic triangulation, since now, in order to calculate the distance of every point on the line, the triangle composed by the cameras, the light projector and the points of the light stripe can be determined. This is sketched in Figure 4.16.

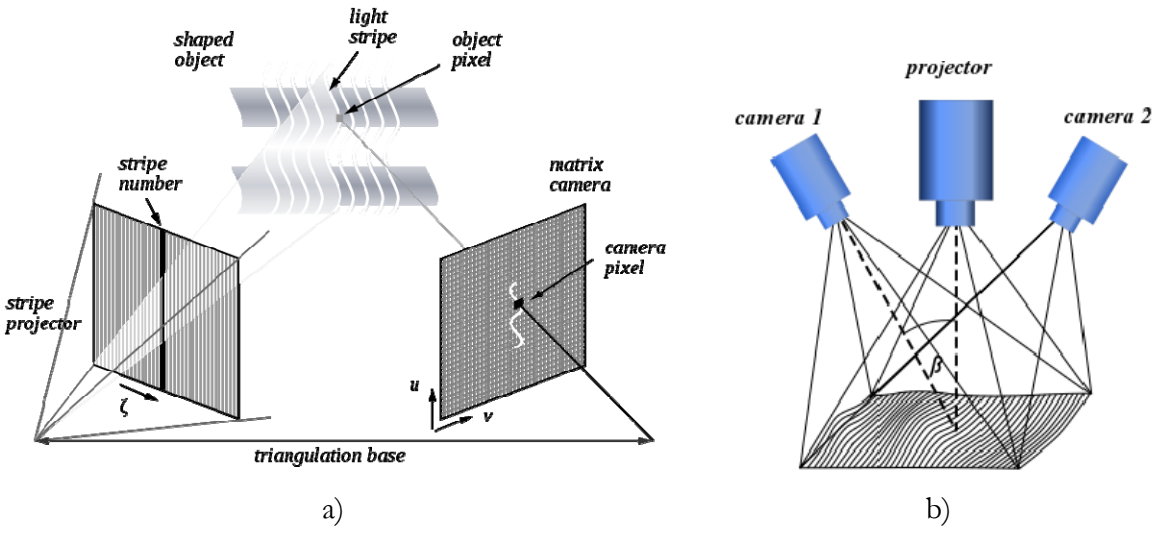

Figure 4.16 Photogrammetric capture of an irregular surface. a) Principle of triangulation with the structured-light 3D scanning. b) Device arrangement of the 3D scanner. (Source: http://www.wikipedia.org)

However, for the particular case of the pile foundation, a single scan cannot possibly provide a complete model of the soil surface, since the projected light will inevitably produce a shadow

behind the pile, hence leaving some parts of the soil surface uncharted. Therefore, multiple scans from many different directions are normally required to capture the whole soil surface, which then have to be brought into a common reference system by means of fixed reference points and then merged to create a complete 3D model.

The resolution of the structured-light scanners depends mainly on the width of the projected stripes and their optical quality (shiny, mirroring or transparent surfaces will in general present problems). Since the reduction of the stripe width is technically limited by the depth of field and by the resolution of the projector and cameras, a phase-shifting method is normally employed to improve the resolution. This way, a number of consecutive exposures are taken with slightly shifted stripes, which then improves the resolution down to a fraction of the stripe width (typically to about 1/10 of it).

4.3.2 Topographic evolution of soil surface

The state of the soil surface around the pile before and after the application of the third cyclic loading schedule is shown exemplarily in Figure 4.17. There, the extrapolated polygonal model of the soil surface can be seen for both states, and the elevations after the test have been calculated relative to the position of the original surface.

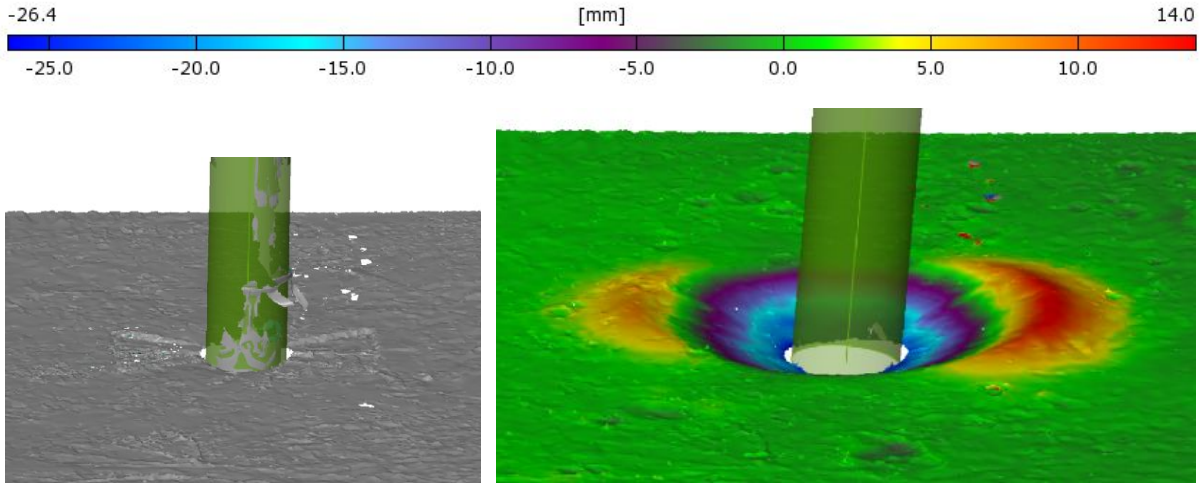

a) b)

Figure 4.17 Measured topography of soil surface before (a) and after (b) the application of 5 million load cycles of lateral load on the pile.

The geometry of the subsided cone can be appreciated in detail by plotting the surface profiles (or soil "slices") along the loading axis and perpendicular to it, as shown in Figure 4.18. There, it can be seen that the depth of the subsided cone is about a third of the pile diameter D and its base (excluding the emerged part) is an almost perfect circle, with a diameter of 3D in both directions. Such circular regularity of the cone is a remarkable feature, since both the lateral loading and the soil heave did only take place along a single direction and in an unsymmetric way. That suggests the existence of out-of-plane displacements within the soil, which was later confirmed by the use of sand markers (see next section).

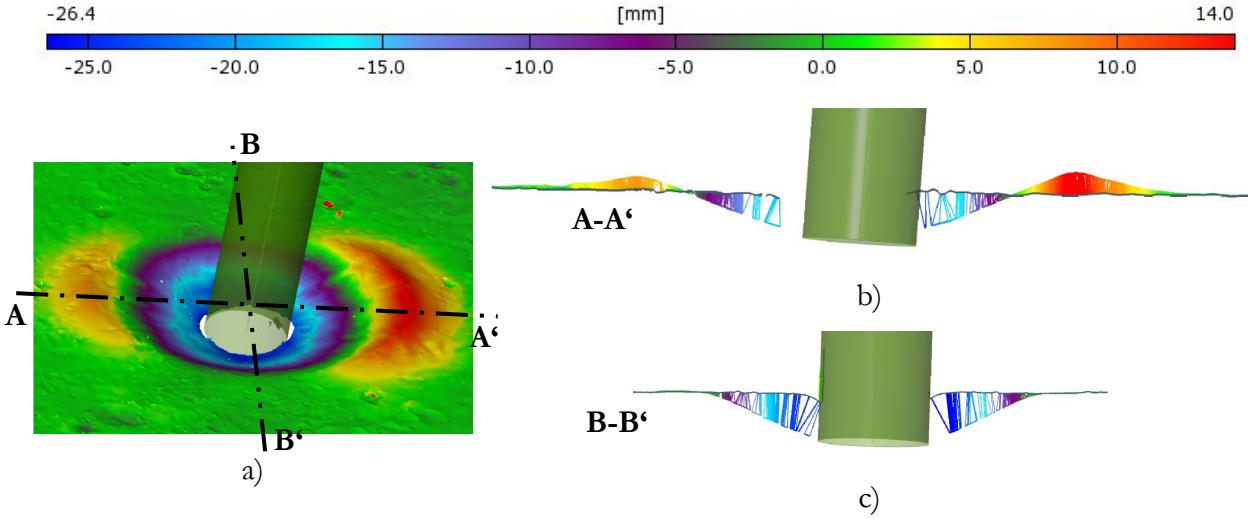

Figure 4.18 Detail of subsided zone (a) and surface profiles along the loading axis (b) and perpendicular to it (c).

Interestingly, the dimensions and geometry of the subsided cone were almost the same for all the tests, with the mere exception of the one-way loading test, which produced an elongation of the subsided zone along of the loading axis (i.e. an ovalization) with a maximum diameter of 7/3 D. This means, that the extension of the densified region is significantly smaller for the one-way test as for the two-way counterparts, which would be consistent with the observations made by Brown *et al.* [1988].

The rest of the tests tended to reach sooner or later a steady form and magnitude of the subsided cone. This would reinforce the idea that the observed subsidence is mainly due to the cyclic densification of the surrounding soil, which after a certain number of load cycles reaches its maximum density, sooner or later depending on the magnitude of the loads. Afterwards, the soil's void ratio in that zone would be practically unaffected by further cycles, regardless of their number and magnitude.

4.3.3 Densification and embedment stiffening

By performing a spatial integration of the surface elevations with respect to a given reference, an estimate of the absolute volume of the soil can be calculated for both the initial and final states.

In none of the tests did the heaved volume add up to account for the whole subsided one, so the cyclic densification of such very dense sand did indeed take place (at least in an average sense) for all the tests. The absolute difference between the subsided and heaved volumes was measured to range between 550 cm^3 and 620 cm^3, which correspond to the 5th test (one-way) and 4th test respectively.

As an order of magnitude, consideration can be made that, since the model pile had 7.5 cm in diameter and 30 cm in embedded length, 620 cm^3 represents around 47% of the soil volume enclosed by the pile.

Now, if the geometry of the volume of soil where the densification is taking place is assumed to be known, it is possible to estimate approximately the final density of the soil within its boundaries, just by considering both the measured initial density and final loss of volume, and assuming as well the conservation of soil mass there.

In order to define the geometry of densified soil, consideration can be made that such short stiff piles tend to behave almost like a rigid body rotating around a single point of zero lateral displacement. The depth of the rotation centre, h_R, which in principle is unknown and variable, probably tending to move upwards as the densification proceeds, can be estimated experimentally by means of strain gauges and a corresponding deflection curve. However, such procedure was not used here, since the interpolation and double integration of measured curvatures with such low number of available strain gauges (only three) would provide a very inaccurate result (see for instance [Yang & Liang, 2007]). Alternatively, a rough approximation can be obtained by considering the soil as an elastic medium with the linearly increasing modulus of subgrade reaction $k = n_H \cdot z$ proposed by Terzaghi, so that the problem can be solved analytically, yielding a depth of rotation centre $h_R = 3L/4$, being L the total embedded pile length [Kolymbas, 1989]. This is sketched in Figure 4.19, along with two possible geometries of the densified volume.

The first possibility considered here is based on the assumption that the soil close to the rotation centre does not experience any densification, since at that depth the pile lateral displacements are zero. Then, assuming a linear geometry up to the limits of the subsided zone observed experimentally, and considering the pile rigid-body motion and proportional displacements at the pile

tip, a double conical geometry with common base at the rotation centre can be defined. This possibility is sketched in Figure 4.19-b.

This way, the volume of soil affected by the densification can be calculated as the aggregated volume of the two cones minus the volume enclosed by the pile, which in this case yields:

$$V_{DENSIF} \approx V_{DC} = V_{TOT} - V_{PILE} = \frac{146}{216}\pi D^2 L \tag{4.16}$$

where V_{DENSIF} denotes the volume of soil affected by the densification, V_{DC} is the volume of this first option (double cone), V_{TOT} is the aggregated total volume of this geometry, $V_{PILE} = \pi D^2 L/4$, while D and L are the pile's diameter and embedded length respectively.

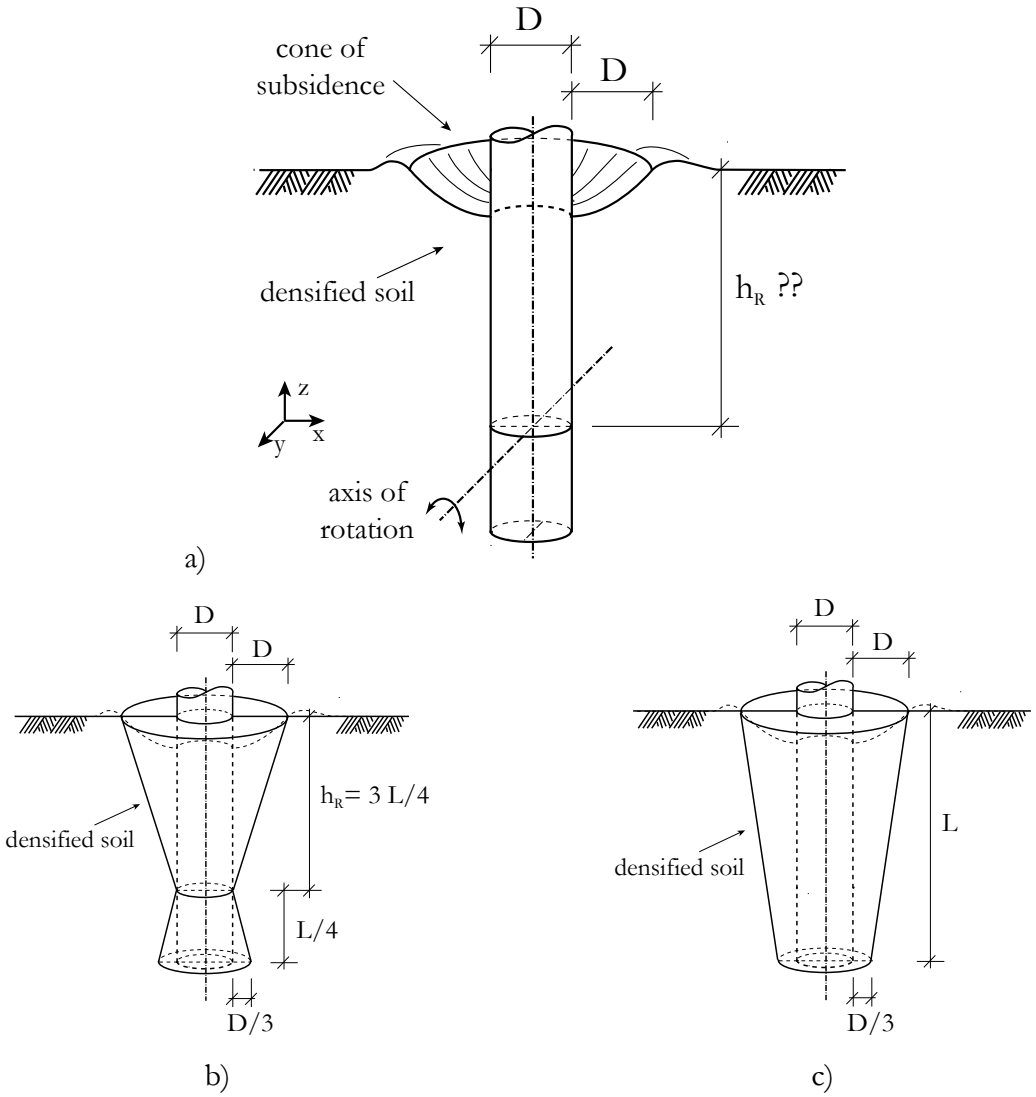

Figure 4.19 Sketches of subsided soil around a laterally loaded pile (a) and two possible simplified geometries of the densified soil volume: Double truncated cone with a common base at the rotation centre (b) and single truncated cone (c).

The geometry of the second option, whose volume is denoted in the following as V_{SC} (volume of single truncated cone), is based on the idea that the densification taking place near the pile tip will cause the subsidence of the soil above it, which means that the soil densified during the initial stages of cycling will tend to move progressively downwards, towards the pile tip. This can be described with the single truncated cone shown in Figure 4.19-c, which then implies the following densification volume:

$$V_{DENSIF} \approx V_{SC} = V_{TOT} - V_{PILE} = \frac{31}{27}\pi D^2 L \tag{4.17}$$

Regarding the depth of subsidence h_S at the pile-soil interface, a conservative estimation can be done by assuming a perfectly conical subsided geometry, sketched in Figure 4.20, which then yields

$$h_S = \frac{6}{5}\frac{\Delta V}{\pi D^2} \tag{4.18}$$

where ΔV is the volume of the subsided geometry (i.e. the volume loss). The real depth of subsidence should in general be shallower, since the observed subsided geometries were in general not perfectly conical but rather more like a revolution paraboloid, as sketched in Figure 4.20.

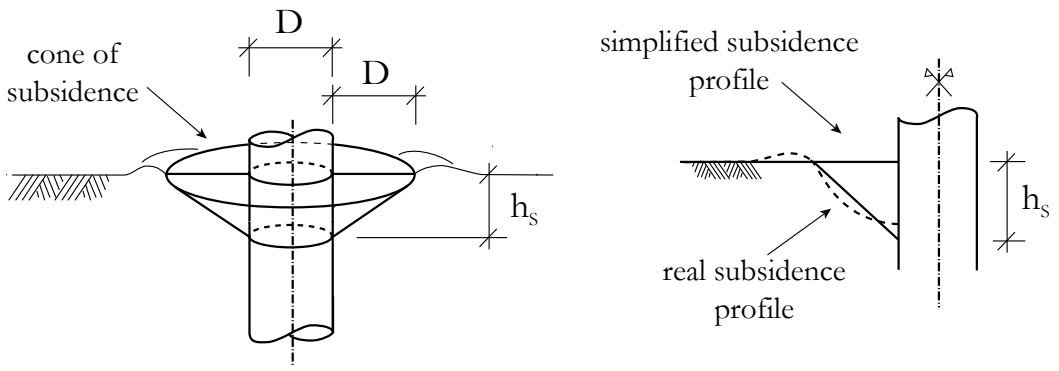

Figure 4.20 Simplified geometry of subsided volume.

And now, in order to analyse the measured data, two alternative ways can be followed:

i. either to calculate the final volume loss assuming maximum density within the selected geometry, and then comparing it to the measured loss of volume,

ii. or to calculate the final density of the soil assuming a given geometry of densified soil and considering the measured subsidence.

4.3.3.1 Volume loss and subsidence depth

By regarding the conservation of the soil mass within the soil geometry affected by the densification, the final (densified) volume can be calculated as

$$V_F = V_0 \frac{\rho_0}{\rho_F} \tag{4.19}$$

and, hence, assuming maximum density at the final state ($\boldsymbol{\rho_F = \rho_{MAX}}$), the volume loss for the two options considered here would be

$$\Delta V_{DC} = V_{DC}\left(1 - \frac{\rho_0}{\rho_F}\right) = \frac{146}{216}\pi D^2 L\left(1 - \frac{\rho_0}{\rho_{MAX}}\right) = 408.5\ cm^3 \tag{4.20}$$

$$\Delta V_{SC} = V_{SC}\left(1 - \frac{\rho_0}{\rho_F}\right) = \frac{31}{27}\pi D^2 L\left(1 - \frac{\rho_0}{\rho_{MAX}}\right) = 693.9\ cm^3 \tag{4.21}$$

where D and L are the diameter and length of the pile, with the values given in Table 4.2, and $\boldsymbol{\rho_0}$ is the initial density of the soil (93% of the Proctor density for these tests).

Therefore, considering that the real loss of volume measured with the 3D scanner ranged between 550 cm^3 and 620 cm^3, it can be concluded that, in this respect, the two simplified geometries used here may represent the bounding limits of the real densified volume. This idea can be expressed as

$$\Delta V_{DC} \le \Delta V_{REAL} \le \Delta V_{SC} \tag{4.22}$$

which may be used in practice for the estimation of the long-term volume loss and subsidence as

$$\Delta V_{LONG-TERM} \le \frac{31}{27}\pi D^2 L\left(1 - \frac{\rho_0}{\rho_{MAX}}\right) \tag{4.23}$$

$$h_S \le \frac{6}{5}\frac{\Delta V_{LONG-TERM}}{\pi D^2} \tag{4.24}$$

4.3.3.2 Final soil density

Another way to look at the results of these tests is to estimate the final density of the surrounding soil by considering a given geometry of soil affected by the densification and imposing the measured volume loss and the conservation of soil mass within the geometry's boundaries. This way

$$\rho_F = \rho_0 \frac{V_0}{V_F} = \rho_0 \frac{V_0}{\left(V_0 - \Delta V_{MEASURED}\right)} \tag{4.25}$$

And now, considering the single-cone and double-cone alternatives introduced before, their respective final densities would be

$$(\rho_F)_{SC} = \rho_0 \frac{\frac{31}{27}\pi D^2 L}{\left(\frac{31}{27}\pi D^2 L - \Delta V_{MEASURED}\right)} = 1.854 \ \ g/cm^3 \tag{4.26}$$

$$(\rho_F)_{DC} = \rho_0 \frac{\frac{146}{216}\pi D^2 L}{\left(\frac{146}{216}\pi D^2 L - \Delta V_{MEASURED}\right)} = 2.013 \ \ g/cm^3 \tag{4.27}$$

where $\boldsymbol{\Delta V_{MEASURED}}$ has been taken exemplarily from the measurements of the 4th test series, and hence as 620 cm^3.

Considering that the maximum density of the Berliner sand used in these tests is $\boldsymbol{\rho_{MAX}}$=1.88 g/cm3, this seems to indicate again that the single-cone geometry can approximate well the extents of soil densification. On the other hand, the double-cone geometry cannot possibly accommodate all the subsided volume, since that would increase its density beyond the limits imposed by $\boldsymbol{\rho_{MAX}}$.

4.3.3.3 Concluding remarks

This all seems to fit well with the hypothesis expressed in the previous section: The soil surrounding the cyclic laterally loaded pile experiences a cyclic densification and after a certain number of load cycles reaches its maximum density, sooner or later depending on the magnitude of

the loads. Afterwards, the soil's void ratio in that zone is practically unaffected by further cycles, regardless of their number and magnitude.

This also agrees with the experimental fact mentioned before, that the cyclic pile-head displacement amplitude tends to reduce until a certain point, where it remains stable. That point would mark the moment where the soil has reached its maximum density.

To conclude this section, the following remarks can also be made:

- The considerations made here are based on the assumption of mass conservation within the region of soil affected by the densification. However, a certain grain migration towards the pile and a constant inflow of material at the pile-soil interface were observed for all the tests, which could appear to contradict the first assumption. As it will be shown in the next section, this is not the case, since the migrating material follows a convective trajectory within a closed cell, which is completely enclosed by the simplified geometries presented here, and thus no net inflow of "new" material did happen.
- The real geometry of the soil affected by the densification is probably much more complex than the simplified options presented here. Since the densifying agent is the pile cyclic displacement, it appears reasonable to assume that the densified region will be larger along the loading axis, and minimal within the plane transversal to it.
- The assumption of an axi-symmetric geometry of densified soil such as the ones employed here can be considered as conservative, since for a given volume of densified soil it will imply less densification, and hence less bedding improvement, along the loading direction.
- The simplified geometries adopted here provide a good quantitative estimate of the volume loss, which can be assumed to be in between these two options. The single-cone geometry would be more conservative, yielding a maximum boundary for the depth of subsidence.
- It may be possible to investigate the geometry of densified soil in detail by means of numerical DEM simulations, which could also provide a better insight into the degree of densification, but that lies out of the scope of the present work and shall be left for future investigations.
- The sand around full-scale piles in the field may compact to a lesser extent than the sand in these model tests due to scale effects caused by greater confining pressures.

- As a final remark, it is important to highlight that such densification will in general lead to a stiffening of the soil around the pile, which in the long term may produce a significant change in the dynamic behaviour of the foundation. Similar conclusions have been drawn by Grabe and Dührkop in the light of their experimental results from model tests [Grabe & Dührkop, 2008].

4.4 Sand Ratcheting Convection

Remarkably, during the tests it was possible to observe a continuous grain migration towards the pile, along with the local subsidence on the surface of the soil discussed in the previous section. In order to investigate the causes of this "steady-state" grain migration, and aiming to find out the final destination of the migrated sand particles, the second and further tests were devised incorporating bands of coloured markers on the soil surface so that they could be identified at the end of the loading schedule, upon removal of the upper layers of soil.

As evident from the recorded images (see an extract in Figure 4.21), the grain migration towards the pile started immediately after the beginning of the loading and within the first few hours (the first hundred thousand load cycles) the first grain marker band (the red grains) had been totally engulfed and the conical soil depression around the pile reached a rather constant depth of about 2 cm.

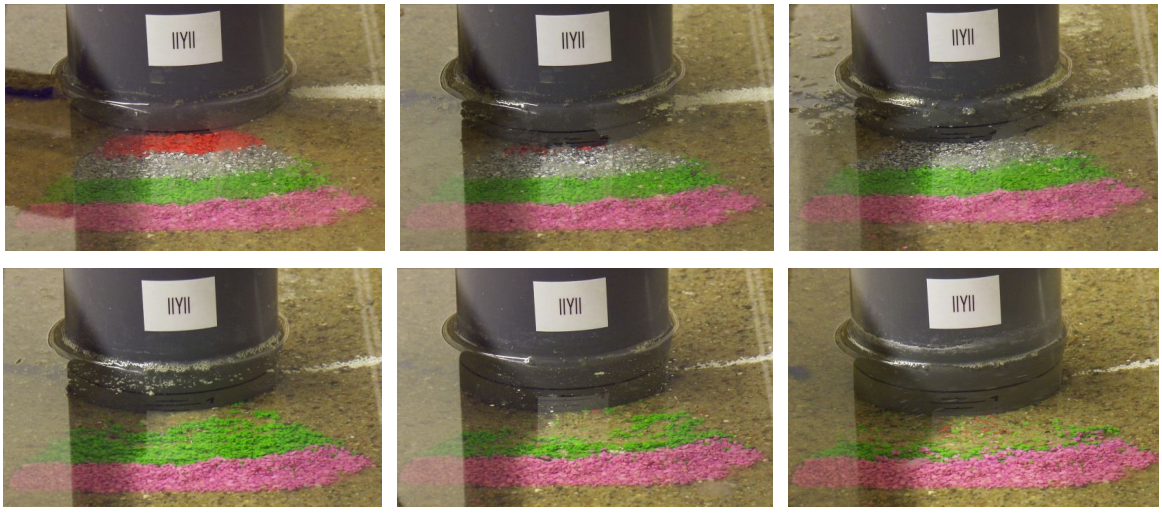

Figure 4.21 Photographic sequence of grain migration during two months of testing and application of 5 million load cycles. Chronological order displayed from left to right and downwards.

Then, the grain migration decelerated slightly in a progressive manner and by the tenth day of loading (approximately the first million load cycles), the second coloured band (the silver-colour markers) had also disappeared from the soil surface and the grain migration speed seemed to stabilise to a constant rate.

By the end of the test after 5 million load cycles, the third band of coloured sand markers (the green sand particles) had also almost completely migrated into the soil-pile interface and the particle migration was still active and at a rather constant speed.

But most remarkably, after approximately 2 million cycles, red markers from the first coloured band (which disappeared within the first few hours of loading) started appearing back into the soil surface at some distance from the pile, and then being mixed and drawn back to the pile along with the rest of sand particles affected by the grain migration (see Figure 4.22). This evidence clearly suggests a convective nature of the grain migration.

Figure 4.22 Surge of red sand markers after approximately 2 million load cycles, returning back to the soil surface.

The fourth band of markers (the pink sand grains), at a distance of 6 cm from the pile wall, did not experience any substantial migration, indicating therefore the limits of the observed phenomena.

Additionally to the grain migration along the loading direction, the recorded images also showed a grain migration within the marker lines perpendicular to it. In fact, this pattern of grain movement towards the pile seemed to happen radially in every direction of the soil's surface plane, and neither happened to cease during the test's runtime.

The average speed of the migrating grains ranged around a millimetre every few hours, as it appeared from the video images. Although it was out of the scope of these investigations, it should

be possible to characterise more accurately the migration at the surface by means of PIV techniques (particle image velocimetry), just as done for instance in [White *et al.*, 2003].

The state of the markers and soil's surface at the end of the test, after the performance of a concluding static capacity loading and the complete drainage of the soil's water, is shown in Figure 4.23.

Figure 4.23 Soil surface and leftover sand markers after 5 million load cycles.

4.4.1 Granular convective cells

After the tests and upon drainage of the water, the excavation of the soil revealed in all cases the existence of two clearly differentiated domains within the soil that suggest a closed-cell convective pattern of grain migration, and, most notably, a dark transition band marking the limit between these two domains (see Figure 4.24).

The first soil domain, which here shall be termed the convected domain, could be observed beside the pile-head and right under the soil depression. All over this domain, it was possible to see a heterogeneous mixture of sand grains and coloured particles from the different marker bands. For the two-way tests, it reached a depth of about 10 cm (i.e. 1/3 of the embedded length) along the pile-soil interface, as measured from the apex of the conical soil depression, and its depth decreased rapidly with the distance from the pile wall. Besides, the domain's most distant point from the pile (the domain's maximum extension) happened to be right below the beginning of the pink marker band at the soil surface, which, as mentioned before, was observed to be practically unaffected by the grain migration, indicating therefore the limit of this hypothetical convective cell. The extents of the convected domain for the different tests is summarised in Table 4.5.

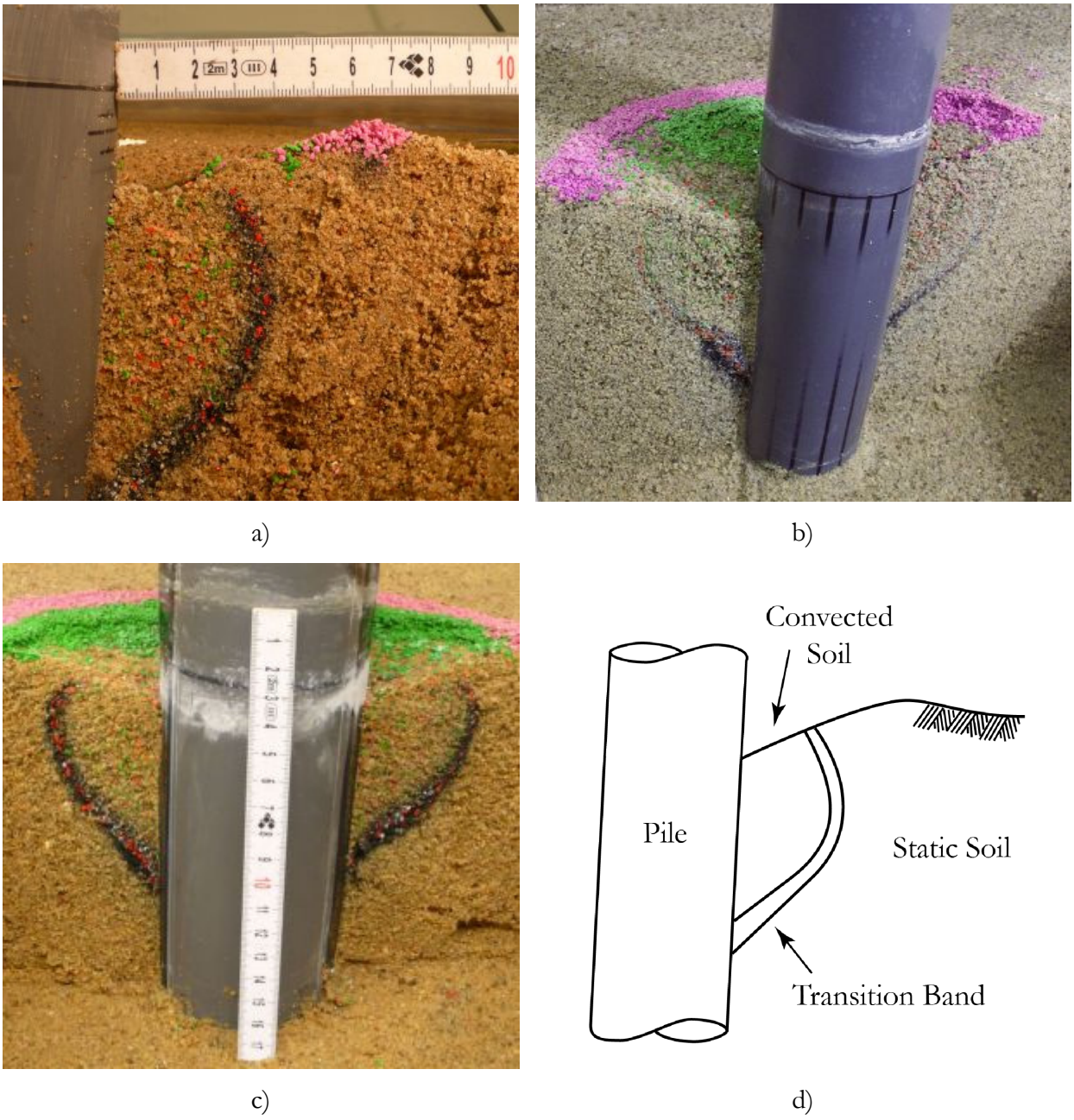

Figure 4.24 Closed cell of granular convection beside the pile-head. Excavated soil after the 2nd, 3rd and 5th tests, shown in (a), (b) and (c) respectively. (d) Sketch of soil domains and transition band.

On the other hand, the second soil domain, henceforth referred to as the static domain (noting that it is not implied that it does not actually move), covered the rest of the soil, from the undisturbed regions at the boundary with the soil container right up to the limits of the transition band (or, more appropriately, transition surface, as will be explained below). Remarkably, this static soil domain was characterised by a complete absence of coloured sand markers, with the mere exception of a few coloured grains unavoidably pressed into it during the cut and removal of the soil after the loading programs.

Table 4.5 Extents of convected soil domain observed in the different tests.

Physical test	Loading range	Depth of convection	Width of convection
2nd test (Two-way)	-10 N to 20 N	9.5 cm	~ 6 cm (*)
3rd test (Two-way)	-10 N to 30 N	10.5 cm	6 cm
4th test (Two-way)	-10 N to 40 N	(**)	(**)
5th test (One-way)	0 N to 30 N	7 cm	5 cm

Depths as measured below subsided soil surface; Widths as measured from pile surface.

(*): Estimated after static lateral capacity test.

(**): During the 4th test, only ceramic spherical markers were used, leading to inconclusive results.

Noteworthy, the transition region between the convected and static domains featured a high population of coloured markers and, especially, the striking presence of very fine dark particles, previously unaccounted for (see Figure 4.25, magnification of the Figure 4.24-a). These dark particles where later identified as coming from the silver-colour coating of the grains of the third marker band. It appears that upon shear under water, the abrasion occurring at the contact between sliding grains did wear off the paint-coating of the silver-coloured sand grains, generating the dark dust-size particles. This fact seems to confirm the hypothesis of two distinct soil domains, a static and a moving one, and the existence of a direct shear surface between them, where the weak coating of the silver markers is worn off.

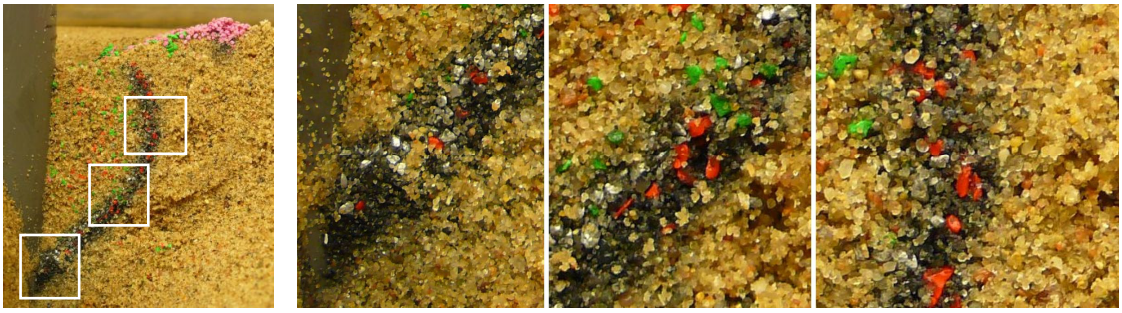

Figure 4.25 Details of the transition band, featuring dark abraded particles of paint coating.

To further reinforce this hypothesis, it can be observed that within the lower parts of the transition surface, where the abrasion of the silver-coloured particles would be just only beginning, there was a much higher population of silver particles than in the upper parts of the limit surface, in which the silver markers would have experienced the abrasion all the way up during their convective migration and thus would have lost most of their colour coating.

The paint-coatings of the other migrated coloured markers (the red and green ones) did not appear to be susceptible to such abrasion under water, at least at the low confining stresses present during the experiment, and thus these markers could be clearly seen all over the convected domain and delimiting surface.

A subsequent removal of the pile exposed the three dimensional nature of the convected domain (see Figure 4.26). It can be observed that the transition band was also present in vertical planes along directions other than the loading line, although only reaching shallower depths. A difference of about 3 cm in the maximum depths of the convected domain was measured between the loading direction, where the convection cell reached its deepest point, and the furthest radial direction within the marker circular sector, which was about 30 degrees off the loading axis in the soil surface plane.

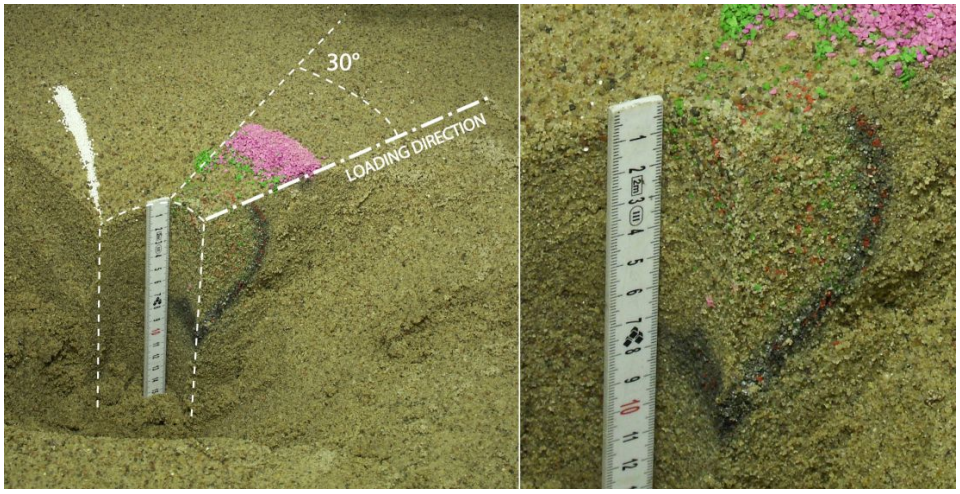

Figure 4.26 Three-dimensional nature of the convective cell, as observed upon removal of the pile.

Also worth mentioning is the pattern of grain displacement in the direction transversal to the loading line, which, as mentioned earlier, was traced with the white ceramic spheres and blue coarse sand particles. As shown in Figure 4.27, the flow of grains in this transversal direction moved out of the vertical plane and deviated clearly towards the less loaded side of the loading direction (the side where the pile was only loaded with a maximum 10 N in all the two-way tests). As evidenced by the video images, both the ceramic spheres and coarse sand markers first migrated radially towards the pile, that is, moving within their vertical plane transversal to the loading direction. But once they reached the pile and penetrated into the soil at the pile-soil interface, they seemed to experience an out-of-plane convection taking them towards the side where the cyclic stresses were lower.

Interestingly, the convected coarse blue particles reached a much shallower depth (around 2 cm under the soil surface) than any other markers, especially than the ceramic markers placed on the opposite side of the pile, which points out to a significant influence of the grain size in the magnitudes of the observed phenomena.

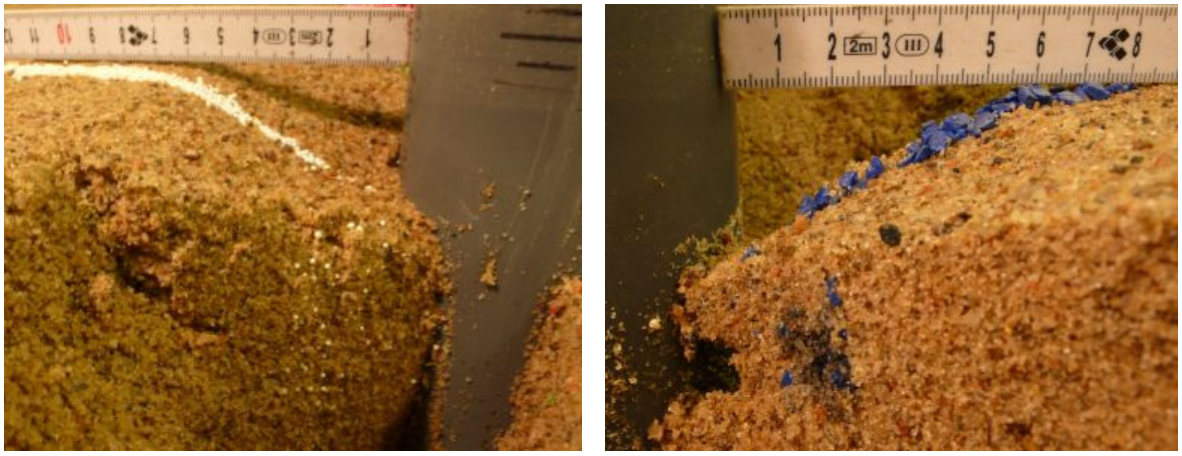

a) b)

Figure 4.27 Out-of-plane convection of sand along the direction transversal to the loading axis, and grain-size effect. a) Small white ceramic spheres and b) Coarse sand blue markers.

In order to assess the effects of the scaling into these phenomena, the coloured sand markers have also been used within the testing series at a bigger scale (1:32) performed by Georgi [Georgi *et al.*, 2009], where the model pile had an outer diameter of 25 cm and an embedded depth of about a meter. The very same phenomena were also observed in those tests and, curiously, the convected domain reached the same proportional depth as in the small scale tests, namely a third of the pile's embedded length (see Figure 4.28) [Georgi *et al.*, 2009].

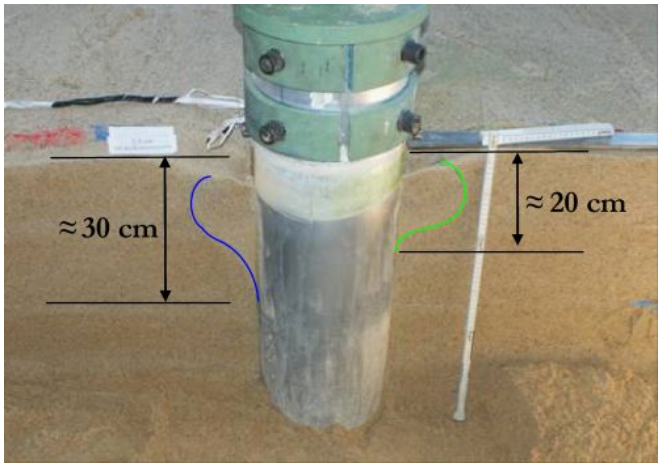

Figure 4.28 Granular convective cells around the monopile in physical tests at a greater scale (1:32). (Source: [Georgi *et al.*, 2009])

For a monopile in prototype-size this would mean a depth of several meters, but the fact that the convected domain was able to hold the scale in these tests has to be regarded with care, since these model tests were carried out under very particular 1-g conditions and the appropriate scaling laws were not strictly followed. It remains unclear whether these phenomena do take place around real-size offshore prototypes, and if so, to what extent.

4.4.2 Quasi-static convection and granular ratcheting

It is important to emphasise that, in contrast to the usual vibratory granular convection that has been broadly mentioned and studied since its discovery in 1831 by Faraday, e.g. in [Faraday, 1831; Kutzner, 1962; Gallas *et al.*, 1992; Herrmann, 1995; Jaeger *et al.*, 1996; Knight *et al.*, 1996; Ehrichs *et al.*, 1998], where the granular matter is subjected to vibrations and relatively high accelerations, the convective flow presented here has instead a quasi-static "ratcheting" nature. During these tests, both the loading frequency and pile-head displacements were so low that the induced accelerations of the soil particles must have been negligible compared to the earth's gravity.

The actual mechanism responsible for the ratcheting convection may be explained in the following manner: every time the pile moves back after a loading peak, a small gap opens at the pile-soil interface allowing the sand grains adjacent to the pile-head to move downwards along the interface. Once they reach a critical depth where the gap is not big enough and they cannot move further down, the sand particles would then be pressed into the soil, moving a little bit further with every load cycle, in a ratchet-like fashion.

Along their way through the soil mass, the migrated grains would be pushed forward by the following grains, and also move directed by gradients of shear stress and towards areas of lower confining stresses, i.e. upwards, setting in motion a whole ratcheting convective cell within the pile-head vicinities.

At the limit where the sand grains are no longer directly affected by the pile-head displacements (and hence rather static), the migrating grains would have to override the standing particles in order to move forward, triggering a direct shear between the convected and the static material.

This hypothetical mechanism seems to be somehow confirmed by the shape of the direct shearing surface and by inspecting the isolines of shear stress within the soil during a loading peak, which can be obtained with a FE model such as the one presented in Chapter 3. As shown in

Figure 4.29, the normals to the isolines of shear stress (i.e. the gradients of shear stress) reproduce quite well the shape of the convected domain and even the characteristical return towards the pile near the soil surface.

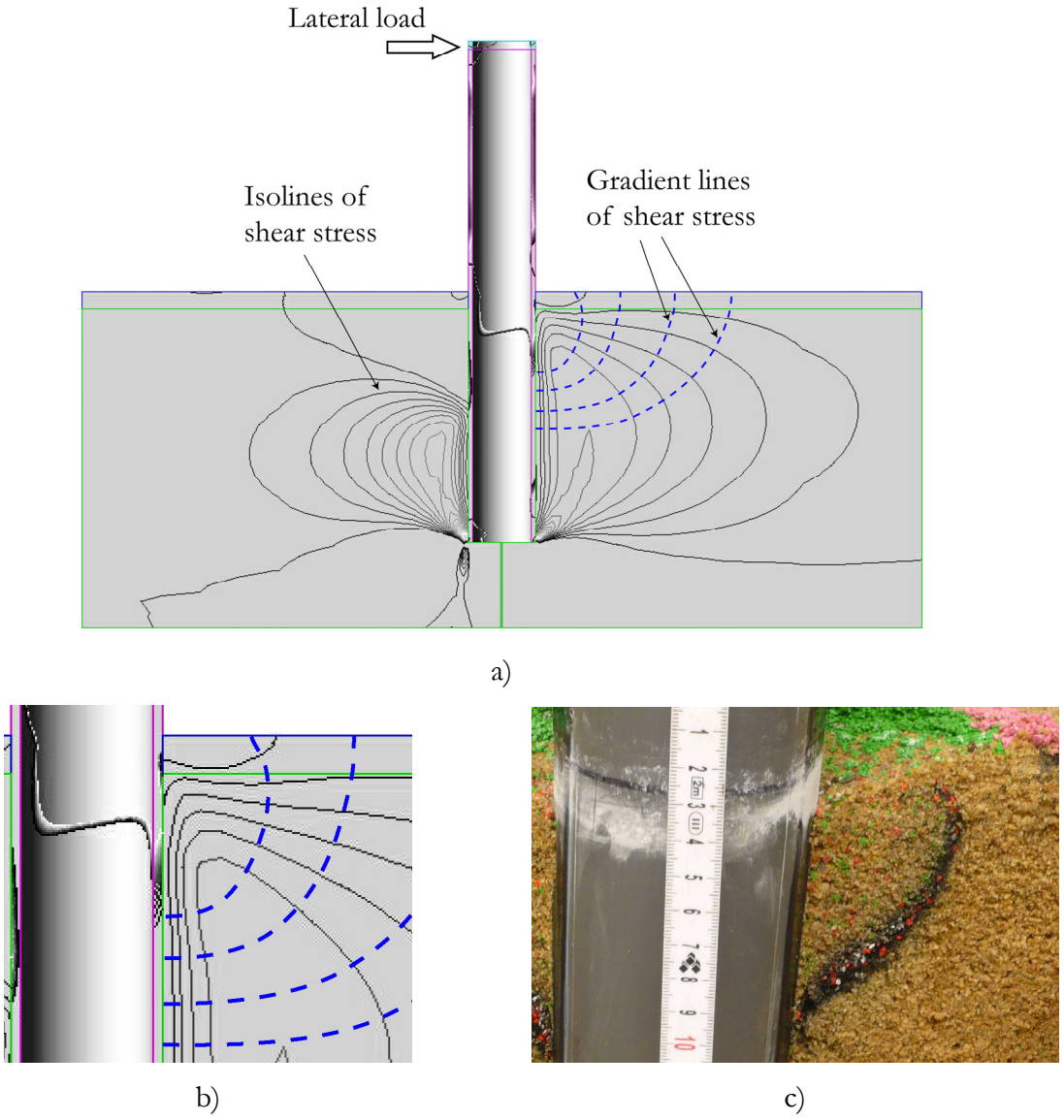

Figure 4.29 Gradients of shear stress as mechanical explanation of convected geometry. (a) Isolines of shear stress obtained by FE analysis. (b) Magnification of soil region near the pile-head. (c) Experimental evidence.

The idea of ratcheting behaviour has already been used in the field of soil mechanics to explain the progressive accumulation of plastic deformations of granular materials under cyclic loads, e.g., in [Festag, 2003; Gudehus, 2003; McNamara *et al.*, 2008; García-Rojo *et al.*, 2004], and numerical studies of granular micromechanics have shown that, even under very small loading, a large number of particle contacts can reach the sliding condition and produce irreversible deformations [Alonso-Marroquin & Herrmann, 2004; Alonso-Marroquin, 2004].

One issue that still needs to be clarified is the role of water in the observed phenomena. Probably, the presence of water may have enhanced the soil migration and convective flow, since the effective stresses within the submerged soil matrix are lower than those within a dry material (where there would be no buoyancy). This, in turn, permits a bigger number of contacts between particles reaching the sliding condition, favouring thus the ratcheting displacements.

In any case, the author believes that these phenomena might also happen in dry sands, although probably to a minor extent, and perhaps even in partially saturated sands.

The effects of any excess pore water pressure and the possibility of soil liquefaction within the convected domain have in principle been disregarded, but they should be object of further investigations, particularly in relation to the loading frequency.

4.4.3 Incremental collapse vs. localised failure

It must also be noted that, despite the striking presence of the shear surface as shown in the pictures, this is not a localised failure of the foundation in the traditional sense. The term "shear surface" is employed here, instead of the more common "shear band", with a double intention: firstly, it stresses the 3-dimensional character of this phenomenon, since this surface seems to surround a heart-shaped volume of soil all around the pile (the term "band" seems more appropriate for a 2D plane strain case). Additionally, it is also meant to avoid confusion with the more common sense of "shear band" as localised failure of the soil. The sliding of a whole block of soil along a shear band, as reported for instance by Bobryakov *et al.* for their experiments [Bobryakov *et al.*, 1990], was never observed in this case, and during the whole runtime of the tests, the soil seems to have kept most of its strength. As a matter of fact, the static capacity tests carried out after each of the cyclic loading schedules did show consistently ultimate values ranging around 150 N at pile-head displacements of 0.1 D.

This way, instead of a localised abrupt failure within the soil, here the foundation rather experiences an attenuation of the permanent displacement rate and an incremental collapse in the sense that such rate never gets down to zero, as discussed previously in Section 4.2.4.

In any case, and regarding the ultimate lateral capacity of the pile, the direct shearing between the convected and static soil domains could lead to the localised damage that eventually might trigger a failure surface, even if such failure surface was never observed in these tests. The material and

mechanical properties of this limiting surface and its hypothetical connection to localised failure should be investigated in detail.

4.5 Practical Implications. Bi-Phasic Model of Long Term Behaviour

The empirical evidence shown in this chapter suggests a two-phase scenario of pile-soil interaction that, to the knowledge of the author, has not been described or reported before. Such scenario could be outlined qualitatively as follows:

"The saturated sand surrounding a flexible pile foundation, subject to a two-way cyclic horizontal loading on the pile-head, undergoes two main distinct phases of deformation and grain displacement: an initial densification-dominated phase and a subsequent convection-dominated phase."

4.5.1 Densification-dominated phase

The first phase, the densification phase (or simply rearrangement phase, if the sand were to be dense enough), starts immediately after the first cycle of loading and is characterised by a progressive subsidence of the soil surface surrounding the pile. During this phase, the cyclic compaction of the soil due to the pile displacements causes a grain rearrangement and, in general, a reduction of inter-granular voids.

This phase would also be characterised by the progressive reduction of the pile cyclic displacement amplitude as a consequence of the hardening of the soil, and in general by the logarithmic accumulation of pile-head permanent displacements described in Section 4.2.4.

The duration of this initial phase would be mainly influenced by the magnitude of the pile displacements and initial relative density of the soil, and it would occur even in absence of particle-crushing or significant pore-pressure accumulations, which don't seem to have happened in the presented tests*). Although it may not be possible to define a clear temporal limit of this phase,

*) As Hettler reckons, grain-crushing and elastic compression of the single grains may be disregarded at low levels of stress (up to 1 MPa) for such sands [Hettler, 1981].

for the presented tests it appears to have lasted for a number of cycles between $N=10^4$ and $N=10^5$.

Concerning the geometry of the soil affected by the densification and the extent of volume loss, a rough estimate may be obtained by assuming the simplified geometries presented in Section 4.3.3, and the maximum soil density within its boundaries.

As mentioned before, Gudehus did propose the same densifying explanation for both the subsidence and grain migration near a cyclically *axially* loaded pile or wall, where the cyclic shearing would cause a net contraction of the soil near the structure, thereby producing a flow of material towards the latter and downwards "until the maximal density of the soil is reached" [Gudehus, 2000]. However, there he did not make any further distinction of phases, nor investigated the geometry of the densified region.

It must also be noted that not all sands have a tendency to densify and, in some circumstances, part of the local subsidence might be also caused by a mere plastic deformation of the soil without reduction in volume, meaning that the subsided volume emerges somewhere else. This seems to have happened to some extent in the presented tests, where the sand was already quite dense and some slight local heave was observed right outside the subsided area. But in any case, as it was shown in Section 4.3.3, the heaved volume of soil never accounted for the whole subsidence, so the densification of such dense sand happened indeed.

In this respect, Brown *et al.* reported a similar "surprising" densification of an already well compacted sand as a result of the two-way cyclic lateral load on a pile [Brown *et al.*, 1988], and in general it can be noted that the shallow (upper) layers of most natural sand deposits might not be so dense to exclude the possibility of further densification.

Finally, it must be stressed again that the soil hardening produced by such densification-dominated phase may modify significantly the eigen-frequencies of the foundation, and hence introduce relevant changes in the dynamic behaviour of the turbine in the long-term. This may have important consequences for the turbine operational thresholds if resonance phenomena are to be avoided.

4.5.2 Convection-dominated phase

After most of the densification has taken place, and once the soil depression reaches a rather constant depth, a second phase starts, namely the convection-dominated phase. During such phase, rather than producing further densification of the soil, the cyclic lateral movements of the pile would mainly cause a convective ratcheting displacement of the sand particles.

Such a convective flow would imply that, despite the permanent grain migration and constant inflow of material into the pile-soil interface, no more significant soil densification is taking place.

This second phase would also be characterised by a fairly constant cyclic displacement amplitude and in general by an over-logarithmic accumulation of pile-head permanent displacements, leading eventually to an incremental collapse in the sense of an ever-decreasing but never vanishing rate of accumulation of permanent displacement. Such over-logarithmic accumulation of displacements could be subdivided into a first stage with constant rate (i.e. a stage of linear accumulation) and a subsequent phase with power-law accumulation that characterises the very long-term behaviour.

Again, it might not be possible to determine precisely the temporal limits of these stages, but in the presented tests, the power-law accumulation of displacements could be observed starting approximately between $N=5\cdot10^5$ and $N=10^6$. In any case, a global approximation of the accumulation during the whole phase may be done by means of a rate degrading function of the number of cycles, as proposed in Section 4.2.4.2.

It is important to stress that these two phenomena, densification and convection, need not be necessarily decoupled. In fact, it appears reasonable that some convective grain migration already takes place simultaneously with the densification during the first loading cycles and, reciprocally, some degree of further densification might also occur during the convection-dominated phase, as the densified soil would approach its maximum density asymptotically.

In a recent paper, Alonso-Marroquin *et al.* have analysed the formation of convective vorticity caused by granular ratchets and report, at a micro-mechanical level (a packing of 400 polygons), the existence of two kinds of deformation regimes: short time regimes featuring a fast accumulation of plastic deformation, and long time ratcheting regimes with slow rates of plastic deformation [Alonso-Marroquin *et al.*, 2008]. In a sense, the experimental evidence and the two-phase model of pile-soil interaction proposed here could be interpreted as the macro-mechanical translation of the micro-mechanical effects discussed therein.

At this point it is also interesting to note the similarities with the experimental results of Bobryakov *et al.* [1990]. Although carried out on a different system (a retaining wall and a raking slope of confined sand, one way loading and plane strain conditions), they also report two stages of soil deformation in their system, namely an initial non-stationary phase with densifying character during the first few load cycles and a subsequent stationary stage "with steady state material density and unchanging specimen surface". The author believes that such correspondence with the two-phase scenario described so far strongly supports the model of pile-soil cyclic interaction proposed here.

The main features of the two phases, along with some proposals for the estimation of the different phenomena, are summarised in Table 4.6.

4.5.3 On the character of the cyclic loading (One-way vs. Two-way)

Considering that the opening of a small gap at the pile-soil interface seems to be a key element for the appearance of such grain migration and convective cell, because it facilitates the downwards movement of the grains adjacent to the pile-head, the depth of the convection cell is probably strongly influenced by the magnitude of the opening gap and the relative size of the migrating grains. As proposed before, the sand grains would only migrate downwards at the interface just until reaching the depth where the gap is not big enough to let them through.

This means that, for a same level of maximum loading, a two-way cyclic load would produce a greater subsidence and grain migration (and thus a deeper convective cell) than a one-way cyclic lateral loading, since the two-way loading would feature a higher cyclic displacement amplitude and hence cause a greater aperture of the pile-soil interface. The single one-way test performed here seems to indicate so (see Table 4.5), and it should be possible to empirically verify the validity of this hypothesis with further tests.

Similar conclusions are drawn by Brown *et al.*, who consider that the sand densification due to lateral pile loading appears to be related to the compaction of the sand falling into the gap behind the pile, and conclude that one-way cyclic lateral load would "undoubtedly" produce less densification than a two-way loading [Brown *et al.*, 1988].

Table 4.6 Bi-phasic phenomenological model of long-term behaviour for a cyclic laterally loaded offshore pile

Phenomena	**Densification-dominated phase**	**Convection-dominated phase**
	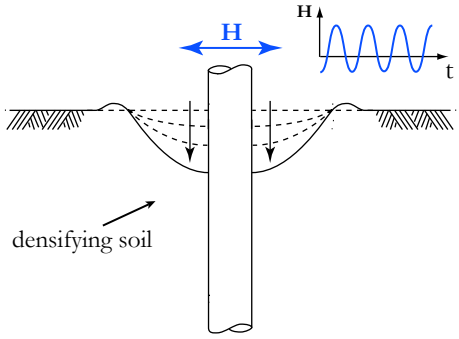	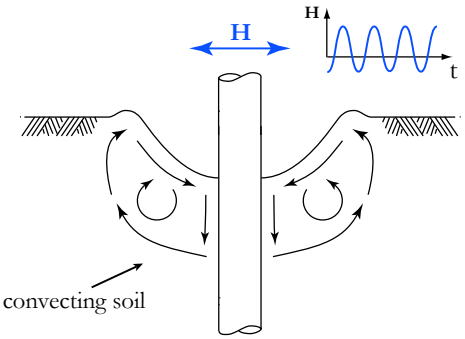
Temporal Extent	$1 < N < 10^4$ to 10^5 (*) (*): load level dependent	(*) 10^4 to $10^5 < N < \infty$ (*): load level dependent
Soil Subsidence	Increasing up to $\Delta V_{LONG-TERM} \leq \frac{31}{27}\pi D^2 L\left(1-\frac{\rho_0}{\rho_{MAX}}\right)$ $h_S \leq \frac{6}{5}\frac{\Delta V_{LONG-TERM}}{\pi D^2}$	Steady state $h_S \approx \frac{6}{5}\frac{\Delta V_{LONG-TERM}}{\pi D^2}$
Soil Density around the pile	Increasing within a certain region (see Section 4.3.3) until $\rho \approx \rho_{MAX}$	Steady state $\rho \approx \rho_{MAX}$
Sand Convection / Direct shearing	?	Closed convective cell: - Trajectory along gradients of shear stress - Depth defined by magnitude of interface gap and soil grain size - Direct shearing at the limit with static soil
Permanent Displacement Accumulation	Logarithmic evolution	Over-logarithmic evolution: - At first, constant rate of accumulation - In the long-term (N > 10^6) the rate decays
	$y_N = y_1\left(1 + B_1\left[ln\left(B_2 N + 1\right) + B_3\delta_N\right]\right)$ where $\delta_N = N\left(1-B_4\right) - \frac{B_4}{B_5}e^{-N\cdot B_5} + C$; $C = B_4 + \frac{B_4}{B_5}e^{-B_5}$	

Furthermore, Grabe *et al.* have also shown, by means of numerical simulations with a hypoplastic constitutive law, how the two-way loading can produce some hardening of the surrounding soil and thus reduce the pile-head displacements, in contrast to a one-way cyclic lateral load causing a progressive collapse [Grabe *et al.*, 2005]. The authors of the simulations interpreted such cyclic hardening as being conditioned by the slippage of soil at the interface after each loading peak, so a clear analogy with the densification phase described here can be highlighted.

4.5.4 Possible implications for offshore operations

Despite the qualitative character of these investigations and the special conditions in which they were carried out (a.o. model tests with single frequency, one directional, two-way loading in a homogeneous clean sand), the practical consequences for the pile design might be manifold. If these phenomena are confirmed to take place also for real in-situ conditions, the model proposed here could be part of a rational framework for an approximate quantification of the long-term cyclic behaviour of lateral pile-soil interaction.

Depending on the soil conditions and expected loads, it might eventually be possible to define the limits of the densification phase and subsidence cone. On the other hand, it may be possible to relate the depth and extent of the convected soil domain to the different design parameters of the pile (flexural stiffness, service loads, grain size distribution, etc...) so that a clearer picture of the pile bedding emerges. This, in turn, might provide a basis for a further re-examination of the current lateral pile design procedures. Applying the existing and future knowledge on granular ratchets to the lateral pile-soil interaction could lead to better estimations of long-term pile-head displacements and a proper adjustment of the p-y curves. The current practice merely prescribes a certain reduction of the static p-y curves for all cases of cyclic loading, irrespective of their duration, magnitude and orientation [API, 2007].

A particularly striking conclusion, if yet unconfirmed, is that if the results of these tests were to be up-scaled back to a prototype-size, it would mean that the granular convective flow could reach a depth of up to 10 meters. However, the fact that so far the convected domain seemed to hold the scale between these tests and those carried out by Georgi [Georgi *et al.*, 2009] has to be regarded with care, since these model tests have been carried out under very particular 1g condi-

tions and the appropriate scaling laws have not been strictly followed. It remains unclear whether these phenomena do take place around real-size offshore prototypes, and if so, to what extent.

Another practical consequence that could be drawn for offshore and under-water operations is related to the scour protection. It seems clear that, despite their obvious resemblance, the conical soil depression reported here is not related to the scour that often occurs in under-water foundations. Local scour is solely caused by the sediment transportation due to the turbulence produced by any foundation that poses an obstacle to the flow of water currents. Given the small dimensions of the confining container and the quasi-static character of the loading, no water currents strong enough to erode the soil surface could have happened during these tests. Therefore, in practice, even if scour is not expected to happen or the appropriate counter-measures are adopted, the soil subsidence will probably still occur due to the densification and grain migration caused by the cyclic loading. A rough estimation of the depth of the subsided cone may be carried out by assuming that a certain volume of soil around the pile reaches the maximum density in the long-term, as proposed in Section 4.3.3.

Finally, it is important to remark again the possible impact of the densification in the dynamic behaviour of the turbine. The shift of the foundation's eigenfrequencies in the long-term due to the hardening of the soil may be estimated by performing a FE dynamic analysis of the pile foundation and assuming maximum soil density within a certain region of the surrounding soil. This may have significant consequences for the turbine operational thresholds if resonance phenomena are to be avoided.

As a closure to the chapter it must also be stressed again that the upper parts of the pile foundations are the most relevant for their lateral bearing capacity [Lesny, 2008; Brown *et al.*, 1988], which highlights the general significance of such phenomenological investigations. A better understanding of the processes inside the soil and of the pile-soil interaction at shallow depths might help improve the design and safety of future foundations.

4.6 Recapitulation

A broad phenomenological model of long-term lateral pile-soil interaction has been presented in this chapter based on experimental results from model tests on a reduced scale with up to five million load cycles. It encompasses a qualitative description of three different stages of pile-head displacement, while a generalised form of a log-linear accumulation law has been found to repro-

duce well the experimental results in the very high cycle range, beyond the first million of load cycles. In this respect, no abrupt failure could be observed in the long-term for the laterally loaded pile, in contrast to the potential unstable behaviour that the axially loaded piles can show under cyclic loads, and the general trend could be described as an attenuating incremental deformation.

Furthermore, a general densification and hardening of the soil were observed in all the tests, as suggested by the marked soil subsidence around the pile and the reduction of bending moments. This was confirmed by means of topographic measurements of the soil surface before and after the tests, which also made possible a quantification of the soil subsidence and the tentative estimation of the geometry and volume of the soil region affected by the cyclic densification. It must be stressed that such densification may not only have a phenomenological interest, but also might bear relevant consequences for the dynamic behaviour of the pile in the long-term.

Finally, some conclusive evidence of granular convective phenomena within the shallow layers of soil around the pile has been put forward, while the existence of a distinct surface where a direct shear of the convecting material takes place has been discussed. A ratcheting mechanism driven by small gaps at the pile-soil interface and gradients of shear stress within the soil has been proposed as a mechanical explanation of the grain migration and convective flow.

5 CONSIDERATIONS FOR DESIGN

Given their phenomenological nature, some of the findings from these investigations will probably be more relevant as a contribution to the general understanding of the mechanical processes involved in the cyclic soil-foundation interaction rather than for a direct application in the design procedures of offshore pile foundations.

However, several of the issues that have been discussed here could and should be reflected in future design approaches, since they might play a relevant role for the safety and serviceability of the offshore wind turbines. Their possible consideration within the frame of a design procedure will be outlined in the following sections, while being divided into short-term and long-term cyclic effects according to the structure of this thesis.

5.1 Short Term Cyclic Lateral Loading

The first important consideration for the design of large-diameter offshore piles is that in general the coupling effects between the pore water pressure and the soil stress are not irrelevant, as assumed systematically in practical pile design. As shown in Chapter 3, the transient increase of PWP generated in the soil during a storm can produce an effective softening of the global stiffness of the foundation, which may only dissipate after the storm subsides.

From a design point of view, the implications of such transient softening could be twofold:

1) ***Ultimate Limit State:*** The extremal loading case for the analysis of the ULS may not take place with an "intact" foundation, but rather happen during an extreme storm (e.g. 50 year return period), which before the arrival of the extreme wave may have generated an excess of PWP in the soil and consequently softened the foundation to some extent. This also applies to the case of foundations in dense sands, even if there the danger of full liquefaction could in principle be disregarded. Therefore, it appears necessary to prove in design that such softening either does not take place or that it does not compromise the overall stability of the pile at ULS.

2) ***Serviceability Limit State:*** The transitory softening of the foundation may give origin to relevant permanent pile displacements, even under the effects of moderate storms with a recurrence period of 1 year. Since such displacements could accumulate with those produced by subsequent storms, the design should also verify that the cumulative inclination of the foundation will not jeopardise the serviceability of the turbine during its operational lifetime.

In this respect, and on the basis of the numerical investigations performed so far, it appears reasonable to distinguish between three possible scenarios:

a) Piles in ***Fully Drained Conditions***, where the transient increments of PWP in the soil can dissipate completely during each loading cycle, and no accumulation of residual pressure nor its consequent softening will take place.

b) Piles in ***Partially Drained Conditions***, where initially the rate of accumulation of PWP in the soil is higher than the rate of dissipation, leading to a net progressive increase of PWP and a softer behaviour of the foundation. However, the dissipation rate will increase as the gradients of PWP around the pile increase, so after a number of cycles the levels of PWP will stabilise and the foundation will not soften further.

c) Piles in ***Undrained Conditions***, where the soil in a close range around the pile will behave essentially undrained. The residual levels of PWP will increase as long as the cyclic loading takes place, which might eventually lead to localised phenomena of cyclic mobility or in extreme cases with loose sand deposits even liquefaction in the soil.

In order to classify a given pile design configuration in the frame of these categories, it is conceivable to define thresholds for the main design parameters (pile diameter, flexural stiffness, soil permeability, etc...) and treat each category differently, according to their propensity to accumulate PWP. In this respect, the categories should not be considered as absolute, since the thresholds should certainly be load dependent. Therefore, a given pile in a given soil could be considered undrained for the ULS but partially or fully drained for the SLS.

Such framework for design is sketched in Figure 5.1 and outlined in the following sections.

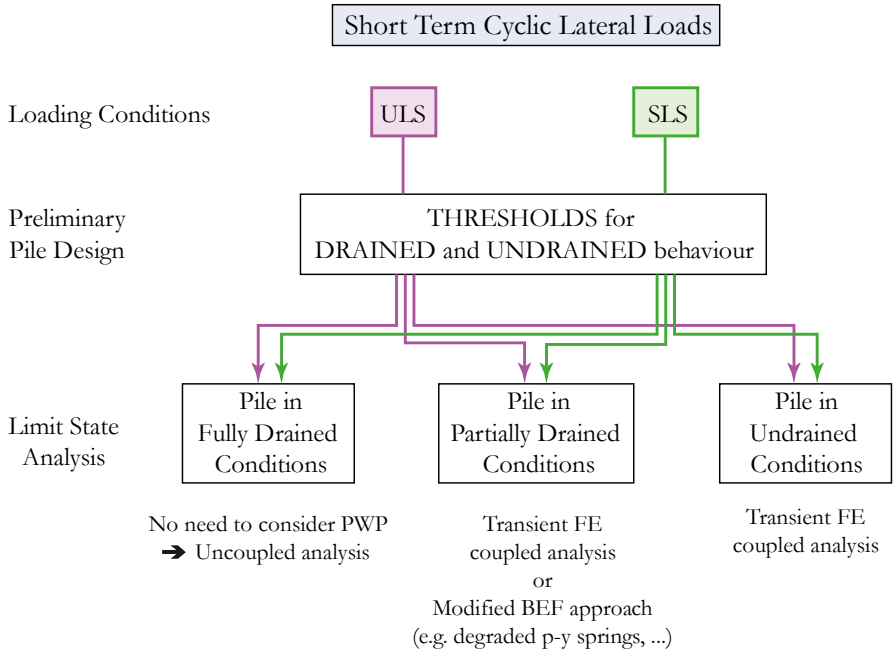

Figure 5.1 Framework for the consideration of short term cyclic lateral loads in the design of large-diameter offshore piles.

5.1.1 Thresholds for drained and undrained behaviour

The existence of different thresholds for the fully drained and undrained behaviour of the large-diameter piles has been discussed in Section 3.6, where some limits were given for the particular cases studied therein.

However, such thresholds are very likely to be dependent on many parameters simultaneously, and not only on those considered there but also on other factors like soil density, load type (one-way or two-way, symmetric or unsymmetric, regular or irregular), load order effects, pile installation method or proximity to other piles, just to name a few.

Therefore, it might not be possible to condense such dependencies in the form of a simple formula or diagram, and perhaps the design criteria will have to be based on given values for given parameter combinations, all of them summarised in the form of design tables.

In any case, further extensive parametrical studies will be required to clarify such extents, quantify the thresholds and bring some light into the inter-dependencies between the different factors.

5.1.2 Piles in Fully Drained Conditions

Whenever it can be substantiated with objective evidence that the loading and foundation parameters are such, that no accumulation of excess PWP around the pile will take place, the design may proceed without further consideration of coupling effects with the pore water.

It must be stressed that this condition does not exempt the design from taking account of *other* cyclic effects such as the accumulation of permanent pile displacements or the cyclic stiffening of the soil. Design procedures for such cyclic effects are currently still subject of research and in general need validation to the special conditions of the offshore wind turbines. Nevertheless, several options have already been proposed, as introduced in Chapter 2 and elsewhere.

5.1.3 Piles in Partially Drained Conditions

For those cases where at some point the rate of dissipation of excess of PWP might compensate or surpass its rate of accumulation, the progressive softening of the foundation will reach a maximum level and then stabilise or decrease. The design should then verify that the requirements for both limit states are met when the foundation experiences the maximum degree of softening.

For this purpose, and since at present there does not exist a simple design procedure that accounts for such PWP-induced softening, it is recommended to perform a transient FE analysis in the following form:

- ***ULS:*** Firstly, a preliminary transient calculation with a 10-minutes load signal from an arbitrary time-history realisation for the extreme storm (50 year recurrence period) should provide the maximum degree of global stiffness degradation. Subsequently, a second FE analysis for the design wave (or design load combination, however it may be defined) should be performed with the initial conditions taken from the maximum degraded state of the preliminary calculation, and the stability of the pile should be demonstrated.
- ***SLS:*** A rough estimate of the permanent pile displacement caused by the PWP-induced softening may be obtained by using a 10-minutes load realisation for the

maximal storm under normal conditions (1 year return period), and then extrapolating it linearly for the rest of the turbine's lifetime, i.e. multiplying it by the number of years of expected operational service. Although such linear extrapolation may appear overly conservative, it might compensate the fact that only 10 minutes of a single storm per year are being considered.

This possible course of action is sketched in Figure 5.2.

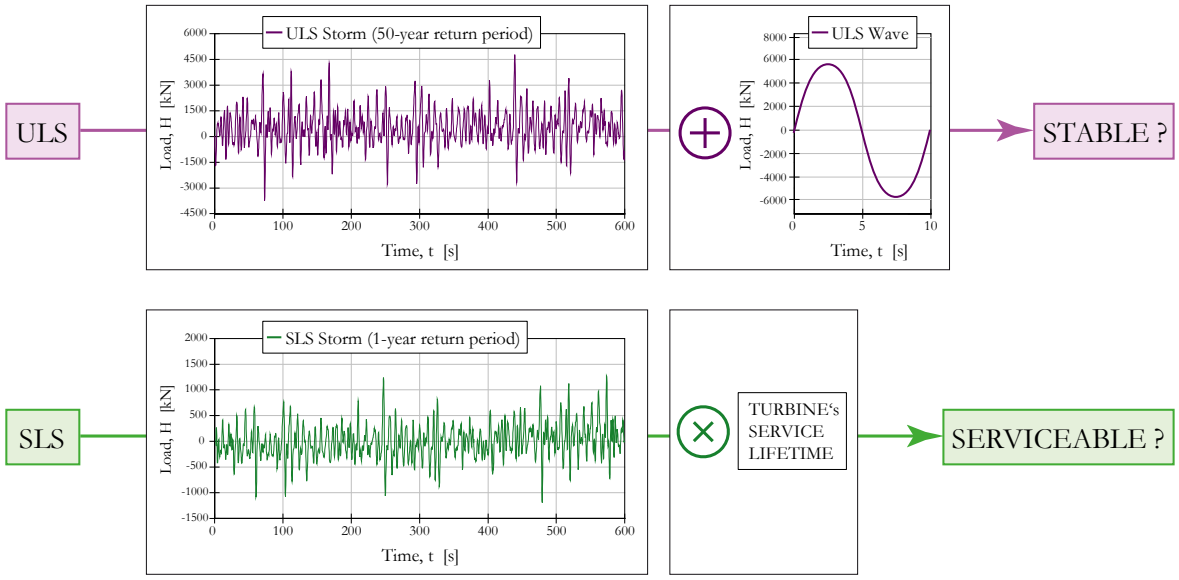

Figure 5.2 Sketch of possible course of action for the verification of limit states for large-diameter offshore piles under consideration of PWP cyclic accumulation.

An essential requirement for the FE calculation model would be to include the three following basic features:

1) A coupled mathematical model for the consideration of the interaction between the pore water and the solid soil skeleton.

2) A constitutive model capable of generating a residual excess of PWP under cyclic loading*). This excludes in principle all the classical elastic-perfectly-plastic models.

*) Strictly speaking, the ability to generate a residual excess of PWP is only a by-product, and not an intrinsic property of any constitutive model. It comes only as a consequence of using a coupled mathematical model along with a constitutive model that generates plastic volumetric strains inside the failure surface and upon stress reversals.

3) A type of finite element that avoids the appearance of spurious pore pressure instabilities.

Suitable options for such requirements have been presented in Chapter 3 and also in [Grabe *et al.*, 2004] or [Tasan *et al.*, 2010a] for instance.

However, for this case, a simpler approach in the frame of the commonly used BEF design techniques (in particular the p-y approach) could be envisaged as an outcome of future extensive parametrical studies. In this respect, the PWP-induced softening could be implemented as a global reduction factor for the initial modulus of subgrade reaction and for the soil's ultimate resistance. That extent lies in any case out of the scope of this thesis and should be addressed in future investigations.

5.1.4 Piles in Undrained Conditions

For piles in undrained conditions, similar considerations as in the previous case apply, but to a greater extent and with the additional danger that the progressive increase of the residual levels of PWP might eventually lead to localised phenomena of cyclic mobility and considerable permanent deformations. In the author's opinion, a literal liquefaction of the soil is very unlikely to occur for the offshore piles, especially in the German bight of the North Sea, where the sand deposits tend to feature very high densities, but the real possibility of cyclic mobility phenomena (the liquefaction counterpart for dense sands) should not be underestimated.

Therefore, for such cases where the soil around the pile could behave essentially undrained, a full FE transient analysis with an appropriate constitutive model (in the frame of the theory of Generalised Plasticity or hypoplastic, for instance) would probably be indispensable. The course of action for the analysis of the limit states could be analogous to the one proposed in the previous section, i.e. to perform transient calculations with representative 10-minutes load signals.

For a discussion about the legal implications of using the FEM for geotechnical design, the interested reader can refer for instance to a recent contribution by Grabe, Hettler and Drewsen [2010], who raise and discuss several topics about the limitations and possibilities of FEM in practical design, both from a technical and juristical point of view.

5.2 Long Term Cyclic Lateral Loading

Concerning the open issues for the long term behaviour mentioned in Chapter 2 and based on the experimental results shown in Chapter 4, some considerations and empirical relations could be used in design to address the following topics:

- **Long term pile-head displacement** in the very high cycle range ($N>10^6$).
- Depth of **soil subsidence** produced by the cyclic densification, additional to the depth of any scouring phenomena that could be expected.
- **Embedment stiffening** due to the soil's cyclic densification, for the dynamic analysis of the foundation in the long term (shift of eigenfrequencies).

Although these considerations are based on the results from model tests and hence for practical design would require not only a validation for the full scale but also some calibration of the material constants, geometry and loads to those being actually considered, they can provide in any case some orientation and an order of magnitude for such phenomena.

5.2.1 Long term pile-head displacement

If a prognosis of the accumulation of permanent lateral displacement in terms of the number of load cycles were to be cast using the explicit accumulation formulas proposed in the literature, the following considerations should be made:

- The logarithmic laws may represent well the initial short-term stage of cycling ($N<10^4$ to 10^5), but tend to underestimate both the rate and the magnitude of the displacements in the long-term.
- The log-linear laws seem to represent very well the accumulation of displacements up to the mid-term range of cycling ($N<10^6$). However, in the long-term stages of cycling the linear term of the law will dominate the behaviour and therefore largely overpredict both the accumulation rate and magnitude of permanent displacements.

Hence, the use of such laws beyond the first million of cycles may be overly conservative for design.

- A generalised form of the log-linear accumulation laws, such as the one proposed in Eqs. 4.12 through 4.14, may provide a more accurate estimation of the permanent displacements in the very high cycle range ($N>10^6$), since it incorporates a degradation factor for the long-term accumulation rate.

5.2.2 Soil subsidence and scouring

Current offshore design guidelines such as GL or DNV already contemplate the possibility of a reduced pile embedment due to hydrodynamic scouring phenomena, while new methods for its quantification and also new mitigation techniques are currently being developed (see e.g. [Haake & Rolfes, 2010]). However, independently of any scour protection measures, the depth of embedment might be further reduced by the progressive compaction of the soil due to the cyclic lateral pile displacements.

Therefore, it might be sensible to include in design an additional reduction of embedment, particularly for the long term dynamic analysis of the pile, since that might affect the shape and frequency of the turbine's characteristic modes of vibration. For this purpose, a simplified geometry of the embedment reduction may be assumed, for instance the conical shape sketched in Figure 5.3.

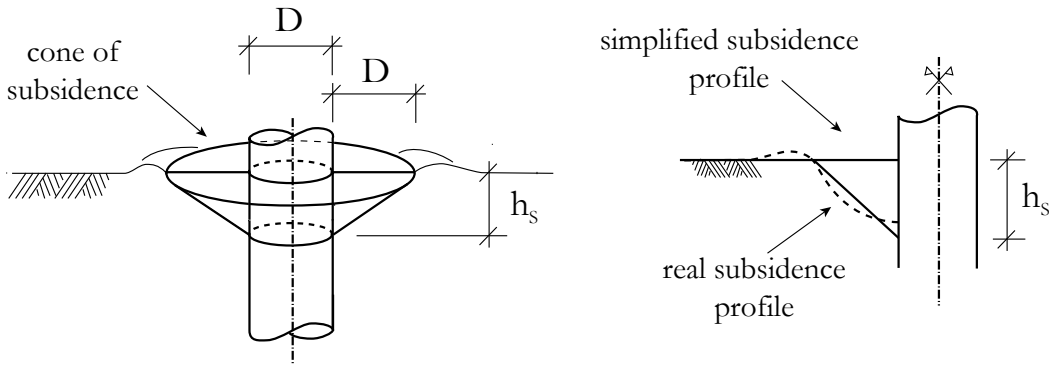

Figure 5.3 Simplified geometry of long-term embedment reduction caused by the cyclic densification of the soil.

Bearing in mind the necessary caution when extrapolating quantities from model scale to full scale, a gross estimate of the magnitude of embedment reduction may be obtained from inexpensive small scale model tests, with the appropriate loads and pile geometry, such as the ones presented in Chapter 4.

In any case, an upper bound*) for the long-term volume loss and densification-induced subsidence may be evaluated by means of Eqs. 4.23 and 4.24.

5.2.3 Embedment stiffening and long term dynamic behaviour

The shift of the foundation's eigenfrequencies in the long-term due to the densification-induced hardening of the soil may be estimated by performing a FE dynamic analysis of the pile foundation while assuming maximum soil density within a certain region of the surrounding soil, for instance the one sketched in Figure 5.4.

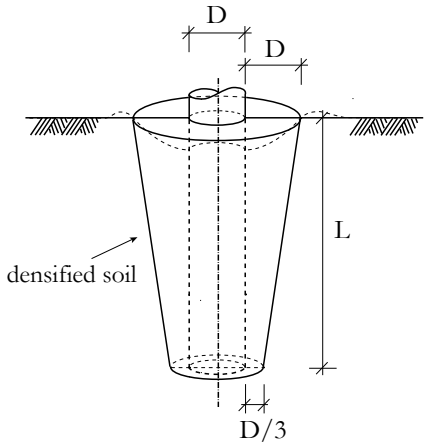

Figure 5.4 Simplified geometry of soil region affected by the long term hardening due to cyclic lateral loading of the pile and progressive densification of the soil.

For such FE analysis, the dynamic properties of the soil within the densified region should be assessed performing laboratory tests on soil samples with the maximum density, although for a preliminary calculation they may be estimated for instance with the formula proposed by Hardin

*) Given the elevated loads employed in these model tests, the amount of soil densification and settlement obtained here are probably higher and not representative of the quantities that may take place in real conditions.

and Black [1966], which provides the dynamic shear modulus G_{DYN} as a function of the void ratio e and mean pressure p:

$$G_{DYN}\,[MPa] = A\frac{(a-e)^2}{1+e}\left(p\,[kPa]\right)^n \tag{5.1}$$

where, in this case, the void ratio $e = e_{MIN}$, and the material constants may be taken as A=6.9, a=2.17 and n=0.5 for sands with round grains and A=3.23, a=2.97 and n=0.5 for angular grains [Wichtmann, 2005].

6 CRITICISM, SUMMARY AND OUTLOOK

For the sake of practicability of the investigations and in view of the elevated computational cost of the study cases presented here, it was necessary to renounce a rigorous modelling of the physical reality of the offshore foundation in several aspects, so certain simplifications had to be introduced inevitably. Nevertheless, their relevance is believed to be minor for the quantities given here, so the orders of magnitude should be appropriate, and in any case they do not preclude the qualitative validity of the phenomena that have been discussed in this thesis. Some of these simplifications and their possible relevance are examined in the first section of this chapter.

Subsequently, the main lines of this work and the principal lessons learnt from it are briefly summarised, and the last part of the chapter is devoted to an outline of the open issues that could be addressed in future investigations.

6.1 Limitations and their relevance

The first main simplification is that the inertia effects have been neglected in the calculations, so just a quasi-static consolidation analysis has been performed. As stated by Taiebat [1999], in general it is difficult to conclude definitively on the need for a dynamic analysis of the response of offshore foundations. Ishihara [1996] classified the wave loading as a static one, although in principle he defined the static events as those where the load application (i.e. a fourth of the load cycle) takes place within tens of seconds, which is not always the case for offshore foundations. On the other hand, Zienkiewicz and Bettess [1982] showed that the dynamic effects are negligible for typical seabed problems under the action of waves of periods no shorter than 10 sec and in which the length of the drainage path is in the order of 10 m. Therefore, while a dynamic analysis probably gives a more accurate picture of the behaviour of offshore foundations its relevance seems to be minor.

Concerning the model constituents, the no-tension joint element obviously departs significantly from the real pile-soil interface behaviour due to the simplified contact laws and conditions (no drainage, a fixed contact topology, no dilatancy, simplified friction, etc…). While this can have a significant impact on the results for long axially loaded piles which heavily rely on the shaft fric-

tion for the development of load resistance, the use of a more rigorous contact description is probably not necessary for the laterally loaded piles studied here, which are mainly influenced by the phenomena occurring perpendicular to the interface.

Regarding the constitutive model, the fact that the state parameters have not been included yet means that the single calibration set for the model parameters is only "right" for a certain depth and not for the whole soil. Without the state parameter, a strict modelling would require that the soil elements at each depth incorporate the material parameters calibrated for their corresponding confining pressure, which is obviously not practicable. However, the set of parameters employed in this study corresponded to a confining pressure of 100 kPa, which can be assumed to be fairly representative of the upper half of the embedment. As mentioned previously, the upper parts of the pile embedment are the most relevant for its lateral load bearing behaviour, so this simplification is believed to have only a small influence on the overall results discussed here.

A perhaps more sensitive issue is the size and degree of refinement of the finite element mesh. In this respect, the adoption of a bigger model incorporating smaller elements perhaps might have rendered a smoother solution and more accurate results. However, that would have brought the computational cost of the studied cases beyond the limits of practicability, while in any case, the use here of the enhanced elements of Simo and Rifai reduces considerably the need for a finer mesh, since they feature a quadratic precision in displacements and are free of locking phenomena (i.e. they do not suffer numerical bending stiffening).

Another issue is that the initial stress state assumed for the soil is also a rough simplification of the real stress conditions of the seabed. Not only that the initial orthotropic stress (a $\boldsymbol{K_0}$ stress state) disregards any stress heterogeneities and pile installation effects, but also the preloading caused by the distributed load on the soil surface has a certain impact on the results. Concerning the former issue, due to its complexity it will have to be addressed in future investigations (some ideas in this respect are given in the Outlook, at the end of this chapter), while the effect of the latter, apart from the beneficial influence on the overall convergence rates, is mainly a shift of the observed phenomena to shallower depths.

The loading conditions have also been severely simplified, particularly for the study case and parametric investigations, where the few cycles of a purely symmetric two-way sinusoidal load with constant period and acting in a single direction are only a crude approximation of the foundation's resultant of the actual loading produced by wind and waves on the turbine. Furthermore, the changing water-level conditions at the seabed surface have also been neglected in this study, which is a factor that can also lead to liquefaction phenomena in the upper metres of soil, as shown by several authors in the past. The limitations concerning the number, character and shape

of the load cycles have been partially addressed with the computation of the realistic storm load signal presented in the end of Chapter 3, although their influence should also be part of a proper parametric study including one-way and unsymmetric two-way loads.

And finally, the representativity of these investigations (both experimental and numerical) is also constrained by the fact that they have not been validated with a real structure (neither field nor centrifuge tests, nor on-site measurements), as well as by the scarcity of results, which are focused on a few pile configurations embedded in a certain sand with a given relative density. The results are likely to vary notably if for instance a longer and slender pile is employed or a different relative density for the sand is considered, which calls for special caution when extrapolating the conclusions from these investigations to different conditions.

6.2 Summary and conclusions

The behaviour of pile foundations for offshore wind turbines deviates from classical assumptions and accumulated experience mainly due to their large diameter, reduced slenderness and elevated ratio of lateral to vertical loads. The offshore environment poses the additional challenge of large numbers of load cycles from wind and waves and the possible influence of transient changes of pore water pressure around the pile, both of them issues that are still not well understood and also not being contemplated in current design guidelines.

The aim of this work was to gain an insight into both aspects, while developing a practicable numerical tool for a short-term prognosis and deriving useful criteria for design. For that purpose, the investigations were broadly structured into a first part with a theoretical orientation for the analysis of short-term transient effects, and a second empirical block for the study of long-term phenomena. Subsequently, some implications for practical design have been explored.

6.2.1 Short-Term Behaviour

In the first part of Chapter 3, some suitable options for the three basic requisites for the coupled transient analysis of an offshore pile foundation have been presented:

- The "u-p_W" mathematical model, to account for the interaction between the soil solid skeleton and the pore water on the basis of Biot's equations of poroelasticity. A general dynamic formulation for a bi-phasic solid-fluid mixture and the particular case of saturated consolidation have been introduced.

- A numerical model that discretises all the equations in the frame of the Finite Element Method for their efficient implementation in a calculation program.

- And most importantly a constitutive model, the Pastor-Zienkiewicz model in the frame of the Theory of Generalized Plasticity, that reproduces the main aspects of sand behaviour and is able to generate a residual excess of pore pressure upon cyclic loading. The latter is a feature essential to these investigations which is not possible with the classical elastic-perfectly-plastic models mainly due to their assumption of elastic behaviour inside the failure surface.

Then, the particular conditions to ensure the stability of the pressure field and to provide a suitable pile-soil interface have been addressed and two efficient options have been proposed, namely the coupled form of the Simo-Rifai EAS element due to Mira *et al.* [2003] and the no-tension isoparametric joint element respectively.

Afterwards, some practicable techniques for the optimization of the computational cost through the choice of an appropriate solution strategy, an efficient handling of the sparse matrices and a parallel computation have been discussed. This proved to be a *conditio sine qua non* for the investigations, since without such optimizations the cost of the calculations presented here would have been simply unaffordable.

The detailed analysis of a case study showed the capabilities of the model and led to the following main conclusions:

- Cyclic lateral displacements of the pile caused by extreme loading do produce a net accumulation of pore pressure in the soil at all depths. This is due to the progressive reduction of pore volume as the sand contracts under cyclic loading and the inability of the soil to dissipate the overpressure completely between consecutive cycles.

- The advancing accumulation of excess of PWP has the consequence of a gradual decrease of effective stress in the soil and the shift of the stress paths towards regions of lower confining pressures, which for the case of dense sands can lead eventually to local phenomena of cyclic mobility and considerable plastic deformations. Therefore, even if liquefaction does not take place, the foundation will experience a general softening and the appearance of residual displacements.

The influence and relevance of some of the main factors that affect the generation of pore pressure around the pile have been discussed on the basis of a parametric study and a tentative formulation to describe the results has been derived. The main findings of the study can be summarised as follows:

- There seems to exist a set of thresholds for the system parameters (a.o. pile diameter, soil permeability, load level, etc…) which mark the onsets for the undrained and fully drained behaviours of the foundation. Although several limits have been quantified here, it is very likely that the different thresholds are not constant but dependent on the rest of influencing factors.

- For piles in undrained conditions, the generation of excess of PWP appears to be directly proportional to the applied load, showing a linear evolution at least in the initial stages of cycling. For the case of piles in partially drained conditions, neither the excess of PWP nor its accumulation rate are proportional to the load level, but as the cycling progresses they seem to approach the undrained behaviour.

- For large-diameter piles under extreme loads, the soil behaviour close to the pile is essentially undrained for the range of sand permeabilities typical of the North Sea, i.e. for permeabilities in the order of magnitude of 10^{-4} m/s. The "drained threshold" above which the high permeability would ensure a fully drained behaviour and no accumulation of PWP seems to be up to three orders of magnitude higher, way beyond the normal permeabilities of clean sands. In any case, such thresholds appear to be load level dependent.

- For load frequencies between 0.01 Hz and 0.2 Hz, i.e. for almost the whole range of frequencies typical of offshore storm events, the investigated cases showed an essentially undrained behaviour under extreme loads, nearly insensitive to the load frequency.

- An increase of pile diameter can have an overall beneficial effect on the absolute levels and accumulation rate of excess of PWP, despite the elongation of the drainage paths around the pile. This can be attributed to the better load transfer and stress distribution into the soil and the consequent lower levels of pile displacement and soil compression.

The so-called order effects and the influence of load irregularities have also been briefly discussed on the basis of two simple examples, whereby a certain significance of the order effects was noticed, particularly for the overall stiffness of the foundation's response. For a given number of

load cycles with a given irregular magnitude, an increasing load order seems to be substantially more damaging than a decreasing one.

And finally, the loading case of a realistic storm time signal has been examined, for which a general increase of pore pressure in the soil was also observed. Remarkably, the excess of PWP did not grow indefinitely during the storm, but at all depths reached a certain "saturation level" where it appeared to stabilise. This implies that the transient softening effect produced by the progressive accumulation of excess of PWP at the different depths can also stabilise at some point without leading necessarily to failure.

It is important to note that although such loss of stiffness might only be transitory and the foundation may be able to regain its original stiffness again once the excesses of PWP are dissipated after the storm (or even higher, due to the soil densification), the general softer behaviour during the storm might give origin to significant levels of permanent displacements, which in general will not be compensated after the storm.

6.2.2 Long-Term Behaviour

A broad phenomenological model of the long-term lateral pile-soil interaction has been discussed based on experimental results from several model tests with up to five million load cycles. It encompasses a qualitative description of three different stages of pile-head displacement, while a generalised form of a log-linear accumulation law has been derived and found to reproduce well the experimental results in the very high cycle range, beyond the first million of load cycles. Further conclusions to be drawn from the tests can be summarised as follows:

- No sudden (brittle) failure could be observed in the long-term for the laterally loaded pile, in contrast to the potential unstable behaviour that the axially loaded piles can show under cyclic loading. The general trend could be described as an attenuating incremental deformation, while none of the tests reached a shakedown state of cyclic displacements.
- A progressive reduction of pile bending moments was registered at a depth of L/2, which can be attributed to an increasing rigidisation of the upper layers of soil produced by its cyclic densification.

- The densification of the soil around the pile also takes place for sands in an already dense state, and it proceeds until the material reaches its maximum density. As a consequence, the soil surface will in general subside (irrespective of any additional scouring phenomena) and the dynamic behaviour of the foundation might change (a shift of its eigenfrequencies caused by the reduced embedment and the increased stiffness of the soil).

Finally, some empirical evidence of a granular convective flow within the shallow layers of soil around the pile has been put forward and the existence of a distinct limiting surface within the soil where a direct shear of the convecting material takes place has been discussed. A ratcheting mechanism driven by small gaps at the pile-soil interface and gradients of shear stress within the soil has been proposed as a mechanical explanation of such convective migration of the sand.

6.2.3 Concluding Remarks

It is important to stress that the long-term hardening and short-term softening discussed here are neither incompatible nor mutually exclusive. The general soil densification and hardening observed in the long term do not preclude the appearance of transient episodes of softening during the storms as a consequence of PWP increments.

Hence the importance of considering the coupling effects between soil stress and pore water pressure in design, even for those cases where a soil liquefaction could in principle be disregarded on the grounds of the high relative density of the soil.

For practical design purposes, it seems sensible to distinguish between piles in fully drained conditions, in partially drained conditions and in undrained conditions, and describe them separately. Some considerations in this respect have been given in the final sections of this thesis.

The second main implication for design is that the long term hardening may carry important consequences for the operation of the turbine and the safety thresholds to avoid dynamic resonance phenomena. This may be taken into account by considering that the soil within a certain region around the pile will strive the maximum density in the long term and deriving the dynamic soil properties in consequence.

6.3 Outlook

The numerical model presented in this thesis has proven to be a versatile tool for the prediction of the short-term behaviour of offshore piles. However, it could be further enhanced in many ways, for instance by including real soil conditions through representative CPT profiles, which could provide the initial state of soil stress and density to be used in the model as profiles of earth pressure coefficient $\boldsymbol{K_0}$ and void ratio $\boldsymbol{e}$. For such feature it would probably be necessary to include some additional state parameter in the constitutive model in order to avoid the need of different calibration sets for the model parameters at the different depths. In this respect, a suitable state parameter has already been proposed by Manzanal, Pastor and coworkers [Manzanal *et al.*, 2010; Pastor *et al.*, 2009], who have recently managed to include it successfully in the GeHo-Madrid FE code, so its adoption for future investigations seems very promising.

Besides, in view of the high cost of the calculations proposed here, a further optimization of the computational cost could be envisaged, for instance through domain decomposition techniques and a better parallelization of the FE program, perhaps including MPI technology to open the possibility of using distributed-memory systems (the so-called processor-clusters or supercomputers). Other possibilities in this direction would be to explore the efficient use of iterative solvers (here not really investigated in detail) and the use of the new external solvers that are currently starting to be implemented for GPU's (graphical processing units), which can achieve a high-performance parallelism in normal computers without the need of a processor-cluster.

Concerning the numerical results presented here and their possible repercussion on design, some kind of empirical validation in realistic conditions would be desirable, either through field tests or at least through tests with a geotechnical centrifuge to ensure the appropriate levels of confining stress in the soil. Furthermore, the observed thresholds and derived functions should be re-examined, particularly in relation to the inter-dependence of the parameters (load level, load frequency, soil permeability, pile diameter, etc...), so this calls for an extensive parametrical study, if possible including larger numbers of load cycles.

Regarding the use of these results for the development of a simple BEF model for design (e.g. some kind of softened p-y springs), perhaps it would be useful to adopt some formulation for the generation of residual PWP around the pile such as the one derived in this thesis, but then it would be necessary to investigate its variation with depth, and also its particular influence on the subgrade reaction modulus and soil's ultimate resistance.

As for further topics of the numerical investigations, it seems important to explore the post-cyclic phenomena, in particular the reconsolidation process after an extreme storm and the speed and extent of soil strength recovery. It would also be interesting to explore the effects of multidirectional cyclic lateral loading, although that would require a full 3D foundation model (not half of it, as conveniently done here) and further optimizations to reduce the computational cost. Another issue that could be worth to investigate is the influence of changing boundary conditions for the pressure field, in particular the influence in the pore pressure accumulation within the soil as the water waves propagate over the seafloor.

On the other hand, it could also be interesting to investigate the evolution of PWP around other kinds of piles, for instance around the piles with wings being currently proposed as an alternative for offshore foundations (e.g. in [Grabe, 2008; Dührkop, 2010]). In this case, although the drainage path in shallow layers may increase (the squeezed water may not flow easily around the pile), the better distribution of loads and lower soil stress levels in front of the pile may imply lower levels of transient PWP increments, just as seems to happen with the large diameter piles studied here.

Finally, some extensions of the empirical investigations can also be conceived, for example through PIV observations and/or DEM simulations for an insight into the "real" geometry of densified soil around the pile, and perhaps for the convective cells of sand grains as well, although the latter technique might be out of reach for the time being, since the long-term densification could require the simulation of thousands of load cycles and the convective phenomena perhaps tens or hundreds of thousands of them.

7 REFERENCES

- **Author's publications in the frame of this doctoral work:**

Cuéllar, P., Baeßler, M., and Rücker, W. (2009): "Ratcheting convective cells of sand grains around offshore piles under cyclic lateral loads". *Granular Matter,* 11(6), 379-390.

Cuéllar, P., Pastor, M., Mira, P., Fernandez Merodo, J. A., Baeßler, M., and Rücker, W. (2010): "Numerical investigations for the pile foundation of an offshore wind turbine under transient lateral load". Proceedings of the 7th European Conference on Numerical Methods in Geotechnical Engineering (NUMGE 2010), in Trondheim (Norway), T. Benz and S. Nordal, eds., CRC Press, Taylor & Francis Group, 913-920.

Cuéllar, P., Baeßler, M., Georgi, S., and Rücker, W. (2010): "Special issues for the coupled transient simulation of laterally loaded offshore piles and novel experimental findings". Proceedings of the Workshop Gründungen für Offshore Windenergieanlagen, in Karlsruhe, Germany. Veröffentlichungen des Institutes für Bodenmechanik und Felsmechanik am KIT, Heft 172, T. Triantafyllidis, ed., 117-138.

- **Bibliographic references:**

Achmus, M., Abdel-Rahman, K., and Kuo, Y.-S. (2008): "Design of monopile foundations for offshore wind energy converters". Geotechnics in Maritime Engineering. 11th Baltic Sea Geotechnical Conference, Gdansk, Poland, 463-470.

Achmus, M., Abdel-Rahman, K., Kuo, Y.-S., and Peralta, P. (2007): "Untersuchungen zum Tragverhalten von Monopilegründungen unter zyklischer Belastung". Proceedings of the Pfahl-Symposium 2007; Braunschweig, Germany.

Achmus, M., Kuo, Y.-S., and Abdel-Rahman, K. (2009): "Behaviour of monopile foundations under cyclic lateral load". *Computers and Geotechnics,* 36, 725-735.

Alizadeh, M., and Davisson, M. T. (1970): "Lateral load tests on piles - Arkansas River project". *Journal of the Soil Mechanics and Foundations Division,* 96(5), 1583-1604.

Allotey, N., and El Naggar, M. H. (2008): "A consistent soil fatigue framework based on the number of equivalent cycles". *Geotechnical and Geological Engineering,* 26, 65-77.

Alonso-Marroquin, F. (2004): "Micromechanical investigation of soil deformation: Incremental response and granular ratcheting" *(Thesis)*, Universität Stuttgart.

Alonso-Marroquin, F., and Herrmann, H. J. (2004): "Ratcheting of granular materials". *Physical Review Letters,* 92(5).

Alonso-Marroquin, F., and Herrmann, H. J. (2005): "The incremental response of soils. An investigation using a discrete-element model". *Journal of Engineering Mathematics,* 52, 11-34.

Alonso-Marroquin, F., Mühlhaus, H. B., and Herrmann, H. J. (2008): "Micromechanical investigation of soil plasticity using a discrete model of polygonal particles". *Theoretical and Applied Mechanics,* 35, 11-28.

Altaee, A., and Fellenius, B. H. (1994): "Physical modeling in sand". *Canadian Geotechnical Journal,* 31, 420-431.

Amestoy, P., Buttari, A., Guermouche, A., L'Excellent, J.-Y., and Ucar, B. (2009): "MUltifrontal Massively Parallel Solver (MUMPS 4.9.1) Users' guide". CERFACS.

Andelfinger, U., and Ramm, E. (1993): "EAS-elements for two-dimensional, three-dimensional, plate and shell structures and their equivalence to HR-elements". *International Journal for Numerical Methods in Engineering,* 36, 1311–1337.

Andersen, K. H. (2009): "Bearing capacity under cyclic loading — offshore, along the coast, and on land. The 21st Bjerrum Lecture presented in Oslo, 23rd November 2007". *Canadian Geotechnical Journal,* 46(5), 513-535.

Andersen, K. H., Hansteen, O. E., Høeg, K., and Prévost, J. H. (1978): "Soil deformations due to cyclic loads on offshore structures". *Numerical Methods in Offshore Engineering*, O. C. Zienkiewicz, R. W. Lewis, and K. G. Stagg, eds., John Wiley & Sons, Ltd., 413-452.

Andersen, K. H., and Hoeg, K. (1992): "Deformations of soils and displacements of structures subjected to combined static and cyclic loads". Proc. 10th European Conference on Soil Mechanics and Foundation Enginnering, Florence, Italy, 1147-1158.

Annaki, M., and Lee, K. L. (1977): "Equivalent uniform cycle concept for soil dynamics". *Journal of the Geotechnical Engineering Division, ASCE,* 103(GT6), 549-564.

API (2007): "Recommended practice for planning, designing and constructing fixed offshore platforms - Working Stress Design (21st edition, Dec. 2000; Errata&Supplement 1, Dec. 2002; Errata&Supplement 2, Sept.. 2005; Errata&Supplement 3, Dec. 2007)", American Petroleum Institute

Ashour, M., and Norris, G. (2000): "Modeling lateral soil-pile response based on soil-pile interaction". *Journal of Geotechnical and Geoenvironmental Engineering, ASCE,* 126(5), 420-428.

ASTM (2007): "Standard Test Methods for Laboratory Compaction Characteristics of Soil Using Standard Effort (12 400 ft-lbf/ft3 (600 kN-m/m3))", ASTM International

Augustesen, A. H., Sørensen, S. P. H., Ibsen, L. B., Andersen, L., Møller, M., and Brødbæk, K. T. (2010): "Comparison of calculation approaches for monopiles for offshore wind tur-

bines". Numerical Methods in Geotechnical Engineering, NUMGE 2010, T. Benz and S. Nordal, eds., 901-906.

Babuska, I. (1973): "The finite element method with Lagrangian multipliers ". *Numerische Mathematik,* 20(3), 179-192.

Bachmann, J., and Overbeck, G. (2008): "FINO3: Offshore-Forschungsplattform für Windenergieanlagen - Geophysikalische und geotechnische Baugrunderkundungen". Proceedings of the Baugrundtagung 2008 in Dortmund. Deutsche Gesellschaft für Geotechnik, DGGT., 111-117.

Baeßler, M., Dahlke, C., Eissfeldt, F., Lüddecke, F., Rücker, W., Vierfuß, U., and Zeiler, M. (2009): "Erste Erfahrungen bei der Realisierung der Tragstrukturen von Offshore-Windenergieanlagen in der deutschen ausschließlichen Wirtschaftszone". *Stahlbau,* 78(4), 267-275.

Bane, M. K., Keller, R., Pettipher, M., and Smith, I. (2000): "A Comparison of MPI and OpenMP Implementations of a Finite Element Analysis Code". Cray User Group (CUG-2000).

Banerjee, P. K., and Davies, T. G. (1978): "The behaviour of axially and laterally loaded single piles embedded in nonhomogeneous soils". *Géotechnique,* 28(3), 309-326.

Barrett, R., Berry, M., Chan, T. F., Demmel, J. W., Donato, J., Dongarra, J. J., Eijkhout, V., Pozo, R., Romine, C., and Van der Vorst, H. A. (1994): *Templates for the Solution of Linear Systems: Building Blocks for Iterative Methods*, SIAM, Society for Industrial and Applied Mathematics.

Bathe, K.-J., and Wilson, E. L. (1976): *Numerical Methods in Finite Element Analysis*, Prentice-Hall.

Been, K., and Jefferies, M. G. (1985): "A state parameter for sands". *Géotechnique,* 35(2), 99 -112.

Beer, G. (1985): "An isoparametric joint/interface element for finite element analysis". *International Journal for Numerical Methods in Engineering,* 21, 585–600.

Belytschko, T., Liu, W. K., and Moran, B. (2000): *Nonlinear finite elements for continua and structures*, John Wiley & Sons, Ltd.

Bentley, K. J., and El Naggar, M. H. (2000): "Numerical analysis of kinematic response of single piles". *Canadian Geotechnical Journal,* 37, 1368-1382.

Biot, M. A. (1941): "General theory of three-dimensional consolidation". *Journal of Applied Physics,* 12(2), 155-164.

Biot, M. A. (1955): "Theory of elasticity and consolidation for a porous anisotropic solid". *Journal of Applied Physics,* 26(2), 182-185.

Biot, M. A. (1956): "Theory of propagation of elastic waves in a fluid-saturated porous solid - I. Low-frequency range". *Journal of the Acoustical Society of America,* 28(2), 168-178.

Biot, M. A., and Willis, P. G. (1957): "The elastic coefficients of the theory of consolidation". *Journal of Applied Physics,* 24, 594-601.

Bitzarakis, S., Papadrakakis, M., and Kotsopulos, A. (1997): "Parallel solution techniques in computational structural mechanics". *Computer Methods in Applied Mechanics and Engineering,* 148(1-2), 75-104.

Bobryakov, A. P., Kosykh, V. P., and Revuzhenko, A. F. (1990): "Temporary structures during the deformation of granular media". *(Translation from) Fiziko-Tekhnicheskie Problemy Razrabotki Poleznykh Iskopaemykh. Mining Institute, Siberian Branch, Academy of Sciences of the USSR.,* 2, 29-39.

Boccotti, P. (2000): *Wave Mechanics for Ocean Engineering*, Elsevier Science B.V.

Bolton, M. D. (1986): "The strength and dilatancy of sands". *Géotechnique,* 36(1), 65-78.

Borgard, D., and Matlock, H. (1980): "Simplified calculation of p-y curves for laterally loaded piles in sand". Earth Technology Corporation, Inc., Houston, TX.

Boulon, M. J., Garnica, P., and Vermeer, P. A. (1995): "Soil-structure interaction: FEM computations". *Mechanics of Geomaterial Interfaces* A. P. S. Selvadurai and M. J. Boulon, eds., Studies in Applied Mechanics (42), Elsevier, 147-171.

Bowman, E. T. (2002): "The ageing and creep of dense granular materials" *(Thesis)*, University Cambridge.

Brezzi, F. (1974): "On the existence, uniqueness and approximation of saddle-point problems arising from Lagrange multipliers". *R.A.I.R.O.,* 8(2), 129-151.

Brezzi, F., and Pitkaranta, J. (1984): "On the stabilization of finite element approximations of the Stokes problem". *Efficient solutions of elliptic problems, Notes on Numerical Fluid Mechanics, 10*, W. Hakbusch, ed., 11-19.

Brinch Hansen, J. (1961): "The ultimate resistance of rigid piles against tranversal forces". *Geoteknisk Instituts bulletin No. 12*, Danish Geotechnical Institute, Copenhagen, 5-9.

Broms, B. (1964): "Lateral resistance of piles in cohesionless soils". *Journal of the Soil Meachanics and Foundations Division ASCE,* 90(SM3), 123-156.

Brown, D. A., Morrison, C., and Reese, L. C. (1988): "Lateral load behavior of pile group in sand". *Journal of Geotechnical Engineering,* 114(11), 1261-1276.

Buckingham, E. (1914): "On physically similar systems; illustrations of the use of dimensional equations". *Phys. Rev.,* 4, 345-376.

Buckingham, E. (1915): "The principle of similitude". *Nature,* 96, 396-397.

Buhl, M. L., and Manjock, A. (2006): "A Comparison of Wind Turbine Aeroelastic Codes Used for Certification ". National Wind Technology Center.

Byrne, B. W., and Houlsby, G. T. (2003): "Foundations for offshore wind turbines". *Philosophical Transactions of the Royal Society A,* 361(1813), 2909-2930.

Cambou, B., and Di Prisco, C. (2000): "Constitutive Modelling of Geomaterials". Hermes Science Publications.

Carol, I., and Alonso, E. E. (1983): "A new joint element for the analysis of fractured rock". Proc. 5th. Int. Congress on Rock Mech., Melbourne, 147-151.

Carol, I., Gens, A., and Alonso, E. E. (1986): "Three dimensional model for rock joints". 2nd International Symposium on Numerical Models in Geomechanics, G. N. Pande, ed., Ghent, 179-189.

Castro, G. (1969): "Liquefaction of sands" *(Thesis)*, Harvard University.

Castro, G., and Poulos, S. J. (1977): "Factors affecting liquefaction and cyclic mobility". *Journal of the Geotechnical Engineering Division ASCE,* 103(GT6), 501–516.

Cerioni, R., Brighenti, R., and Donida, G. (1995): "Use of incompatible displacement modes in a finite element model to analyze the dynamic behavior of unreinforced masonry panels ". *Computers and Structures,* 57(1), 47-57

Chan, A. (1988): "A unified Finite Element Solution to Static and Dynamic Geomechanics problems" *(Thesis)*, University College of Swansea

Chandra, R., Dagum, L., Kohr, D., Maydan, D., McDonald, J., and Menon, R. (2001): *Parallel Programming in OpenMP*, Academic Press, Morgan Kaufmann Publishers.

Cheang, L., and Matlock, H. (1983): "Static and cyclic lateral load tests on instrumented piles in sand". The Earth Technology Corporation, Long Beach, California.

Chorin, A. J. (1968): "Numerical solution of incompressible flow problems". *Studies in Numerical Analysis 2*, J. M. Ortega and W. C. Rheinboldt, eds., 64-71.

Chow, F. C., Jardine, R. J., Brucy, F., and Nauroy, J. F. (1997): "Time related increases in the shaft capacities of driven piles in sand". *Géotechnique,* 47(2).

Chrisochoides, N. (2005): "A survey of parallel mesh generation methods". Brown University.

Cuéllar, V., Bazant, Z. P., Krizek, R. J., and Silver, M. L. (1977): "Densification and hysteresis of sand under cyclic shear". *Journal of the Geotechnical Engineering Division, ASCE,* 103(5), 399-416.

Darcy, H. (1856): *Les Fontaines Publiques de la Ville de Dijon*, Dalmont, Paris.

Davis, T. A. (2006): *Direct Methods for Sparse Linear Systems*, Society for Industrial and Applied Mathematics.

Davisson, M. T., and Prakash, S. (1963): "A Review of Soil-Pole Behavior". *Highway Research Record,* 39, 25-48.

Davisson, M. T., and Salley, J. (1970): "Model study of laterally loaded piles". *Journal of the Soil Mechanics and Foundations Division, ASCE,* 96(5), 1605-1627.

Day, R. A., and Potts, D. M. (1994): "Zero thickness interface elements - Numerical stability and application". *International Journal for Numerical and Analytical Methods in Geomechanics,* 18, 689-708.

Demmel, J. W., Gilbert, J. R., and Xiaoye, S. L. (2009): "SuperLU Users' Guide". Computer Science Division, University of California.

Desai, C. S., and Siriwardane, H. J. (1984): *Constitutive laws for engineering materials with emphasis on geologic materials*, Prentice Hall.

Dietrich, T. (1966): "Modellversuche mit biegsamen langen Dalben unter wiederholter Belastung im Sand". *Mitteilungsblatt der Bundesanstalt für Wasserbau,* 23, 1-40.

DNV (2004): Offshore Standard DNV-OS-J101 "Design of offshore wind turbine structures", Det Norske Veritas

Dongarra, J. J., Duff, I. S., Sorensen, D. C., and van der Vorst, H. A. (1998): *Numerical Linear Algebra for High-Performance Computers*, Society for Industrial and Applied Mathematics.

Douglas, D. J., and Davis, E. H. (1964): "The movement of buried footings due to moment and horizontal load and the movement of anchor plates". *Géotechnique,* 14(2), 115-132.

Dowling, N. E. (1971): "Fatigue failure predictions for complicated stress-strain histories". *T. & A. M. REPORT NO. 337*, Department of Theoretical and Applied Mechanics, University of Illinois, Urbana, Illinois.

Duff, I. S., Grimes, R. G., and Lewis, J. G. (1992): "Users' guide for the Harwell–Boeing sparse matrix collection (release 1)". *Technical Report RAL-TR-92-086*, Rutherford Appleton Laboratory, Oxfordshire, England.

Dührkop, J. (2010): "Zum Einfluss von Aufweitungen und zyklischen Lasten auf das Verformungsverhalten lateral beanspruchter Pfähle in Sand" *(Thesis)*, Veröffentlichungen des Instituts für Geotechnik und Baubetrieb der TU Hamburg-Harburg, Heft 20.

Dührkop, J., and Grabe, J. (2008): "Monopilegründungen von Offshore-Windenergieanlagen – Zum Einfluss einer veränderlichen zyklischen Lastangriffsrichtung". *Bautechnik,* 85, 317-321.

Duncan, J. M., Evans, L. T., and Ooi, P. S. K. (1994): "Lateral load analysis of single piles and drilled shafts". *Journal of Geotechnical Engineering, ASCE,* 120(5), 1018-1033.

Egglezos, D. N., and Bouckovalas, G. D. (1999): "Permanent strain and pore pressure relations for cyclic loading of sand". Earthquake Geotechnical Engineering, Séco e Pinto, ed., Balkema, Rotterdam.

Ehrichs, E. E., Flint, J. K., Jaeger, H. M., Knight, J. B., Nagel, S. R., Karczmar, G. S., and Kuperman, V. Y. (1998): "Convection in vertically vibrated granular materials". *Philosophical Transactions of the Royal Society A,* 356, 2561-2567.

Evans, L. T., and Duncan, J. M. (1982): "Simplified analysis of laterally loaded piles". University of California, Berkeley.

Faraday, M. (1831): "On a Peculiar Class of Acoustical Figures; and on Certain Forms Assumed by Groups of Particles upon Vibrating Elastic Surfaces ". *Philosophical Transactions of the Royal Society of London,* 121, 299-340.

Farhat, C., Wilson, E. L., and Powell, G. (1987): "Solution of finite element systems on concurrent processing computers". *Engineering with Computers,* 2, 157-165.

Felippa, C. A. (2001): *Nonlinear Finite Element Methods*, Department of Aerospace Engineering Sciences and Center for Space Structures and Controls, University of Colorado, USA.

Fellenius, B. H. (1975): "Test loading of piles and new proof testing procedure". *Journal of the Geotechnical Engineering Division, ASCE,* 101(GT9), 855-869.

Fernandez Merodo, J. A. (2001): "Une approche a la modelisation des glissements et des effondrements de terrains: Initiation et propagation" *(Thesis)*, Ecole Centrale Paris.

Fernandez Merodo, J. A., and Pastor, M. (2002): "Finite element modelling of landslides". *Numerical Modelling in Geomechanics*, M. Pastor and C. Tamagnini, eds., Revue francaise de génie civil, Hermes Science Publications, 1193-1212.

Festag, G. (2003): "Experimentelle und numerische Untersuchungen zum Verhalten von granularen Materialien unter zyklischer Beanspruchung" *(Thesis)*, Technische Universität Darmstadt.

FINO-Offshore: "FINO - Research Platforms in the North and Baltic Seas", http://www.fino-offshore.com/

Fleming, K., Weltman, A., Randolph, M., and Elson, K. (2009): *Piling Engineering*, Taylor & Francis.

Frank, R., Guenot, A., and Humbert, P. (1982): "Numerical analysis of contacts in geomechanics". Proceedings of the 4th International Conference on Numerical Methods in Geomechanics, Edmonton, Canada, 37-42.

Franke, E., and Muth, G. (1985): "Scale effect in 1g model tests on horizontally loaded piles". Proceedings of the 11th International Conference on Soil Mechanics and Foundation Engineering, 1011-1014.

Frehner, M., Schmalholz, S. M., Saenger, E. H., and Steeb, H. (2008): "Comparison of finite difference and finite element methods for simulating two-dimensional scattering of elastic waves". *Physics of the Earth and Planetary Interiors,* 171, 112-121.

Frossard, E. (1983): "Une équation d'écoulement simple pour les matériaux granulaires". *Géotechnique,* 33(1), 21-29.

Gallas, J. A. C., Herrmann, H. J., and Sokolowski, S. (1992): "Convection cells in vibrating granular media". *Physical Review Letters,* 69(9), 1371-1374.

Ganendra, D. (1993): "Finite element analysis of laterally loaded piles" *(Thesis)*, Imperial College of Science, Technology and Medicine, University of London.

García-Rojo, R., McNamara, S., and Herrmann, H. J. (2004): "Discrete element methods for the micro-mechanical investigation of granular ratcheting". *Proceedings of the ECCOMAS 2004*.

Garcia Nuñez, J. R. (2007): "Análisis comparativo del fenómeno de licuación en arenas. Aplicación a Tumaco (Colombia)" *(Thesis)*, Escuela Técnica Superior de Ingenieros de Caminos, Canales y Puertos. Universitat Politecnica de Catalunya.

George, J. A., and Liu, J. W. (1987): "The evolution of the minimum degree ordering algorithm". *ORNL/TM-10452*, Oak Ridge National Laboratory.

Georgi, S., Baeßler, M., Cuéllar, P., and Rücker, W. (2009): "AP 03: Modellversuche. Anwendungsorientiertes Bemessungs- und Überwachungsmodell für Gründungskonstruktionen von Offshore-Windenergieanlagen unter zyklischer Belastung". Presentation at the Workshop "Pfahlgründungen von Offshore-Windkraftanlagen", 29. April, 2009. TU-Berlin, Germany.

Ghaboussi, J., and Wilson, E. L. (1972): "Variational formulation of dynamics of fluid saturated porous elastic solids". *Journal of the Engineering Mechanics Division, ASCE,* 98, 947-963.

Ghaboussi, J., Wilson, E. L., and Isenberg, J. (1973): "Finite element for rock joints and interfaces". *Journal of the Soil Mechanics and Foundations Division, ASCE*, 849-862

GL WIND (2005): GL WIND IV-2 "Rules and Guidelines IV Industrial Services -2 Guideline for the Certification of Offshore Wind Turbines", Germanischer Lloyd Industrial Services GmbH

Goldscheider, M., and Gudehus, G. (1976): "Einige bodenmechanische Probleme bei Küsten- und Offshore-Bauwerken". Proceedings of the Baugrundtagung 1976 in Nürnberg, Germany, Deutsche Gesellschaft für Erd- und Grundbau e.V., 507-522.

Goodman, R. E., Taylor, R. L., and Brekke, T. L. (1968): "A model for the mechanics of jointed rock". *Journal of the Soil Mechanics and Foundations Division, ASCE,* 94(SM3), 637-659.

Gotschol, A. (2002): "Veränderlich elastisches und plastisches Verhalten nichtbindiger Böden und Schotter unter zyklisch-dynamischer Beanspruchung" *(Thesis)*, Universität Kassel.

Gould, N. I. M., Hu, Y., and Scott, J. A. "A numerical evaluation of sparse direct solvers for the solution of large sparse, symmetric linear systems of equations". *RAL-TR-2005-005*, Computational Science and Engineering Department, Atlas Centre, Rutherford Appleton Laboratory, Oxfordshire.

Grabe, J. (2008): "Pile foundations for nearshore and offshore structures". Geotechnics in Maritime Engineering. 11th Baltic Sea Geotechnical Conference, Gdansk, Poland, 445-462.

Grabe, J., and Dührkop, J. (2008): "Zum Tragverhalten von überwiegend horizontal belasteten Pfählen". Proceedings of the DGGT Baugrundtagung 2008 in Dortmund, Deutsche Gesellschaft für Geotechnik e.V.

Grabe, J., Dührkop, J., and Mahutka, K.-P. (2004): "Monopilegründungen von Offshore-Windenergieanlagen. Zur Bildung von Porenwasserüberdrücken aus zyklischer Belastung". *Bauingenieur,* 79, 418-423.

Grabe, J., Hettler, A., and Drewsen, G.-F. (2010): "Zwischenruf: Entspricht die Anwendung der FEM in der Geotechnik dem Stand der Technik?". Proceedings of the 31st DGGT Baugrundtagung in Munich, Germany, Deutsche Gesellschaft für Geotechnik e.V. (DGGT), German Geotechnical Society, 241-246.

Grabe, J., and Mahutka, K.-P. (2005): "Abschätzung der horizontalen Bettung mittels dynamischer Pfahlprüfung". *Bautechnik,* 82(Heft 4), 227-235.

Grabe, J., Mahutka, K.-P., and Dührkop, J. (2005): "Monopilegründungen von Offshore-Windenergieanlagen - Zum Ansatz der Bettung". *Bautechnik,* 82(1), 1-10.

Grabe, J., and Rudolph, C. (2010): "Zum lateralen Lastabtrag von Pfählen". Proceedings of the Workshop Offshore-Gründungen von Windkraftanlagen 2010, Karlsruhe, Germany.

Grashuis, A. J., Dietermann, H. A., and Zorn, N. F. (1990): "Calculation of cyclic response of laterally loaded piles". *Computers and Geotechnics,* 10(4), 287-305.

Green, R. A., and Terri, G. A. (2005): "Number of equivalent cycles concept for liquefaction evaluations - Revisited". *Journal of Geotechnical and Geoenvironmental Engineering, ASCE,* 131(4), 477-488.

Griffiths, D. V. (1985): "Numerical modelling of interfaces using conventional finite elements". Proceedings of the 5th International Conference on Numerical Methods in Geomechanics, Nagoya, Japan, 837–844.

Gropp, W., Lusk, E., and Skjellum, A. (1999): *Using MPI: portable Parallel Programming with the Message Passing Interface (2nd edition)*, MIT Press, Cambridge, MA, USA.

Gudehus, G. (2000): "Nichtlineare Bodendynamik in der Geotechnik". Baugrundtagung 2000, Hannover, VGE Verlag GmbH, Essen, 263-270.

Gudehus, G. (2003): "Ratcheting und DIN 1054". 10. Darmstädter Geotechnik-Kolloquium, 159-172.

Gudehus, G., Darve, F., and Vardoulakis, I. (1984): "Constitutive Relations for Soils". Balkema.

Gutknecht, M. H. (2005): "Krylov Space Solvers". International Symposium on Frontiers of Computational Science, Nagoya.

Haake, G., and Rolfes, R. (2010): *GIGAWIND alpha ventus Jahresbericht 2009. Ganzheitliches Dimensionierungskonzept für OWEA-Tragstrukturen anhand von Messungen im Offshore-Testfeld alpha ventus*, Institut für Statik und Dynamik, Leibniz Universität Hannover.

Haldar, A. K., Reddy, D. V., and Arockiasamy, M. (1990): "Foundation shakedown of offshore platforms". *Computers and Geotechnics,* 10, 231-245.

Han, J., and Frost, J. D. (2000): "Load-Deflection response of transversely isotropic piles under lateral loads". *International Journal for Numerical and Analytical Methods in Geomechanics,* 24, 509-529.

Hanche-Olsen, H. (2004): "Buckingham's Pi-Theorem". A note for the Mathematical Modelling course, Faculty of Mathematics, Norwegian University of Science and Technology (NTNU).

Haraldsson, A. (2003): "Formulierung und Simulation der Kontaktvorgänge in der Baugrund-Tragwerk-Interaktion" *(Thesis)*, Universität Hannover.

Hardin, B. O., and Black, W. L. (1966): "Sand stiffness under various triaxial stresses". *Journal of the Soil Meachanics and Foundations Division ASCE,* 92(SM2), 27-42.

Hardy, S. (2003): "The implementation and application of dynamic finite element analysis to geotechnical problems" *(Thesis)*, Imperial College of Science, Technology and Medicine, University of London.

Hartmann, S., Tebbens, J. D., Quint, K. J., and Meister, A. (2009): "Iterative solvers within sequences of large linear systems in non-linear structural mechanics". *Journal of Applied Mathematics and Mechanics,* 89(9), 711–728.

Heeres, O. M. (2001): "Modern strategies for the numerical modeling of the cyclic and transient behavior of soils" *(Thesis)*, Technische Universiteit Delft.

Helm, J., Laue, J., and Triantafyllidis, T. (2000): "Zur Verformungsentwicklung von Böden unter zyklischer Beanspruchung". *Bautechnik,* 77(6), 405-415.

Herrmann, H. J. (1995): "Physics of granular media". Chaos, Solitons and Fractals, Elsevier Science, 203-212.

Herrmann, L. R. (1978): "Finite element analysis of contact problems". *Journal of the Engineering Mechanics Division, ASCE,* 104(5), 1043-1057

Hetenyi, M. (1946): *Beams on Elastic Foundation*, The University of Michigan Press, Ann Arbor.

Hettler, A. (1981): "Verschiebungen starrer und elastischer Gründungskörper in Sand bei monotoner und zyklischer Belastung" *(Thesis)*, Veröffentlichungen des Institutes für Bodenmechanik und Felsmechanik der Universität Fridericiana in Karlsruhe.

Hettler, A. (1983): "Modelluntersuchungen für Gründungen in Sand". *Bauingenieur,* 58, 41-48.

Hettler, A. (1986): "Horizontal belastete Pfähle mit nichtlinearer Bettung in körnigen Böden" *(Thesis)*, Institut für Bodenmechanik und Felsmechanik, Universität Fridericiana in Karlsruhe.

Hettler, A., and Gudehus, G. (1980): "Estimation of shakedown displacement in sand bodies with the aid of model tests". Proceedings of the International Symposium on Soils under Cyclic and Transient Loading, Swansea, 3-8.

Hildebrandt, A., Stahlmann, A., and Schlurmann, T. (2009): "Field Data Derived from Offshore Wind Energy Converters – Assessment and Correlation of Dynamic Wave Loads". 33rd Biennial congress of the International Association of Hydraulic Engineering and Research (IAHR), Vancouver (Canada).

Hillmer, B., Borstelmann, T., Schaffarczyk, P. A., and Dannenberg, L. (2007): "Aerodynamic and structural design of multiMW wind turbine blades beyond 5M". *The Science of Making Torque from Wind (Journal of Physics: Conference Series 75)*, IOP Publishing Ltd.

Hinz, P. (2009): "Beurteilung des Langzeitverhaltens zyklisch horizontal belasteter Monopile-Gründungen" *(Thesis)*, Universität Duisburg-Essen.

Hinz, P., Lesny, K., and Richwien, W. (2007): "Prognose des Langzeitverhaltens von Monopilegründungen". Proceedings of the HTG-Kongress 2007, Dresden, Germany.

Holzlöhner, U. (1983): "Modellversuchstechnik". Symposium Messtechnik im Erd- und Grundbau, Deutsche Gesellschaft für Erd- und Grundbau e.V., Essen, 119-126.

Hughes, T. J., Franca, L. P., and Balestra, M. (1986): "A new finite element formulation for computational fluid dynamics: V. Circumventing the Babuska–Brezzi condition: A stable Petrov–Galerkin formulation of the Stokes problem accommodating equal-order interpolations". *Computer Methods in Applied Mechanics and Engineering,* 59(1), 85-99.

Ibrahimbegovic, A., and Wilson, E. L. (1991): "A modified method of incompatible modes". *Communications in Applied Numerical Methods,* 7, 187-194.

Ishihara, K. (1996): *Soil Behaviour in Earthquake Geotechnics*, Oxford University Press.

Ishihara, K., Tatsuoka, F., and Yasuda, S. (1975): "Undrained deformation and liquefaction of sand under cyclic stresses". *Soils and Foundations - Japanese Society of Soil Mechanics and Foundation Engineering,* 15(1), 29-44.

ISO (2007): ISO 19902:2007 "Petroleum and natural gas industries - Fixed steel offshore structures", ISO, International Organization for Standardization

Jaeger, H. M., Nagel, S. R., and Behringer, R. P. (1996): "Granular solids, liquids and gases". *Review of Modern Physics,* 68(4), 1259-1273.

Jardine, R., Chow, F., Overy, R., and Standing, J. R. (2005): "ICP design methods for driven piles in sands and clays", Imperial College London

Jardine, R., and Standing, J. R. (2000): "Pile Load Testing Performed for HSE Cyclic Loading Study at Dunkirk, France". *Offshore Technology Report - OTO 2000 007.*

Jardine, R., Standing, J. R., and Chow, F. (2006): "Some observations of the effects of time on the capacity of piles driven in sand". *Géotechnique,* 56(4), 227-244.

Jefferies, M., and Been, K. (2006): *Soil Liquefaction. A critical state approach*, Taylor & Francis.

Johannesson, P. (2005): "Extrapolation of fatigue loads". Presentation at the 4th Conference on Extreme Value Analysis, Gothenburg, Sweden.

Johannesson, P., and Thomas, J.-J. (2002): "Extrapolation of rainflow matrices". *Extremes,* 4(3), 241-260.

Juirnarongrit, T., and Ashford, S. (2005): "Effect of pile diameter on the modulus of sub-grade reaction". *Report No. SSRP–2001/22*, Department of Structural Engineering, University of California, San Diego.

Kagawa, T. (1986): "Cyclic and loading-rate effects on pile responses". Proceedings of the International Conference on Numerical Methods in Offshore Piling, Nantes, 417–32.

Kaggwa, W. S., Booker, J. R., and Carter, J. P. (1991): "Residual strains in calcareous sand due to irregular cyclic loading". *Journal of Geotechnical Engineering, ASCE,* 117(2), 201-218.

Kahle, H. (2009): "Offshore Windenergieanlagen. Erfahrungen in Design und Ausführung". Proceedings of 5th Hans Lorenz Symposium. Veröffentlichungen des Grundbauinstitutes der Technischen Universität Berlin, Heft Nr. 47, 167-182.

Karypis, G., and Kumar, V. (1995): "Multilevel graph partitioning schemes". Department of Computer Science, University of Minnesota, Minneapolis.

Karypis, G., and Kumar, V. (1998): "A Fast and High Quality Multilevel Scheme for Partitioning Irregular Graphs". *SIAM Journal on Scientific Computing,* 20(1), 359 - 392.

Katona, M., and Zienkiewicz, O. C. (1985): "A unified set of single step algorithms. Part 3: The Beta-m method, a generalization of the Newmark scheme". *International Journal for Numerical Methods in Engineering,* 21, 1345-1359.

Kluge, K. (2007): "Soil Liquefaction around Offshore Pile Foundations – Scale Model Investigations" *(Thesis)*, Faculty of Architecture, Civil Engineering and Environmental Sciences University of Braunschweig – Institute of Technology and the Faculty of Engineering University of Florence.

Knight, J. B., Ehrichs, E. E., Kuperman, V. Y., Flint, J. K., Jaeger, H. M., and Nagel, S. R. (1996): "Experimental study of granular convection". *Physical Review E,* 54(5), 5726-5738.

Knothe, K., and Wessels, H. (1999): *Finite Elemente. Eine Einführung für Ingenieure*, Springer.

Kohlmeier, M., Mittendorf, K., Kossel, T., Habbar, A., and Zielke, W. (2007): "Wave Load Prediction Methods in Offshore Wind Turbine Modelling and their Influence on Fatigue Load Analysis". Proceedings of the European Offshore Wind Conference 2007, Berlin.

Kolymbas, D. (1989): *Pfahlgründungen*, Springer-Verlag.

Kolymbas, D. (1991): "An outline of hypoplasticity ". *Archive of Applied Mechanics,* 61(3), 143-151.

Kolymbas, D. (1993): *Modern Approaches to Plasticity*, Elsevier.

Kolymbas, D., Herle, I., and Wolffersdorf, P.-A. v. (1995): "Hypoplastic constitutive equation with internal variables". *International Journal for Numerical and Analytical Methods in Geomechanics,* 19(6), 415-436.

Kuhlemeyer, R. L. (1979): "Static and dynamic laterally loaded floating piles". *Journal of the Geotechnical Engineering Division, ASCE,* 105(GT2), 289-304.

Kuhn, M. R. (2005): "Scaling in granular materials". *Powders and Grains (2005)*, R. García-Rojo, H. J. Herrmann, and S. McNamara, eds., Taylor & Francis Group, London, 115-122.

Kuo, J. S. H. (1982): "Joint opening nonlinear mechanism: Interface smeared crack model". *EERC Report 82/10*, University of California, Berkeley.

Kuo, Y.-S. (2008): "On the behavior of large-diameter piles under cyclic lateral load" *(Thesis)*, Leibniz Universität Hannover.

Kutzner, C. (1962): "Über die Vorgänge in körnigen Schüttungen bei der Rüttelverdichtung" *(Thesis)*, Technische Hochschule Karlsruhe.

LeBlanc, C. (2009): "Design of Offshore Wind Turbine Support Structures - Selected topics in the field of geotechnical engineering" *(Thesis)*, Department of Civil Engineering, Faculty of Engineering, Aalborg University.

Lee, K. L., and Focht, J. A. (1975): "Liquefaction potential at Ekofisk tank in the North Sea". *Journal of the Geotechnical Engineering Division ASCE,* 101(1), 1-18.

Lehane, B. M., Schneider, J. A., and Xu, X. (2005): "The UWA-05 Method for Prediction of Axial Capacity of Driven Piles in Sand". ISFOG 2005: Proc. 1st Int. Symp. Frontiers in Off-

shore Geotechnics, S. Gourvenec and M. Cassidy, eds., Taylor & Francis, London, University of Western Australia, Perth, 683-689.

Lesny, K. (2008): "Gründung von Offshore-Windenergieanlagen - Entscheidungshilfen für Entwurf und Bemessung". *Bautechnik,* 85(8), 503-511.

Lesny, K., Richwien, W., and Hinz, P. (2007): "Bemessung von Gründungen für Offshore-Windenergieanlagen". Proceedings of the 5th Symposium Offshore-Windenergie, Bau- und umwelttechnische Aspekte, 18.April 2007, Hannover.

Levy, N. H., Einav, I., and Hull, T. (2009): "Cyclic shakedown of piles subjected to two-dimensional lateral loading". *International Journal for Numerical and Analytical Methods in Geomechanics,* 33, 1339-1361.

Lin, S.-S., and Liao, J.-C. (1999): "Permanent strains of piles in sand due to cyclic lateral loads". *Journal of the Geotechnical and Geoinvironmental Engineering,* 125(9), 798-802.

Lindgren, G., and Rychlik, I. (1987): "Rain flow cycle distributions for fatigue life prediction under Gaussian load processes". *Fatigue Fract. Engng. Mater. Struct.,* 10(3), 251-260.

Little, R. L., and Briaud, J.-L. (1988): "Full scale cyclic lateral load tests on six single piles in sand". *GL-88-27*, Civil Engineering Department, Texas A&M University, Texas, USA.

Liu, M. D., and Carter, J. P. (2001): "A general method for defining the number of cycles of repeated loading". *International Journal for Numerical and Analytical Methods in Geomechanics,* 25, 71-81.

Lobo-Guerrero, S., and Vallejo, L. E. (2005): "DEM analysis of crushing around driven piles in granular materials". *Géotechnique,* 55(8), 617-623.

Lobo-Guerrero, S., and Vallejo, L. E. (2007): "Influence of pile shape and pile interaction on the crushable behavior of granular materials around driven piles: DEM analyses". *Granular Matter,* 9, 241-250.

Long, J. H., and Vanneste, G. (1994): "Effect of cyclic lateral loads on piles in sand". *Journal of the Geotechnical Engineering Division ASCE,* 120(1), 33-42.

Lu, J. (2006): "Parallel finite element modeling of earthquake ground response and liquefaction" *(Thesis)*, University of California, San Diego.

Mahtab, M. A., and Goodman, R. E. (1970): "Three-dimensional finite element analysis of jointed rock slopes". Proceedings of the Second Congress of the International Society of Rock Mechanics, 353-360.

Manguoglu, M., Sameh, A., and Schenk, O. (2009): "PSPIKE: A Parallel Hybrid Sparse Linear System Solver". Proceedings of the 15th International Euro-Par Conference on Parallel Processing, Lecture Notes in Computer Science, 797-808.

Manoliu, I., Dimitriu, D. V., and Dobrescu, G. (1985): "Load-deformation characteristics of drilled piers". Proceedings of the 11th International Conference on Soil Mechanics and Foundation Engineering, San Francisco, 1553-1558.

Manzanal, D. G. (2008): "Modelo constitutivo basado en la teoría de la plasticidad generalizada con la incorporación de parámetros de estado para arenas saturadas y no saturadas" *(Thesis)*, Universidad Politecnica de Madrid, ETS Ingenieros de Caminos, Canales y Puertos, Madrid (Spain).

Manzanal, D. G., Fernandez Merodo, J. A., and Pastor, M. (2010): "Generalized plasticity state parameter-based model for saturated and unsaturated soils. Part 1: Saturated state". *International Journal for Numerical and Analytical Methods in Geomechanics*.

Markowitz, H. M. (1957): "The elimination form of the inverse and its application to linear programming". *Management Science,* 3, 255-269

Marques, O. A. (1993): "A partitioned skyline LDL^T factorization". *Technical Report TR/PA/93/53*, CERFACS, Centre Europeen de Recherche et de Formation Avancee en Calcul Scientifique, Toulouse, France.

Marr, W. A., and Christian, J. T. (1981): "Permanent displacements due to cyclic waveloading". *Journal of the Geotechnical Engineering Division, ASCE,* 107(GT8), 11291149.

Martin, G. R., Lam, I., and Tsai, C.-F. (1980): "Pore-pressure dissipation during offshore cyclic loading". *Journal of the Geotechnical Engineering Division, ASCE,* 106(GT9), 981-996.

Matlock, H. (1970): "Correlations for design of laterally loaded piles in soft clay". Second Annual Offshore Technology Conference, Houston, Texas, 1970.

Matlock, H., Bryant, L. M., and Foo, S. H. C. (1978): "Simulation of Lateral Pile Behavior Under Earthquake Motion". Proceedings of the ASCE Geotechnical Engineering Div. Specialty Conference, Pasadena, CA. USA, 600-619.

Matlock, H., and Reese, L. C. (1960): "General solutions for laterally loaded piles". *Journal of the Soil Meachanics and Foundations Division ASCE,* 86(SM5), 63-91.

Matthies, H. G., Nath, C., Schellin, T. E., Garrad, A. D., Wastling, M. A., Quarton, D. C., Wei, J., Scherweit, M., and Siebers, T. (1995): *Study of offshore wind energy in the EC*, Verlag Natürliche Energie, Brekendorf, Germany.

McClelland, B., and Cox, W. R. (1976): "Performance of pile foundations for fixed offshore structures". Proceddings, BOSS'76, International Conference on Behaviour of Offshore Structures, Vol. 2. Technical University of Trondheim, Norway, 528–544.

McClelland, B., and Focht, J. A. (1958): "Soil modulus for laterally loaded piles". *Transactions of the American Society of Civil Engineers,* 123(2954), 1049-1086.

McNamara, S., García-Rojo, R., and Herrmann, H. J. (2008): "Microscopic origin of granular ratcheting ". *Physical Review E,* 77.

Mindlin, R. D. (1936): "Force at a point in the interior of a semi-infinite solid". *Physics,* 7, 195-202.

Miner, M. A. (1945): "Cumulative damage in fatigue". *Journal of Applied Mechanics,* 67, 159-164.

Mira, P. (2001): "Análisis por elementos finitos de problemas de rotura de geomateriales" *(Thesis)*, Universidad Politecnica de Madrid, ETS Ingenieros de Caminos, Canales y Puertos, Madrid (Spain).

Mira, P. (2010). <*Personal communication*>

Mira, P., Pastor, M., Li, T., and Liu, X. (2003): "A new stabilized enhanced strain element with equal order of interpolation for soil consolidation problems". *Computer Methods in Applied Mechanics and Engineering,* 192(37-38), 4257-4277

Mira, P., Pastor, M., Li, T., and Liu, X. (2004): "Failure problems in soils - An enhanced strain coupled formulation with application to localization problems". *Revue Française de Génie Civil,* 8, 735-759.

Mittendorf, K. (2006): "Hydromechanical Design Parameters and Design Loads for Offshore Wind Energy Converters" *(Thesis)*, Fakultät für Bauingenieurwesen und Geodäsie der Leibniz Universität Hannover.

Mlakar, P. F. (1987): "Nonlinear response of concrete gravity dams to strong earthquake-induced ground motion". *Computers & Structures,* 26, 165-173.

Muir Wood, D. (2004): *Geotechnical Modelling*, Spon Press, Taylor & Francis Group.

Murchison, J. M., and O'Neill, M. W. (1984): "Evaluation of p-y relationships in cohesionless soils". *Analysis and Design of Pile Foundations*, J. R. Meyer, ed., 174-191.

Niemunis, A. (2000): "Akkumulation der Verformung infolge zyklischer Belastung des Bodens – numerische Strategien". Beiträge zum Workshop "Boden unter fast zyklischer Belastung: Erfahrungen und Forschungsergebnisse", Veröffentlichung des Institutes für Grundbau und Bodenmechanik Universität Bochum.

Niemunis, A., Wichtmann, T., and Triantafyllidis, T. (2004): "Explicit accumulation model for cyclic loading". Proceedings of the International Conference on Cyclic Behaviour of Soils and Liquefaction Phenomena, in Bochum, Germany, 65-76.

Niemunis, A., Wichtmann, T., and Triantafyllidis, T. (2005): "A high-cycle accumulation model for sand". *Computers and Geotechnics,* 32(4), 245-263.

Norman, C. D., and Anderson, F. A. (1985): "Reanalysis of Cracking in Large Concrete Dams in the U.S. Army Corps of Engineers". Proceedings of the 15th Int. Conference on Large Dams, Lausanne, Switzerland.

Norris, G. (1986): "Theoretically based BEF laterally loaded pile analysis". Proceedings of the 3rd International Conference on Numerical Methods in Offshore Piling, Nantes, France, 361-386.

Oñate, E. (2000): "A stabilized finite element method for incompressible viscous flows using a finite increment calculus formulation ". *Computer Methods in Applied Mechanics and Engineering,* 82(3-4), 355-370.

Ovesen, N. K. (1980): "The use of physical models in design - The scaling law relationships". *Design Parameters in Geotechnical Engineering*, British Geotechnical Society, London, 319-323.

Palmgren, A. G. (1924): "Die Lebensdauer von Kugellagern". *Zeitschrift des Vereines Deutscher Ingenieure (VDI Zeitschrift),* 68(14), 339–341.

Pande, G. N., and Sharma, K. G. (1979): "On joint/interface elements and associated problems of numerical ill-conditioning". *International Journal for Numerical and Analytical Methods in Geomechanics,* 3, 293-300.

Pastor, M., Drempetic, V., Fernandez Merodo, J. A., and Mira, P. (2006): "Modelling marine structures foundations: a rational approach". *Advances in Geomaterials and Structures. Proceedings of the first Euro-Mediterranean Symposium on Advances in Geomaterials and Structures* F. Darve, L. Doghri, R. El Fatmi, H. Hassis, and H. Zenzri, eds., 203-208.

Pastor, M., Fernandez Merodo, J. A., Herreros, M. I., Mira, P., Gonzalez, E., Haddad, B., Quecedo, M., Tonni, L., and Drempetic, V. (2008): "Mathematical, Constitutive and Numerical Modelling of Catastrophic Landslides and Related Phenomena". *Rock Mechanics and Rock Engineering,* 41(1), 85-132.

Pastor, M., Manzanal, D. G., Fernandez Merodo, J. A., Mira, P., Blanc, T., Drempetic, V., Pastor, M. J., Haddad, B., and Sanchez, M. (2009): "From solids to fluidized soils: diffuse failure mechanisms in geostructures with applications to fast catastrophic landslides". *Granular Matter.*

Pastor, M., Mira, P., and Fernandez Merodo, J. A. (2002): "Practical aspects of the finite element method". *Numerical Modelling in Geomechanics*, M. Pastor and C. Tamagnini, eds., Revue francaise de génie civil, Hermes Science Publications, 1147-1168.

Pastor, M., Quecedo, M., and Zienkiewicz, O. C. (1996): "A mixed displacement-pressure formulation for numerical analysis of plastic failure". *Computers & Structures,* 62(1), 13-23.

Pastor, M., and Zienkiewicz, O. C. (1986): "A generalized plasticity, hierarchical model for sand under monotonic and cyclic loading". 2nd International Symposium on Numerical Models in Geomechanics, G. N. Pande and W. F. Van Impe, eds., Ghent, Belgium, 131-150.

Pastor, M., Zienkiewicz, O. C., and Chan, A. H. C. (1990): "Generalized Plasticity and the Modelling of Soil Behaviour". *International Journal for Numerical and Analytical Methods in Geomechanics,* 14, 151-190.

Pastor, M., Zienkiewicz, O. C., and Leung, K. H. (1985): "Simple model for transient soil loading in earthquake analysis, II. Non-associative models for sands". *International Journal for Numerical and Analytical Methods in Geomechanics,* 9, 477-498.

Pastor, M., Zienkiewicz, O. C., Li, T., Xiaoqing, L., Fernandez Merodo, J. A., and Mira, P. (1999): "Modelización del comportamiento sísmico de geoestructuras". *Física de la Tierra,* 11, 175-201.

Pietruszczak, S. (1999): "On homogeneous and localized deformation in water-infiltrated soils". *International Journal of Damage Mechanics,* 8, 233-253.

Pöschel, T., Saluena, C., and Schwager, T. (2001): "Can we scale granular systems?". Powders & Grains'2001, Kishino, ed., Rotterdam, 2001, Balkema, 439-442.

Potts, D. M., and Zdravkovic, L. (1999): *Finite Element Analysis in Geotechnical Engineering: Theory*, Thomas Telford.

Poulos, H. G. (1971): "Behavior of laterally loaded piles: Part 1 - Single piles". *Journal of the Soil Mechanics and Foundations Division, ASCE,* 97(5), 711-731.

Poulos, H. G. (1982): "Single pile response to cyclic lateral load". *Journal of the Geotechnical Engineering Division ASCE,* 108(3), 355-375.

Poulos, H. G. (1988): *Marine geotechnics*, Unwin Hyman Ltd (Pub.).

Poulos, H. G., and Davis, E. H. (1980): *Pile Foundation Analysis and Design*, Rainbow Bridge Book Co.

Quell, P., Knops, M., Heinicke, M., Rettenmeier, A., Kühn, M., Rücker, W., Baessler, M., Rolfes, R., Haake, G., Hahn, B., Benesch, M., van Radecke, H., Finger, K., Neumann, T., and Herklotz, K. (2007): "Offshore Wind Energy Research in Germany - RAVE – Research at Alpha VEntus". *European Offshore Wind 2007 Conference & Exhibition*. December 4-6, 2007, Berlin, 1-10.

Rackwitz, F. (2003): "Numerische Untersuchungen zum Tragverhalten von Zugpfählen und Zugpfahlgruppen in Sand auf der Grundlage von Probebelastungen" *(Thesis)*, Veröffentlichungen des Grundbauinstitutes der Technischen Universität Berlin.

Rahman, M. S., Seed, H. B., and Booker, J. R. (1977): "Pore pressure development under offshore gravity structures". *Journal of the Geotechnical Engineering Division, ASCE,* 103(GT12), 1419-1436.

Randolph, M. F. (1981): "The response of flexible piles to lateral loading". *Géotechnique,* 31(2), 247-259.

Randolph, M. F. (2003): "Science and empiricism in pile foundation design". *Géotechnique,* 53(10), 847–875.

Randolph, M. F., and Carter, J. P. (1979): "The effect of pile permeability on the stress changes around a pile driven into clay". Proceedings of the 3rd International Conference on Numerical Methods in Geomechanics, Aachen, Germany, 1097-1105.

Randolph, M. F., Cassidy, M., Gourvenec, S., and Erbrich, C. (2005): "Challenges of offshore geotechnical engineering". Proceedings of the 16th International Conference on Soil Mechanics and Geotechnical Engineering, Millpress Rotterdam Netherlands, 123-176.

Rankine, W. (1857): "On the stability of loose earth". *Philosophical Transactions of the Royal Society of London,* 147.

Reese, L. C. (1977): "Laterally loaded piles: Program documentation". *Journal of the Geotechnical Engineering Division, ASCE,* 103(GT4), 287-305.

Reese, L. C., Cox, W. R., and Koop, F. D. (1974): "Analysis of laterally loaded piles in sand". Proceedings of the 6th Annual Offshore Technology Conference in Houston, Texas, 473-483.

Reese, L. C., and Matlock, H. (1956): "Non-dimensional solutions for laterally loaded piles with soil modulus assumed proportional to depth". Proceedings Eighth Texas Conference on Soil Mechanics and Foundation Engineering.

Reese, L. C., and Van Impe, W. F. (2001): *Single piles and pile groups under lateral loading*, A.A.Balkema Publishers, Rotterdam.

Remaud, D. (1999): "Pieux sous charges laterales: Etude experimentale de l'effet de groupe" *(Thesis)*, Ecole Centrale de Nantes.

Richter, T. (2009): "Geotechnische Spezialaufgaben bei der Gründung von Offshore-Anlagen. Was ist bekannt? Wo ist wissenschaftliches Neuland?". BAW-Kolloquium, Aktueller Stand und Herausforderungen der Geotechnik im Verkehrswasserbau, on September 24th, 2009 in Karlsruhe, Germany.

Richwien, W., Lesny, K., and Hinz, P. (2005): "Tragstruktur - Gründung". Jahresbericht GIGAWINDplus 2004, W. Zielke, ed., Universität Hannover, 20-32.

Rosquoët, F., Garnier, J., Thorel, L., and Canepa, Y. (2004): "Horizontal cyclic loading of piles installed in sand: study of pile head displacement and maximum bending moment". Proceedings of the International Conference on Cyclic Behaviour of Soils and Liquefaction Phenomena, Bochum, Germany, 363-368.

Rosquoët, F., Thorel, L., Garnier, J., and Canepa, Y. (2007): "Lateral cyclic loading of sand-installed piles". *Soils and Foundations,* 47(5), 821-832.

Rücker, W. (2007): "Offshore wind energy plants: Problems and possible solutions". Proceedings of the EVACES 2007 Conference in Porto, Portugal, 55-72.

Russo, G., and Viggiani, C. (2008): "Piles under horizontal load: An overview". Proceedings of the 2nd Internation Conference on Foundations, ICOF2008.

Sagaseta, C., Cuéllar, V., and Pastor, M. (1991): "Cyclic loading". Deformation of soils and displacements of structures. Proceedings 10th European Conference on Soil Mechanics and Foundation Engineering, Firenze, Italy, 981–999.

Sanavia, L., and Schrefler, B. A. (2002): "A finite element model for water saturated and partially saturated geomaterials". *Numerical Modelling in Geomechanics*, M. Pastor and C. Tamagnini, eds., Hermes Science Publications.

Savidis, S., Rackwitz, F., Richter, T., Röhner, J., and Schneider, N. (2004): "Verhalten von Pfählen in wassergesättigten Sanden unter zyklischen Horizontallasten". *Bauingenieur,* 79, 383-385.

Savidis, S., Rackwitz, F., and Tasan, H. E. (2007): "1g-Modellversuche mit zyklisch horizontal belasteten Einzelpfählen im wassergesättigten Sand". Pfahl-Symposium 2007, J. Stahlmann, ed., Braunschweig, Germany, 115-130.

Schenk, O., and Gärtner, K. (2004): "Solving unsymmetric sparse systems of linear equations with PARDISO". *Future Generation Computer Systems,* 20, 475–487.

Schenk, O., and Gärtner, K. (2009): "Parallel Sparse Direct and Multi-Recursive Iterative Linear Solvers PARDISO".

Schwarz, P. (2002): "Beitrag zum Tragverhalten von Verpresspfählen mit kleinem Durchmesser unter axialer zyklischer Belastung" *(Thesis)*, Technischen Universität München.

Sedran, G., Stolle, D. F. E., and Horvath, R. G. (2001): "An investigation of scaling and dimensional analysis of axially loaded piles". *Canadian Geotechnical Journal,* 38, 530-541.

Seed, H. B., Martin, P. P., and Lysmer, J. (1975): "The generation and dissipation of pore water pressures during soil liquefaction". *UCB/EERC-75/26*, Earthquake Engineering Research Center, University of California, Berkeley.

Seed, R. B., Cetin, K. O., Moss, R. E. S., Kammerer, A. M., Wu, J., Pestana, J. M., Riemer, M. F., Sancio, R. B., Bray, J. D., Kayen, R. E., and Faris, A. (2003): "Recent advances in soil liquefaction engineering: A unified and consistent framework". *Report no. EERC 2003-06*, Earthquake Engineering Research Center, College of Engineering, University of California, Berkeley.

Shen, C., Harder, L., Vrymoed, J., and Bennet, W. (1978): "Dynamic response of a sand under random loadings". Proceedings of ASCE Speciality Conference on Earthquake Engineering and Soil Dynamics, 853-863.

Shieh-Beygi, B., and Pietruszczak, S. (2008): "Numerical analysis of structural masonry: mesoscale approach". *Computers and Structures,* 86, 1958-1973.

Siddharthan, R. (1987): "Wave-induced displacements in seafloor sands". *International Journal for Numerical and Analytical Methods in Geomechanics,* 11, 155-170.

Simo, J., and Rifai, M. (1990): "A class of mixed assumed strain methods and the method of incompatible modes". *International Journal for Numerical Methods in Engineering,* 29, 1595-1638.

Skrikerud, P. E., and Bachmann, H. (1986): "Discrete crack modelling for dynamically loaded, unreinforced concrete structures". *Earthquake Engineering and Structural Dynamics,* 14(2), 297–315.

Sørensen, S. P. H., Ibsen, L. B., and Augustesen, A. H. (2010): "Effects of diameter on initial stiffness of p-y curves for large-diameter piles in sand". Numerical Methods in Geotechnical Engineering, NUMGE 2010, T. Benz and S. Nordal, eds., 907-912.

Stahlmann, J., Gattermann, J., and Kluge, K. (2007): "FINO 3 - Forschungsansätze für Offshore Windenergieanlagen". Proceedings of the Pfahl-Symposium 2007, in Braunschweig, Germany, J. Stahlmann, ed., Institut für Grundbau und Bodenmechanik der Technischen Universität Braunschweig, 207-223.

Stewart, H. E. (1986): "Permanent strains from cyclic variable-amplitude loadings". *Journal of Geotechnical Engineering,* 112(6), 646-660.

Stieß, M. (2009): "Ähnlichkeitslehre und Dimensionsanalyse". *Mechanische Verfahrenstechnik - Partikeltechnologie 1*, Springer, 97-104.

Swane, I. C. (1983): "The cyclic behaviour of laterally loaded piles" *(Thesis)*, University of Sydney.

Taiebat, H. A. (1999): "Three dimensional liquefaction analysis of offshore foundations" *(Thesis)*, University of Sidney.

Taiebat, H. A., and Carter, J. P. (2000): "A semi-empirical method for the liquefaction analysis of offshore foundations". *International Journal for Numerical and Analytical Methods in Geomechanics,* 24, 991-1011.

Tamagnini, C., Castellanza, R., and Nova, R. (2002): "Implicit integration of constitutive equations in computational plasticity". *Numerical Modelling in Geomechanics. Revue Française de Génie Civil (6)*, M. Pastor and C. Tamagnini, eds., Hermes Science Publications, 1051-1067.

Tamagnini, C., and Viggiani, G. (2002): "Constitutive modelling for rate-independent soils: a review". *Numerical Modelling in Geomechanics*, M. Pastor and C. Tamagnini, eds., Hermes Science Publications.

Tasan, H. E. (2011): "Zur Dimensionierung der Monopile-Gründungen von Offshore-Windenergieanlagen" *(Thesis)*, Technische Universität Berlin.

Tasan, H. E., Rackwitz, F., and Savidis, S. (2010a): "Behaviour of cyclic laterally loaded large diameter monopiles in saturated sand". Numerical Methods in Geotechnical Engineering, NUMGE 2010, T. Benz and S. Nordal, eds., Taylor & Francis Group, 889-894.

Tasan, H. E., Rackwitz, F., and Savidis, S. (2010b): "Porenwasserdruckakkumulation bei zyklisch horizontal belasteten Monopiles mit großen Durchmessern". *Bautechnik,* 87(8), 449-461.

Tatsuoka, F. (1972): "Shear tests in a triaxial apparatus. A fundamental research on the deformation of sand" *(Thesis)*, University of Tokyo (in Japanese).

Tatsuoka, F., and Ishihara, K. (1974): "Drained Deformation of Sand Under Cyclic Stresses Reversing Direction". *Soils and Foundations - Japanese Society of Soil Mechanics and Foundation Engineering,* 14(3), 51 - 65.

Taylor, R. L., Beresford, P. J., and Wilson, E. L. (1976): "A non-conforming element for stress analysis". *International Journal for Numerical Methods in Engineering,* 10, 1211–1219.

Temizer, I. (2004): "Continuum theory of mixtures". *ME 285 PROJECT*, Mechanical Engineering Department, University of Califonia, Berkeley.

Terzaghi, K. (1943): *Theoretical Soil Mechanics*, John Wiley & Sons, Inc. New York, London.

Terzaghi, K. (1955): "Evaluation of coefficients of subgrade reaction". *Géotechnique,* 5(4), 297-326.

Titze, E. (1970): "Über den seitlichen Bodenwiderstand bei Pfahlgründungen". *Bauingenieur-Praxis,* (77).

Tobita, Y. (1996): "Importance of incremental nonlinearity in the deformation of granular materials". N. A. Fleck and A. C. E. Cocks, eds., *IUTAM Symposium on Mechanics of Granular and Porous Materials*. 139–150.

Triantafyllidis, T. (2003): "Bodenverflüssigung infolge zyklischer Belastung". *GEOLEX,* 2(2), 5-20.

Truesdell, C. (1957): "Sulle basi della termomeccanica". *Rendiconti della Classe di Scienze Fisiche, Accademia Nazionale dei Lincei,* 22, 33–38.

Tsotsos, S., Georgiadis, M., and Damaskinidou, A. (1989): "Numerical analysis of liquefaction potential of partially drained seafloors". *Coastal Engineering,* 13, 117-128.

Turner, J. P., Kulhawy, F. H., and Charlie, W. A. (1987): "Review of load tests on deep foundations subjected to repeated loading". Geotechnical Engineering Group, Cornell University.

Tzamtzis, A. D., and Asteris, P. G. (2004): "FE analysis of complex discontinuous and jointed structural systems (Part 1: Presentation of the method - A state-of-the-art review)". *Electronic Journal of Structural Engineering,* 1, 75-92.

Verdeyen, J., and Gillet, J. (1968): "Évaluation des valeurs du coefficient de réaction horizontal des sols". *Revue C Genie Civil,* 4(10), 303-331.

Verdure, L., Garnier, J., and Levacher, D. (2003): "Lateral cyclic loading of single piles in sand". *International Journal of Physical Modelling in Geotechnics,* 3, 17-28.

Walz, B. (2006): "Der 1g-Modellversuch in der Bodenmechanik - Verfahren und Anwendung". Vortrag zum 2. Hans Lorenz Symposium, Grundbauinstitut der Technische Universität Berlin, 13-26.

Wang, Z. (2000): "Behaviour of soils and foundation structures under cyclic loads" *(Thesis)*, Mitteilungen aus dem Fachgebiet Grundbau und Bodenmechanik der Universität Duisburg-Essen, Heft 25.

Wellmann Jelic, A. (2007): "Paralleles Simulationskonzept für zeitabhängige Zuverlässigkeitsanalysen bei stochastischen Ermüdungsprozessen" *(Thesis)*, Ruhr-Universität Bochum.

White, D. J. (2005): "A general framework for shaft resistance on displacement piles in sand". Frontiers in Offshore Geotechnics: ISFOG 2005, S. Gourvenec and M. Cassidy, eds., 697-703.

White, D. J., and Bolton, M. D. (2004): "Displacement and strain paths during plane-strain model pile installation in sand". *Géotechnique,* 54(6), 375-397.

White, D. J., and Lehane, B. M. (2004): "Friction fatigue on displacement piles in sand". *Géotechnique,* 54(10), 645-658.

White, D. J., Take, W. A., and Bolton, M. D. (2003): "Soil deformation measurement using particle image velocimetry (PIV) and photogrammetry". *Géotechnique,* 53(7), 619-631.

Wichtmann, T. (2005): "Explicit accumulation model for non-cohesive soils under cyclic loading" *(Thesis)*, Fakultät für Bauingenieurwesen der Ruhr-Universität Bochum.

Wichtmann, T., Niemunis, A., and Triantafyllidis, T. (2008): "Predictions of long-term deformations for monopile foundations of offshore wind power plants". Geotechnics in Maritime Engineering. 11th Baltic Sea Geotechnical Conference, Gdansk, Poland, 785-792.

Wichtmann, T., and Triantafyllidis, T. (2005): "Dynamische Steifigkeit und Dämpfung von Sand bei kleinen Dehnungen". *Bautechnik,* 82(4), 236-246.

Wiemann, J. (2007): "Bemessungsverfahren für horizontal belastete Pfähle. Untersuchungen zur Anwendbarkeit der p-y Methode" *(Thesis)*, Mitteilungen aus dem Fachgebiet Grundbau und Bodenmechanik der Universität Duisburg-Essen.

Wilson, E. L., Taylor, R. L., Doherty, W. P., and Ghaboussi, J. (1973): "Incompatible displacement models". *Numerical and Computer Methods in Structural Mechanics*, S. J. Fenves, N. Perrone, A. R. Robinson, and W. C. Schnobrich, eds., Academic Press, New York, 43-57.

Wilson, S. D., and Hilts, D. E. (1967): "How to determine lateral load capacity of piles". *Wood Preserving News,* (July), 1-5.

Winkler, E. (1867): *Die Lehre von der Elasticitaet und Festigkeit mit besonderer Rücksicht auf ihre Anwendung in der Technik für polytechnische Schulen, Bauakademien, Ingenieure, Maschinenbauer, Architekten, etc*, Verlag von H. Domenicus, Prag.

Winter, H., and Hettler, A. (1983): "Ähnlichkeit bei Randwertproblemen und ihre Anwendung in der Sandmechanik". *Ingenieur-Archiv,* 53, 27-39.

Wood, W. L. (1990): *Practical time-stepping schemes (Oxford Applied Mathematics and Computing Science Series)*, Clarendon Press, Oxford.

Wriggers, P., and Imhof, M. (1993): "On the treatment of nonlinear unilateral contact problems". *Archive of Applied Mechanics,* 63, 116-129.

Wriggers, P., and Simo, J. C. (1985): "A note on tangent stiffness for fully nonlinear contact problems". *Communications in Applied Numerical Methods,* 1, 199-203.

Wu, W., Bauer, E., and Kolymbas, D. (1996): "Hypoplastic constitutive model with critical state for granuar materials". *Mechanics of Materials,* 23, 45-69.

Yamada, Y., and Ishihara, K. (1982): "Yielding of loose sand in three-dimensional stress conditions". *Soils and Foundations,* 22(3), 15-31.

Yang, K., and Liang, R. (2007): "Methods for deriving p-y curves from instrumented lateral load tests". *ASTM Geotechnical Testing Journal,* 30(1), 31-38.

Youd, T. L. (1972): "Compaction of Sands by Repeated Shear Straining". *Journal of the Soil Mechanics and Foundations Division, ASCE,* 98(7), 709-725.

Zavarise, G., Wriggers, P., and Schrefler, B. A. (1998): "A method for solving contact problems". *International Journal for Numerical Methods in Engineering,* 42, 473-498.

Zavarise, G., Wriggers, P., Stein, E., and Schrefler, B. A. (1992): "Real contact mechanisms and finite element formulation - a coupled thermomechanical approach". *International Journal for Numerical Methods in Engineering,* 35, 767-785.

Zienkiewicz, C., Chan, A. H. C., Pastor, M., Schrefler, B. A., and Shiomi, T. (1999): *Computational Geomechanics with Special Reference to Earthquake Engineering*, John Wiley & Sons.

Zienkiewicz, O. C., Best, B., Dullage, C., and Stagg, K. G. (1970): "Analysis of non Linear Problems in Rock Mechanics with Particular Reference to Jointed Rock Systems". Second Congress of the International Society for Rock Mechanics, Belgrad, Yugoslavia, 501-509.

Zienkiewicz, O. C., and Bettess, P. (1982): "Soils and other saturated media under transient, dynamic conditions: General formulation and validity of various simplifying assumptions". *Soil Mechanics - Transient and Cyclic Loads*, G. N. Pande and O. C. Zienkiewicz, eds., Wiley, 1-16.

Zienkiewicz, O. C., Chang, C. T., and Bettess, P. (1980): "Drained, undrained, consolidating dynamic behaviour assumptions in soils". *Géotechnique,* 30, 385-395.

Zienkiewicz, O. C., and Mroz, Z. (1984): "Generalized plasticity formulation and applications to geomechanics". *Mechanics of engineering materials*, C. S. Desai and R. H. Gallagher, eds., Wiley, 655-679.

Zienkiewicz, O. C., and Pande, G. N. (1977): "Some useful forms of isotropic yield surfaces for soil and rock mechanics". *Finite Elements in Geomechanics*, G. Gudehus, ed., John Wiley & Sons, 171-190.

Zienkiewicz, O. C., and Shiomi, T. (1984): "Dynamic behaviour of saturated porous media: the generalized Biot formulation and its numerical solution". *International Journal for Numerical and Analytical Methods in Geomechanics,* 8, 71-96.

Zienkiewicz, O. C., and Taylor, R. L. (2000): *The Finite Element Method*, Butterworth-Heinemann.

Zienkiewicz, O. C., Wood, W. L., and Taylor, R. L. (1990a): "An alternative single-step algorithm for dynamic problems". *Earthquake Engineering and Structural Dynamics,* 8(1), 31-40.

Zienkiewicz, O. C., Xie, Y. M., Schrefler, B. A., Ledesma, A., and Bicanic, N. (1990b): "Static and dynamic behaviour of soils: a rational approach to quantitative solutions. II. Semi-saturated problems". *Proceedings of the Royal Society of London. Series A. Mathematical and Physical Sciences,* 429, 285-309.

A APPENDIX

A.1 Weak form of the u-p_W formulation. Gauss's Divergence Theorem

Starting from the weighted residual equations shown in (3.40) and (3.41), which read

$$\int_\Omega \delta u\left(\nabla\cdot(\sigma' - m p_W) + \rho b - \rho\ddot{u}\right)d\Omega = 0 \tag{a.1}$$

$$\int_\Omega \delta p_W\left(m\nabla\cdot\dot{u} + \nabla\cdot\left(k\left(\rho_W b - \nabla p_W\right)\right) + \frac{\dot{p}_W}{Q^*}\right)d\Omega = 0 \tag{a.2}$$

the integrals can be decomposed in their single addends as

$$\int_\Omega \delta u\nabla\cdot\sigma' d\Omega - \int_\Omega \delta u\nabla m p_W d\Omega + \int_\Omega \delta u\rho b d\Omega - \int_\Omega \delta u\rho\ddot{u}d\Omega = 0 \tag{a.3}$$

$$\int_\Omega \delta p_W m\nabla\cdot\dot{u}d\Omega + \int_\Omega \delta p_W\nabla\cdot(k\rho_W b)d\Omega - \int_\Omega \delta p_W\nabla\cdot(k\nabla p_W)d\Omega + \int_\Omega \delta p_W\frac{\dot{p}_W}{Q^*}d\Omega = 0 \tag{a.4}$$

Now the terms containing the divergence operator can be integrated by parts, which yields

$$\begin{aligned}&\int_\Omega \nabla\cdot(\delta u\sigma')d\Omega - \int_\Omega \sigma'\nabla\cdot\delta u d\Omega - \int_\Omega \nabla\cdot(\delta u m p_W)d\Omega + \int_\Omega m p_W\nabla\cdot\delta u d\Omega + \\ &+ \int_\Omega \delta u\rho b d\Omega - \int_\Omega \delta u\rho\ddot{u}d\Omega = 0\end{aligned} \tag{a.5}$$

$$\begin{aligned}&\int_\Omega \delta p_W m\nabla\cdot\dot{u}d\Omega + \int_\Omega \nabla\cdot(\delta p_W k\rho_W b)d\Omega - \int_\Omega k\rho_W b\nabla\delta p_W d\Omega - \\ &- \int_\Omega \nabla\cdot(\delta p_W k\nabla p_W)d\Omega + \int_\Omega k\nabla p_W\nabla\delta p_W d\Omega + \int_\Omega \delta p_W\frac{\dot{p}_W}{Q^*}d\Omega = 0\end{aligned} \tag{a.6}$$

At this point, it is useful to introduce the Gauss's divergence theorem (also known as Green's theorem, or in its more general form, Stokes' theorem), which states that the volume integral of the divergence of a vector field over a volume is equal to the outward flux of the field through the closed surface that limits the volume. Mathematically, this is expressed with the following equivalence

$$\int_\Omega (\nabla\cdot F)d\Omega = \oint_\Gamma F\cdot n d\Gamma \tag{a.7}$$

Making use of this theorem, the equations (a.5) and (a.6) can be transformed into

$$\int_\Gamma (\delta u \sigma')nd\Gamma - \int_\Omega \sigma' \nabla \cdot \delta u d\Omega - \int_\Gamma (\delta u m p_W)nd\Gamma + \int_\Omega m p_W \nabla \cdot \delta u d\Omega + \\ + \int_\Omega \delta u \rho b d\Omega - \int_\Omega \delta u \rho \ddot{u} d\Omega = 0 \tag{a.8}$$

$$\int_\Omega \delta p_W m \nabla \cdot \dot{u} d\Omega + \int_\Gamma (\delta p_W k \rho_W b)nd\Gamma - \int_\Omega k \rho_W b \nabla \delta p_W d\Omega - \\ - \int_\Gamma (\delta p_W k \nabla p_W)nd\Gamma + \int_\Omega k \nabla p_W \nabla \delta p_W d\Omega + \int_\Omega \delta p_W \frac{\dot{p}_W}{Q^*} d\Omega = 0 \tag{a.9}$$

and now recalling the boundary conditions defined for this problem as

$$t = \sigma' n - p_W n = \tilde{t} \qquad \text{in } \Gamma_t \tag{a.10}$$

$$q = k(\rho_W b - \nabla p_W)n = \tilde{q} \qquad \text{in } \Gamma_q \tag{a.11}$$

it is possible to group and rearrange the terms, producing the following expressions

$$\int_\Omega \sigma' \nabla \cdot \delta u d\Omega - \int_\Omega m p_W \nabla \cdot \delta u d\Omega + \int_\Omega \delta u \rho \ddot{u} d\Omega = \int_\Omega \delta u \rho b d\Omega + \int_\Gamma \delta u t d\Gamma \tag{a.12}$$

$$\int_\Omega \delta p_W m \nabla \cdot \dot{u} d\Omega + \int_\Omega k \nabla p_W \nabla \delta p_W d\Omega + \int_\Omega \delta p_W \frac{\dot{p}_W}{Q^*} d\Omega = \\ = \int_\Omega k \rho_W b \nabla \delta p_W d\Omega - \int_\Gamma \delta p_W q d\Gamma \tag{a.13}$$

And finally, considering symmetry of the terms and transposing, the equations can be recast as

$$\int_\Omega \delta u^T \nabla^T \cdot \sigma' d\Omega - \int_\Omega \delta u^T \nabla^T m p_W d\Omega + \int_\Omega \delta u^T \rho \ddot{u} d\Omega = \\ = \int_\Omega \delta u^T \rho b d\Omega + \int_{\Gamma_t} \delta u^T t d\Gamma_t \tag{a.14}$$

$$\int_\Omega \delta p_W m^T \nabla \cdot \dot{u} d\Omega + \int_\Omega \nabla^T \delta p_W k \nabla p_W d\Omega + \int_\Omega \delta p_W \frac{\dot{p}_W}{Q^*} d\Omega = \\ = \int_\Omega \nabla^T \delta p_W k \rho_W b d\Omega - \int_{\Gamma_q} \delta p_W q d\Gamma_q \tag{a.15}$$

which are the expressions that have been used in the section 3.1.2.

A.2 Convergence of the non-linear algorithm. Tolerance criteria

As shown in Section 3.1.2, the set of non-linear algebraic equations given by (3.72) may be solved by means of a linear approximation of the residual using the Newton-Raphson algorithm. This way, a linear system of equations will arise in the following form

$$K \cdot \Delta u = Res \tag{a.16}$$

where $\boldsymbol{K}$ is the coefficient matrix (the assembled Jacobian), $\boldsymbol{\Delta u}$ is a vector containing the corrections to the variables and $\boldsymbol{Res}$ is the vector of out-of-balance forces (i.e. the residual), expressed as

$$Res = f - f^i \tag{a.17}$$

However, the variables' updates obtained from the solution of the linearized system of equations will, in general, not make the residuals zero, and further iterative corrections will be required. Such iterative process can be described as

$$K^i \cdot \Delta u^i = f - f^i \tag{a.18}$$

$$u^{i+1} = u^i + \Delta u^i \tag{a.19}$$

By using the *classical* Newton-Raphson method, the assembled Jacobian matrix is recalculated for every single iteration and the norm of the residual will in principle converge at a quadratic rate [Zienkiewicz & Taylor, 2000]. This means that if the residual ratio is in the order of 10^{-p} for a given iteration, then the following iteration will reduce the residual ratio to an order of 10^{-2p}. This is a very powerful feature, but it comes at the price of having to update the assembled Jacobian in every iteration.

Since the computation, assembly and factorization (in the case of direct Gaussian solvers) of the Jacobian matrix is normally the most expensive part of a FE analysis, several variations of the Newton method have been proposed (a good review is given, for instance, in [Felippa, 2001]). A first variation of the method is the so-called Modified Newton-Raphson, where the Jacobian is calculated only at the beginning of the increment or just with a low frequency (once every several iterations). This has the advantage that the factorization of the Jacobian can be stored and reused for several iterations, which can save a lot of computational effort. However, it has the inconvenient that the convergence rate is no longer quadratic and in general may require many more ite-

rations than the classical Newton-Raphson algorithm. Further procedures, as the Quasi-Newton methods, have been developed in order to improve the convergence rate and have been described, for instance, in [Zienkiewicz & Taylor, 2000] and [Felippa, 2001].

In any case, for most of the iterative processes the numerical solution is only approximately achieved and some tolerance criteria will be required in order to finish the iteration. The criteria adopted in the FE program GeHoMadrid are based on residual *ratios* instead of using absolute values of the error. This way, a computed solution will be accepted whenever *both* of the following inequalities are satisfied

$$\frac{\left\| f - f^{i} \right\|}{\left\| f \right\|} < Tol_F \quad \text{and} \quad \frac{max\left(f - f^{i} \right)}{max\left(f \right)} < Tol_F \tag{a.20}$$

Additionally, a convergence criterion is also enforced for the iterative increments of the variables. This ensures that, once the mechanical equilibrium is achieved (i.e. the "force residual" is small enough), the variables remain stable.

$$\frac{\left\| \Delta u^{i} \right\|}{\left\| u^{i+1} \right\|} < Tol_U \quad \text{and} \quad \frac{max\left(\Delta u^{i} \right)}{max\left(u^{i+1} \right)} < Tol_U \tag{a.21}$$

Now the key issue is to choose appropriate tolerance levels $\boldsymbol{Tol_F}$ and $\boldsymbol{Tol_U}$ that can be achieved in a reasonable amount of iterations and still keep the error level from becoming significant. This choice will in general be problem-dependent, but a reasonable value may be in the order of 10^{-6}. Zienkiewicz and Taylor recommend a tolerance of half the machine precision whenever a full Newton scheme is used, since quadratic convergence would imply that the next residual would reach the full precision [Zienkiewicz & Taylor, 2000]. On the other hand, the modified or the quasi-Newton methods do require many more iterations to achieve high precision, and for these cases a much higher tolerance is often used (up to 0.01, according to Zienkiewicz and Taylor). This, however, may lead to instability of the solution if the problem involves a large number of steps, since the error accumulates with every step.

For the present work, in which every simulation required a large number of time steps and a considerable amount of iterations per time step, a tolerance threshold of 10^{-7} has been usually employed. However, for the analysis of the storm event shown in Section 3.7, a much lower tolerance (10^{-9}) was required due to the large time span (600 seconds) and the consequently high number of time steps to be computed (around 20,000 time steps).

A.3 Formulation of the saturated consolidation case

Starting from the general dynamic formulation shown in equations (3.51) and (3.52), the particular case of the saturated consolidation may be obtained by neglecting the terms associated to accelerations of the solid skeleton, which yields

$$\int_{\Omega} B^T \sigma' d\Omega - Q\overline{p}_W = f_u \tag{a.22}$$

$$Q^T \dot{\overline{u}} + H\overline{p}_W + C\dot{\overline{p}}_W = f_p \tag{a.23}$$

and considering the fulfilment of these equations in the time station ***N+1***, they can be expressed as

$$\int_{\Omega} B^T \sigma'_{N+1} d\Omega - Q\overline{p}_{N+1} = f^U{}_{N+1} \tag{a.24}$$

$$Q^T \dot{\overline{u}}_{N+1} + H\overline{p}_{N+1} + C\dot{\overline{p}}_{N+1} = f^P{}_{N+1} \tag{a.25}$$

Now the time discretisation can be introduced again by means of a Newmark recurrence scheme, but for this particular case it is possible to employ the GN11 (i.e., the first order scheme) for both variables $\boldsymbol{u}$ and $\boldsymbol{p_w}$. This way the variables at consecutive time stations are related as

$$\overline{u}_{N+1} = \overline{u}_N + \Delta t \dot{\overline{u}}_N + \beta \Delta t \Delta \dot{\overline{u}}_N \tag{a.26}$$

$$\overline{p}_{N+1} = \overline{p}_N + \Delta t \dot{\overline{p}}_N + \theta \Delta t \Delta \dot{\overline{p}}_N \tag{a.27}$$

where

$$\Delta \dot{\overline{u}}_N = \dot{\overline{u}}_{N+1} - \dot{\overline{u}}_N \tag{a.28}$$

$$\Delta \dot{\overline{p}}_N = \dot{\overline{p}}_{N+1} - \dot{\overline{p}}_N \tag{a.29}$$

Here as well, the parameters $\boldsymbol{\beta}$, and $\boldsymbol{\theta}$ of the Newmark scheme must comply with the restrictions for numerical stability

$$\beta \geq \frac{1}{2} \quad \text{and} \quad \theta \geq \frac{1}{2} \tag{a.30}$$

And now, introducing the expressions (a.26) through (a.29) into (a.24) and (a.25), the system of non-linear equations arises [Mira, 2001]

$$G^{U}{}_{N+1} = \int_{\Omega} B^{T} \sigma'_{N+1} d\Omega - Q\theta\Delta t\Delta\dot{\bar{p}}_{N} - F^{U}{}_{N+1} = 0 \tag{a.31}$$

$$G^{P}{}_{N+1} = Q^{T}\Delta\dot{\bar{u}}_{N} + H\theta\Delta t\Delta\dot{\bar{p}}_{N} + C\Delta\dot{\bar{p}}_{N} - F^{P}{}_{N+1} = 0 \tag{a.32}$$

where now

$$F^{U}{}_{N+1} = f^{U}{}_{N+1} + Q\left(\bar{p}_{N} + \Delta t\dot{\bar{p}}_{N}\right) \tag{a.33}$$

$$F^{P}{}_{N+1} = f^{P}{}_{N+1} - Q^{T}\dot{\bar{u}}_{N} - H\left(\bar{p}_{N} + \Delta t\dot{\bar{p}}_{N}\right) - C\dot{\bar{p}}_{N} \tag{a.34}$$

Employing the Newton-Raphson technique, the non-linear system of equations is firstly expressed in the following form

$$G(x) = 0 \tag{a.35}$$

where in this case

$$x = \begin{Bmatrix} \Delta\dot{\bar{u}} \\ \Delta\dot{\bar{p}} \end{Bmatrix} \quad \text{and} \quad G = \begin{Bmatrix} G^{U} \\ G^{P} \end{Bmatrix} \tag{a.36}$$

And now, taking the Taylor series of equation (a.35) and disregarding the terms of second and higher order, the system is formulated as

$$G(x_i) + \frac{\partial G}{\partial x}_{x=x_i} dx_i = 0 \tag{a.37}$$

where the first term can be taken to the right-hand side, producing

$$J dx_i = -G(x_i) \tag{a.38}$$

where $\boldsymbol{J}$ is the Jacobian matrix, defined in this case as

$$J = \begin{bmatrix} \partial G^{U} / \partial\Delta\dot{\bar{u}} & \partial G^{U} / \partial\Delta\dot{\bar{p}} \\ \partial G^{P} / \partial\Delta\dot{\bar{u}} & \partial G^{P} / \partial\Delta\dot{\bar{p}} \end{bmatrix} \tag{a.39}$$

This matrix may now be approximated as

$$J \approx \begin{bmatrix} K_{T}\beta\Delta t & -Q\theta\Delta t \\ Q^{T} & H\theta\Delta t + C \end{bmatrix} \tag{a.40}$$

where the tangent matrix $\boldsymbol{K_T}$ is again the standard stiffness matrix, defined as

$$K_{T} = \int_{\Omega} B^{T} D^{EP} B d\Omega \tag{a.41}$$

And finally, introducing (a.40) back into (a.38), the system of equations is written as

$$\begin{bmatrix} K_T \beta \Delta t & -Q\theta\Delta t \\ Q^T & H\theta\Delta t + C \end{bmatrix} \begin{Bmatrix} d(\Delta \dot{\bar{u}}_N) \\ d(\Delta \dot{\bar{p}}_N) \end{Bmatrix} = -\begin{Bmatrix} G^U \\ G^P \end{Bmatrix} \tag{a.42}$$

A.4 Definitions of stress and strain invariants

The stress state in an isotropic material can be represented by the stress invariant scalars $\boldsymbol{p}$, $\boldsymbol{q}$ and $\boldsymbol{\theta}$, which are often referred to as mean confining stress, deviatoric stress and Lode's angle, respectively, and using the conventional notation of soil mechanics are defined as:

$$p = -\frac{1}{3} I_1 \tag{a.43}$$

$$q = \sqrt{3 J_2} \tag{a.44}$$

$$\theta = -\frac{1}{3} sin\left(\frac{3\sqrt{3}}{2} \frac{J_3}{J_2^{3/2}} \right)^{1/2} \tag{a.45}$$

where $\boldsymbol{I_1}$ is the first invariant of the stress tensor and $\boldsymbol{J_2}$ and $\boldsymbol{J_3}$ are the second and third invariants of the deviatoric stress tensor respectively, which in turn are defined as

$$I_1 = \sigma_{ii} = \sigma_{xx} + \sigma_{yy} + \sigma_{zz} = \sigma_1 + \sigma_2 + \sigma_3 \tag{a.46}$$

$$J_2 = \frac{1}{2} tr\left(s^2\right) = \frac{1}{2}\left(s_{ij} s_{ji}\right) = \frac{1}{2}\left(s_1^{\,2} + s_2^{\,2} + s_3^{\,2}\right) \tag{a.47}$$

$$J_3 = \frac{1}{3} tr\left(s^3\right) = \frac{1}{3}\left(s_{ij} s_{jk} s_{ki}\right) = s_1 s_2 s_3 \tag{a.48}$$

and the deviatoric stress tensor $\boldsymbol{s}$ is defined as

$$s = \sigma - \frac{1}{3} I_1 I \tag{a.49}$$

being $\boldsymbol{I}$ the unitary second order tensor or Kronecker's delta.

Their work-conjugated strain invariants can be defined incrementally as

$$d\varepsilon_V = d\varepsilon_{ii} \tag{a.50}$$

$$d\varepsilon_S = \frac{2}{3} tr\left(de^2\right) = \frac{2}{3} de_{ij} de_{ji} \tag{a.51}$$

where the deviatoric strain tensor $\boldsymbol{e}$ is defined as

$$de = d\varepsilon - \frac{1}{3} d\varepsilon_V I \tag{a.52}$$

In the particular case of triaxial conditions, where the second and third principal stresses σ_2 and σ_3 are identical, the invariants take the following simplified form:

$$p = -\frac{1}{3}\left(\sigma_1 + 2\sigma_3\right) \tag{a.53}$$

$$q = \sigma_1 - \sigma_3 \tag{a.54}$$

$$d\varepsilon_V = d\varepsilon_1 + 2d\varepsilon_3 \tag{a.55}$$

$$d\varepsilon_S = \frac{2}{3}\left(d\varepsilon_1 - d\varepsilon_3\right) \tag{a.56}$$

A.5 Estimation of design loads for an offshore turbine

In general, the main load components to be taken into account for the structural assessment of the wind turbine's foundation are the turbine's own weight and those produced by the wind and wave action. Further loads, as for instance those originating from sea currents, sea ice, earthquake motion, operational loads or a boat impact, may play a significant role depending on the turbine's design and the specific site location, and can be estimated on the basis of the usual offshore guidelines (e.g. [GL WIND, 2005; DNV, 2004; API, 2007; ISO, 2007]).

Aerodynamic loads. The flow of air and its interaction with the wind turbine produces in general both quasi-static and dynamic loads on the structure that can be collectively termed as aerodynamic loads. They are conditioned by the design parameters (e.g. the aerodynamic shape of the blades, the rotational speed of the rotor, the turbulence generation, etc.) as well as by the wind characteristics (average wind speed at hub height, speed distribution with height, air density, etc.), which are stochastic by nature.

Additionally, there are a number of factors that may have a relevant influence on the wind loads, as for instance the wind field perturbations caused by the structure itself (wake and upwind effects), stall and aeroelastic effects, possible flow asymmetries or the dynamic response when the turbine is at standstill conditions under strong wind, and, therefore, their importance should also be assessed during design [GL WIND, 2005].

The main lines of the calculation process for the quasi-static wind loads may be summarized as follows:

- Determination of the temporal statistics for the wind speed at the wind-farm site, which can be approximated by means of a suitable distribution, typically the Weibull distribution (see for instance [Mittendorf, 2006]).
- Then, the wind speed at a given height (usually 10 m) is calculated for the extreme event, for instance the strongest wind gust (3 seconds in duration) with a return period of 50 years.
- The maximum wind speed for service conditions is defined by the rotor design (the cut-off speed above which the blades are rotated in order to offer minimum resistance to wind flow).

- Calculation of the wind-speed distribution with height, for instance by means of the Hellmann distribution.
- The quasi-static pressure of the flowing wind upon the structure at every height can be then estimated through the Bernoulli equation.
- The integration of the pressure over the structure, considering the exposed surfaces, the angle of attack and the aerodynamic form coefficients, provides finally the total horizontal loads and overturning moments.

On the other hand, the aerodynamic loads acting on the rotor itself (thrust, drag and lift forces) are usually computed combining the so-called Blade Element Momentum Theory (BEM) and a vortex theory for small perturbations [Hillmer *et al.*, 2007], or by means of three-dimensional CFD codes. A comparison of different calculation programs is given, for instance, in [Buhl & Manjock, 2006].

Hydrodynamic loads. In addition to the drag and inertia forces exerted by the passing waves on the offshore structure, further loads, such as those caused by the sea currents, by the breaking waves or by the wave-slamming (impact) effects, need to be considered. They can all be loosely termed as hydrodynamic loads, and depend mainly on the kinematics of the waves, the density and depth of the water and on the shape of the support structure [GL WIND, 2005].

The calculation process for the single wave loads may be roughly sketched as follows:

- Upon consideration of the local site statistics of the sea state parameters (wave height and period), the maximum wave height and corresponding period are determined for both the extreme (50 year return period) and service (1 year return period) storm conditions. A first approximation may also be obtained from suitable charts and tables in the offshore guidelines (e.g. in [DNV, 2004]) or by means of empirical formulas relating the wind velocity to the significant wave height and period, such as the Pierson-Moskowitz or JONSWAP spectral formulations [Mittendorf, 2006].
- Then, the "design wave" kinematics (wave length and water orbital velocities and accelerations) are defined at every depth by means of a suitable wave theory (for instance, Airy's Linear Wave Theory for deep waters).
- The distributed drag and inertia forces per unit length of submerged structure can be then estimated by introducing the water particle velocities and accelerations into the Morison equation. This equation also requires the provision of the hydrodynamic

coefficients, which may be obtained from the literature and mainly depend on the Reynolds and Keulegan-Carpenter numbers as well as on the surface roughness of the structure (see for instance [GL WIND, 2005], [Mittendorf, 2006] or [Hildebrandt *et al.*, 2009]).

- The resulting lateral loads and overturning moments can be computed then by integration of the distributed forces along the length of the supporting structure that is exposed to the action of the waves.

Considerations for cyclic loading. The consideration of a single wave or wind gust cannot possibly represent the loading conditions of the offshore wind turbine, since the sea states and wind conditions are irregular and stochastic in nature, and the structure will be subject to billions of load cycles of different magnitude during its lifetime.

For the assessment of the turbine's response to extreme short-time events, a transient calculation can be performed by adopting a suitable load history time signal of a certain length (for instance, 600 seconds). Such time signal can in principle be derived by means of an inverse Fourier transform of a wave spectrum (e.g. the JONSWAP spectrum) defined by a significant wave height and peak period (see for instance [Kohlmeier *et al.*, 2007] or [Boccotti, 2000]) or be directly based on measured data of wind speed and sea water level. However, in order to assess the performance of the structure during its design life, it is necessary to extrapolate the short-time data in some suitable way that provides the magnitude and occurrence of both the large cycles in low numbers (i.e. the extreme events) as well as the lower cycles in large numbers (relevant for fatigue analysis where appropriate).

When extrapolating a given time "block" signal, a first and simple option would be to repeat that very same block a number of times (say, one thousand times) so that it covers the whole time span under consideration. However, such approach does not permit any cycles other than those already observed in the given block, and certainly not all the possible cycles [Johannesson & Thomas, 2002]. This kind of "repetitive" extrapolation is characterised by a load spectrum with a horizontal part in the range of low number of cycles and usually underestimates the value of the highest single event.

In order to overcome this limitation, the generated time signal composed of N identical time blocks can be modified by randomly changing the measured peak and trough values according to an extreme value theory (e.g. the Peak Over Threshold, POT, approach) [Johannesson, 2005]. This way, the load spectrum is also extrapolated in the large amplitude area and an estimation of

the single highest load "outside" the measured data can be obtained. This is illustrated in Figures A.1-a and A.2.

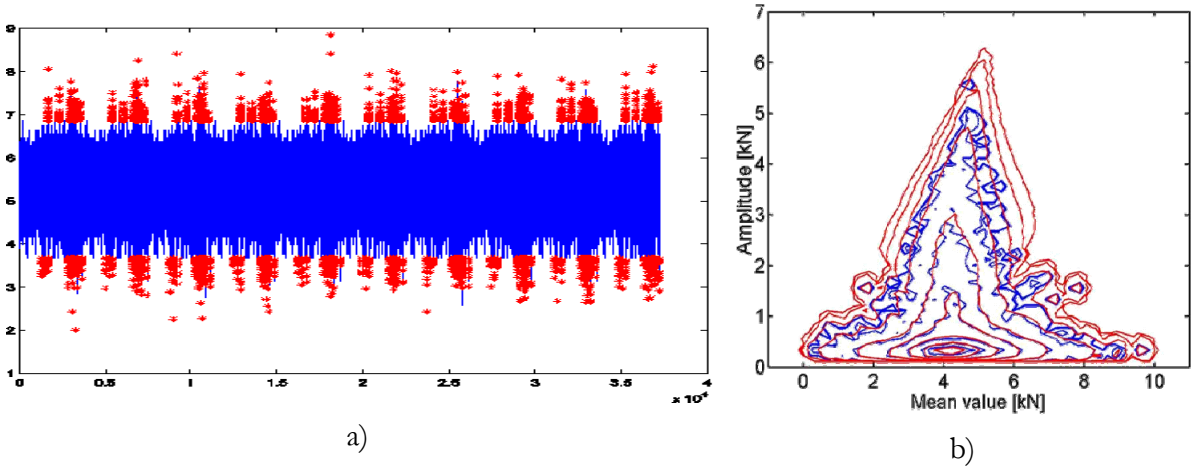

a) b)

Figure A.1 Extrapolation of load data (in blue colour, the measured data, and in red the extrapolation). a) 10-fold POT extrapolation of a train load time signal. b) Rainflow Matrix extrapolation with isolines of level up-crossing intensity. Extracted from [Johannesson, 2005].

An alternative approach for the extrapolation may be based on the Rainflow counting procedure proposed by Rychlik (e.g. in [Lindgren & Rychlik, 1987]), where the load time signal is filtered and the cycles are classified according to their amplitude and occurrence as well as on their average values. In this respect, Johannesson and Thomas propose to "expand" (or extrapolate) the shape of the Rainflow matrix to a certain "limiting shape", which would be approximated to an "extreme value" rainflow matrix in the areas of the large cycles and a "smoothed" rainflow matrix in the areas of the low intensity cycles [Johannesson & Thomas, 2002]. Such procedure is illustrated in Figure A.1-b, while its resulting load spectrum is also shown in Figure A.2.

This way, the extrapolated load spectrum provides the highest wave for an "extreme load case" calculation and can also be used for long-term fatigue analysis (if appropriate), usually by means of a Wöhler-type curve and the Miner-Palmgren's damage linear accumulation method.

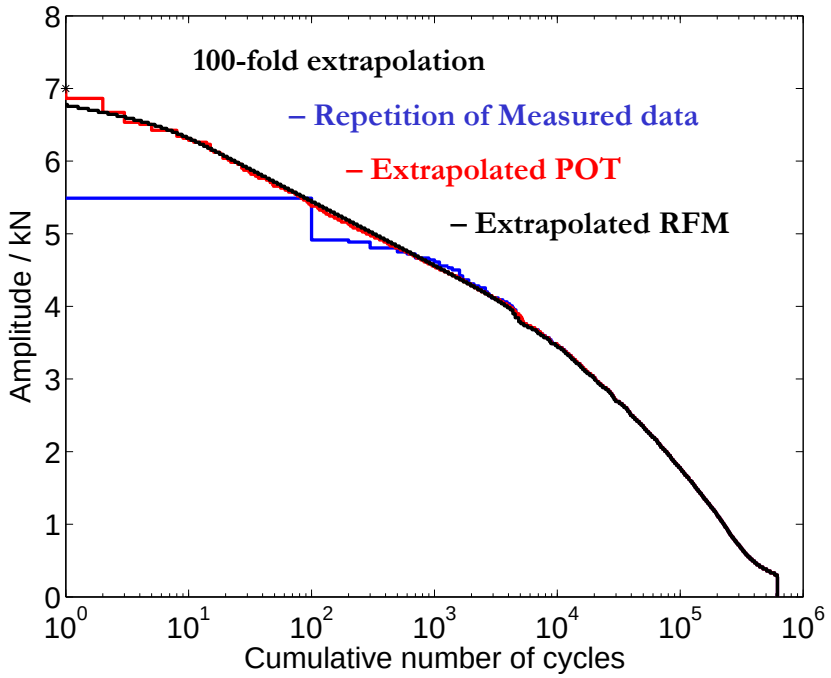

Figure A.2 Load spectrum for a 100-fold time extrapolation of measured data: blue line shows the 100 times repetition of measured data, while the red and black lines are the POT and the Rainflow Matrix extrapolations, respectively. Extracted from [Johannesson, 2005].

A.6 Adjustment of accumulation law to the experimental data

As shown in Section 4.2.4.2, the following formulation has been employed for the generalized long-term approximation of permanent pile-head displacements:

$$y_N = y_1 \left(1 + B_1\left[ln\left(B_2 N + 1\right) + B_3\, \delta_N\right]\right) \tag{A.57}$$

$$\delta_N = N\left(1 - B_4\right) - \frac{B_4}{B_5}\, e^{-N \cdot B_5} + C \tag{A.58}$$

$$C = B_4 + \frac{B_4}{B_5}\, e^{-\cdot B_5} \tag{A.59}$$

where y_1 and y_N are the permanent pile-head displacements after the first and Nth load cycles respectively, and B_1, B_2, B_3, B_4 and B_5 are constants, whose values for the different tests are given in Table 7.1.

The Log-Linear approximation shown in the following figures was obtained using the same formulation and constants, except for the B_4 constant, which was set equal to zero.

Table 7.1 Calibration of permanent displacement accumulation law to the experimental data

Cyclic test	y_1 [mm]	B_1	B_2	B_3	B_4	B_5
1st test series (-10N to 10N)	0.005	0.415	0.062	5.54E-5	0.999	1.55E-6
2nd test series (-10N to 20N)	0.088	1.105	0.0115	1.45E-5	0.91	5.5E-7
3rd test series (-10N to 30N)	0.274	1.95	0.002	2.75E-5	0.14	3.9E-7
4th test series (-10N to 40N)	0.366	1.55	0.0115	4.35E-4	0.976	2.05E-5
5th test series (0N to 30N)	0.459	0.675	0.0075	5.25E-6	0.82	4.5E-7

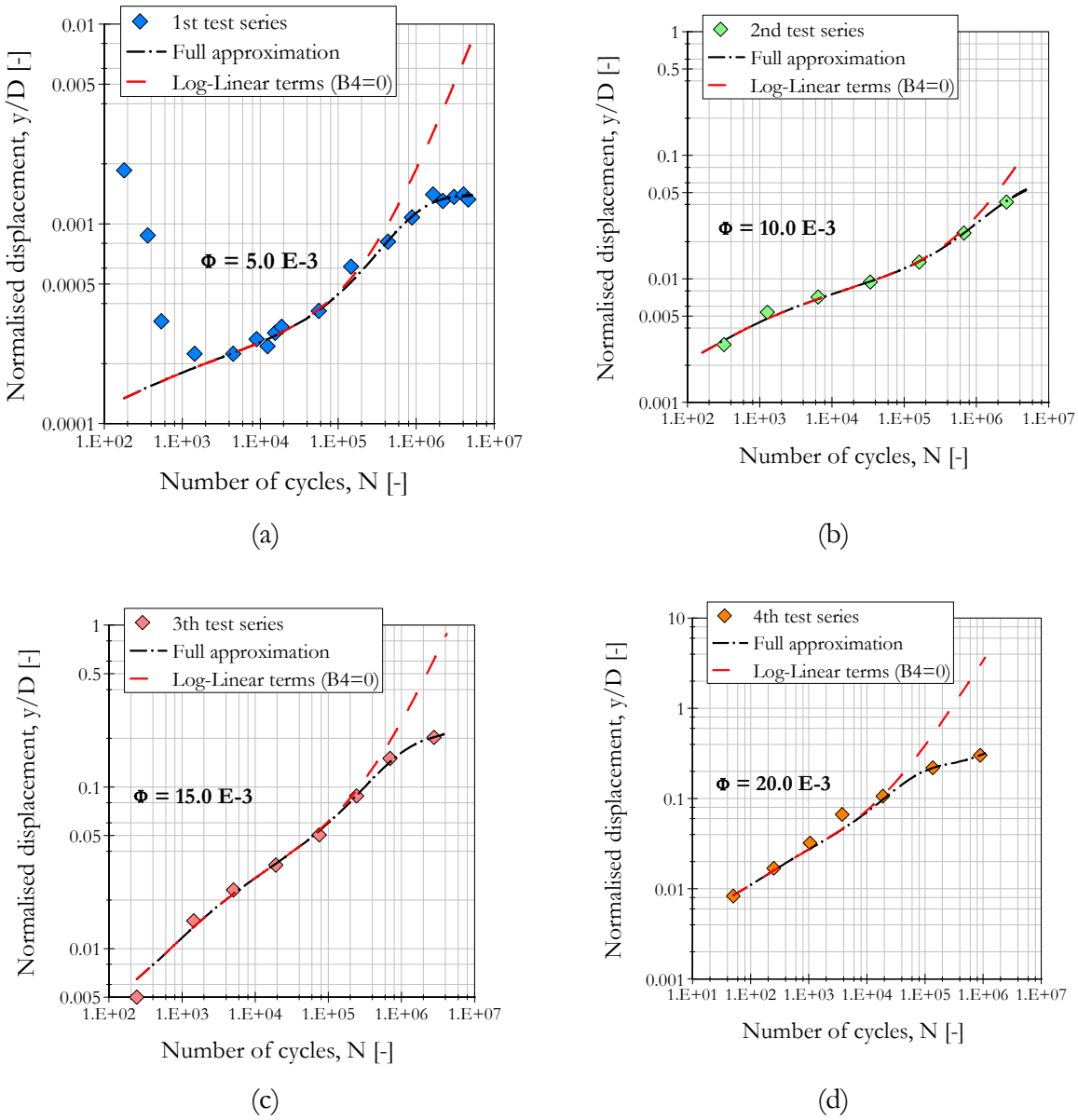

Figure 7.1 Dimensionless horizontal displacements versus number of cycles. Comparison of generalised approximation versus its Log-Linear counterpart obtained by setting B_4 equal to zero. (a) 1st test series (-10N to 10N). (b) 2nd test series (-10N to 20N). (c) 3rd test series (-10N to 30N). (d) 4th test series (-10N to 40N). (e) 5th test series (0N to 30N).

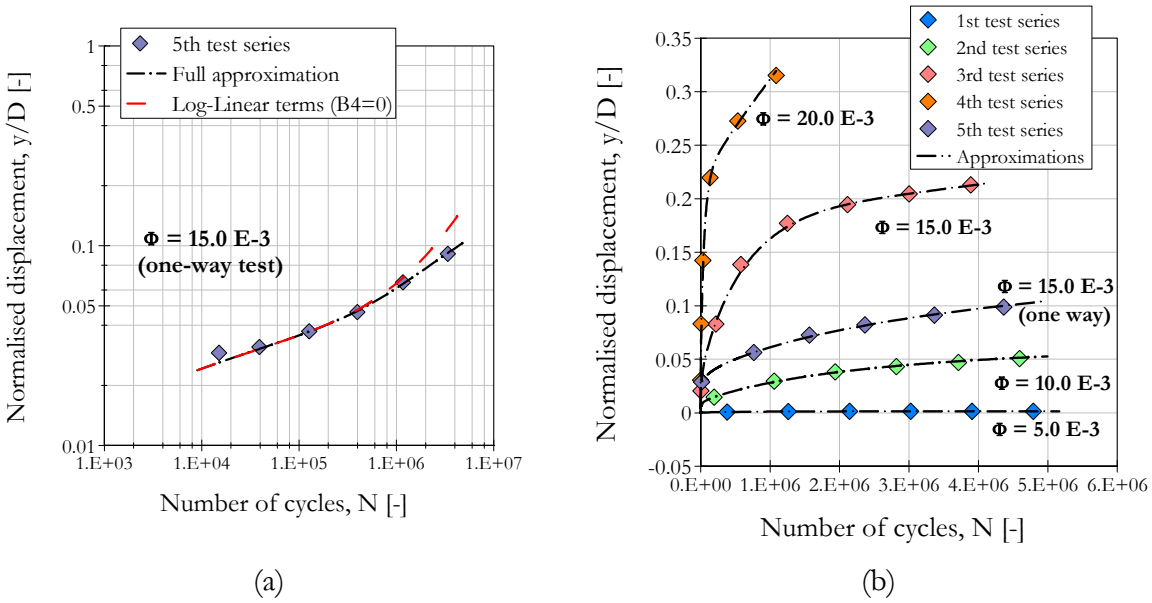

(a) (b)

Figure 7.2 Dimensionless horizontal displacements versus number of cycles. (a) Comparison of generalised approximation versus its Log-Linear counterpart for the 5th test series (0N to 30N). (b) Summary of the generalised approximation for all tests, in natural representation.